NUMERICAL MODELLING OF TIDAL FLOWS

IN

THE ARABIAN GULF

A Thesis Submitted for the Degree of Doctor of Philosophy

by

Mohammad Bashir

Department of Mathematics & Statistics, Brunel University

September 1993

ACKNOWLEDGEMENT

I would like to express my sincere thanks to my supervisor, Dr E.H. Twizell, for his constant support and encouragement throughout the course of this research work. His suggestions and criticisms were valuable and most relevent. I am pleased I had this opportunity to work with him.

I would also like to thank my honorary supervisors Dr A.Q.M Khaliq and Professor A.Y. Al-Hawaj. Dr Khaliq's untiring assistance and suggestions are much appreciated. Also, Professor Al-Hawaj has always been very helpful and supportive during the course of this work.

The academic discussion during the course of this work with colleagues at the University of Bahrain and at Brunel University, England are greatly acknowledged.

I am also indebted to the Academic Computing Departments at Brunel University, England, and at the Western Illinois University, U.S.A. Their faculty members were of great help in assisting the use of SURFER IV, MAP VIEWER and GRAPHER software packages, by Golden Software Co., for drawing contours and other graphic work.

Finally, I would like to thank my son, Tariq, for his valuable assistance with the computer graphics. I also would like to thank my wife, Jean, and daughter, Fouzia, for their constant support.

ABSTRACT

The main purpose of this thesis is the prediction of tidal movements in the Gulf, which are essential factors for shipping, fishing, and coast protection. The search for suitable predictions of tide propagation and flow problems has undergone a great advance with the arrival of the digital computer. The development of numerical methods permits the formulation of different efficient hydrodynamic models to compute every tide phenomenon with precision and to handle a great amount of information.

A two dimensional hydrodynamic model for tidal flow in the Arabian Gulf is developed. The basic hydrodynamic equations are solved with an explicit finite difference method using a staggered grid to reproduce the various tidal constituents in the Arabian Gulf Tidal forcing term at the open boundary (Strait of Harmouz) is approximated in a novel way. A detailed discussion is presented on the treatment of open and closed boundaries. Simulations have been made over several representative tidal cycles using this finite difference model, and the results compare favourably with existing data in different locations in the Arabian Gulf. Contour diagrams for amplitudes and phases are presented for the four dominant constituents M_2 (principal lunar), S_2 (principal solar), K_1 (lunar solar diurinal) and O_1 (principal lunar diurnal) in the Arabian Gulf. Due to the explicit nature of the finite difference scheme, this hydrodynamic model can be efficiently implemented on parallel as well as serial computers.

CONTENTS

CHAPTER 6 Numerical experiment and discussion

CHAPTER ONE

INTRODUCTION

Most numerical models presently being used for computing tidal flows are based on shallow water equations. In recent years, finite difference methods have been formulated for the numerical solution of shallow water equations in order to predict tidal movements, which are essential for shipping, fishing and coastal protection. Finite-difference schemes due to Hansen (1962), Leendertse (1967), Mathews and Mungall (1972), Flather and Heaps (1975), Lardner et al. (1982) and Duff (1983) are the most widely used techniques among these methods. Lardner et al. (1982) modified the Leendertse (1967) scheme to study tide movements in various regions of the Arabian Gulf. A detailed discussion of various schemes is documented in Chapter 3, section 3.3.

The hazards of pollution in the Arabian Gulf have increased significantly in the last two decades as a result of the high levels of production and transportation of petroleum and also of the growing industrialization and urban development around its shores.

The intensive oil traffic and rapid industrial development in the Arabian Gulf impose extreme demands on the maritime operations of the region, such as predicting currents around offshore drillings and other installations; monitoring pollution and determining tanker routes would be undeniably a useful tool. A particularly important part of such a model involves modelling the tidal movements in the Arabian Gulf.

Chapter 2 discusses first the phenomenon and general history of tides and then from section 2.3 to the end of the chapter the theory of tides is represented.

Section 2.1 discusses the affect of the moon on tides. The historical background, in section 2.2, presents the work of philosophers and scientists who realized there was a relation between the motion of the sea and the celestial bodies and how this understanding came to be studied from a mathematical point of view. The work of well known scientists of the past two centuries, in the field of tidal theory, is documented.

Sections 2.3 to 2.8 introduce the dynamics of oceans. Section 2.3 is about the determination of tide generating forces. In section 2.4 the tidal disturbing forces due to the sun and the moon are discussed in detail.

In section 2.5 the corresponding response of the oceans to the forces in 2.4 is discussed on the basis of the equilibrium theory, and when the inertia of the ocean is retained but the rotation of the earth is neglected, the limitations of this theory are indicated.

Three species of tide (diurnal, semi-diurnal and long period) are discussed in section 2.6. The details of the four dominant tidal constituents of the Arabian Gulf M_2 (principal lunar), S_2 (principal solar), K_1 (lunar solar diurnal) and O_1 (principal lunar diurnal) with their period and relative size are given in Table 2.1. Section 2.7 discusses the importance of coriolis acceleration and a term for coriolis acceleration is derived, which is necessary to understand the movement of the oceans. Sub-section 2.7.2 discusses large-scale movement of the ocean.

"Tides in the Gulf", in section 2.8, discusses cases in which one side of an approximating rectangular Gulf is connected to the open sea and the three remaining sides of the Gulf are bound by land. This is a similar situation to that occurring in the Arabian Gulf where the author's numerical modelling was carried out.

Chapter 3 is concerned with tidal flow in the Arabian Gulf. Section 3.1 discusses the physical geography of the basin and the factors which govern the tidal flow. In section 3.2 the complexity of the tides is discussed and also the effect that tidal ranges have on currents. In section 3.3, an in-depth review of the literature is documented.

Chapter 4 presents the mathematical model. In section 4.1 the basic equations for fluid flow, equation of continuity and the equations of motions for the model are set out. Section 4.2 discusses the reduction of the model equations to shallow water equations, while section 4.3 discusses the closed and open ocean boundary conditions. In section 4.4 initial conditions throughout the region are presented and finally in section 4.5 different formulae for the Chezy coefficient are given.

Chapter 5 presents a detailed discussion of the numerical scheme. Section 5.1 discusses some general aspects of nonlinear shallow water equations (SWE). In section 5.2 an explicit finite difference method is proposed for the numerical approximation of shallow water equations (5.1). Section 5.3 and 5.4 deal with the numerical approximation of shallow water equations (5.1) near the boundaries. Boundary treatment near closed boundaries is described in section 5.3 while section 5.4 is devoted to open boundaries. In section 5.5 the numerical treatment of tide flats is discussed. Section 5.6 deals with the topography of the Arabian Gulf bottom. Section 5.7 covers the method of grid identification, namely the 3 types of grid cell occurring in the solution domain. Section 5.8 deals with the stability condition necessary for the explicit finite difference scheme and finally section 5.9 discusses the stopping criteria and convergence.

In the final chapter, Chapter 6, the results of the numerical experiments are presented and evaluated. Section 6.1 shows the results of the computation of amplitudes and phases of tidal constituents M_2, S_2, K_1 and O_1 in the Arabian Gulf. Section 6.2 demonstrates the accuracy of the numerical model explicit finite difference method, EFDM, for simulation of the tidal amplitudes and phases.

Section 6.3 gives the results of error analysis for the four tides. Measured and computed amplitudes and phases for the tides M_2, S_2, K_1 and O_1 at 74 tidal stations shown in Figure 6.2b in the Arabian Gulf are tabulated. Histograms of errors and percentage errors in calculated amplitudes and phases are also given, as are the sizes of errors and their cumulative distribution. Comparison of observed and computed amplitudes of each of M_2, S_2, K_1 and O_1 tides at an average of 18 stations is shown in a series of figures.

In section 6.4 the results of well-known hydrodynamical models in Arabian Gulf by Lardner et el. (1982), Evans-Roberts (1979) and Von Trepka (1968) are discussed. Their results are compared with the present model. Contour diagrams generated by the simulation of several important tidal constituents are discussed. Contour diagrams for amplitudes and phases for the constituents M_2, S_2, K_1 and O_1 are generated using SURFER IV by Golden Software Co, U.S.A.

CHAPTER TWO

HISTORY AND THEORY OF TIDES

HISTORY OF TIDES

2.1 THE PHENOMENON OF TIDES.

Tides are produced by the attraction of both sun and moon on the oceans and can be seen as a regular rise and fall of water within a range of several feet. They usually occur twice every day with the interval between one high water period and the next averaging 12 hours and 25 minutes.

Even elementary observations made at the sea-shore reveal that ocean tides are affected more strongly by the moon than by the sun. The time of high and low water is closely related to the position of the moon, that is, to its passage over the meridian which occurs, on average 50 minutes later on each succeeding day. However, between the moon's passage over the meridian and high water there is a time lapse which differs from place to place and also differs for the same place depending on the propagation of the tide from the ocean into coastal waters. Also, there is a variation, from day to day, in the height to which the water rises. A spring tide occurs during a new moon when the sun and moon are on the same side of the earth, as well as at full moon when they are diametrically opposite. At full moon the tidal range - equalling the difference in height between high and low water- is often greatest. During the moon's first or third quarter the range is smallest and that is when a neap tide occurs. Apart from the regular changes in the ranges the tides at some places are subject to various irregularities. The ranges of two successive tides are usually not the same at any given place.

This is known as the diurnal inequality of the tide, the extent of this effect differs from place to place. When the moon is in perigee (that is, nearest the earth) the range of the tide is greater by nearly 20 per cent than when it is in apogee (furthest

point from earth). The maximum tidal range occurs during the moon's new or full phases i.e. when it is in perigee.

In certain seas, namely in parts of the Gulf of Mexico, the Gulf of St. Lawrence, the Indonesian Archipelago and the China Sea, the tides are even more irregular. In those areas the water levels rise and fall only once daily during a part of each month. However, in such diurnal tides the tidal fluctuations are quite small compared to the so-called semi-diurnal tides.

The tidal phenomenon is obviously a complicated one. There is no general theory that will explain all the irregularities of tides. However, the available theory enables us to establish a practical method for the determination of tides at certain points along the coast and in estuaries. Numerical computations can be used to determine the coefficients which fix the tides at any given point in detail.

For an introduction to the theory of tides, reference is made to Darwin (1907) and for more modern theories to the books of Proudman (1953), Defant (1961) and Hill (1962).

2.2 HISTORICAL BACKGROUND.

Nearly two thousand years ago naturalists like Pliny and Strabo (1962) suspected that there was a relation between the celestial bodies and the motion of the sea. Kepler (1601-1630) realized that the attracting forces of the sun and moon were involved but it was Newton who first discussed the origin of tides from a mathematical viewpoint. In his work "Philosophiae Naturalis Principia Mathematica" (1687) he dealt with the problem of tides by assuming the entire earth to be covered with water, and showed that the surface of the water would then become a spheroid as a result of the pull of the moon (or sun). The fact that the main axis of the spheroid would be directed toward the moon explained the twice-daily occurrence of ebb and flow. Newton derived the phenomenon of the spring and neap tides from the positions of the moon and sun. He also demonstrated the effect of the difference in the distance between the earth and the sun, with respect to the moon. However, Newton's development

was qualitative and unsuitable for practical application.

In 1738 the French Academy of Science held a competition for the best tidal theory. One of the prize winners was Bernoulli (1741) who extended Newton's theory of the course of tides at the equator. Both Newton and Bernoulli postulated a so-called equilibrium surface which the water mass on the earth assumes under the influence of the pull of a celestial body and which changes continuously so that the main axis is constantly directed towards the celestial body. Neither men considered the forces of inertia and consequently the motion of the particles themselves. Newton's hypothesis is in fact incompatible with the actual motion of the particles, which is a subject for hydrodynamic theories.

Laplace (1796-1825) attempted to improve Newton's work in this respect. Volume IV of his work "La Mécanique Celeste" is devoted to the theoretical and practical study of the sea's oscillations. A large part of his work deals with the tides at Brest but the theory is not adequate when considering the many variations in terrestrial conditions. Nevertheless, the results of Laplace's theory, which describes the general principles of the correspondence between the periodic forces and the sea's motion, are useful for showing how tidal observations must be analysed for theoretical and practical purposes.

These principles form the foundation of the harmonic method which was developed by Thomson in about 1868. While Laplace combined all periodic terms into one formula, Thomson based his method on the development of a sum of periodic terms, the so-called tidal constituents. Since the amplitude and phase of each tidal constituent may be determined from observations and since the period is known from the theory of harmonic analysis, the tides can be forecast at any given place. After Thomson, the theory of harmonic analysis, especially the methods for numerical computation of the harmonic constituents, was extended by Darwin and other investigators. The course of a tide along the coast may be determined approximately from the known values of the harmonic constants of the tides at points along the coast, but this does not hold for tides in the seas due to a lack of observation points. Because of this fact, it would be of great

importance if the tidal motion in the oceans could be determined by mathematical means. Mention should also be made of the most important investigators in this field. Following the fundamental work of Newton, Bernoulli and Laplace the problem of tides was considered by Airy (1842) and, later, Poincare developed mathematical methods in volume III of "Lecons de Mécanique Celeste, Theorie des Marées". Taylor (1920) and Proudman (1953), and more recently Van Dantzig and Lauwerie (1960) have all used analytical mathematical methods.

The theoretical study of the tidal motion in coastal waters and rivers started in the first half of the nineteenth century. The hydraulic study of steady flow in inland rivers where no tidal flow occurs began in the last part of the eighteenth century. It is clear that a study of the tides must also be based on these hydraulic studies, especially when the influence of friction is being considered. Since the numerous variations in the dimensions of a river and the irregularities in the coast line considerably complicate the application of simple methods of calculation, original tidal research was for the most part of an empirical nature. Mathematical tools, based on real functions, for solving linear differential equations were well known in those days; the introduction of complex quantities dates from the time of Gauss and the solution of partial differential equations is based on the work of Cauchy.

As a result, at the beginning of the nineteenth century, it was already possible to begin theoretical studies of tidal motion in shallow water. In the publication of Airy, in.1842, it is shown that due to the non-linear character of propagation an originally pure sinusoidal wave is distorted such that higher harmonics are introduced. In addition, De Saint Venant (1871) approached the propagation of tidal and other similar long waves in another way: his method is based on some of the features of the characteristic formulation of differential equations which were not yet completely developed.

An important contribution to the theory of tides in shallow waters was made by Massau, in 1900. He was one of the original users of the theory of characteristics which then had been extensively studied by the French school of mathematicians in the

latter part of the nineteenth century and first part of the twentieth century (Hadamard (1923), Picard (1950), Goursat (1923) and others). However, at that time his work attracted little attention, possibly because its practical use was not clearly understood. With the development of modern methods of numerical calculation Massau's work finally received full recognition.

During this century hydraulic engineering problems in tidal waters greatly intensified the need for hydraulic studies, and consequently the practical computation of the actual tides in rivers became important. This was the case in the Netherlands where extensive tidal computations were made in connection with the closure of the Zuiderzee. Lorentz (1926) was one of the members of the Netherlands Government Commission and made important contributions to the methods of solving tidal problems. After the closure of the Zuiderzee, in 1932, the actual modifications in the tidal motion in the Waddenzee agreed with the results of the earlier computed predictions. The basic method used in the work of the Commission was the Fourier or harmonic method. After the Second World War methods based on the characteristics of hyperbolic partial differential equations were applied to tidal motion. The work done by Massau has been mentioned already. This subject was also dealt with extensively by Schönfeld (1955), who applied the theory more generally to long waves in shallow waters. Solutions of tidal computations on computers has now greatly extended our knowledge of tides in coastal waters as well as in the ocean.

THEORY OF TIDES

2.3 THE TIDE-GENERATING FORCES AND TIDAL MOVEMENT

The sun and the moon are the only celestial bodies that need to be considered for the determination of tide-generating forces. Because of their greater distance or smaller size, other celestial bodies have a negligible effect on the tidal force.

To derive mathematical expressions for the tide-generating forces of the sun and the moon, the principal factors to be taken into consideration are the rotation of the earth, the revolution of the moon around the earth in an orbit inclined to the equator of the earth, and the motion of the earth around the sun along the ecliptic which is also inclined to the equator. The system of the moon and the earth go around the sun once a year. Since the earth is 80 times heavier than the moon, the centre of the gravity of the earth and moon lies inside the earth.

Consider a balance of forces affecting a unit mass at a point of the earth's surface. This mass moves in the gravitational field conditioned by the attraction force of the earth $\mathbf{G}(X)$, the moon, the sun and other perturbing bodies of the solar system. Denote the attraction forces of these bodies by $\sum_i \underline{\mathfrak{I}}_i(X)$.

The displacement of the mass at the point X will be controlled also by the forces of pressure $\mathbf{P}(X)$ and friction $\mathbf{F}(X)$.

Introducing an inertial system of co-ordinates with the origin at a point O, let C be the centre of the earth, and B_i ($i = 1, 2, 3, \ldots$) be the centres of the purturbing bodies (Figure 2.1). Then Newton's second law for the point X can be represented by

$$\frac{d_a^2}{dt^2}\underline{OX} = \mathbf{P}(X) + \mathbf{G}(X) + \sum_i \underline{\mathfrak{I}}(X) + \mathbf{F}(X). \qquad (2.1)$$

Here the operator $\frac{d_a}{dt}$ refers to the inertial system of co-ordinates.

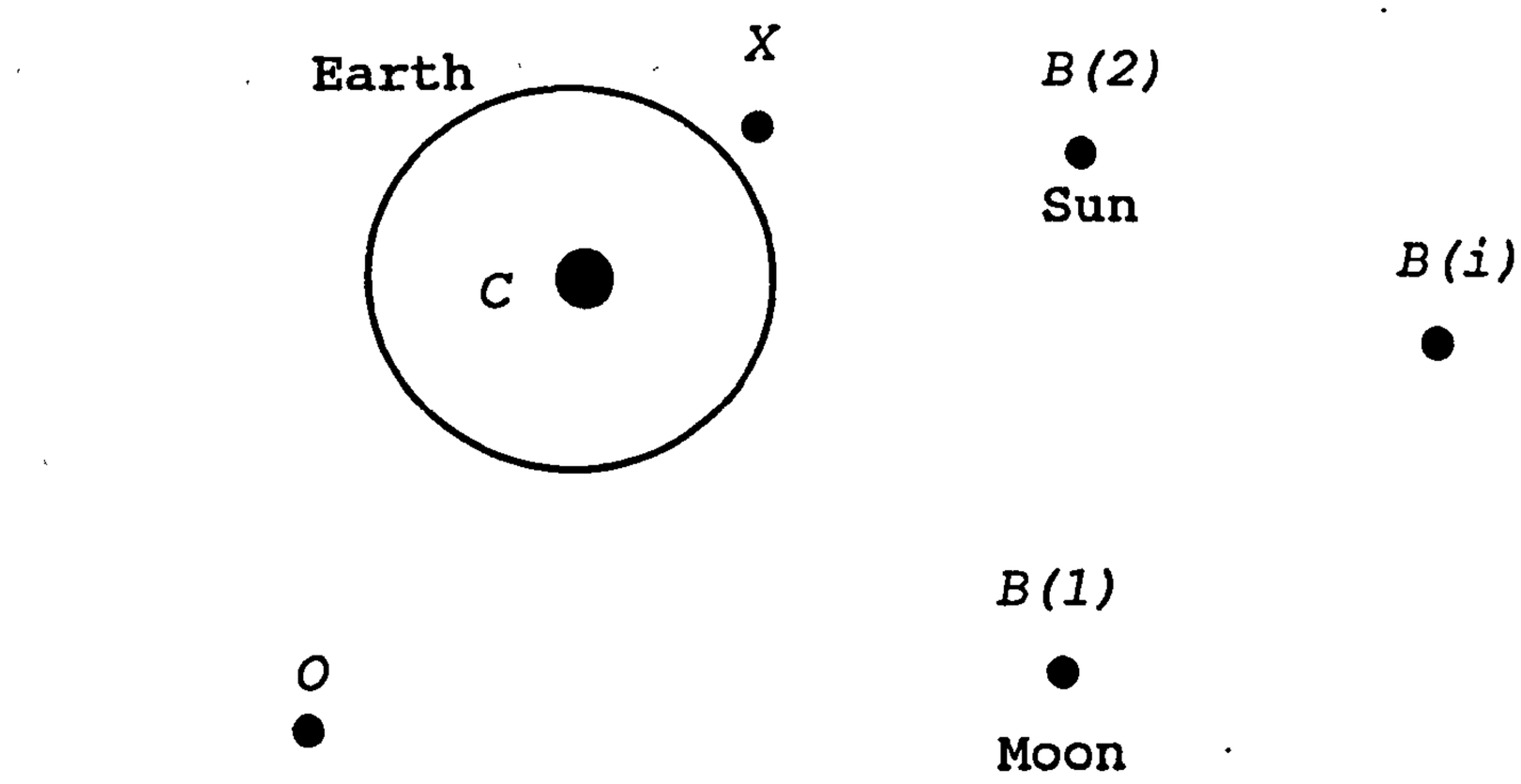

Figure 2.1

Figure 2.1 represents the position of the considered point X, the centre of the earth C and purturbing bodies B_i with respect to the origin of the inertial system of coordinates.

Compare the orders of magnitude of $\mathfrak{I}(X)$ and $\mathbf{G}(X)$. For the moon and the sun $R \langle\langle D$ (Figure 2.2). Hence

$$|\mathfrak{I}(X)| \approx |\mathfrak{I}(C)| \approx \frac{\gamma M}{D^2} ,$$

where γ is the gravitational constant, M is the mass of the perturbing body B and D is its distance

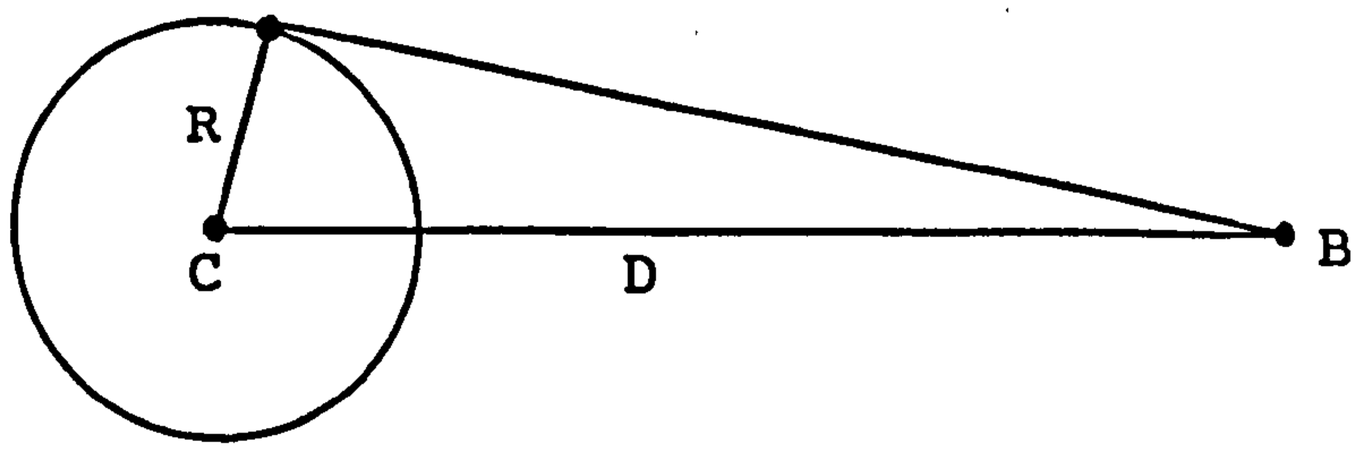

Figure 2.2

from the centre of the earth. Since

$$|\mathbf{G}(X)| \approx \gamma\left({}^{M_E}\!/_{R^2} \right) ,$$

where M_E is the earth's mass, R is the distance between the centre of the earth and the point X, then

$$|\underline{\mathfrak{I}}(X)|/|\mathbf{G}(X)| \approx \left({}^{M}\!/_{M_E} \right)\left({}^{R}\!/_{D} \right)^2 .$$

The mass ratios between the moon and the earth and the sun and the earth are known to be

$$M_{moon}/M_E = 1 / 81.30 ; \quad M_{sun}/M_E = 332,958 . \tag{2.2}$$

respectively.

If R is set equal to the equatorial radius of the earth r, then R/D is the equatorial parallax its mean value for the moon and the sun being

$$\frac{r}{c_{moon}} = 0.016593; \quad \frac{r}{c_{sun}} = 4.2615\times10^{-5} \tag{2.3}$$

respectively. Here R/c is the mean value of R/D with respect to the orbit. Thus

$$\frac{|\underline{\mathfrak{I}}(X)|}{|\mathbf{G}(X)|} \approx \begin{cases} 3.4\times10^{-6} & \text{for the moon,} \\ 6.0\times10^{-4} & \text{for the sun.} \end{cases}$$

The sun is seen to exert a greater attraction than the moon. Remember that, when moving along its orbit, the earth is subjected to acceleration. Use Newton's second law again and obtain

$$\frac{d^2}{dt^2}\underline{OC} = \sum_i \underline{\mathfrak{I}_i}(C);$$

subtracting this relation from equation (2.1) gives

$$\frac{d^2}{dt^2}\underline{CX} = \mathbf{P}(X) + \mathbf{G}(X) + \sum_i \mathbf{T}_i(X) + \cdot \mathbf{F}(X) \qquad (2.4)$$

where $\mathbf{T}_i(X) \equiv \underline{\mathfrak{I}_i}(X) - \underline{\mathfrak{I}_i}(X)$ is the tide-generating force. Thus, the tide-generating force is determined as the resultant of the forces of attraction of a unit mass at the points X (arbitrary points on the surface) and (the earth's centre) exerted by the perturbing body. The direction of $\mathbf{T}(X)$ coincides with that of the vector sum of $\underline{\mathfrak{I}_1}(X)$ and $-\underline{\mathfrak{I}_1}(X)$ forces. Figure 2.3 presents the direction and the magnitude of the tide-generating force at eight points of the meridional section of the sphere centred at the point C.

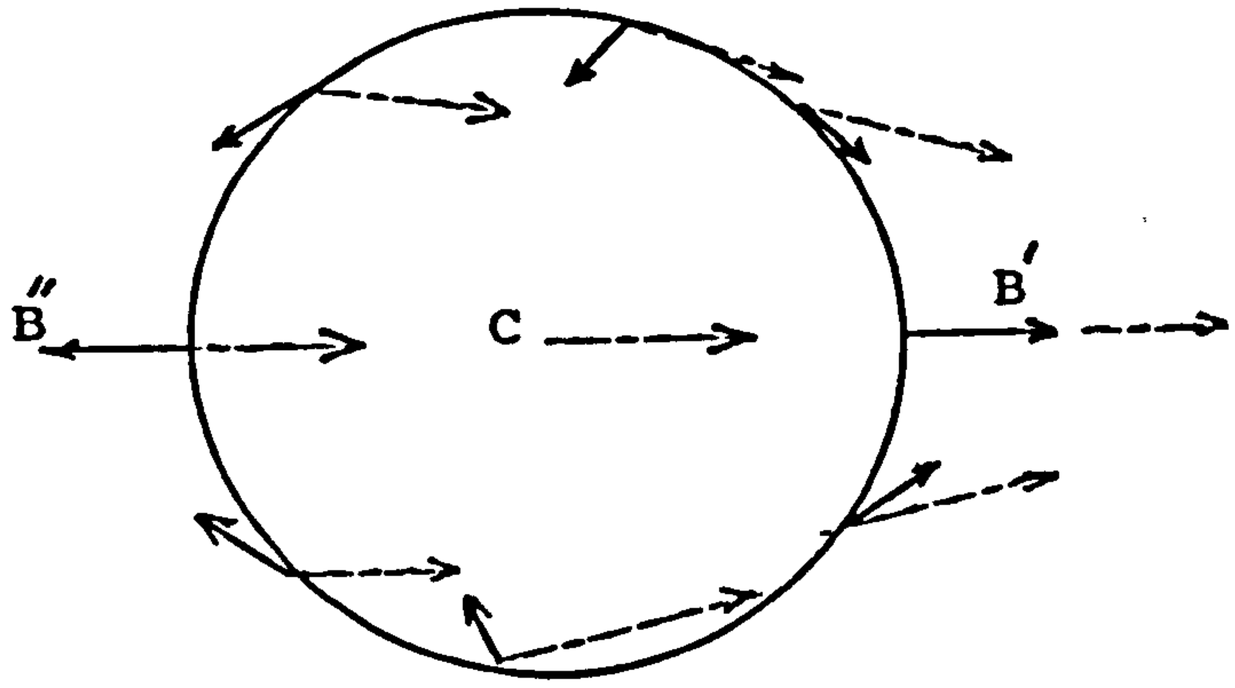

Figure 2.3

In Figure 2.3 the tide-generating force (full arrows) is shown at eight points of the sphere meridional section. Dashed arrows denote the force of attraction at the point X. In the centre of sphere $\mathfrak{I}(X) = \mathfrak{I}(C)$.

In the case discussed, when the distance from the perturbing body B (the moon or the sun) to the centre of the earth greatly exceeds its radius (that is, for small values of the

parallax), the distributions $\mathbf{T}(X)$ in the sublunar and antilunar (analogously in subsolar and antisolar), the earth's hemispheres will be almost mirror images of each other.

The order of magnitude of $\mathbf{T}(X)$ can be evaluated by the difference between the vectors $\underline{\mathfrak{I}}(X)$ and $\underline{\mathfrak{I}}(C)$ at the point B' (Figure 2.3) where their directions coincide,

$$\text{If} \quad R \ (\equiv C B') \quad << \quad D \ (\equiv C B) \ , \quad \text{then}$$

$$|\mathbf{T}(B')| = \frac{\gamma M}{(D-R)^2} - \frac{\gamma M}{D^2} \approx \frac{2\gamma M R}{D^3}.$$

Comparing $|\mathbf{T}(B')|$ with $|\mathbf{G}(B')| \approx {}^{\gamma M_E}\!/_{R^2}$ gives

$$\frac{|\mathbf{T}(B')|}{|\mathbf{G}(B')|} \approx 2\left(\frac{M}{M_E}\right)\left(\frac{R}{D}\right)^3.$$

Hence, unlike the moon's and the sun's attraction, forces which, when referred to those of the earth, are proportional to the squared parallax, the tide-generating force normalized in the same way is proportional to $\left({}^{r}\!/_{c}\right)^3$.

Equalities (2.2) and (2.3) afford

$$\frac{M_{moon}}{M_E}\left(\frac{r}{c_{moon}}\right)^3 = 0.5603 \times 10^{-7}$$

$$\frac{M_{sun}}{M_E}\left(\frac{r}{c_{sun}}\right)^3 = 0.2580 \times 10^{-7} \qquad (2.5)$$

The tide-generating forces of the moon and the sun appear to be of the same order of magnitude and about 10^7 times less than the gravitational force of the earth. However, despite this fact, they cannot be neglected. Indeed, in the ocean (as well as in both the atmosphere and lithosphere) the force G is counteracted by the force of the hydrostatic pressure which

nearly equals **P**, so that the sum **P+G** can be negligible when compared to **G**

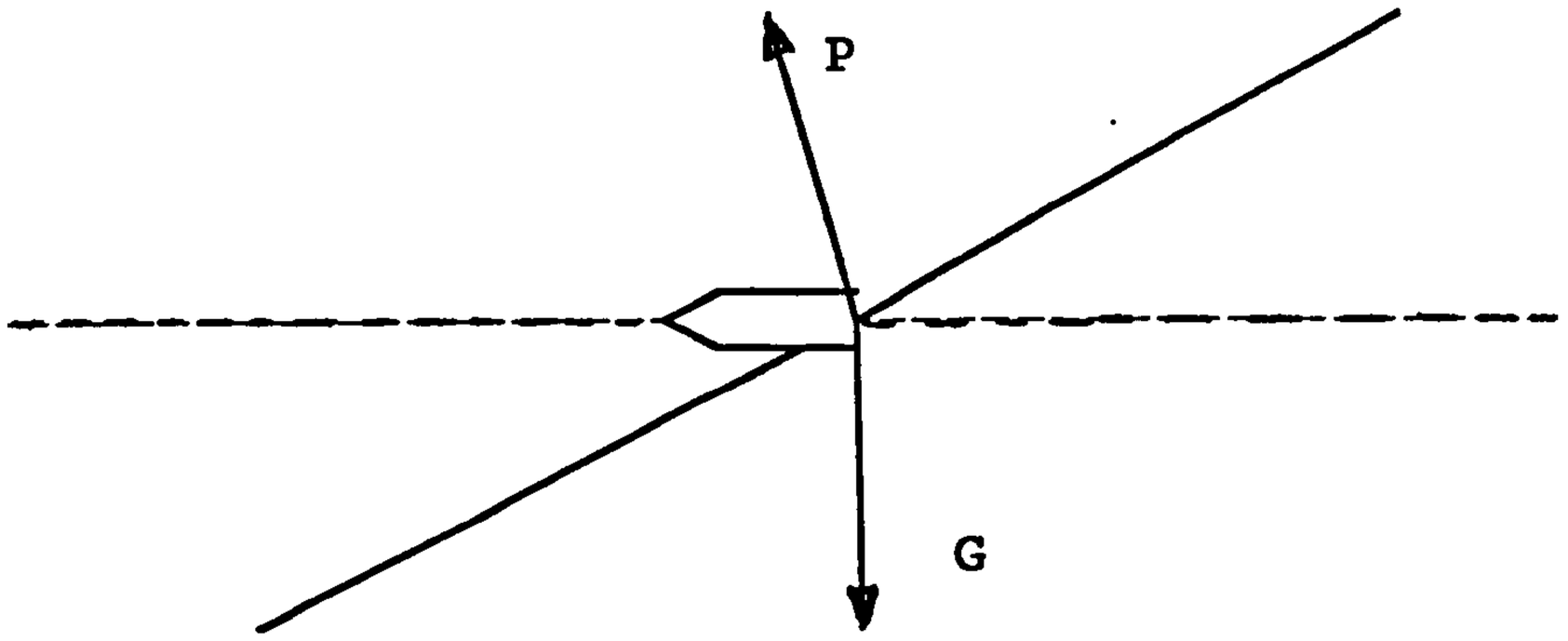

Figure 2.4 Balances of forces of the earth's attraction and hydrostatic pressure.

This conclusion is illustrated by Figure 2.4 in which the surface normal to **G** and hydrostatic component of the force **P** are presented in dashed lines, while the resultant **P+G**, equal in order of magnitude to the tide-generating force and oriented almost perpendicular to **G**, is denoted by an arrow.

This discrepancy in the directions of the **G** and **T** forces results in the fact that the latter leads to the horizontal shift of particles along the earth's surface and hence to the accumulation of the mass in the vicinity of the points B' and B" Figure 2.3. The accompanying vertical (radial) shifts are of a kinematic nature. They are induced by the law of conservation of mass rather than by the radial component of the tide-generating force.

This is in outline of the tide-generating mechanism in the atmosphere, hydrosphere and lithosphere of the earth.

2.4 THE TIDE POTENTIAL (Disturbing Potential)

We set up here the quantitative analysis of the inference of the bodies (sun, moon etc.) upon the ocean and we follow Lamb's "Hydrodynamics" (1932) quite closely in much of the treatment.

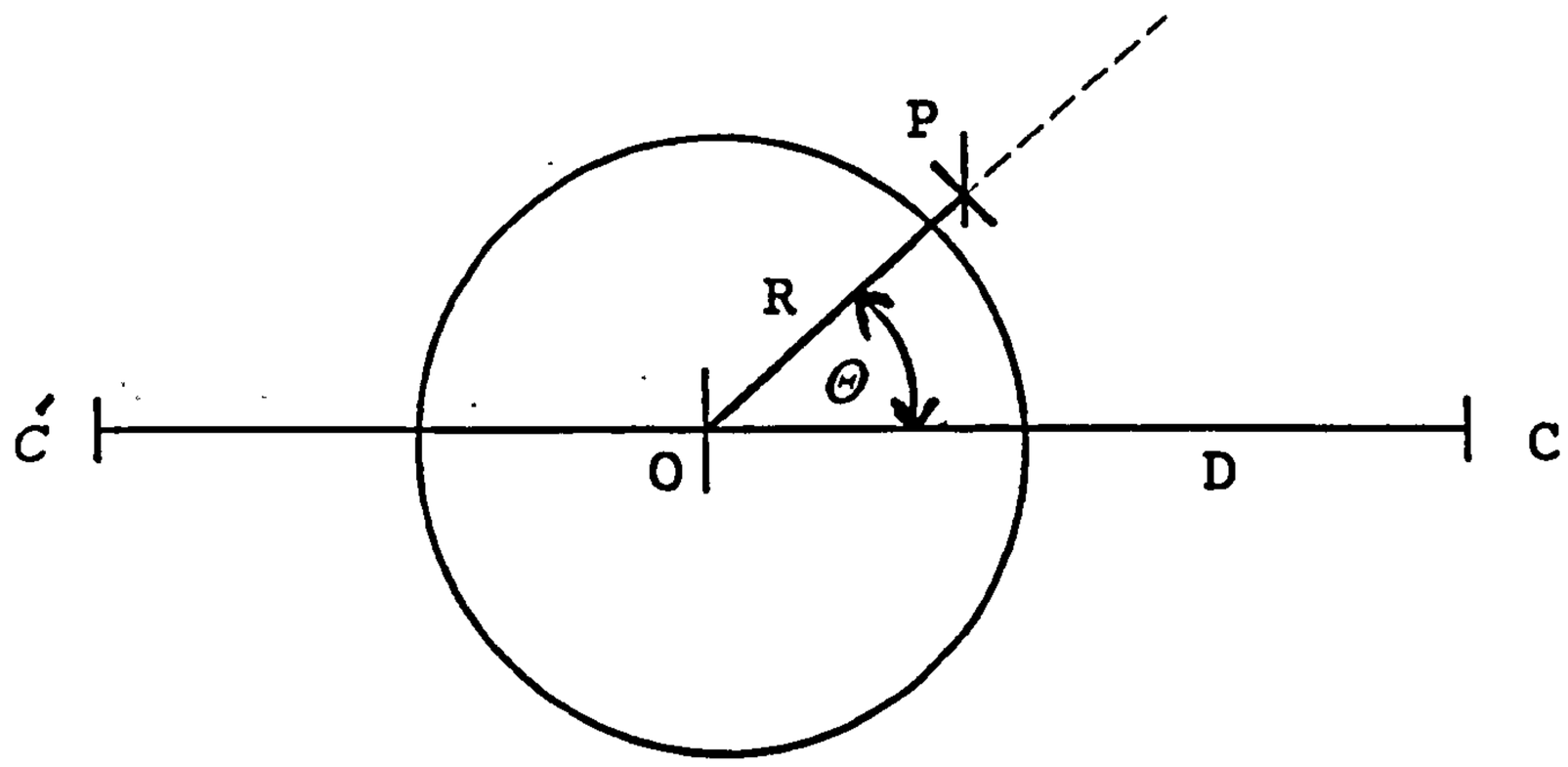

Figure 2.5

In Figure 2.5, O is the centre of the earth, C is a disturbing body represented as a point mass because of its distance from O. P is a representative point within the ocean and let us suppose that C is the moon

Let

$$OP = R$$

$$OC = D$$

Mass of Earth $= M_E$

Mass of the Moon $= M$

Zenith angular distance $= COP = \Theta$

Universal constant of gravitation $= \gamma$

Newton's law of gravitation states that two particles of masses m_1 , m_2 distance d_{12} apart will attract one another with a force of magnitude

$$\gamma\, m_1\, m_2 \,/\, d_{12}^2$$

directed along the line joining them. It is also a general result of gravitational theory that a spherical body, such as the moon, will attract an outside body as if all its mass is concentrated at its centre. Suppose now we have a unit mass at the point P, then the attraction upon this mass due to the moon will be

$$\gamma M / CP^2 \quad \text{along } \vec{PC} \tag{2.6}$$

Rather than work with forces, it is easier to introduce the gravitational potential V such that

$$\mathbf{F} = -\operatorname{grad} V \tag{2.7}$$

in which case we can say that the attractive force in (2.6) arises from the potential V where

$$V = -\gamma M / CP \tag{2.8}$$

hence

$$V = -\frac{\gamma M}{\{ D^2 + R^2 - 2DR\cos\Theta \}^{1/2}} \tag{2.9}$$

The problem is a little more complicated than this, however, since we shall require to relate all theory relative to the centre of the earth as origin and the centre of earth is attracted to the moon by the force

$$\gamma M M_E / D^2$$

This means that the centre of the earth has an acceleration of magnitude $\gamma M / D^2$ along the direction OP.

In applying Newtonian equations, it is essential that we have a Newtonian frame of reference which is either at rest or at most in uniform motion and, therefore, the effect of this acceleration has to be removed. If, for a moment , we look upon the direction OC as the X-axis, we have a uniform acceleration of our axes system of magnitude $\gamma M / D^2$ in the X-direction and this can be said to arise from a potential V^* given by

$$V^* = -\frac{\gamma M}{D^2} x = -\frac{\gamma M}{D^2} R \cos \Theta \qquad (2.10)$$

where, $\left(-\frac{\partial V}{\partial x} = \frac{\gamma M}{D^2} \right)$

It follows, therefore, that in order to relate movements of the ocean relative to the centre of the earth as origin of coordinates, we have to use the gravitational potential Ω defined by

$$\Omega = V - V^* = -\frac{\gamma M}{\{ D^2 + R^2 - 2DR\cos\Theta \}^{1/2}} + \frac{\gamma M}{D^2} R\cos\Theta \qquad (2.11)$$

where we have subtracted the effect V^*. This is the exact disturbing potential that one should use for each of the disturbing bodies, moon, sun, planets. Because of the fact that $D >> R$, we can use an approximation to equation (2.11) which can be derived as follows; we have

$$\Omega = -\frac{\gamma M}{D} \left\{ 1 - 2\frac{R}{D}\cos\Theta + \frac{R^2}{D^2} \right\}^{-1/2} + \frac{\gamma M}{D^2} R\cos\Theta$$

We can expand binomially to obtain

$$\Omega = -\frac{\gamma M}{D} \left\{ 1 + \frac{\left(-\frac{1}{2}\right)}{1} \left(-2\frac{R}{D}\cos\Theta + \frac{R^2}{D^2} \right) + \frac{\left(-\frac{1}{2}\right)\left(-\frac{3}{2}\right)}{2!} \left(-\frac{2R}{D}\cos\Theta + \frac{R^2}{D^2} \right)^2 \cdots \right\}$$

$$+ \frac{\gamma M}{D^2} R\cos\Theta$$

that is

$$\Omega = -\frac{\gamma M}{D}\left\{ 1+\frac{R}{D}\,Cos\,\Theta+\frac{R^2}{D^2}\left(-\frac{1}{2}+\frac{3}{2}\,Cos^2\Theta \right) \right.$$

$$\left. +\ O\left(\frac{R^3}{D^3}\right) \right\} + \frac{\gamma M}{D^2} R\,Cos\Theta\ ,$$

$$= -\frac{\gamma M}{D} - \frac{\gamma M R^2}{D^3}\left(-\frac{1}{2}+\frac{3}{2}Cos^2\Theta \right) + \ldots\ldots \qquad (2.12)$$

The exact expansion of Ω in ascending powers of R/D can, of course, be written down in terms of Legendre polynomials, as follows. We use the generating function definition of Legendre polynomials, namely

$$\frac{1}{(\ 1-2hx+h^2\ )^{1/2}} = \sum_{n=0}^{\infty} h^n\,P_n(x) \quad |2hx-h^2| < 1 \qquad (2.13)$$

and this gives the result

$$\Omega = -\frac{\gamma M}{D}\sum_{n=0}^{\infty}\frac{R^n}{D^n}P_n(\ Cos\Theta\ ) + \frac{\gamma M}{D^2}R\,Cos\Theta \qquad (2.14)$$

Since $P_0(x) = 1$, $P_1(x) = x$, $P_2(x) = -\frac{1}{2}+\frac{3}{2}x^2$, etc.,

we return to formula (2.12).

The constant term $-\gamma M/D$ is unimportant since the potential is always undefined to the extent of an additive constant and, henceforth, we shall use the expression

$$\Omega \;=\; \frac{3}{2}\,\frac{\gamma M R^2}{D^3}\left(\;\frac{1}{3}\;-\;Cos^2\Theta\;\right) \qquad (2.15)$$

for the disturbing potential. The rapidity of convergence in expanding by the binomial series can be assessed if we bear in mind that

$$R \;\approx\; 6400 \;\; \text{kms}\,, \; D_{moon} \;=\; 384{,}800 \;\; \text{kms}$$

and

$$D_{sun} \;=\; 149{,}664{,}900 \;\; \text{kms.}$$

It is of interest to observe that the approximate potential (2.15) could have been deduced if we had placed a mass $\frac{1}{2}M$ at C and a mass $\frac{1}{2}M$ at C' where $OC = OC'$, for, in this case, we would have

$$\Omega \;=\; \left\{ -\;\frac{\frac{1}{2}\gamma M}{\left(\;D^2 \;+\; R^2 \;-\; 2\,D\,R\,Cos\Theta\;\right)^{1/2}} \right.$$

$$\left. -\;\frac{\frac{1}{2}\gamma M}{\left(\;D^2 + R^2 \;+\; 2\,D\,R\,Cos\Theta\;\right)^{1/2}} \right\} \qquad (2.16)$$

and, upon expansion, (2.15) would be recovered. A mass at such a position C' is known as the anti-moon. There are various ways in which (2.15) can be developed, but the above derivation given by Lamb is clear. Physical reasoning in deducing the necessity for an anti-moon may be found in Darwin's (1911) popular book on Tidal Theory.

We can now state the tidal problem. Given the disturbing tidal potential (2.15) for each disturbing body, find the resulting shape of ocean. This is a problem of enormous difficulty, due largely to the difficulty of incorporating the rotation of the earth in a proper way. We shall deal with the problem in various ways,the first of these being the equilibrium tidal theory due to Laplace (1749-1827) who produced his monumental work "Traité de Mécanique Céleste", 5 volumes, between 1799-1825.

In addition to the simple equilibrium theory, Laplace produced a dynamical theory of tides to which we shall also refer later. Contributions to tidal theory came in the 19th century from Kelvin, Darwin and Hough, most of which is summarized adequately in Lamb's "Hydrodynamics". In this century, the Laplace-Hough theory has been criticized by the Norwegian mathematician Solberg (1937), in "Astophisica Norvegica". In all the above theories , it is assumed that the free upper surface of the ocean is a surface of constant pressure, that is, the variable influence of moving pressure, systems like cyclones, depressions and anti-cyclones is neglected. We shall have occasion to discuss these effects later. Furthermore, it is usually assumed that the ocean floor is either a sphere or spheroidal shape and the influence of the rapid shallowing effects near the coasts and the further influence of covering estuary or inlet will have to be considered separately.

2.5 THE EQUILIBRIUM TIDAL THEORY

The tidal force which generates the tides upon the earth can be determined accurately from the known movements of the sun and the moon with respect to the earth. Since these movements have a periodic character, the tides may also be developed into periodic constituents. It is, however, not yet possible to deduce from these known forces the theoretical periodic constituents of the tide at any point on the ocean or adjacent seas by assuming terrestrial conditions similar to those actually existing. It is only possible to determine the tides on the earth under idealized conditions, such as those applied in the equilibrium theory. In this theory, it is supposed that the oceans cover the entire earth. Then, the horizontal component of the tidal force will move the water particles such that at any moment an equilibrium surface is maintained. (See for the discussion of the equilibrium tide Doodson (1921), Lamb (1945) and Villain (1943,1944)).

The equilibrium conditions are satisfied when the free surface is normal to the resultant of gravitational force and the

tide-generating forces. Furthermore, it is assumed that the free surface maintains its equilibrium form at all times. However, the sun and the moon change their positions continuously with respect to the earth; this causes a corresponding motion of the water particles. Thus the equilibrium surface will change continuously with time at every point on the earth. Furthermore, in the equilibrium theory, it is implicitly assumed that the water has a negligible inertia and can respond instantaneously to the forces. Actually, however, the inertial forces are very important.

Fortunately, experience confirms that the real tide has constituents everywhere analogous to those predicted by the equilibrium tide and that the periods of the existing constituents are the same as those of the equilibrium constituents. However, every terrestrial component lags behind its corresponding equilibrium constituent, and in addition, its amplitude is different. As a result, the tides as they exist can be compared with the equilibrium tide which is considered the standard.

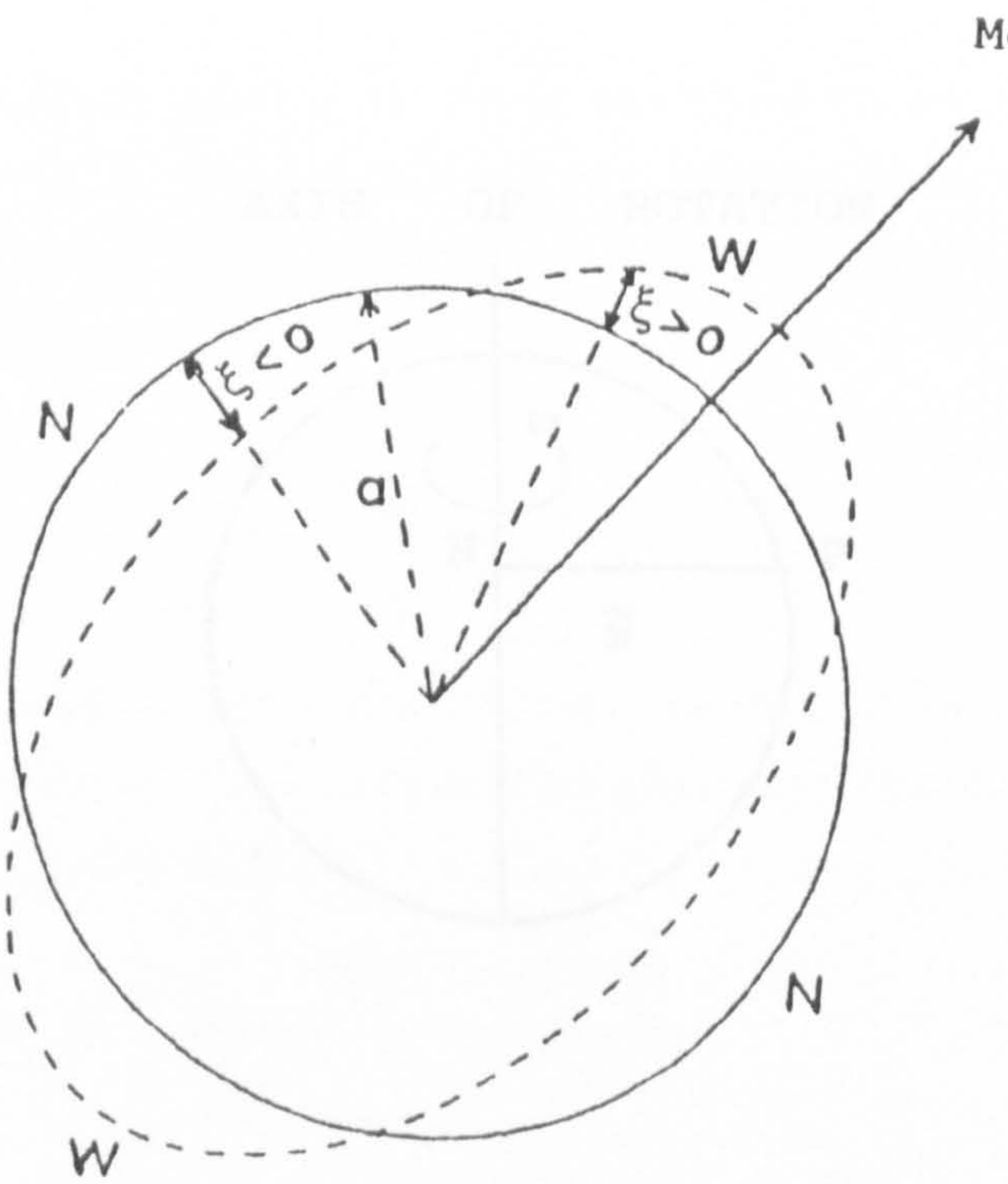

Figure 2.7

When there is no tidal force, the free water surface is perpendicular to the gravitational force. This surface is denoted by N in Figure 2.7. The value of potential of the gravitational force is constant at any point N, and W the surface perpendicular to the resultant of the gravitational and the tidal forces.

In the equilibrium theory of the tides, it is assumed that the free surface of the ocean takes the equilibrium form which might be maintained if the disturbing body were to remain in a fixed position relative to the rotating earth. The theory will then be as follows in the case of an incompressible liquid. The equations of motion will contain terms arising from the pressure gradient, from the earth's gravitational field (potential function Ψ), from the external disturbing potential Ω and from the acceleration due to steady rotation of the ocean about the earth's axis with angular velocity ω . If we write $PN = \tilde{\omega}$, the acceleration will be $\omega^2 PN = \omega^2 \tilde{\omega}$ directed from P to N and, hence, if $\hat{\tilde{\omega}}$ is a unit vector along the normal to the axis of rotation,

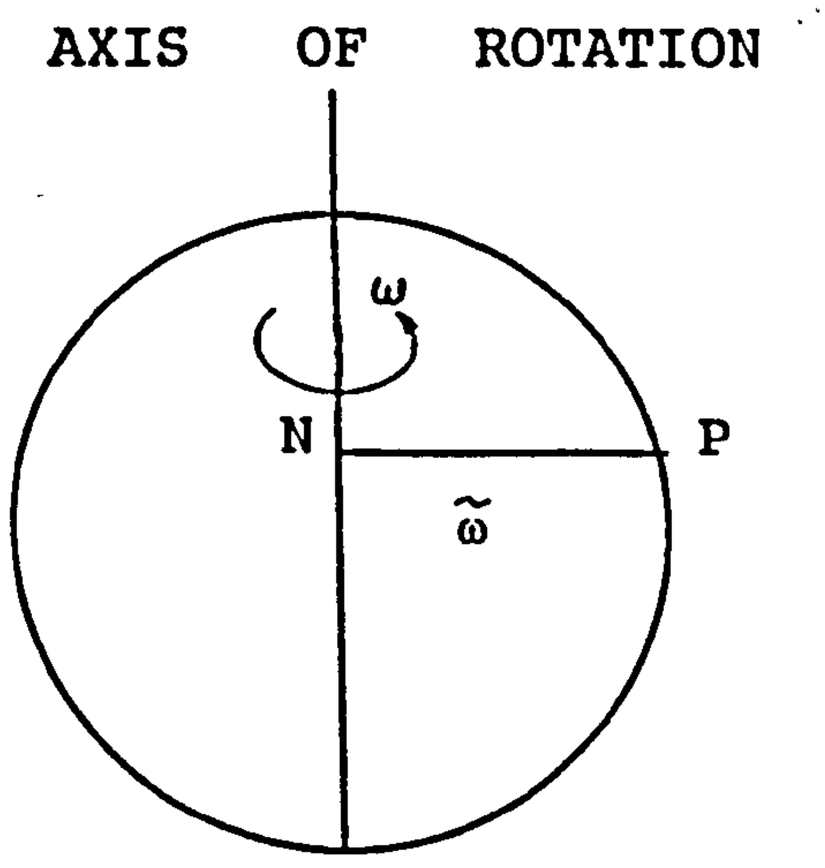

Figure 2.8

we have the following vectorial form for the equation of motion:

$$-\omega^2\,\tilde{\omega}\,\hat{\tilde{\omega}} \;=\; -\frac{1}{\rho}\,\mathrm{grad}\,P \;-\; \mathrm{grad}\,\Psi \;-\; \mathrm{grad}\,\Omega \qquad (2.17)$$

$$= \;-\;\mathrm{grad}\left(\;\frac{P}{r} \;+\; \psi \;+\; \Omega\;\right),$$

P being the pressure and ρ the density.

Bearing in mind that

$$\omega^2\,\tilde{\omega}\,\hat{\tilde{\omega}} \;=\; \mathrm{grad}\left(\;\frac{1}{2}\,\omega^2\,\tilde{\omega}^2\;\right),$$

we then have the integral of (2.17) in the form

$$\frac{P}{r} + \Psi + \Omega - \frac{1}{2}\omega^2\,\tilde{\omega}^2 \;=\; \text{constant} \qquad (2.18)$$

The free surface of the ocean is assumed to be a constant pressure surface. Such surfaces are known sometimes in oceanography as level surfaces. The equation of the free surface of the ocean is therefore

$$\Psi + \Omega - \frac{1}{2}\,\omega^2\,\tilde{\omega}^2 \;=\; \text{constant} \qquad (2.19)$$

In order to assess the influence of Ω in (2.19), we can proceed as follows. When Ω is neglected entirely, the free surface of the ocean will be the surface

$$\Psi \;-\; \frac{1}{2}\,\omega^2\,\tilde{\omega}^2 \;=\; \text{constant} \qquad (2.20)$$

We have $\Psi = -\gamma M_E \;/\; R$, where R represents the distance of P from the centre of the earth. Thus the constant pressure surfaces in the absence of the disturbing potential Ω will be given by

$$\frac{\gamma M_E}{R} + \frac{1}{2}\omega^2 \tilde{\omega}^2 = \text{constant} \qquad (2.21)$$

If a is the radius of the earth and we take "$g = \gamma M_E / a^2$" (this ,in fact, is erroneous since g as a rule includes the effect of the rotation of the earth) the magnitude of the 'equatorial bulge' in a constant pressure surface can now be calculated and is given approximately by $\omega^2 a^2 / 2g$. With $g = 9.8$ m/sec^2, $a = 6400$ kms, $\omega = 7.29 \times 10^{-3}$ and the equatorial bulge is approximately 13 kms.

This gives a mean slope of the constant-pressure surfaces of around $14/\pi a = 7/6000 \approx 1/900$ to the horizontal. It should also be noted that the earth itself is a spheroid with polar radius 3950 miles (6357 kms) and equatorial radius 3963.5 miles (6378 kms) so that the earth's equatorial bulge is 13 miles (21 km). This gives some idea of the shape of the constant pressure surface in the absence of the disturbing potential Ω.

In order to estimate the effect of the disturbing potential, let us now suppose that the displacement of a level surface (2.21) arising from the disturbing potential Ω is ξ along the normal at a point P, see Figure 2.9

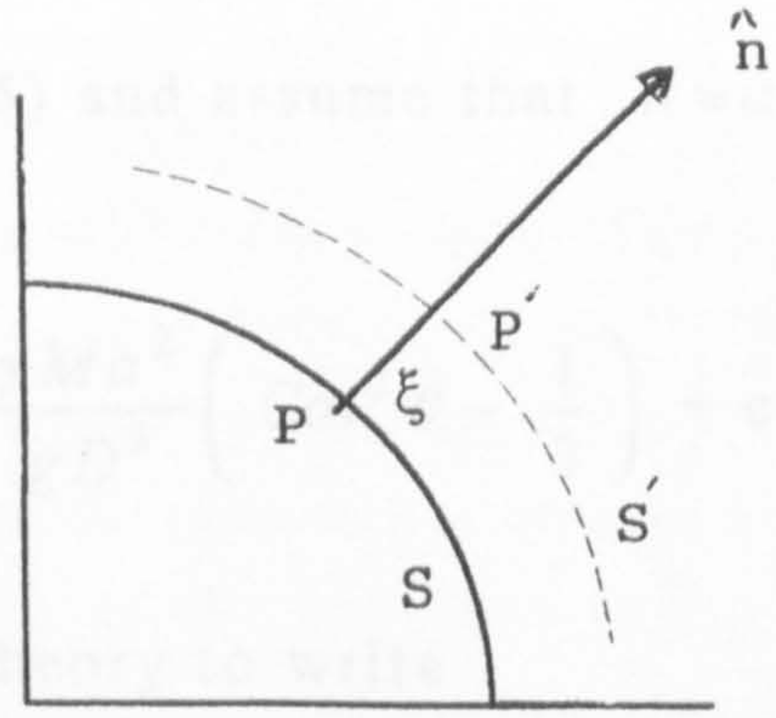

Figure 2.9

We have $PP' = \bar{\xi}$ and, to a first approximation,

$$\left(\Psi - \frac{1}{2}\omega^2 \tilde{\omega}^2 \right)_{S'} =$$

$$\left(\Psi - \frac{1}{2}\omega^2 \tilde{\omega}^2 \right)_s + \bar{\xi} \frac{\partial}{\partial n} \left(\Psi - \frac{1}{2}\omega^2 \tilde{\omega}^2 \right) \Big|_s$$

The usually accepted definition of " g " is

$$g = \frac{\partial}{\partial n} \left(\Psi - \frac{1}{2}\omega^2 \tilde{\omega}^2 \right) \Big|_s \qquad (2.22)$$

hence the departure of the level surface due to the disturbing potential is given by

$$g\bar{\xi} + \Omega = \text{constant}$$

and according to the equilibrium theory, the surfaces of constant pressure will depart from the surfaces (2.21) by the amount

$$\bar{\xi} = -\frac{\Omega}{g} + \text{constant} \qquad (2.23)$$

If we now use (2.15) and assume that $R \approx a$, we obtain the formula

$$\bar{\xi} = \frac{3}{2} \frac{\gamma M a^2}{g D^3} \left(Cos^2 \theta - \frac{1}{3} \right) + \text{constant} \qquad (2.24)$$

It is usual in tidal theory to write

$$H = \frac{3}{2} \frac{\gamma M a^2}{g D^3} \approx \frac{3}{2} \frac{M}{M_E} \left(\frac{a}{D} \right)^3 a \qquad (2.25)$$

using the approximation $g = \gamma M_E / a^2$, and, in terms of H,

we have

$$\bar{\xi} = H\left(Cos^2\Theta - \frac{1}{3} \right) + C , \qquad (2.26)$$

where C is constant. The principal value of the equilibrium tidal theory lies in the remarkable simplicity of the formula (2.26). The surface (2.26) is called the equilibrium tidal spheroid and some of the principal features may be noted ; the maximum elevation of the tidal spheriod will occur at $\Theta = 0$, $\Theta = \pi$, that is, at the zenith and nadir positions and the minimum at $\Theta = \pi/2$

$$\bar{\xi}_{max} = \frac{2}{3} H \quad , \quad \bar{\xi}_{min} = -\frac{1}{3} H. \qquad (2.27)$$

Accordingly, the total variation in the height of the equilibrium tidal spheroid is H . It is a fairly easy matter to calculate H for the moon and the sun and we have the following results

$$\text{Lunar } H = 55 \text{ cms}, \quad \text{Solar } H = 24 \text{ cms} \qquad (2.28)$$

It will be observed that the enormously more massive sun makes a smaller contribution to tide height than does the moon because of its distance from the earth. It still remains, of course, to see whether (2.28) can be accepted when we depart from the assumptions of the equilibrium theory. The final point which can be made in concluding this section is that the equilibrium theory would be valid for the oceans for a moving sun or moon if the ocean responded immediately to the presence of the disturbing masses. The departure of the shape of the oceans from the above equilibrium theory is due indeed to the inertia of the ocean mass. This effect of inertia can be investigated in the dynamic theory of tides. When there is the instantaneous response of the ocean to the disturbing masses, it is useful to analyze the structure of the equilibrium tidal spheroid from the known " motion " of the sun and the moon-daily, seasonally and annually. This response is discussed in section 2.6. Below, we indicate the broad result of the shape of a constant pressure surface according to the

equilibrium theory.

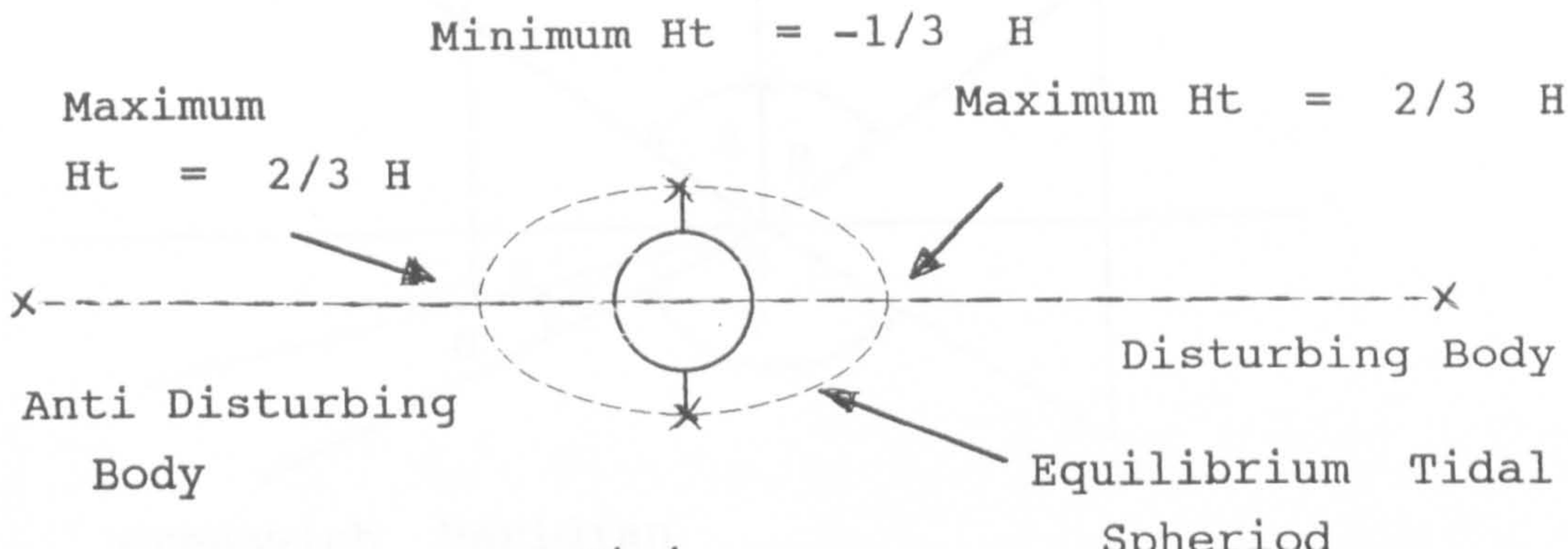

Figure 2.10

One further point should be made in that the movement of the earth about the sun and that of the moon about the earth are slightly elliptic orbits and this effect is obscured by the approximation $R \approx a$ made in (2.24).

2.6 THE THREE KINDS OF TIDES ACCORDING TO THE EQUILIBRIUM THEORY, DUE TO THE ROTATION OF THE EARTH AND ORBITAL MOTION OF THE DISTURBING BODIES.

Owing to the diurnal rotation of the earth and the orbital motion of the disturbing body, the position of the tidal spheroid relative to the earth is continually changing so that the level of the water at any particular place will continually rise and fall. It is convenient to analyse this by introducing spherical polar coordinates with the N-polar axis as axis of reference. Let θ be the co-latitude of P and ϕ the longitude measured from Greenwich (ϕ positive to east).

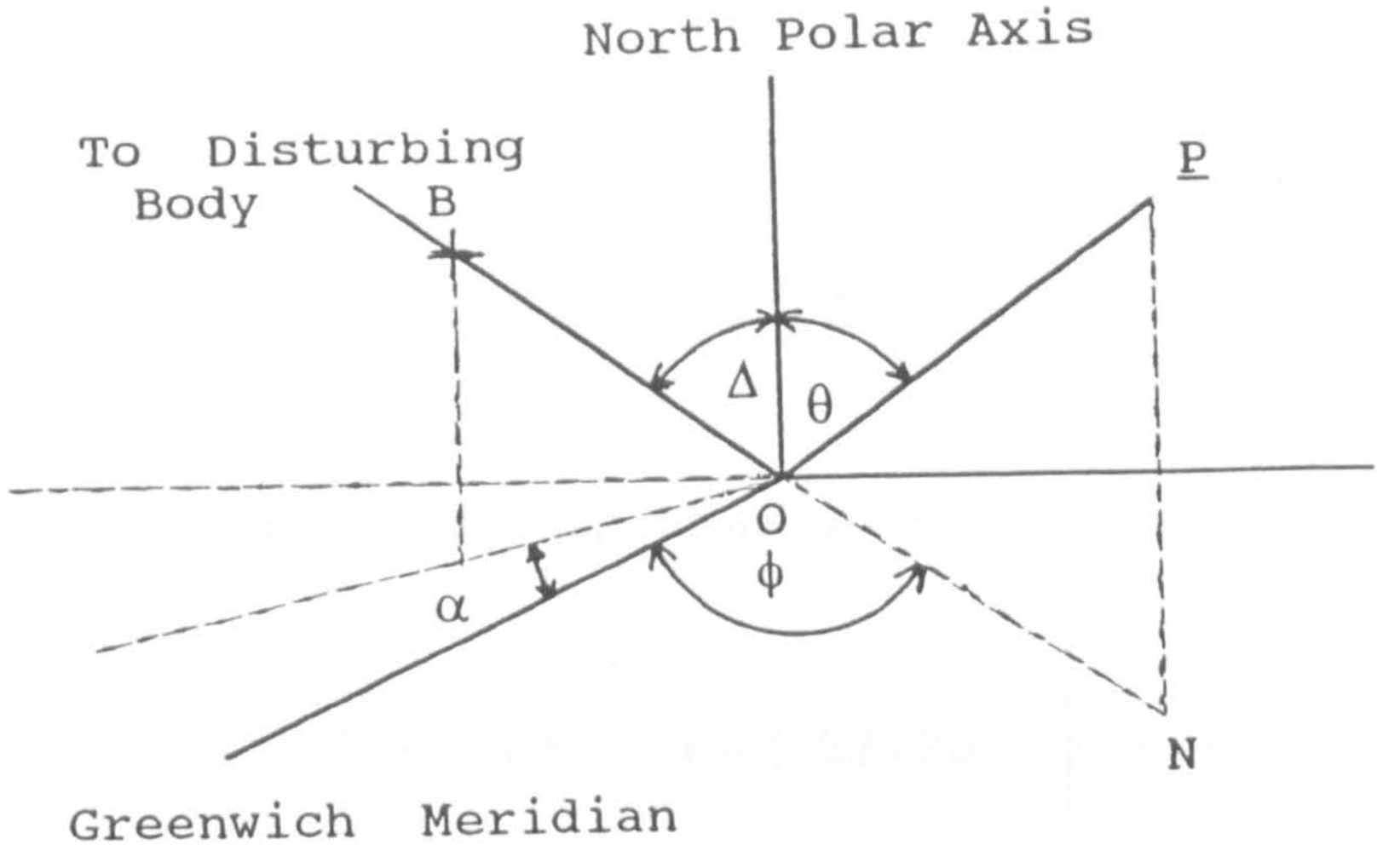

Figure 2.11

Let Δ be the co-latitude and $-\alpha$ the longitude of the disturbing body. Thus α is an angle to the west of Greenwich and we shall refer to it as the hour angle. The angle Θ which we have used in the previous section will be the angle BOP in Figure 2.11. The direction cosines of these two lines are as follows:

$$OP \equiv (\; Sin\,\theta\, Cos\,\phi, \;\; Sin\,\theta\, Sin\,\phi, \;\; Cos\,\theta \;)$$

$$OB \equiv (\; Sin\,\Delta\, Cos\alpha, \;\; -\, Sin\,\Delta\, Sin\,\alpha, \;\; Cos\,\Delta \;)$$

hence,

$$Cos\,\Theta = Cos\,\theta\, Cos\,\Delta + Sin\,\theta\, Sin\,\Delta\, Cos(\; \phi + \alpha \;) \qquad (2.29)$$

It now follows from (2.26) that

$$\overline{\xi} = H \left\{ Cos^2\,\theta\, Cos^2\,\Delta + 2\, Sin\,\theta\, Cos\,\theta\, Sin\,\Delta\, Cos\,\Delta\, Cos(\; \phi + \alpha \;) + \right.$$

$$\left. + \; Sin^2\,\theta\, Sin^2\,\Delta\, Cos^2(\; \phi + \alpha \;) - \frac{1}{3} \right\} + C$$

that is,

$$\bar{\xi} = H\left\{\left(Cos^2\theta\, Cos^2\Delta + \frac{1}{2} Sin^2\theta\, Sin^2\Delta - \frac{1}{3} \right) + \right.$$

$$+ \frac{1}{2} Sin2\theta\, Sin2\Delta\, Cos(\phi+\alpha) +$$

$$\left. + \frac{1}{2} Sin^2\theta\, Sin^2\Delta\, Cos(2\phi+2\alpha) \right\} + C$$

$$= H\left\{ \frac{3}{2}\left(Cos^2\theta - \frac{1}{3} \right)\left(Cos^2\Delta - \frac{1}{3} \right) + \right.$$

$$+ \frac{1}{2} Sin2\theta\, Sin2\Delta\, Cos(\phi+\alpha) +$$

$$\left. + \frac{1}{2} Sin^2\Phi\, Sin^2\Delta\, Cos(2\phi+2\alpha) \right\} + C$$

Accordingly, the form of the equilibrium tidal spheroid in terms of (θ, ϕ) will be

$$\bar{\xi} = \frac{3}{2} H\left(Cos^2\theta - \frac{1}{3} \right)\left(Cos^2\Delta - \frac{1}{3} \right)$$

(Tide of first species)

$$+ \frac{1}{2} H\, Sin2\theta\, Sin2\Delta\, Cos(\phi+\alpha)$$

(Tide of second species)

$$+ \frac{1}{2} H\, Sin^2\theta\, Sin^2\Delta\, Cos(2\phi+2\alpha)$$

(Tide of third species)

$$+ C$$

(2.30)

The first, second and third species tides are defined in (2.30), each of them represents a partial tide and the results are superposed. In what follows, we shall use the phrases "solar day " to mean 24 hours and " lunar day " to mean 24 h. 50.47 mins.

2.6.1 FIRST SPECIES TIDE

This tide is represented, from (2.30) , by

$$\frac{3}{2}H\left(\ Cos^2\theta - \frac{1}{3}\ \right)\left(\ Cos^2\Delta - \frac{1}{3}\ \right)$$

$$\equiv \frac{2}{3}H P_2(\ Cos\theta\ )\,P_2(\ Cos\Delta\ ) \qquad (2.31)$$

This tidal species, being independent of the longitude angle ϕ, gives a tide which is constant in height around a circle of latitude; furthermore, it is symmetrical about the equator. There are nodal lines at

$$Cos^2\theta_0 = \frac{1}{3} \quad \text{where} \quad \theta_0 = 90^\circ \pm 35^\circ 16'.$$

The amount of the tidal elevation in any latitude other than $\pm\theta_0$ will depend upon the function $P_2(Cos\Delta)$. In the case of the moon, we can get some idea of the time variations in Δ by noting that the plane orbit of the moon is inclined to the plane of the earth's orbit about the sun (the plane of the ecliptic) by $5^\circ 8'$ and that the time of a complete revolution of the moon about the earth back to its starting direction is 27 days, 7 hours, 40 minutes. The summer season description is shown in Figure 2.12.

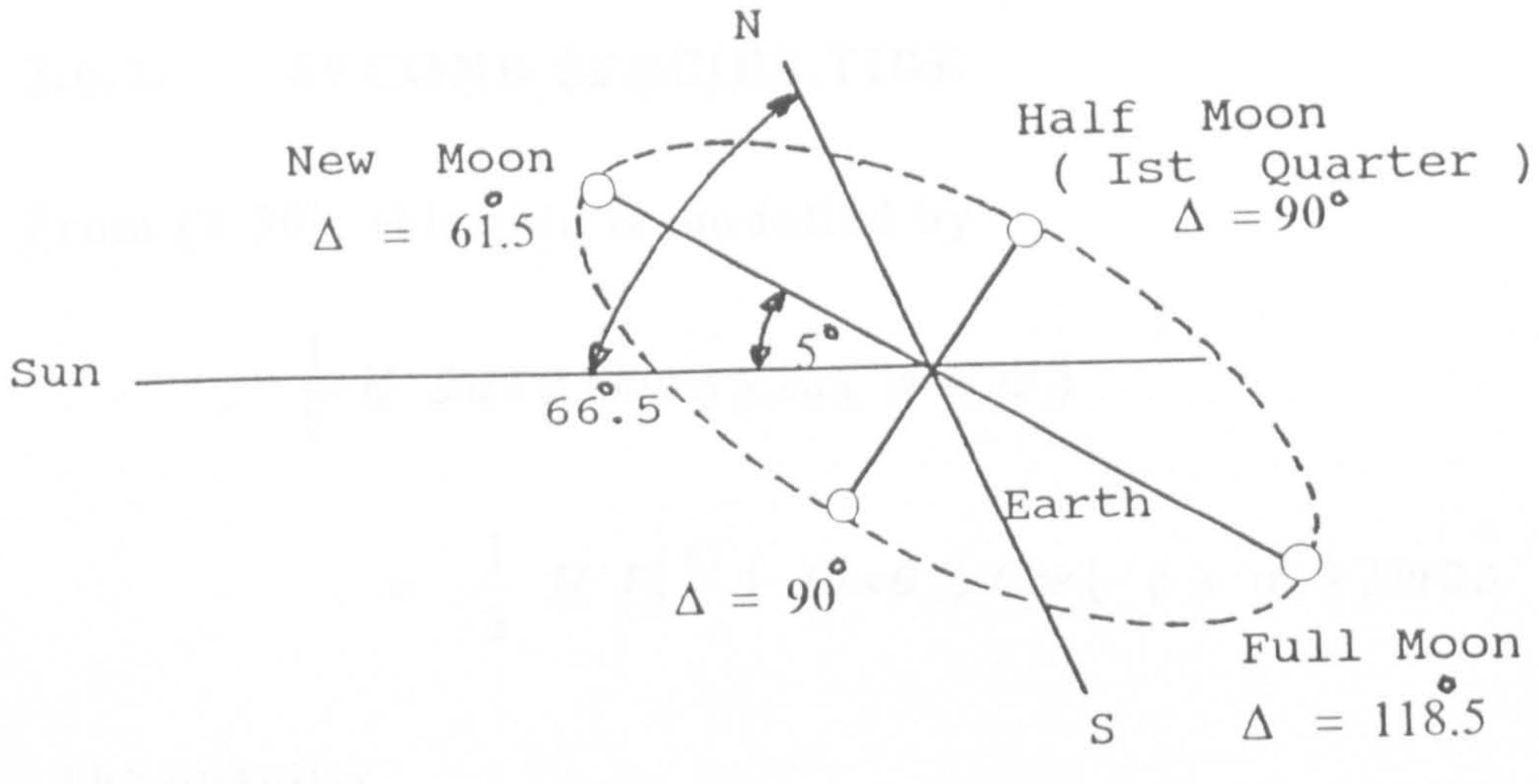

Figure 2.12

It will be clear from the figure that in performing the complete orbit in the summer season, the angle Δ will increase from 61.5° at new moon to 118.5° at full moon in approximately 14 days and then return to 61.5° in the second 14 days of the cycle. From (2.31), it is clear that the fluctuation of the Δ term will depend upon a term $1/2 Cos 2\Delta$; hence the period associated with the fluctuation will be 14 days (approximately). These are the lunar fortnightly tides. In the case of the sun as a disturbing body, because of the inclination of the axis of rotation of the earth at an angle of 66.5° to the plane of the ecliptic, there is, of course, a variation of Δ in the range $66.5^\circ \le \Delta_{sun} \le 113.5^\circ$ in six months and the associated tide is the "solar semi-annual tide". It may be observed finally that the mean value of $\left(Cos^2 \Delta - 1/3 \right)$ with respect to time is 1/6 and, being non-zero, it follows that this type of tide implies a permanent change in level of the ocean.

2.6.2. SECOND SPECIES TIDE

From (2.30), this tide is modelled by

$$\frac{1}{2} H \; Sin2\theta \; Sin2\Delta \; Cos(\; \phi + \alpha \;)$$

$$\equiv \frac{1}{3} H \; P_2^{(1)} (\; Cos\theta \;) \; Cos(\; \phi + \alpha \;) \; Sin2\Delta \qquad (2.32)$$

The quantity

$$P_m^{(s)} (\; Cos\theta \;) \; Coss\phi \qquad (s \; < \; m)$$

is known as the tesseral harmonic and the present case corresponds to $s = 1$, $m = 2$. The nodal lines on the sphere are the meridian, which is 90° from that of the disturbing body and the equator. The disturbance of level is greatest in the meridian of the disturbing body at distances 45° N and S of the equator. The oscillation at any one place goes through a period with the hour angle Δ, that is, in a lunar day or solar day; in addition, however, there is a variation in amplitude with Δ giving a 14 day lunar effect and a 6 monthly solar effect. This term, therefore, gives the "diurnal" tides but with variable amplitude as shown below in Figure 2.13 in the case of the lunar tides. The beat effects may be noted and are called spring tides.

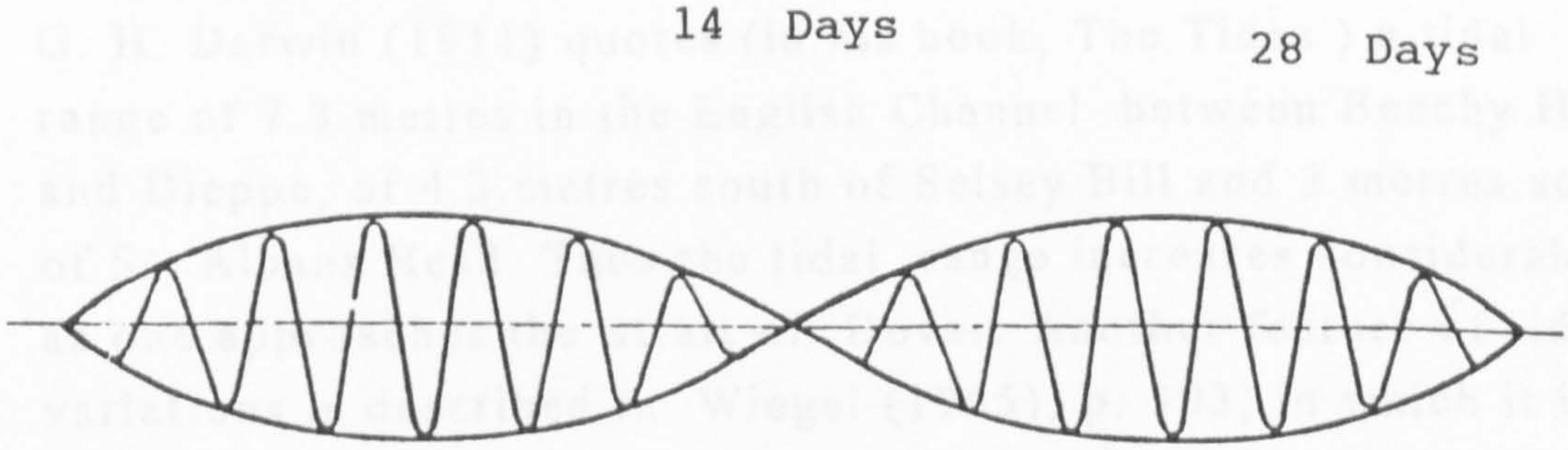

Figure 2.13

2.6.3. THIRD SPECIES TIDE

This tide is modelled by

$$\frac{1}{2} H \, Sin^2 \Delta \, Sin^2 \theta \, Cos(\; 2\alpha \; + \; 2\phi \;)$$

$$\equiv \frac{1}{6} H \, Sin^2 \Delta \; P_2^2 (Cos \theta) \, Cos (2\alpha + 2\phi)$$

The quantity

$$P_m^{(s)} (\; Cos\theta \;) \; Coss\phi \qquad (s \; = \; m)$$

is known as a sectional harmonic and this term with $s = 2$, $m = 2$ will give a tidal spheroid with the following nodal lines; meridians which are distant $45^\circ E$ and W from that of the disturbing body, together with nodal points at the N and S poles. The oscillation at any one point goes through its period with 2α in a half (lunar or solar) day; there is a slower variation in amplitude of the tide with the term $Sin^2\Delta$ so then there is a 14 day (lunar) or 6 monthly longer term variation. Here, therefore, we have the origin of the lunar and solar " semi-diurnal tides" and the associated spring tides 14 day period and equinoctial spring tides (6 monthly solar) as stated earlier. When the three partial tides are combined , the maximum range in the open ocean will be 55 cms (lunar) and 24 cms (solar) so that the greatest tidal range on the equilibrium theory is 80 cms. This value, of course , is considerably exceeded in certain locations. Thus, G. H. Darwin (1911) quotes (in his book, The Tides) a tidal range of 7.3 metres in the English Channel between Beachy Head and Dieppe, of 4.3 metres south of Selsey Bill and 2 metres south of St. Albans Head. Thus the tidal range increases considerably as one approaches the Strait of Dover. Another feature of tide variations is described in Wiegel (1965), p. 303, in which it is made clear that stations on the Atlantic coast of the United States all indicate a gradual increase in the height of mean sea level. This has been true since 1900 and may be associated

with the melting of polar ice, although Wiegel does not suggest this.

Some of the more important constituents with their size relative to the largest, the M_2 or principal lunar constituent, taken as 100 are given in Table 2.1. There are up to sixty-five constituents which are recognized as significant in some circumstances, e.g. in describing tides in river estuaries.

2.7 THE ACCELERATION RELATIVE TO AXES WHICH ARE IN STEADY ROTATION

2.7.1 CORIOLIS ACCELERATION

In order to understand the movements of the oceans, it is necessary to explain the idea of Coriolis acceleration and to make this clear, we proceed from first principles.

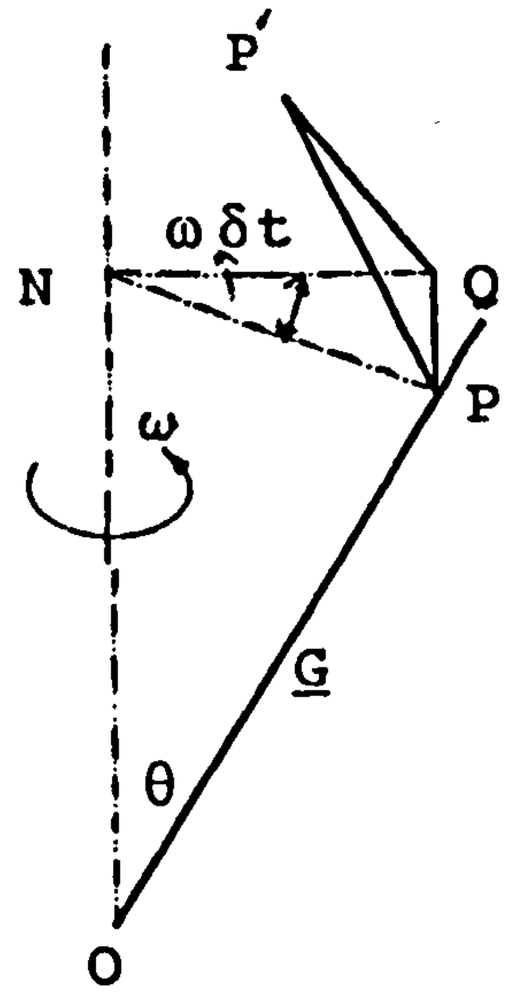

Figure 2.14

Suppose that we have two sets of axes with the same fixed origin O, one set of axes being fixed Newtonian frame and the other a frame which is in rotation relative to the other with angular velocity ω .

Table 2.1 Characteristics of the principal tide-generating force constituents.

Species and name	Symbol	Period (solar hour)	Relative size
Semi-diurnal:			
Principal lunar	M_2	12.42	100
Principal solar	S_2	12.00	47
Larger lunar elliptic	N_2	12.66	19
Luni-solar semi-diurnal	K_2	11.97	13
Diurnal:			
Luni-solar diurnal	K_1	23.93	58
Principal lunar diurnal	O_1	25.82	42
Principal solar diurnal	P_1	24.07	19
Larger lunar elliptic	Q_1	26.87	8
Long period:			
Lunar fortnightly	M_f	327.9	17
Lunar monthly	M_m	661.3	9
Solar semi- annual	S_{sa}	4383	8

Suppose that we have a vector **G** relative to the fixed system of axes. We require to know a relation connecting the time rate of change of **G** relative to the fixed and moving frames. We shall denote the amount of change in **G** in time δt relative to the fixed axes $(d\mathbf{G})_{fixed}$ and relative to the $(d\mathbf{G})_{moving}$.

It is clear from Figure 2.14 that we have the relation:

$$(d\,\mathbf{G})_{fixed} = (d\,\mathbf{G})_{moving} + \vec{\mathbf{PQ}} \qquad (2.33)$$

and since

$$\vec{\mathbf{PQ}} = PN.\omega\,\delta t = |\,\mathbf{G}\,|\,Sin\,\theta\;\omega\;\delta t$$

we have

$$\vec{\mathbf{PQ}} = (\omega \times \mathbf{G})\,\delta t$$

and hence

$$\left(\frac{d\mathbf{G}}{dt}\right)_{fixed} = \left(\frac{d\mathbf{G}}{dt}\right)_{moving} + (\omega \times \mathbf{G}), \qquad (2.34)$$

G being a vector relative to the fixed system of axes.

Case 1. **G** = **r**, **r** being the position vector

$$\left(\frac{d\mathbf{r}}{dt}\right)_{fixed} = \left(\frac{d\mathbf{r}}{dt}\right)_{moving} + (\omega \times \mathbf{r}). \qquad (2.35)$$

Hence

$$\mathbf{v}_{fixed} = \mathbf{v}_{moving} + (\omega \times \mathbf{r}) \qquad (2.36)$$

Case 2. $\mathbf{G} = \mathbf{v}_{fixed} = \mathbf{v}_f$, $\mathbf{v}_f$ being the velocity vector.

Here we have

$$\left(\frac{d\mathbf{v}_f}{dt}\right)_{fixed} = \left(\frac{d\mathbf{v}_f}{dt}\right)_{moving} + \left(\omega \times \mathbf{v}_f\right)$$

The left hand side is the absolute acceleration $\mathbf{a}_f$ and we have, therefore,

$$\mathbf{a}_f = \left(\frac{d\mathbf{v}_f}{dt}\right)_m + \left(\omega \times \mathbf{v}_f\right)$$

and, using (2.36), we obtain in the moving frame, by differentiating (2.36)

$$\left(\frac{d\mathbf{v}_f}{dt}\right)_m = \left(\frac{d\mathbf{v}_f}{dt}\right)_m + \omega \times \left(\frac{d\mathbf{r}}{dt}\right)_m$$

and ω is fixed relative to the moving axes. Hence we obtain

$$\mathbf{a}_f = \left(\frac{d\mathbf{v}_m}{dt}\right)_m + \left(\omega \times \mathbf{v}_f\right)$$

$$= \mathbf{a}_m + \omega \times \mathbf{v}_m + \omega \times \left\{\mathbf{v}_m + \mathbf{w} + \mathbf{r}\right\}$$

and hence

$$\mathbf{a}_f = \mathbf{a}_m + 2\omega \times \mathbf{v}_m + \omega \times (\omega \times \mathbf{r}). \qquad (2.37)$$

In the case of the earth, ω is the angular velocity of the earth about the polar axis and $\omega \times (\omega \times \mathbf{r})$ is a vector of magnitude $\tilde{\omega}\,\omega^2$ along PL. We incorporate this term in our definition of g, the gravitational acceleration, and the remaining terms in (2.37), namely

$$\mathbf{a}_f = \mathbf{a}_m + 2\omega \times \mathbf{v}_m \qquad (2.38)$$

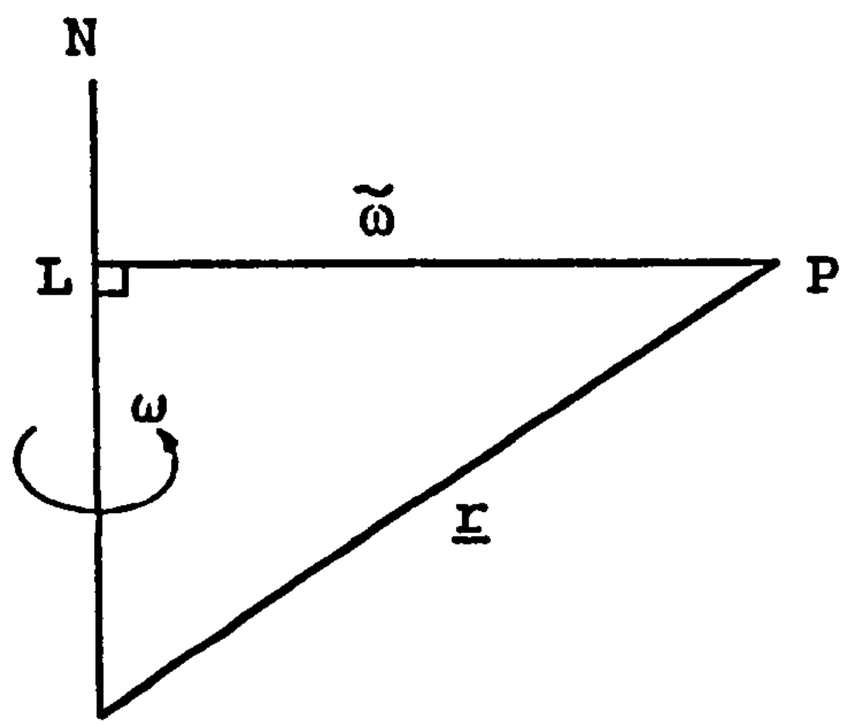

Figure 2.15

constitute the acceleration formula required. The term $2\omega \times \mathbf{v}_m$ is called the Coriolis acceleration. Whenever we use axes which are in rotation relative to some other fixed set of axes, it is always necessary to take into account the Coriolis acceleration; in particular, in the case of the movements of the ocean and atmosphere on a substantial scale, the Coriolis acceleration plays a dominant role. We can illustrate the importance of this concept in a simple example as follows.

Example 1.

The distribution of pressure in a uniform stream of incompressible liquid moving steadily from W to E with speed U in latitude $\lambda\,(\lambda \rangle 0)$. Now we shall take axes rotating steadily with the earth at angular velocity ω and, since the flow is steady and uniform relative to this set of axes, we have

$$\mathbf{a}_m = 0$$

in (2.37). Hence, omitting the term $\omega \times (\omega \times \mathbf{r})$ for the reason stated earlier, we have

$$\mathbf{a}_f \;=\; 2(\,\omega \times \mathbf{v}_m\,)$$

We can now set up the fluid motion equations using the following standard right-handed axes system:

Ox drawn to the East,

Oy drawn to the North

Oz drawn vertically upwards.

We then have

$$\mathbf{v}_m \;=\; u\mathbf{i}$$

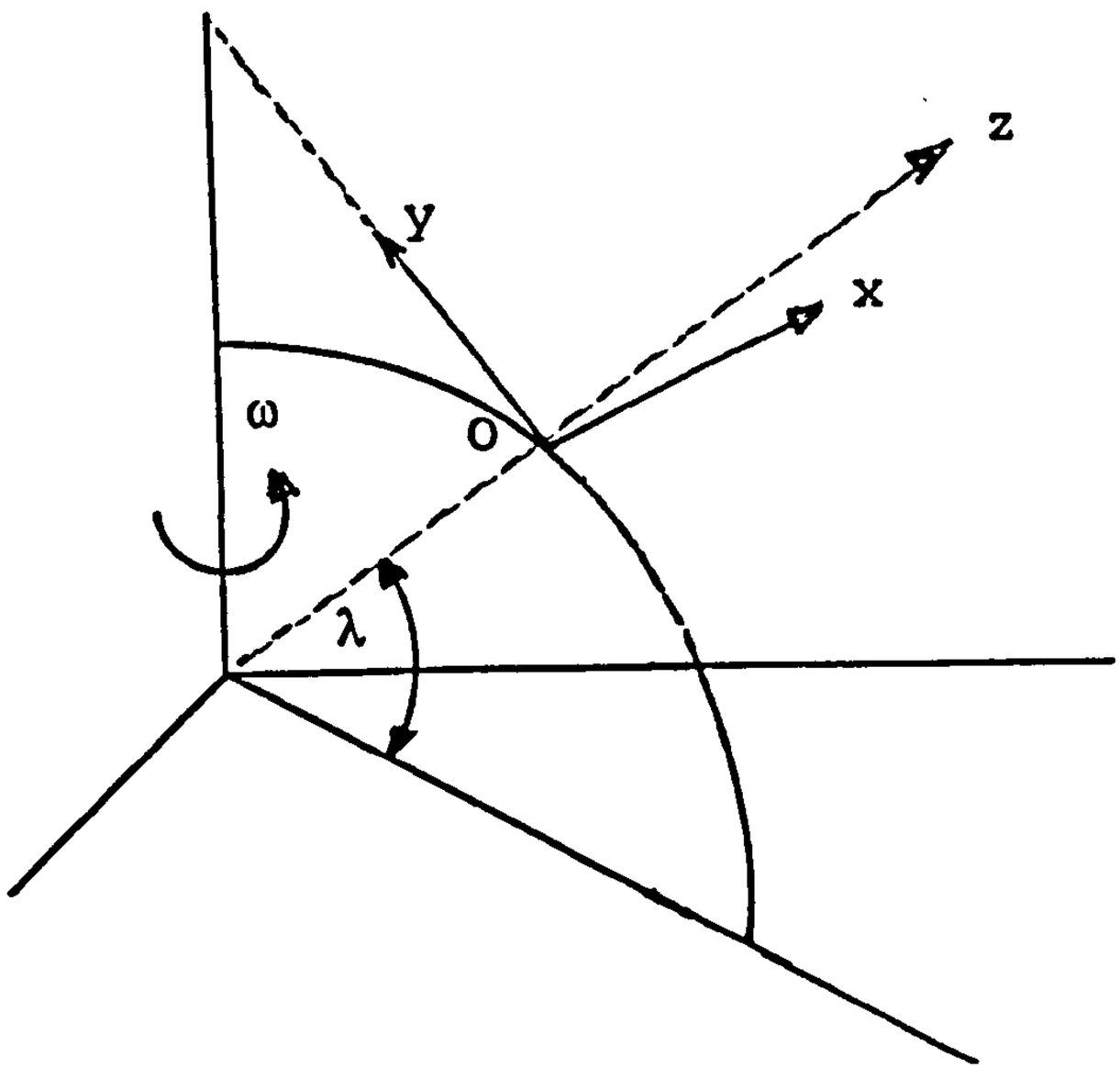

Figure 2.16

and the components of ω relative to this frame will be

$$\omega \;=\; O\mathbf{i} + \omega\, Cos\lambda\, \mathbf{j} + \omega\, Sin\lambda\, \mathbf{k}.$$

The fluid motion equations, including the gravity term $-g\,\mathbf{k}$ will then be

$$2\,(\,\omega \times \mathbf{v}_m\,) \;=\; -\,\frac{1}{\rho}\,grad\,P \;-\; g\mathbf{k}.$$

We have

$$2(\ \omega \times \mathbf{v}_m\ ) \;=\; \begin{vmatrix} \mathbf{i} & \mathbf{j} & \mathbf{k} \\ 0 & \omega Cos\lambda & \omega Sin\lambda \\ U & 0 & 0 \end{vmatrix}$$

$$= \; 2\omega U\ Sin\lambda \mathbf{j} - 2\omega U\ Cos\lambda \mathbf{k}$$

and thus

$$2\omega U\ Sin\lambda \mathbf{j} - 2\omega U\ Cos\lambda \mathbf{k}$$

$$= \; -\frac{1}{\rho}\left\{\ P_x \mathbf{i} \;+\; P_y \mathbf{j} \;+\; P_z \mathbf{k}\ \right\} \;-\; g\mathbf{k}\ .$$

It follows that

$$\frac{\partial P}{\partial x} \;=\; 0,$$

$$\frac{\partial P}{\partial y} \;=\; -2\omega\rho U\ Sin\lambda\ ,$$

$$\frac{\partial P}{\partial z} \;=\; -g\rho + 2\omega\rho U\ Cos\lambda\ ,$$

and the pressure formula is

$$\frac{P}{\rho} \;=\; \text{constant} \;-\; z(\ g - 2\omega U\ Cos\lambda\ ) \;-\; 2\ \omega U\, y\ Sin\lambda.$$

The first striking feature about the above solution is that the pressure gradient in the x-direction is zero even though the flow is taking place in this direction. Engineers accustomed to balancing a pressure gradient along a pipe in the laboratory to the fluid flow along the axes of the pipe will see that quite new rules prevail in the above situation. The constant pressure surfaces are the planes

$$y\,(\,2\omega U\,Sin\lambda\,) + z\,(\,g - 2\,\omega U\,Cos\lambda\,) \;=\; \text{constant.}$$

If we take $\omega = 7.29\times10^{-5}$ rads/sec.,

$$U \;=\; 1.6 \text{ kms / hour} \;=\; 45 \text{ cms / sec.}$$

$$g \;=\; 9.8 \text{ metres/sec}^2$$

then

$$2\omega U \;=\; 6.52 \times 10^{-5} \text{ metres/sec}^2 .$$

In view of the smallness of $2\omega U$ compared with $g\,(\,10^{-5}$ *to* $1\,)$, we see that the slope of the constant pressure surfaces is about 0.3×10^{-5} in latitude $30°$, and the stream is higher on the south side than on the north side.

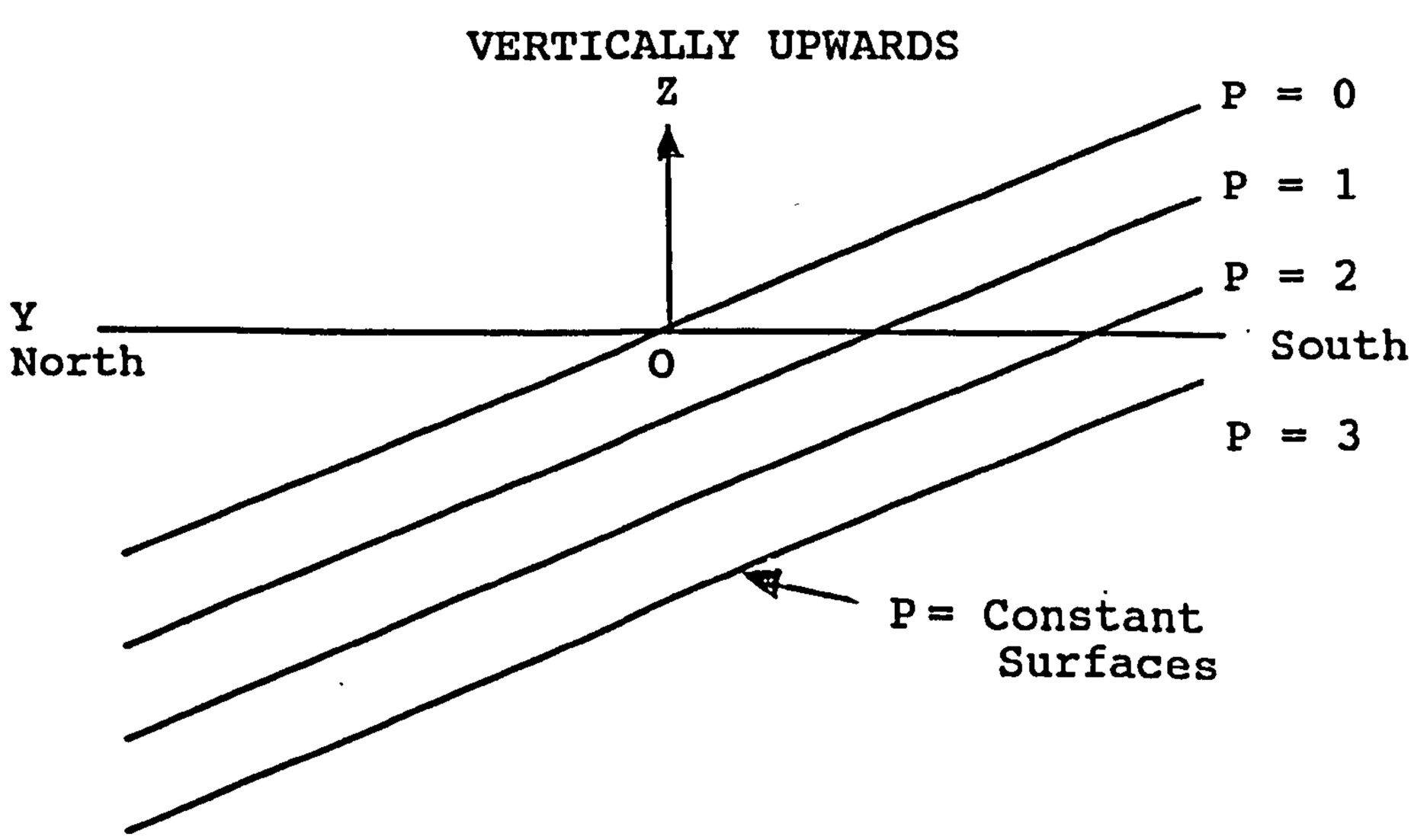

Figure 2.17

If the stream is 32 kms wide, then the difference in height between the north and south ends will be about 10 cms.

The important feature which it is necessary to emphasize is that the horizontal pressure gradient is directed to the north (omitting the hydrostatic term) when the flow is to the east. If the flow is reversed, the pressure gradient is also reversed.

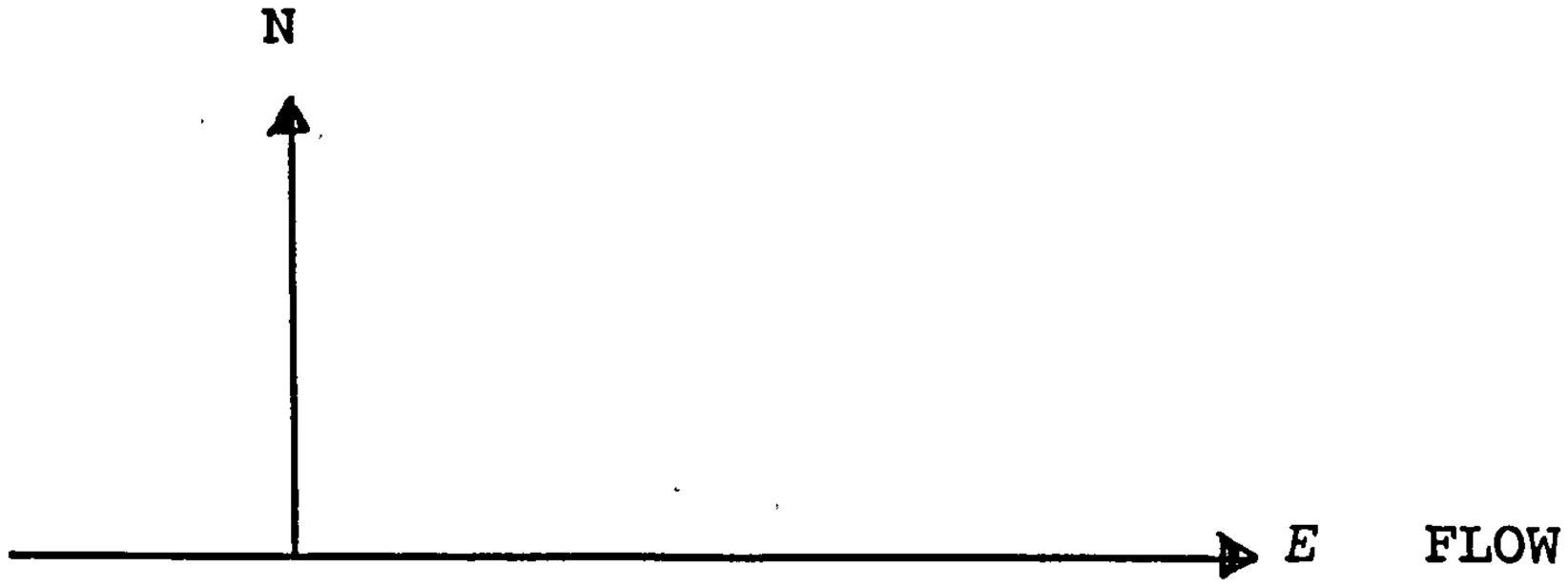

Figure 2.18

It should also be observed that in the southern hemisphere ($\lambda < 0$), the direction of the horizontal pressure gradient is opposite to that in the northern hemisphere.

We may also observe in Figure 2.18 that , if we take two points A and B at the same horizontal level -- A being to the north of B in the stream --the pressure at A will be less than that at B . Thus we can express the above flow rule as follows; the low pressure will lie on the left hand side if an observer is looking along the direction of a stream in the northern hemisphere.

It is easily established that the same general rule applies for a stream which is moving in a direction other than W to E. Flows in which the pressure gradient balances the Coriolis acceleration are called geostrophic flows.

Example 2

The equations of motion relative to axes which are rotating steadily with the angular velocity of the earth and the equation of continuity.

We now use formula (2.38) in setting up the equations of motion which would be valid for an observer located on the earth's surface and rotating steadily with the earth. Let ρ be the density at P and let $\delta\tau$ be an element of volume at P; then the mass acceleration will be

$$\rho \mathbf{a}_f \, \delta\tau$$

The external forces acting on the element will be as follows:

$-\nabla P \delta\tau$ pressure gradient

$-\rho g \hat{\mathbf{n}} \, \delta\tau$ gravitational force normal to level surfaces and including the term $\omega \times (\omega \times \mathbf{r})$

$\vec{\mathbf{D}} \, \delta\tau \;\; (= \mu \nabla^2 V \, \delta\tau)$ viscous force

$-\rho \nabla \Omega \, \delta\tau$ external force arising from planetary bodies and sun.

Combining these terms, we have the equation of motion

$$\mathbf{a}_f = -\frac{1}{\rho}\nabla P - g\hat{\mathbf{n}} + \vec{\mathbf{D}} - \nabla\Omega$$

hence

$$\mathbf{a}_m + 2\omega \times \mathbf{v}_m = -\frac{1}{\rho}\nabla P - g\hat{\mathbf{n}} + \vec{\mathbf{D}} - \nabla\Omega,$$

where $\mathbf{v}_m$ is the velocity relative to the moving frame and $\mathbf{a}_m$ the acceleration relative to the frame. The choice of the moving frame is made according to the problem investigated.
For example, if ZOX is the plane through the meridian of Greenwich and we take for convenience $\mathbf{V} = \mathbf{v}_m$, then

$$\mathbf{a}_f = \mathbf{a}_m + 2\omega \times \mathbf{v}_m = \frac{d\mathbf{V}}{dt} + 2(\omega \times \mathbf{V})$$

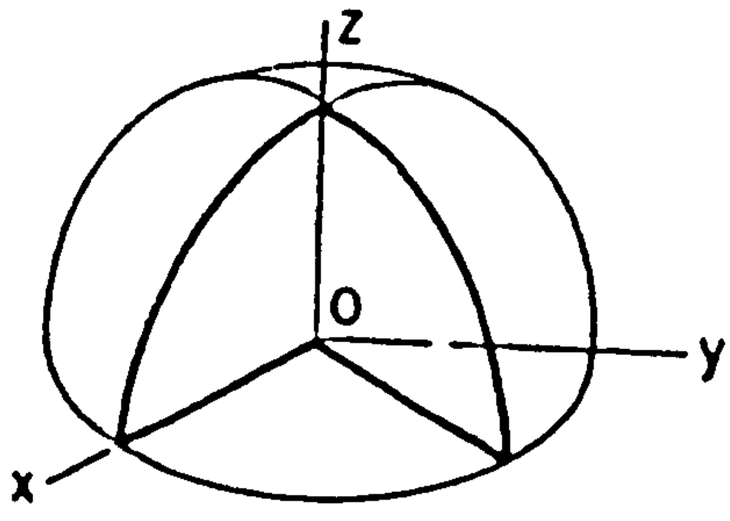

Figure 2.19

The equation of motion is then

$$\frac{d\mathbf{V}}{dt} + 2(\omega \times \mathbf{V}) = -\frac{1}{\rho}\nabla P - g\hat{\mathbf{n}} + \vec{\mathbf{D}} - \nabla\Omega \qquad (2.39)$$

and the operator $d\mathbf{V}/dt$ is interpreted, as is usual in hydrodynamics, as the operator following the motion, that is

$$\frac{d}{dt} \equiv \frac{\partial}{\partial t} + (\mathbf{V}.\nabla) . \qquad (2.40)$$

The equation of continuity in general will be

$$\frac{d\rho}{dt} + \rho \,\mathrm{div}\, \mathbf{V} = 0 . \qquad (2.41)$$

In almost all circumstances in dealing with oceanographic problems, the rate of change of density following the motion is zero, that is

$$\frac{d\rho}{dt} = 0 . \qquad (2.42)$$

This is satisfied either because ρ is constant every where or, in certain situations, because the density of an element remains

constant following the motion of an element in a heterogeneous medium. Thus the equation of continuity assumes the form

$$\text{div } \mathbf{V} = 0. \tag{2.43}$$

2.7.2 LARGE SCALE MOVEMENTS OF THE OCEAN

We assume, following Laplace, that

(a) the vertical velocity in the ocean is ignorable;

(b) the vertical acceleration is ignorable;

(c) the movement in the horizontal is so small that second degree terms in the equations are ignored compared with first degree terms.

The assumptions (a) and (b) are a consequence of the shallowness of the oceans compared with their horizontal extent. For, if H is the mean depth of oceans and L is the typical horizontal dimension, we can think of the large-scale movements in the ocean as a gradual rising of water through a height H as the particle or element of volume covers the horizontal distance L. Hence, if we take w to be the vertical velocity and V_h to be the typical horizontal velocity, then for the large scale movements we have

$$\frac{w}{V_h} \approx \frac{H}{L} \tag{2.44}$$

In a similar way, if dw/dt is the vertical acceleration and dV_h/dt the horizontal acceleration, then

$$\frac{\frac{dw}{dt}}{\frac{dV_h}{dt}} \approx \frac{H}{L} \tag{2.45}$$

Since we have H = 6.4 kms, L = 3840 kms, it follows that the ratio H/L is about 1/600. It is observed that a typical horizontal movement in the open ocean is at most 0.8 kms per hour, that is,

805 metres per hour and, using (2.44), we get an order of magnitude for w, namely about 1.22 metres per hour. This figure may be too great and (2.44) should be looked upon as a crude guide. In a similar way one can get from (2.44) an estimate of the vertical acceleration, for if dV_h/dt is calculated by saying that an element of volume has its speed increased from zero to 805 metres per hour in 6 hours (the semi-diurnal tidal oscillation), then the horizontal acceleration will be, on average, about 135 metres per (hour)^2. It then follows from (2.45) that

$$\frac{dw}{dt} \approx \frac{1}{600} \cdot 135 \text{ metres /(hour)}^2 \qquad (2.46)$$

It is now possible to deduce a result of considerable importance concerning the equation of motion in the vertical direction. If OZ is the vertical axis at P, the equation of motion in the vertical is

$$\text{(vertical acceleration)} = -\frac{1}{\rho}\frac{\partial P}{\partial z} - g - \frac{\partial \Omega}{\partial z} \qquad (2.47)$$

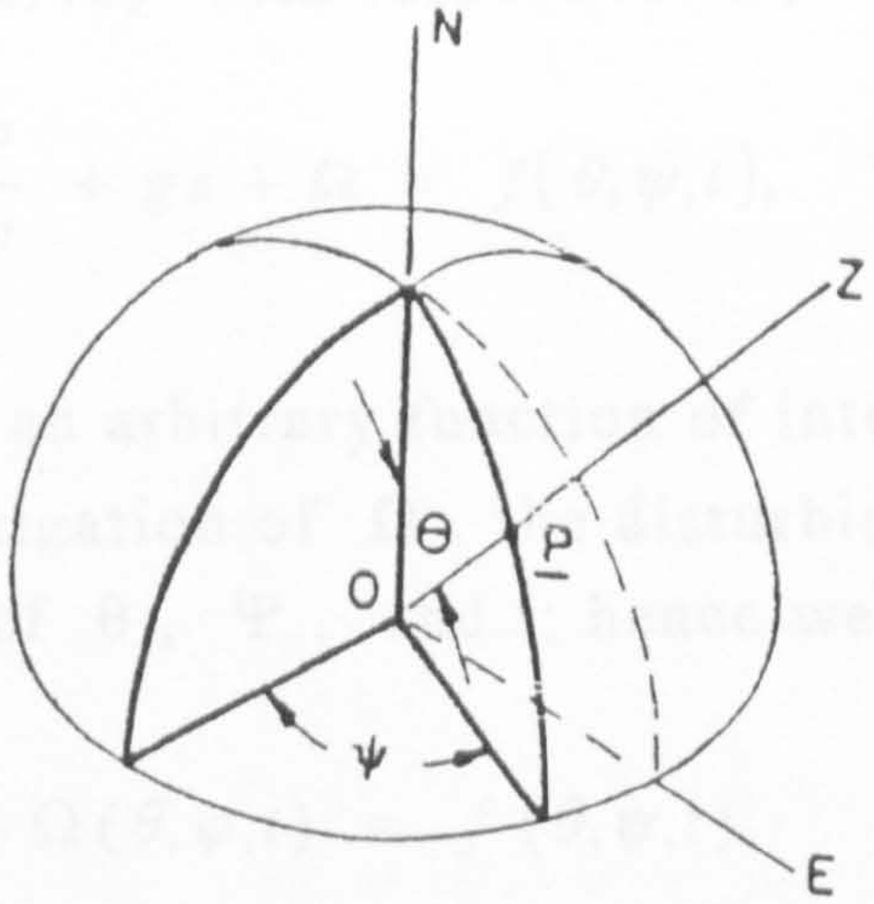

Figure 2.20

We see from (2.46) and (2.38) that the vertical acceleration terms, including both dw/dt and the appropriate component of the Coriolis acceleration, are both quite negligible compared with the gravitational acceleration g . Hence, a very good approximation to the vertical equation of motion is the hydrostatic equation

$$0 = -\frac{1}{\rho}\frac{\partial P}{\partial z} - g - \frac{\partial \Omega}{\partial z} \tag{2.48}$$

This equation can be integrated with respect to Z as follows. Let θ be the co-latitude of p and the longitude (measured positively towards the east). Then we can take the equation of ocean surface to be

$$z = \xi(\theta, \psi, t) \tag{2.49}$$

Let us now assume that the pressure is constant over the ocean surface so that

$$P = P_0 \quad \text{on} \quad z = \xi(\theta, \psi, t) \tag{2.50}$$

When we integrate (2.48) with respect to z , we obtain

$$\frac{P}{\rho} + gz + \Omega = f(\theta, \psi, t), \tag{2.51}$$

where $f(\theta, \psi, t)$ is an arbitrary function of integration. We know from our investigation of Ω , the disturbing potential, that it is only a function of θ , Ψ , and t; hence we can write

$$\frac{P}{\rho} + gz + \Omega(\theta, \psi, t) = f(\theta, \psi, t)$$

If we now apply (2.50) we have at the surface

$$\frac{P_0}{\rho} + g\xi(\theta, \psi, t) + \Omega(\theta, \psi, t) = f(\theta, \psi, t)$$

and hence, by subtraction, we obtain a useful form of hydrostatic equation which is

$$P = P_0 - \rho g \{ z - \xi(\theta, \psi, t) \} \qquad (2.52)$$

We can think of $z = 0$ as being the mean height of the oceans and the bottom of the ocean will then be $z = -h(\theta, \psi, t)$ and the pressure at the bottom will be given by

$$P_{bottom} = P_0 + \rho g(h + \xi) \qquad (2.53)$$

The pressure increases by one atmosphere

$$\approx \quad 1000 \text{ millibars} \quad \approx \quad 10^6 \quad \text{dynes / cm}^2$$

for each 9.8 metres of depth approximately. For accurate calculations of the pressure with depth, the variation of S with salinity must be taken into account. We may note that the salinity S of sea water is the number of grams of salt in one kilogram of sea-water. Typical values of S range from zero near Antarctica to around 35 % near the equator (see Defant (1961), Chapter 4, for details and read to find details concerning daily fluctuations, seasonal variations, variations with latitude and with depth).

Equation (2.51) is of fundamental importance in constructing the tidal equations, but before we make use of it we consider the assumption (c) stated at the outset of this section. The complete acceleration is given by

$$\frac{d\mathbf{V}}{dt} + 2(\omega \times \mathbf{V})$$

$$= \frac{\partial \mathbf{V}}{\partial t} + (\mathbf{V} \cdot \nabla) \mathbf{V} + 2(\omega \times \mathbf{V}) \qquad (2.54)$$

and, in this expression, V occurs to the first degree in the first and third terms and to the second degree in the so- called inertia terms, namely $(\mathbf{V} \cdot \nabla) \mathbf{V}$. There will be situations later in which we shall retain the inertia terms but, in tidal movements, V is

sufficiently small that it is permissible to ignore the second degree terms compared with the first degree terms. Hence, in this case, we can take the acceleration vector to be

$$\left\{ \frac{\partial \mathbf{V}}{\partial t} + 2(\omega \times \mathbf{V}) \right\}_{horiz} , \qquad (2.55)$$

where $\{ \}_{horiz}$ implies that we retain only the two horizontal components of this vector. The right-hand side of the two horizontal equations of motion will be

$$\left\{ -\frac{1}{\rho} \text{grad } P - \text{grad } \Omega \right\}_{horiz} \qquad (2.56)$$

If we replace p in (2.56) using (2.52) and we replace Ω by introducing the equilibrium tide height (2.23), $\Omega = -g\bar{\xi}$, we have

$$\left\{ -\frac{1}{\rho} \text{grad } P - \text{grad } \Omega \right\}_{horiz}$$

$$= -g \text{ grad} \left\{ \xi(\theta, \psi, t) - \bar{\xi}(\theta, \psi, t) \right\}_{horiz} \qquad (2.57)$$

Hence the two horizontal equations of motion will be obtained from

$$\left\{ \frac{\partial \mathbf{V}}{\partial t} + 2(\omega \times \mathbf{V}) \right\}_{horiz}$$

$$= -g \text{ grad} \left\{ \xi(\theta, \psi, t) - \bar{\xi}(\theta, \psi, t) \right\}_{horiz} \qquad (2.58)$$

Equation (2.58) makes clear the result that the departures in tide height from the equilibrium tide height are directly related to the acceleration vector. Equation (2.58) also shows that, in a steady-state situation (that is, when V and ξ do not contain the time t), we have

$$\left\{ 2(\ \omega \times \mathbf{V}\ ) \right\}_{horiz} = -g \left\{ \text{grad}\ \xi(\ \theta, \psi\ ) \right\}_{horiz} \qquad (2.59)$$

and this equation is a more general statement of a geostrophic flow than was given earlier. In order to make this perfectly clear, let us choose a system of axes $P(x,y,z)$ at a point P on the ocean, such that Pz is along the upward vertical, Px is in the horizontal plane at P and directed to the east, Py is in the horizontal plane and directed to the north.

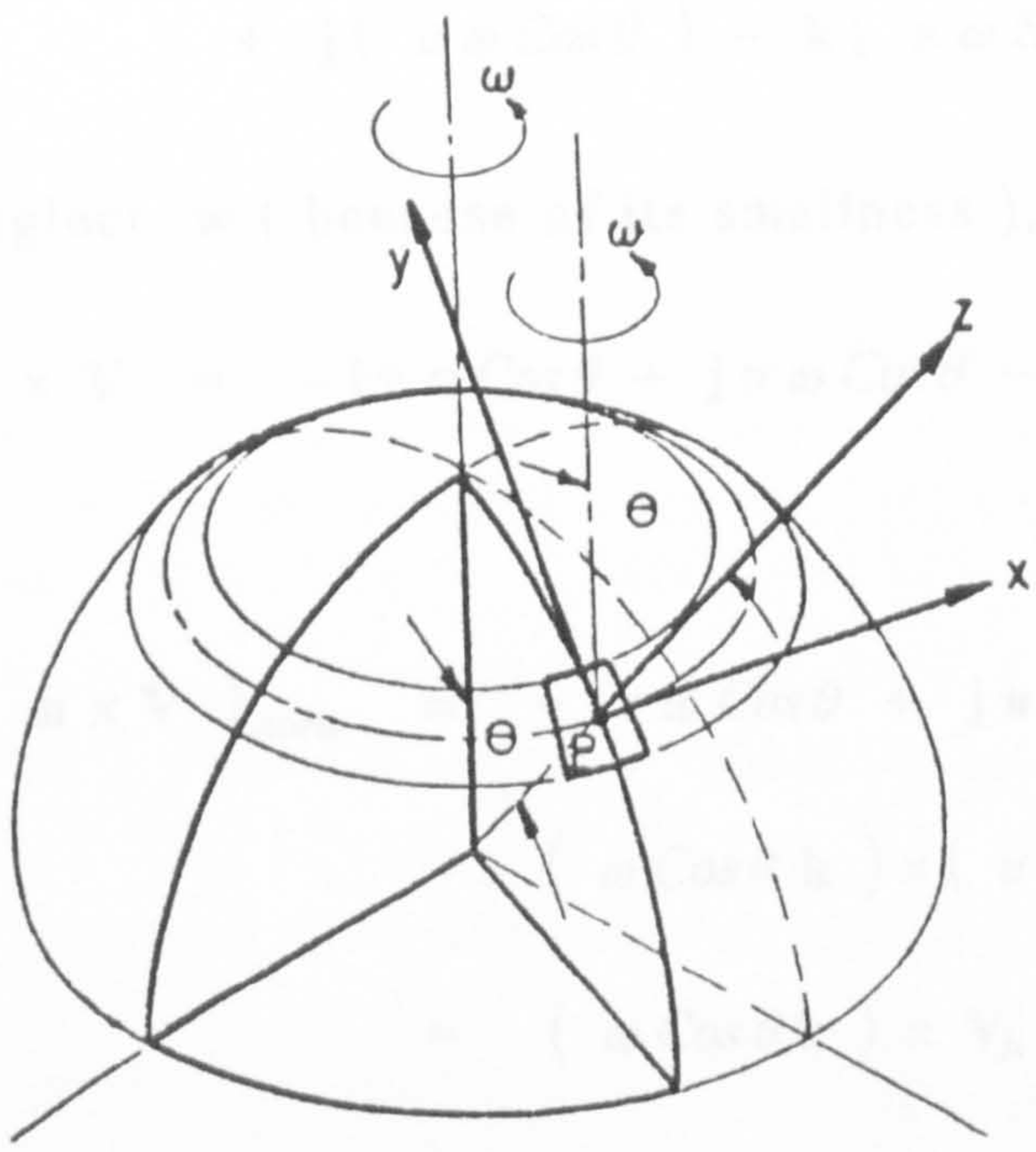

Figure 2.21

The velocity components of the ocean are denoted by (u,v,z) relative to this set of axes and it then follows that, since

$$\omega = \omega \, Sin\theta \, \mathbf{j} + \omega \, Cos\theta \, \mathbf{k} \, ,$$

we have, in general, the result

$$\omega \times \mathbf{V} = \begin{vmatrix} \mathbf{i} & \mathbf{j} & \mathbf{k} \\ 0 & \omega \, Sin\theta & \omega \, Cos\theta \\ u & v & w \end{vmatrix}$$

$$= \mathbf{i}(\; w \, \omega \, Sin\theta - v \, \omega \, Cos\theta \;)$$

$$+ \mathbf{j}(\; u \, \omega \, Cos\theta \;) - \mathbf{k}(\; u \, \omega \, Sin\theta \;) \qquad (2.60)$$

When we neglect w (because of its smallness), we have

$$\omega \times \mathbf{V} = -\mathbf{i} \, v \, \omega \, Cos\theta + \mathbf{j} \, u \, \omega \, Cos\theta - \mathbf{k} \, u \, \omega \, Sin\theta$$

and thus

$$(\; \omega \times \mathbf{V} \;)_{horiz} = -\mathbf{i} \, v \, \omega \, Cos\theta + \mathbf{j} \, u \, \omega \, Cos\theta$$

$$= (\; \omega \, Cos\theta \, \mathbf{k} \;) \times (\; u \, \mathbf{i} + v \, \mathbf{j} \;)$$

$$= (\; \omega \, Cos\theta \, \mathbf{k} \;) \times \mathbf{V}_h \, , \qquad (2.61)$$

where $\mathbf{V}_h$ is the horizontal velocity. Suppose now we construct the curves of constant height,

$$\xi(\theta, \psi) = \text{constant},$$

on the free surface of the ocean, then $-g$ grad ξ will be a vector along the

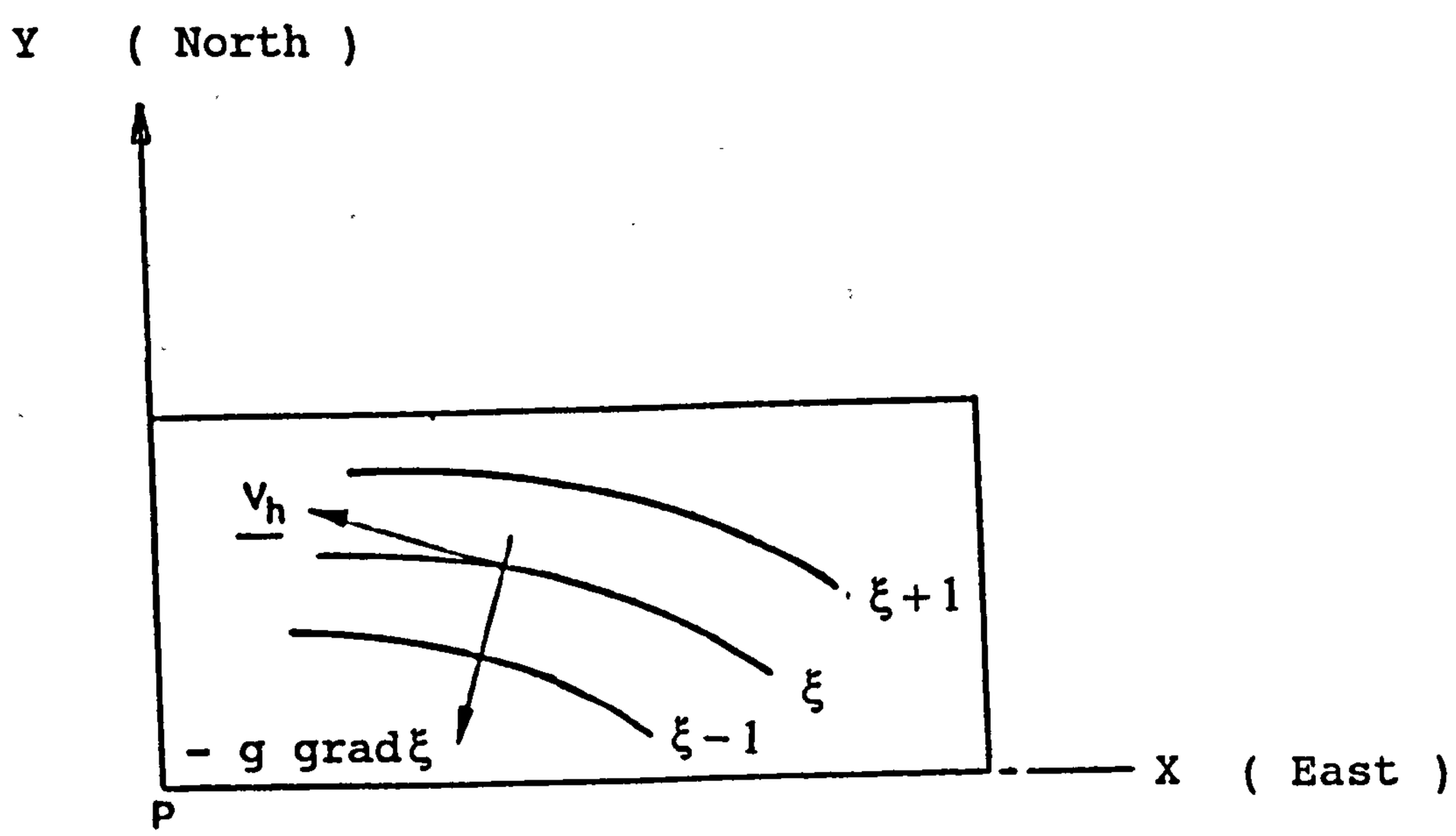

Figure 2.22

normal to the curves ξ = constant, as shown in Figure 2.22 above; this is, therefore, the direction of the vector $(\omega Cos\theta \mathbf{k}) \times \mathbf{V}_h$ and since k is in the vertical direction, it follows that $\mathbf{V}_h$ will be in the direction indicated in the figure, provided we are in the northern hemisphere ($Cos\theta > 0$). If we have a parallel situation in the southern hemisphere ($Cos\theta < 0$), $\mathbf{V}_h$ will be in the opposite direction.

We continue now with the discussion of continuity

$$\text{div } V = 0 .$$

When we separate the horizontal and vertical terms, we can write this in the form

$$(\text{div } \mathbf{V}_h)_h + \frac{\partial w}{\partial z} = 0 , \qquad (2.62)$$

where $\mathbf{V}_h = \mathbf{i}u + \mathbf{j}v$ using the axes described above and

$$(\text{div } \mathbf{V}_h)_h = \frac{\partial u}{\partial x} + \frac{\partial v}{\partial y} \qquad (2.63)$$

we discuss this in the light of the discussion leading to equations (2.58). The pressure gradient terms in (2.58) contain only θ, ψ, t, the coordinate z being absent. Thus, equations (2.58) imply that the acceleration does not vary with z. If, therefore, at some instant of time $t = 0$ the acceleration is independent of z, then it will always remain so. Assuming that this is so, we can deduce that the horizontal components of velocity are not dependent upon the z-coordinate. The picture that we then have of the movement of the ocean is as follows.

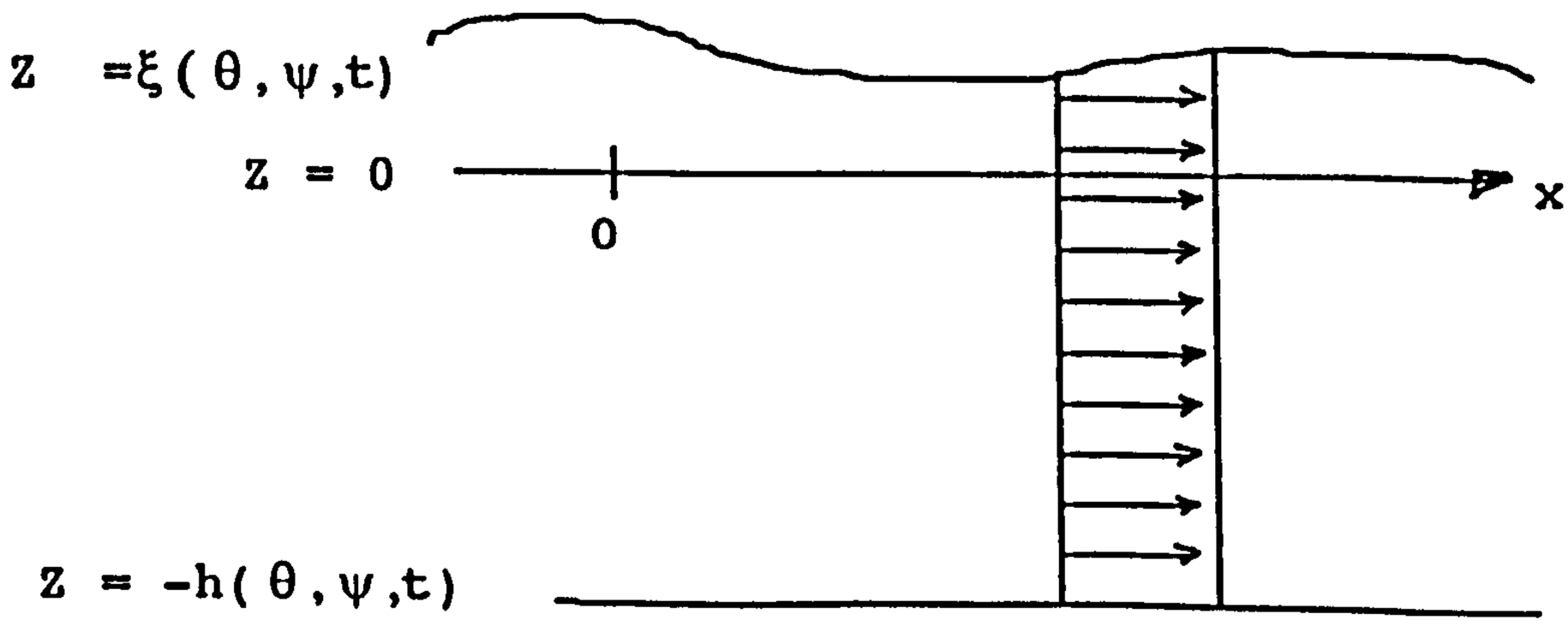

Figure 2.23

One of the consequences of the fact that V_h is independent of the vertical coordinate z is that we can integrate (2.62) with respect to z and obtain

$$\left(\text{div } \mathbf{V}_h \right)_{horiz} \int_{-h}^{z} dz + \left[w \right]_{-h}^{z} = 0 \qquad (2.64)$$

hence

$$w\big|_z = w\big|_{z=-h} - \left(z+h \right)\left(\text{div } \mathbf{V}_h \right)_{horiz} \qquad (2.65)$$

This formula indicates the distribution of vertical velocity and shows that there is a linear variation with the coordinate z. In particular we can specialize (2.65) to the free surface $z = \xi(\theta, \psi, t)$ to obtain

$$w|_{z=\xi} = w|_{z=-h} - (\xi + h)(\operatorname{div} \mathbf{V}_h)_{horiz} \tag{2.66}$$

Now at the free surface we must have the relation

$$w|_{z=\xi} = \frac{d\xi}{dt} = \left\{ \frac{\partial}{\partial t} + (\mathbf{V}\cdot\nabla)_{horiz} \right\} \xi(\theta, \psi, t)$$

$$w|_{z=\xi} = \frac{\partial \xi}{\partial t} + (\mathbf{V}\cdot\nabla)\xi . \tag{2.67}$$

Similarly, at the bottom of the ocean (assuming that it has a moving surface), we have

$$w|_{z=-h} = -\frac{dh}{dt} = -\left\{ \frac{\partial}{\partial t} + (\mathbf{V}_h\cdot\nabla) \right\} h$$

$$= -\frac{\partial h}{\partial t} - (\mathbf{V}_h\cdot\nabla)h . \tag{2.68}$$

Hence, on substituting (2.67) and (2.68) in (2.65), we obtain

$$\frac{\partial \xi}{\partial t} + (\mathbf{V}_h\cdot\nabla)\xi =$$

$$-\frac{\partial h}{\partial t} - (\mathbf{V}_h\cdot\nabla)h - (\xi + h)\operatorname{div} \mathbf{V}_h$$

and we can combine various terms in this expression to produce

$$\frac{\partial}{\partial t}(\xi + h) + \operatorname{div}_h\left\{ (\xi + h)\mathbf{V}_h \right\} = 0, \tag{2.69}$$

where div_h signifies that it is only the horizontal components of this operator which are being retained. Equation (2.69) is a

general form of the equation of continuity which we shall have occasion to use later, but there are two special forms of (2.69) which are also useful.

Special Case (a).

In tidal theory where we are concerned with movements in the open ocean and it is usual to ignore ξ in comparison with h in the term $\mathrm{div}_h(\,)$. If, also, we take the ocean to be of uniform depth h_0, then (2.69) becomes

$$\frac{\partial \xi}{\partial t} + h_0 \, \mathrm{div}_h \, \mathbf{V}_h = 0 \qquad (2.70)$$

Special Case (b).

Suppose that we have a narrow channel and x is a coordinate measuring length along the channel. Suppose that the cross-sectional area of the channel at the position x is $A(x)$ and the breadth of the channel at the free surface is $b(x)$. It will be assumed that both $A(x)$ and $b(x)$ are slowly varying functions of x.

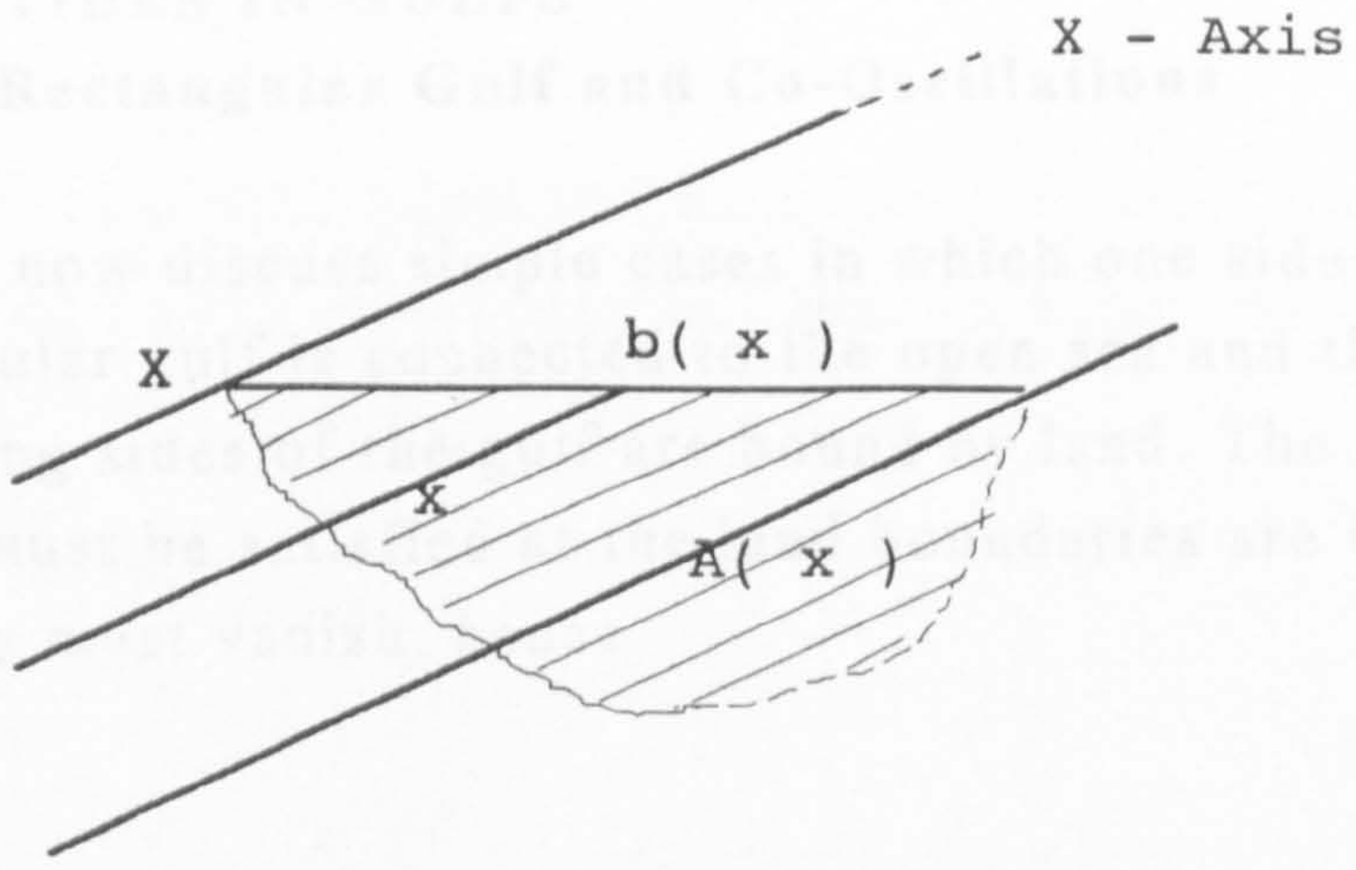

Figure 2.24

If $\xi(X,t)$ measures the departure of the water in the channel from its undisturbed level, then it is quite easy to deduce that the form of the equation of continuity is as follows

$$b\frac{\partial \xi}{\partial t} + \frac{\partial}{\partial X}\left(uA \right) = 0, \qquad (2.71)$$

where u is the velocity component in the horizontal direction along the channel. The horizontal velocity component transverse to the channel is ignored.

We shall now study a tidal problem in which the influence of geometrical boundaries is reduced to a minimum in order to illustrate the way in which the dynamical terms modify the results of the equilibrium theory. The problem deals with narrow channels - the three with latitude walls and the one with meridianal walls. The influence of geometrical walls introduces further complications into the problem and we deal with this by studying oscillations of water movement. Afterwards, we return to discuss tidal movements in gulfs which are connected to the open ocean.

2.8 TIDES IN GULFS

Rectangular Gulf and Co-Oscillations

We can now discuss simple cases in which one side of a rectangular gulf is connected to the open sea and the three remaining sides of the gulf are bound by land. The conditions which must be satisfied at the land boundaries are that the normal velocity must vanish, hence

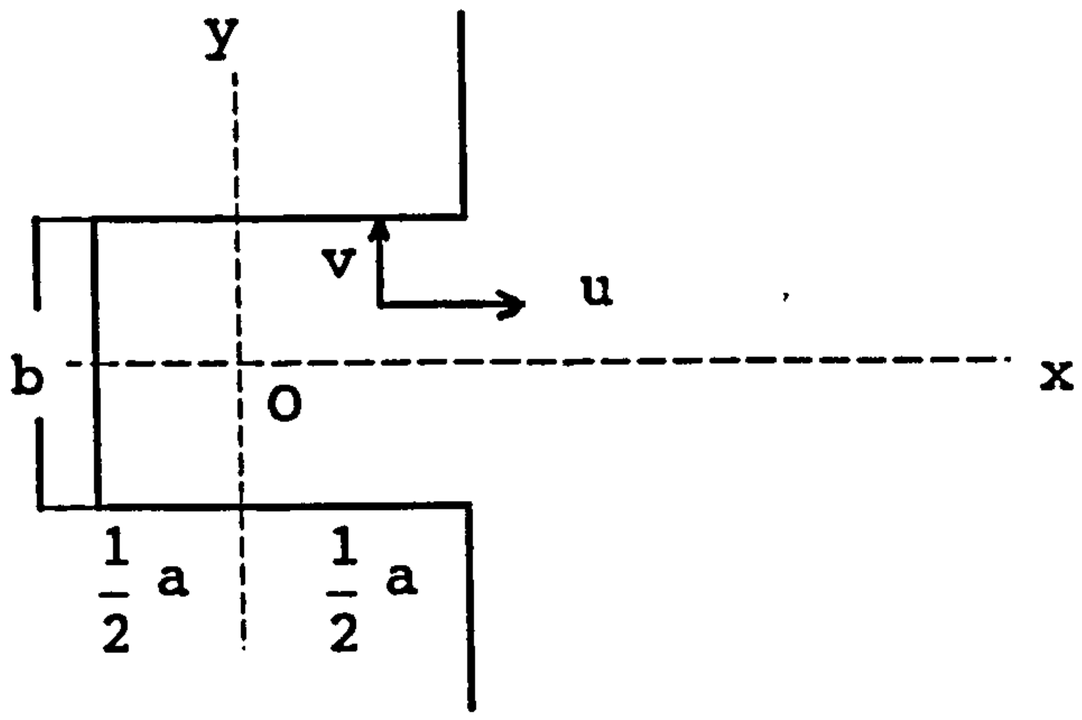

Figure 2.25

$$u = 0, \quad x = -\frac{1}{2}a \tag{2.72}$$

and we shall deal with the case of zero rotation and of no motion in the y-direction. At the end $x = \frac{1}{2}a$, we must have the height ξ of the gulf oscillation occurring in the ocean, that is, we must have

$$\xi|_{x=\frac{1}{2}a} = \alpha\, Cos\left(\frac{2\pi t}{T}\right), \tag{2.73}$$

where α is a prescribed constant, α_{moon} or α_{sun} and T is the prescribed period which may be lunar or solar. Within the gulf, the liquid motion will satisfy

$$\frac{\partial u}{\partial t} = -g\frac{\partial \xi}{\partial x} \qquad \xi = \xi(x,t) \tag{2.74}$$

$$\frac{\partial \xi}{\partial t} + h_0\frac{\partial u}{\partial x} = 0 \qquad u = u(x,t) \tag{2.75}$$

Let us look for a solution of the problem in which

$$\xi = f(x)\,Cos\left(\frac{2\pi t}{T}\right) \tag{2.76}$$

$$\xi|_{x=\frac{1}{2}a} = f\left(\frac{1}{2}a\right)Cos\left(\frac{2\pi t}{T}\right) \qquad \text{at } x = \frac{1}{2}a \tag{2.77}$$

Comparing (2.73) and (2.77), we get

$$f\left(\frac{1}{2}a\right) = \alpha \tag{2.78}$$

Then, from (2.74)

$$\frac{\partial u}{\partial t} = -g\,f'(x)\,Cos\left(\frac{2\pi t}{T}\right) \tag{2.79}$$

and by integrating with respect to t, we obtain

$$u = -\frac{gT}{2\pi}f'(x)Sin\left(\frac{2\pi t}{T}\right) \tag{2.80}$$

$$u|_{x=-\frac{1}{2}a} = \frac{-gT}{2\pi}f'\left(-\frac{1}{2}a\right)Sin\left(\frac{2\pi t}{T}\right) = 0$$

and

$$f'\left(-\frac{1}{2}a\right) = 0 \tag{2.81}$$

If we now substitute for u and ξ in (2.75), we obtain,

$$-\frac{2\pi}{T}f(x)\,Sin\left(\frac{2\pi t}{T}\right) - h_0\left(\frac{gT}{2\pi}\right)\frac{d^2f}{dx^2}\,Sin\left(\frac{2\pi t}{T}\right) = 0$$

hence, f(x) must satisfy the differential equation

$$\frac{d^2f}{dx^2} + \frac{1}{gh_0}\frac{4\pi^2}{T^2}f = 0 \tag{2.82}$$

The general solution for f will be

$$f = A\,Cos\,kx + B\,Sin\,kx \tag{2.83}$$

where k^2 has been introduced for convenience and is defined by

$$k^2 = \frac{1}{gh_0}\frac{4\pi^2}{T^2} \tag{2.84}$$

It follows from (2.80) that, in order to satisfy (2.72), we must make f(x) satisfy

$$f'\left(-\frac{1}{2}a\right) = 0$$

and, in order to satisfy (2.73), we must have

$$f\left(\frac{1}{2}a\right) = \alpha \tag{2.85}$$

Hence

$$k\,A\,Sin\,\frac{1}{2}ka + k\,B\,Cos\,\frac{1}{2}ka = 0$$

$$A\,Cos\,\frac{1}{2}ka + B\,Sin\,\frac{1}{2}ka = \alpha\,.$$

and the solutions for A , B will be given by

$$\frac{A}{Cos\,\frac{1}{2}ka} = \frac{B}{-Sin\,\frac{1}{2}ka} = \frac{\alpha}{Cos\,\frac{1}{2}ka} \tag{2.86}$$

Thus the solution of the problem will be given by

$$f(x) = \alpha\frac{Cos\,k\left(\frac{1}{2}a + x\right)}{Cos\,ka} \tag{2.87}$$

$$\xi = \frac{\alpha}{Cos\, ka} Cos\, k\left(\frac{1}{2}a + x\right) Cos\left(\frac{2\pi t}{T}\right) \qquad (2.88)$$

$$u = \frac{\alpha}{Cos\, ka}\left(\frac{gT}{2\pi}\right) Sin\, k\left(\frac{1}{2}a + x\right) Sin\left(\frac{2\pi t}{T}\right) \qquad (2.89)$$

The interpretation of this solution is as follows. It is clear from (2.89) that u will satisfy the condition (2.72) and from (2.88) that ξ will satisfy (2.73). The value of ξ on the coast line $x = -\frac{1}{2}a$ will be

$$\xi\big|_{x=-\frac{1}{2}a} = \frac{\alpha}{Cos\, ka} Cos\left(\frac{2\pi t}{T}\right) \qquad (2.90)$$

When $Cos\, ka > 0$, this oscillation will be in phase with the oscillation at the entrance to the gulf. When $Cos\, ka < 0$, the oscillation will be exactly opposite in phase to the oscillation at the gulf entrance. If $Cos\, ka$ is small or, if indeed, it vanishes, this is the phenomenon of resonance and the condition for resonance is

$$Cos\, ka = 0 \qquad (2.91)$$

Resonance will occur, therefore, when

$$ka = \frac{\pi}{2}, \frac{3\pi}{2}, \ldots\ldots \qquad (2.92)$$

The quantity k is defined in (2.84) and, using this, the resonance condition will be

$$\frac{a^2}{gh_0}\frac{4\pi^2}{T^2} = \frac{\pi^2}{4}, \frac{9\pi^2}{4}, \ldots \qquad (2.93)$$

2.8.1 FORCED OSCILLATIONS IN THE ARABIAN GULF

As the shape of the Arabian Gulf is quite similar to Rectangular Gulf (Section 2.8). We take an origin $x = 0$ at the west end of x is along the length of the Arabian Gulf. The equation of motion is then

$$\frac{\partial u}{\partial t} = -g\frac{\partial \xi}{\partial x} \qquad \xi = \xi(x,t)$$

In order to incorporate the variable cross-section and variable breadth of the free surface, we take the equation of continuity in the form (2.40), namely

$$b\frac{\partial \xi}{\partial t} + \frac{\partial}{\partial x}(uA) = 0 \qquad . \qquad (2.94)$$

If we now postulate that there is zero velocity u at the west end of the Arabian Gulf, then

$$u = 0 \quad , \; x = 0 \; .$$

We shall assume also the semi-diurnal tidal oscillation M_2 is known at $x = 0$ and let us suppose that this is known in the form

$$\xi|_{x=0} = \alpha \, Cos\left(\frac{2\pi t}{T} + \gamma\right),$$

where α is a known amplitude (for M_2 , $\alpha = 0.9$ m) and γ a known phase angle (for M_2 , $\gamma = 345^\circ$). The problem now is to determine the characteristics of the forced oscillation. It is clear from the above equations that the forced oscillation in ξ within the channel is given by

$$\xi = \alpha \, z(x) \, Cos\left(\frac{2\pi t}{T} + \gamma\right), \qquad (2.95)$$

where, clearly, we must have

$$z(0) = 1$$

from (2.95), It is also clear that the tidal velocity u must be of the form

$$u = \alpha U(x) Cos\left(\frac{2\pi t}{T} + \gamma\right) = \alpha\xi \qquad (2.96)$$

where $U(x)$ is prescribed velocity at the open boundary.

The equations (2.95) and (2,96) are used in Explicit Finite Difference Method (EFDM) as a driving force at the open boundary at Strait of Harmouz in Chapter 5.

CHAPTER THREE

3.0 TIDAL FLOW IN ARABIAN GULF

3.1 FACTORS GOVERNING FLOW IN THE GULF

The Arabian Gulf or, as it is sometimes called, the Persian Gulf, covers the seaway from the Tigris-Euphrates river estuary in the north to the Strait of Harmouz in the south. The average length of the Gulf is 1000 km and the width varies between 55 and 340 km to give a total area of approximately 240,000 square kilometres. The Gulf is relatively small compared to other off-shore oil producing areas such as the North Sea, twice its size, or the Gulf of Mexico, five times as large. It is also relatively young geographically, having been formed only three or four million years ago.During its brief history it has been reduced several times to an estuary of the Tigris-Euphrates river system when world-wide sea level lowering occurred. The most recent such episodes ended less than 20,000 years ago with the Gulf following the sea level rise known as the "Flandrian Transgression", and reaching its present level about 5000 years ago (Kassler, 1973).

The entire basin lies on the continental shelf, the slope of which into deeper waters occurs only in the Gulf of Oman. The result is that the Gulf is very shallow, rarely deeper than 100 metres, with an average depth of between 31 and 37 metres. It is asymmetrical in profile with a gentle slope from the western to the eastern side. A wide area of mud-bottom is found in the northern and eastern parts of the Gulf with the sand bottom predominant in the southern and western parts. Rock is present at the bottom of the Strait of Hormouz and in reef and island margin areas. The coast line on the eastern side is marked by mountains and cliffs whereas the western coast is mainly sandy. Industrial and commercial activities in populated areas have affected the shore line and altered near-shore current patterns.

Studies by Emery (1956) found nearly-uniform surface temperatures in the Gulf of around 32° *C*. A compilation of winter surface temperatures by Schott (1918) and Blegvad (1944) show a variation of between 16° *C* in the northern Gulf to about 24° *C* at the Strait of Harmouz.

Privett (1959) has estimated the evaporation rate for the Gulf to vary between 0.2 and 0.6 gm/cm^2 per day. This means that the volume of water evaporated each year is equivalent to the volume of four million Nowruz spills. Privett claims that evaporation is at a maximum in December and a minimum in May.

The inflow of water from the Gulf of Oman, near the Iranian Coast, and conditions in the Strait of Harmouz have been observed by Sonu (1979). In the Strait of Harmouz, the inflow was estimated to occupy the top 30 m. of the water column, a mixing layer the middle 20 m and the outflow the bottom 30 m. Current observations were made from on board ship, near Kish Island, off the Iranian coast, but no effort was made to remove the tidal oscillations (which probably exceeds the residual flow in this area), or even to report at what time in the tidal cycle the observations were made.

Fresh-water inflow has been estimated (Grasshof, 1976) at between 5 to 10 cubic kilometres per year. This represents only about 1.3% to 28% of the water loss to evaporation. Since precipitation is light in the region, consideration of the differential flow through the Strait of Harmouz is crucial to the water balance in the Gulf. Koske (1972), assuming a shear flow through Harmouz, computed a flushing time for the basin of about 2.5 years. Hughes and Hunter (1979), using a less restrictive model, derived a time for 90% flushing of 2.5 years. They also estimated the turnover time, the time it takes for all the water in the Gulf to come within the influence of the open sea boundary, of 230 days. However, if the interaction of vertical mixing is included with the residual current in the Gulf, in their estimate, the turnover time increases to 2.4 years.

Highly saline conditions are found in the Arabian Gulf. Surface salinity in the summer ranges from 37% in the Gulf of Oman to 42% just off the coast of Bahrain. Salinities as high as

70% have been reported in the Gulf of Salwah at its extreme southern extremity (Basson et al., 1977). The salinity in winter is higher than in summer, apparently due to the variation of fresh-water influx through the Shatt Al-Arab and to meteorological effects particularly evaporation (Schott, 1918). As evaporation exceeds precipitation in the Gulf, the saline-dense water sinks and passes out of the Strait of Harmouz giving rise to a compensating surface flow of less dense water into the Gulf.

Off-shore winds in the Gulf area blow mainly from the northwest and are particularly strong in early summer, due to a counter-clockwise wind circulation around a low pressure area over the Asian continent. The so-called "shamals" (Arabic for north) blow down the Gulf with gusts of as much as 100 km/hour (Williams,1979). The most serious interference with this wind pattern occurs in winter or early spring when passing depressions effect the Gulf in their movement from west to east. These can cause wind flow to change from north-west to south-east. Such exceptional wind patterns can last for a number of days before they revert to normal patterns (Wennink and Nelson-Smith, 1977).

According to Perrone (1981) the usual relationship between wind speed and wave heights that are developed for deep water may not hold for the shallow Arabian Gulf, the maximum depth of which is only about 100 m. He claims the shallowness of the Gulf, as well as its stratification, will make the wave heights much larger than those that are inferred from deep water relationships. Observations made from oil rigs suggest that persistent gale force winds blowing for up to 12 hours can generate wind waves with amplitudes up to 4m. Sometimes waves up to 5m could be generated in a few hours.

In the northern part of the Arabian Gulf wind wave amplitudes are usually smaller because of limited fetch and also due to the fact that this area is affected by short duration shamals. According to Perrone (1981) the following three factors combine to generate waves up to 5m in the southern part of the Arabian Gulf during shamals of three to five days duration

(i) The increase in wind speed in the southern Gulf: this contributes to locally generated seas.

(ii) The longer duration of gale force winds over the whole Gulf: the northern part of the Gulf generates swell which travels into the southern part.

(iii) The lack of fetch limitation: the entire Gulf experiences at least gale force winds with the strongest winds in the south.It may take several days for the swell to decay following shamal winds. On the basis of a geostrophic force balance across the Gulf, and a frictional balance along the Gulf, Hunter (1982) indicated the circulation schematically as shown in Figure 3.1.

According to Perrone (1981) two areas of the Arabian Gulf appear to experience stronger than average shamal conditions. These are shown in Figure 3.2.

The effect of the earth's rotation would be to deflect these flows to the right, giving a surface flow west and north-west along the Iranian coast and a deep flow to the south-east and east along the coasts of Saudi Arabia, Qatar, Bahrain and the United Arab Emirates. The deep flow would be further constrained to these latter coastlines as it is in these regions that the shallow sea areas of high evaporation lie. This circulation pattern would be modified by forcing by the wind and atmospheric pressure, but it has been generally supported by observations of drifts of ships at sea.

Evidence for this anti-clockwise residual circulation in the Gulf, driven mainly by evaporation has been described by Schott (1918), Barlow (1932a,1932b,1932c), British Admiralty (1941), Emery (1956), Sugden (1963), Hartman et al. (1971), Szekielda et al. (1972), Purser and Seibold (1973), Grasshoff (1976), Szekielda (1976) and Brewer et al. (1978).

The north-western part of the Gulf is influenced by the fresh water inflow of the Tigris, the Euphrates and the Karum (entering the Gulf via the Shatt Al-Arab). This inflow appears to be deflected to the right by Coriolis force to form a river plume approximately 20 km wide, flowing along the Iraqi coast

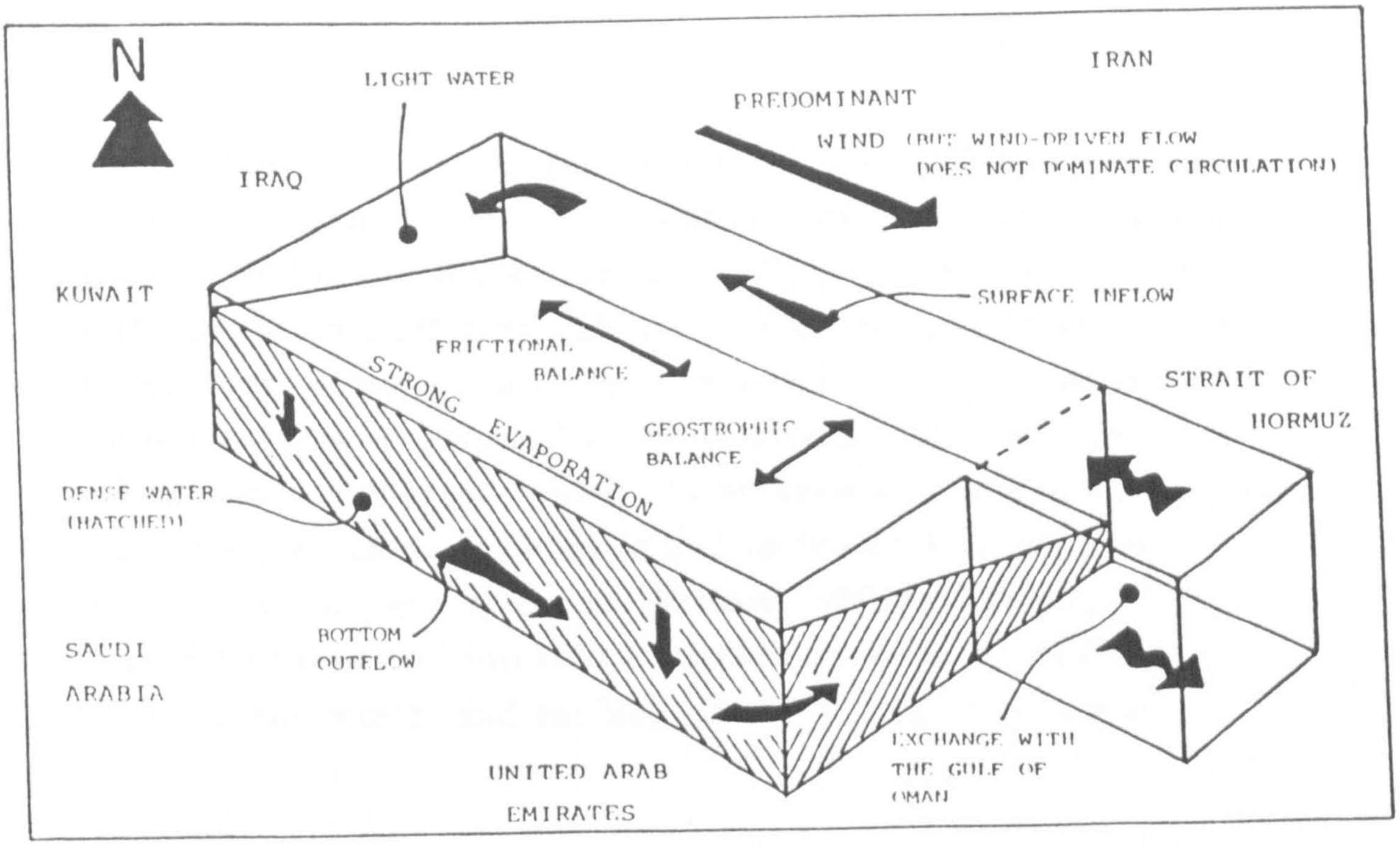

Figure 3.1 The probable circulation pattern in the Gulf (after Hunter, 1982).

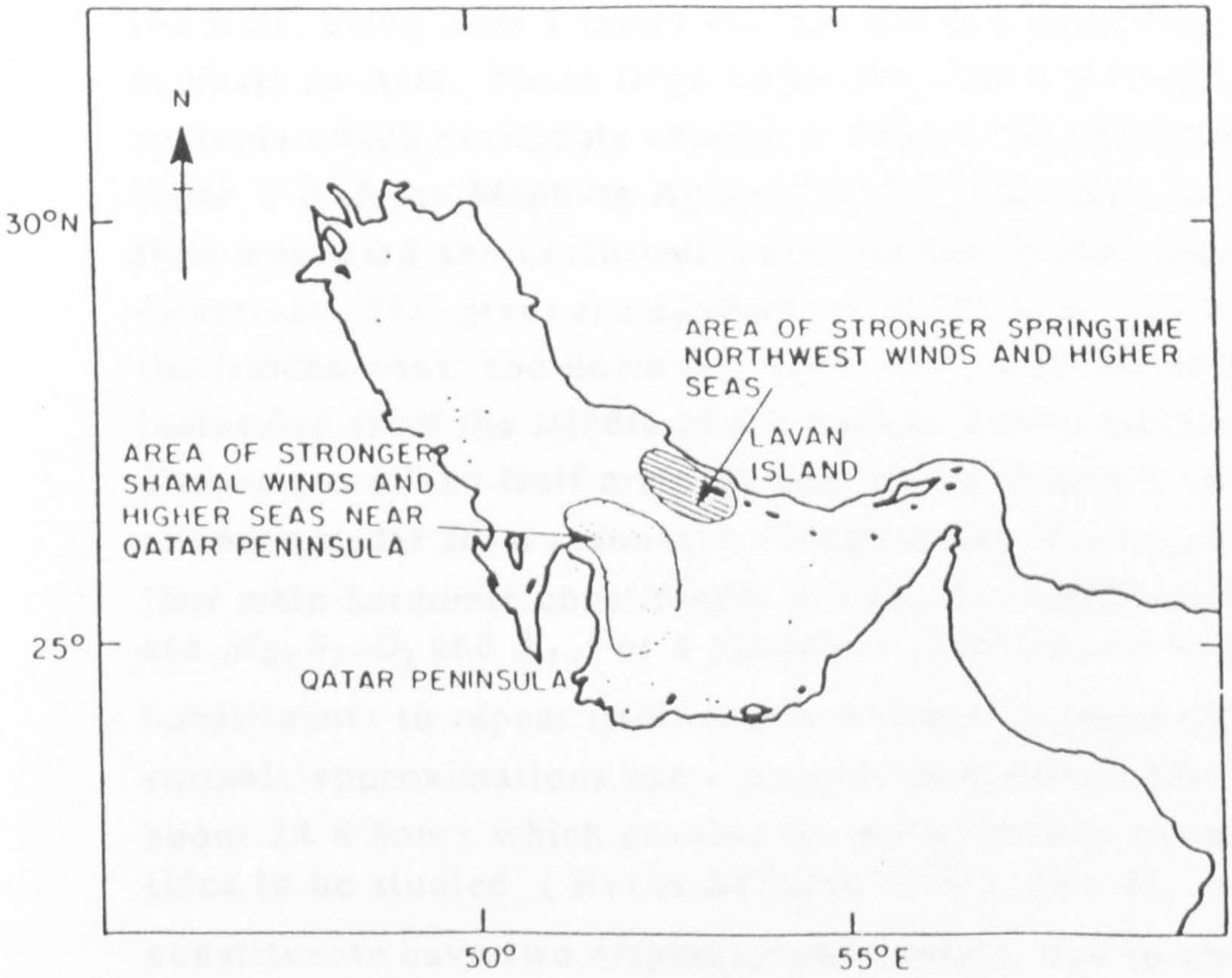

Figure 3.2 Areas of stronger than normal northwesterly winds and higher seas.

into Kuwaiti waters (Mathews et al., 1979). This phenomenon is also indicated by observations at a somewhat larger scale by Dubach (1964) and Brewer et al. (1978). The residual circulation in the southern Gulf area and the Gulf of Oman is influenced by the seasonal effect of the south-west and north-east monsoons. These give rise to seasonal reversal of currents in the north Indian ocean (Warren, 1966)- being generally to the west during the winter, north-east monsoon and to the east during the summer, south-west monsoon. Barlow (1952c) reported observations which indicated a surface outflow in the Gulf of Oman during winter and surface inflow during the summer.

3.2 TIDES IN THE ARABIAN GULF.

The tides in the Gulf are complicated, consisting of a variety of tidal types (Figure 3.3). The tidal ranges are large throughout the Gulf, being over 1 metre everywhere and exceeding 3 metres at Shatt Al-Arab. These large amplitudes cause strong tidal currents which commonly exceed 0.5m/sec. at maximum ebb or flood (Defense Mapping Agency,1975). The tides generally flow westward and north-westward and ebb in the opposite directions. This gives the appearance of the tide progressing up the Iranian coast and down the Saudi side, with the range increasing from the middle of the Gulf in Kelvin wave style. The dimensions of the Gulf are such that the oscillations in the tide are not too far from resonance (Hughes and Hunter,1979). The four main harmonic constituents of the tidal regime in the Gulf are M_2, S_2, O_1 and K_1. For a particular combination of the main constituents to repeat itself requires about 19 years although suitable approximations can construct an artificial tide cycle of about 24.8 hours which enables the main features of the Gulf tides to be studied (Evans-Roberts,1979). The M_2 and S_2 constituents have two amphihidromic points, one in the north-western part of the Gulf and the other in the south-western part (See Figures 6.3-6.6). The O_1 and K_1 have a single amphidromic point.

3.3 LITERATURE REVIEW.

To combat oil pollution, to simulate tides and tidal currents or to predict storm surges in the Gulf, a comprehensive knowledge of the dynamics of the Arabian Gulf is necessary. In recent years a lot of work on this has been done but some aspects are still to be revealed.

Data collection regarding different parameters which are necessary to control and clean up the pollution, predict tides, tidal currents and storm surges, can be made both by measurement and by the development of a numerical model. Numerical modeling has been applied in many fields of applied sciences to reproduce certain phenomena both quantitatively and qualitatively where the measurements can be very costly and slow. Since numerical models were used for the first time in planning major engineering works in a coastal sea.

In fact, more than 60 years have passed since numerical models were used for the first time in planning major engineering works in a coastal sea. The basis for the tide and storm surge computations for the purpose of predicting the effect of the closure of the Zuiderzee in the Netherlands, was established by the Nobel prize winning physicist Lorentz (1926). The studies made for this closure were successful. It appeared after the closure that the water movements and tidal heights agreed well with the predictions made by computation.

In the last 20 years significant changes have occurred. Industrial development, expansion of navigation and increased habitation of low areas near the coast have necessitated increased construction. In coastal areas such as those of the Arabian Gulf, hydraulic modeling of these regions is difficult and expensive. Assessment of the fate of discharged pollutants and of the affect of construction on the environment are difficult to make using these models. Consequently, interest in numerical simulations has increased, particularly with the availability of digital computers

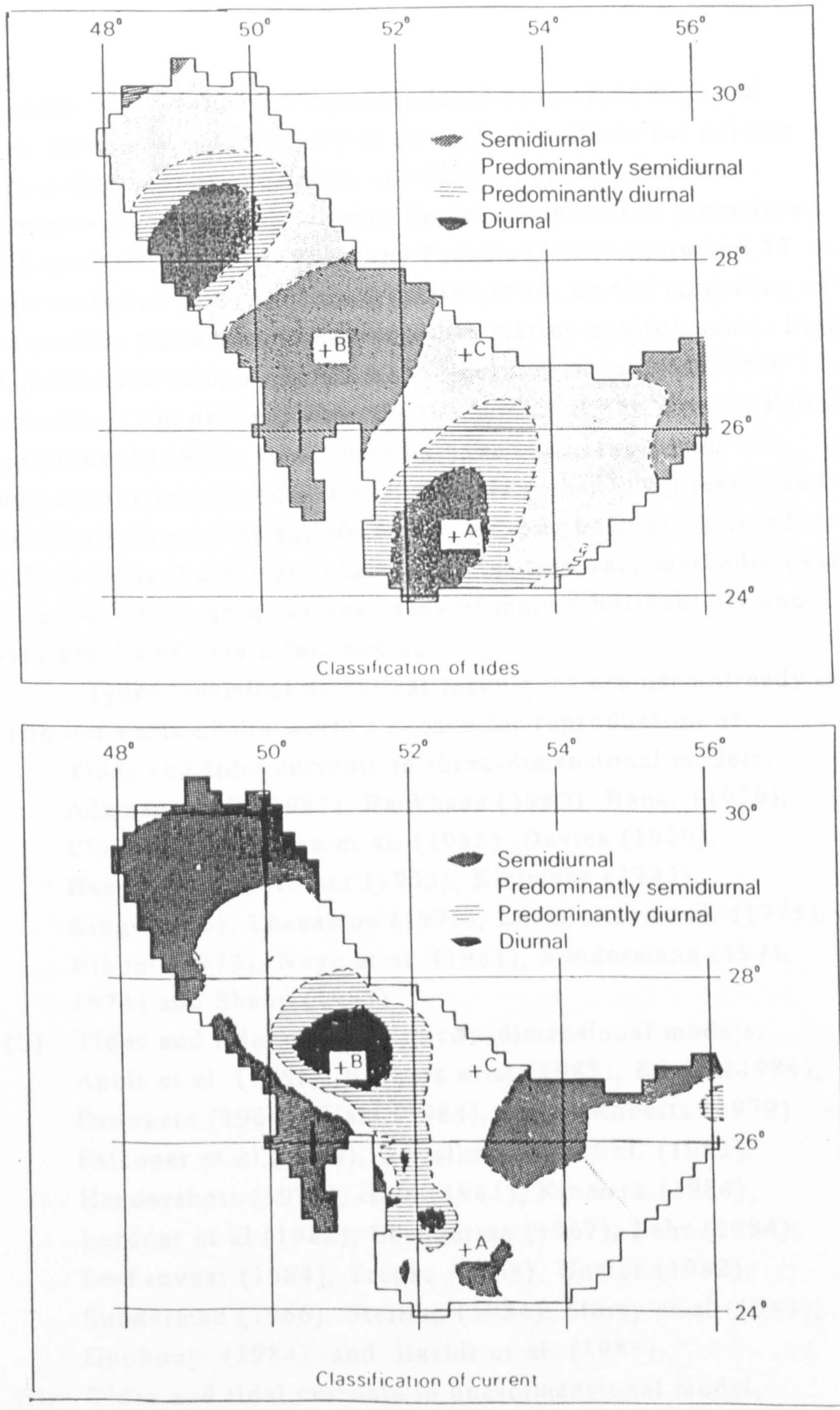

Figure 3.3 Classification of tidal types following Evans-Roberts (1979).

to perform the numerous computational operations required. Also, advances in the theory of numerical methods for solving partial differential equations, the basis of these numerical simulations, make it possible to design computation procedures with minimized errors. Rath and Francis (1977) evaluated 17 representative papers, published after 1964, on the modelling of the surface movement of spilled oil in marine environments. Eight of these used computational techniques and considered tidal currents as the driving force for the model. In the view of Pond and Pickard (1978), tidal currents have been studied for two reasons: the instrumentation required is rather complicated and less likely to operate satisfactorily for long periods unattended, and secondly the current characteristics may vary markedly over distances of hundreds or even tens of metres horizontally and over depths of only a few metres.

Hydrodynamical numerical techniques are used already in different parts of the world's oceans for reproduction of

(i) Tides and tidal currents in three-dimensional models, Adamec et al. (1981), Backhaus (1980), Bauer (1979), Chen (1978), Crean et al. (1983), Davies (1980), Heaps (1980), Hunter (1983), Kielmann (1983), King (1985), Laevastue (1975), Leendertse et al. (1975), Nihoul (1978), Noye et al. (1981), Sundermann (1971, 1974) and Sheng (1983).

(ii) Tides and tidal currents in two-dimensional models, Apelt et al. (1985), Beckers et al.(1985), Krohn (1984), Dronkers (1964), Elahi (1984), Evans-Roberts (1979), Falconer et al.(1984), Gopalkrishnan et al. (1983), Hendershott (1977), Holz (1981), Kinmark (1984), Lardner et al (1982), Leendertse (1967), Lehr (1984), Le-Provost (1984), Trepka (1968), Uncles (1982), Sunderman (1966), Stelling (1984), Murty et al.(1983), Guohong (1984) and Bashir et al. (1989).

(iii) Tides and tidal currents in one-dimensional model, Wang (1983).

(iv) Pollutants dispersion models, Davydov et al. (1984), Galt (1984), Galt et al. (1984), Dippner (1984), Henry et al. (1984), Holly et al. (1984), Kullenberg (1983), Laevastue et al. (1974), Griffiths et al. (1981), Matsuda (1979), Hires et al. (1983), Post (1984), Taylor (1975) and Zeidler (1976).

(v) Water and tidal circulation models, Chiang et al. (1982), Blumberg et al. (1985), Roovers et al. (1984), Miller (1984), Spaulding (1983), Noye et al. (1981), Henry et al. (1984), Goussebaile et al. (1984) and Hamilton et al. (1982).

(vi) Free surface models, Davies (1985), King (1985) and Kawahara et al. (1983).

(vii) Residual currents models, Lardner et al. (1988) and Falconer (1985).

(viii) Salinity models, Owen (1984) and Wang (1983).

(ix) Storm surge models, Elahi et al. (1981) and Howarth et al. (1981).

(x) Temperature distribution model, Falconer (1984).

El-Sabh (1984) edited a report on the symposium workshop held at King Fahad University, Dharan, on oceanographic modelling of the Kuwait Action Plan (KAP) region which includes the Arabian Gulf and the Bay of Oman. The report presents an up-to-date state of knowledge of oceanographic modeling in the region. Out of 12 papers, seven do not represent original work on tidal modelling of the Arabian Gulf. Lehr (1984) and Le Provost (1984) nicely reviewed works of Evans-Roberts (1979), Lardner et al. (1982) and Tepka (1968). Le Provost (1984) constructed co-tidal charts from observed data, which is not a science but an art. McCammon et al. (1977) and Elahi (1979) presented work co-tidal charts of the northern Arabian Sea and Gulf of Oman but not the Arabian Gulf. Hunter (1984) made a valuable contribution on the residual circulation and mixing process in the Arabian Gulf due to pressure gradient arising from evaporation-induced density variations and horizontal variation in water density. Natural-depth distribution is not considered in the three-dimensional, five-level numerical

model of Hunter (1983), though it would appear to be so from the results reported. Quite a good survey of details required in modelling the Arabian Gulf are available in the work of Hughes and Hunter (1979) and Hunter (1980). MEPA's marine weather service has a hydrodynamical model which is capable of predicting sea level pressure, surface winds, singular waves, mean currents, water heights and surface currents for the Arabian Gulf (Al Deghaiter,1984). Only the abstract of this contribution is available, hence nothing can be said about the merit of the method and results of the model.

Gault (1984), Gault et al. (1984), Hunter (1984) and Lehr (1984) discussed oil spill in the Arabian Gulf. Dippner (1984), Post (1984) and Lardner et al. (1988) presented models of oil spills and pollutant dispersion.

CHAPTER FOUR

4.0 MATHEMATICAL MODEL

4.1 THE MODEL EQUATIONS

For the model formulation a system of rectangular cartesian co-ordinates is used in which the origin O is within the equilibrium level of sea-surface, OX points westward, OY points northward and OZ is directed vertically upwards. The western boundary of the analysis area (Figure 4.1) corresponds to the east coast of Saudi Arabia, Kuwait and Bahrain. The eastern boundary is the coast of Iran, the southern boundary is the coast of U.A.E and Qatar and the northern boundary is the coast of Iran and Iraq. There is only one open-sea boundary at the Strait of Harmouz situated along longitude 56° 30′ E.

The physical state of a gulf can be completely described by

Velocity vector	$\langle V_x, V_y, V_z \rangle$
Pressure	P
Temperature	T
Salinity	S
Density	ρ

where $\langle V_x, V_y, V_z \rangle$ are velocity components in the x,y and z-directions of a Cartesian co-ordinate system (Fig.4.2)

These seven quantities can be determined using the following laws of Physics, which are taken as axiomatic in developing a study of the dynamics of an ocean.

1. Conservation of mass.
2. Conservation of energy (temperature and salinity).
3. Conservation of angular momentum.
4. Newton's Laws of motions and gravitation.
5. Equation of state.

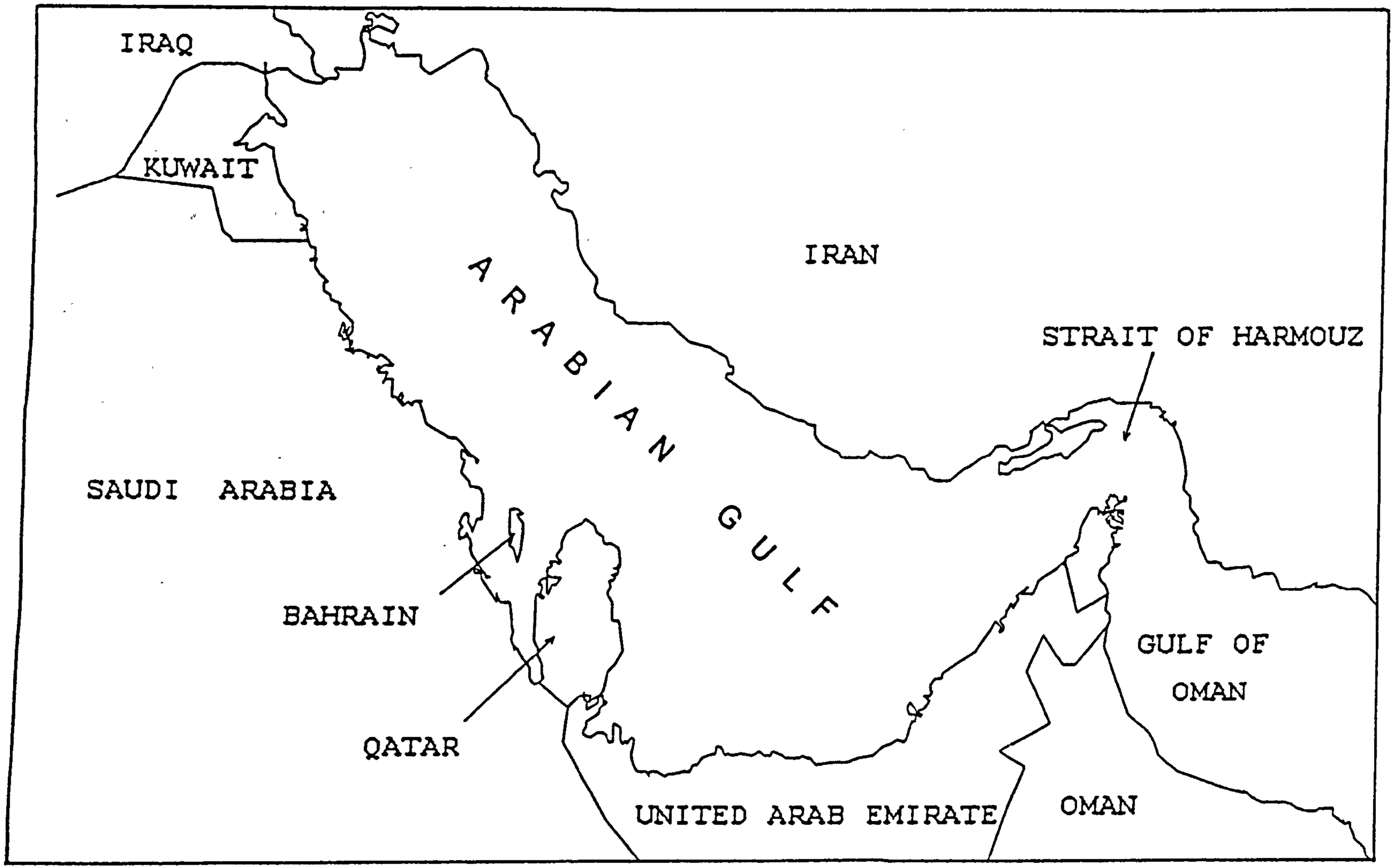

Figure 4.1 Geography of Arabian Gulf.

These conservation Laws lead to the following non-linear partial differential equations. (see Chapter 2)

1. Equation of continuity

$$\frac{\partial \rho}{\partial t} + \frac{\partial}{\partial x_i}(\rho V_i) = 0 \qquad (4.1)$$

2. Equation of motion

$$\frac{\partial V_i}{\partial t} + V_j \frac{\partial V_i}{\partial x_j} = \frac{1}{\rho}\left(K_i - \frac{\partial P}{\partial x_i} \right) + \nu \frac{\partial^2 V_i}{\partial x_j \partial x_i}, \qquad (4.2)$$

where K is the kinematic eddy diffusivity and ν is the kinematic modular viscosity.

3. Equation of dispersion

$$\frac{\partial C}{\partial t} + V_j \frac{\partial C}{\partial x_j} + \beta(C) \frac{\partial^2 C}{\partial x_j^2} \qquad (4.3)$$

4. Equation of state

$$\rho = F(P,T,S) \qquad (4.4)$$

If the variable C represents temperature T, then equation (4.3) is known as the equation of heat conduction and $\beta(T)$ is known as the coefficient of thermo-diffusion. If C represents the salinity S, then equation (4.3) is known as the equation of diffusion and $\beta(S)$ is known as the coefficient of salinity - diffusion.

A complete solution can be achieved if the necessary initial conditions and boundary conditions, for instance at the air-water interface (surface), water-solid interface (bottom), heat exchange or waste discharge are known.

The nature of the flow in the Gulf allows certain simplifications of equations (4.1-4.4), which can be modified to represent the incompressible, turbulent baraclinic flow under the following conditions:

1. Water is incompressible.
2. Density variations are important only for buoyancy forces and considered uniform in the vertical direction.
3. Vertical accelerations can be neglected.
4. Eddy viscosity is considered to be zero.
5. Turbulent diffusion can be described by turbulent exchange coefficients.
6. Flow is quasi-hydrostatic.
7. Boussinesq's approximation is valid.
8. The affect of the Earth's rotation can be taken into account by the Coriolis parameter f and its variation is unimportant.
9. Salinity can be taken as constant.
10. Meterological conditions are ignored; that is, surface stress is zero and evaporation is neglected.
11. Astronomical tide generating forces are unimportant.

By means of the above conditions the following system is obtained:

$$\frac{\partial u}{\partial t} + u\frac{\partial u}{\partial x} + v\frac{\partial u}{\partial y} + w\frac{\partial u}{\partial z} - fv$$

$$= -\frac{1}{\rho}\frac{\partial P}{\partial x} + \frac{\partial}{\partial x}\left(A_h \frac{\partial u}{\partial x} \right) +$$

$$+ \frac{\partial}{\partial y}\left(A_h \frac{\partial u}{\partial y} \right) + \frac{\partial}{\partial z}\left(A_v \frac{\partial u}{\partial z} \right) \qquad (4.5)$$

$$\frac{\partial v}{\partial t} + u\frac{\partial v}{\partial x} + v\frac{\partial v}{\partial y} + w\frac{\partial v}{\partial z} + f u$$

$$= - \frac{1}{\rho}\frac{\partial P}{\partial y} + \frac{\partial}{\partial x}\left(A_h \frac{\partial v}{\partial x} \right)$$

$$+ \frac{\partial}{\partial y}\left(A_h \frac{\partial v}{\partial y} \right) + \frac{\partial}{\partial z}\left(A_v \frac{\partial v}{\partial z} \right) \qquad (4.6)$$

$$\frac{\partial u}{\partial x} + \frac{\partial v}{\partial y} + \frac{\partial w}{\partial z} = 0 \qquad (4.7)$$

$$\frac{\partial C}{\partial x} + u\frac{\partial c}{\partial x} + v\frac{\partial c}{\partial y} + w\frac{\partial c}{\partial z}$$

$$= \frac{\partial}{\partial x}\left(K_h \frac{\partial c}{\partial x} \right) + \frac{\partial}{\partial y}\left(K_h \frac{\partial c}{\partial y} \right)$$

$$+ \frac{\partial}{\partial z}\left(K_v \frac{\partial c}{\partial z} \right) \qquad (4.8)$$

where A_h and A_v are kinematic eddy viscosities in the horizontal and vertical directions, u, v and w are velocity components in the X, Y and Z-directions of a cartesian co-ordinate system (Figure 4.2), and f is the constant Coriolis parameter.

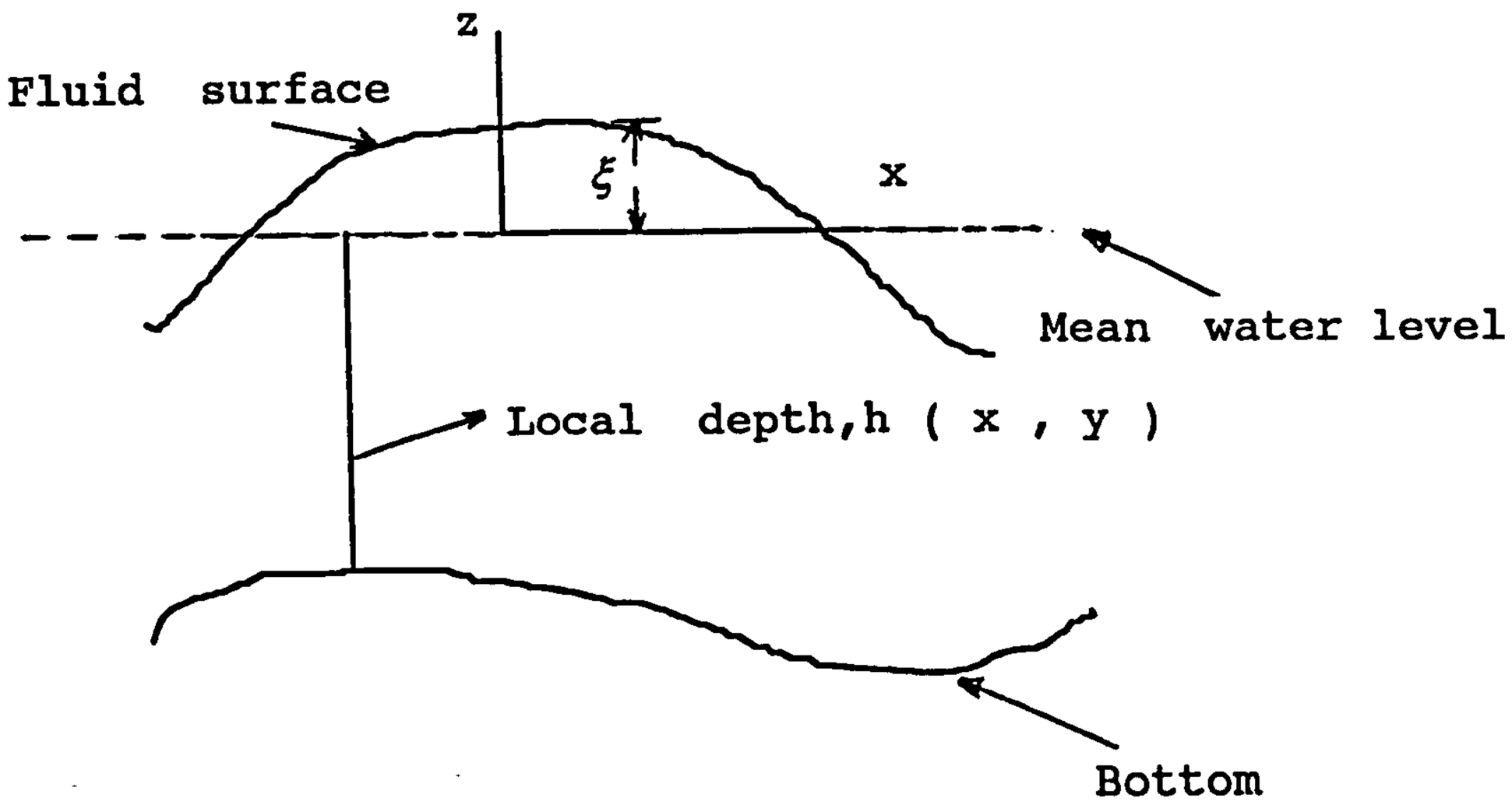

Figure 4.2 Free surface geometry in (x , y , z) coordinate system

The assumption of hydrostatic equilibrium to

$$P = P_s + g\left(\rho_0 + \int_z^h \Delta P \, dz\right) \tag{4.9}$$

4.2 REDUCTION TO SHALLOW WATER EQUATIONS

The above equations, (4.1)-(4.9), are sometimes linearized by neglecting the convective terms.

The equations are vertically integrated from the bottom ($-h$) to the surface (ξ) to represent a single-layer two-dimensional model.

$$\int_{-h}^{\xi} (System)\, dz = 0 \tag{4.10}$$

Under the condition $F(x,y,z,t) = 0$ on the boundary, it follows that

$$\frac{dF}{dt} = \frac{\partial F}{\partial t} + u\frac{\partial F}{\partial x} + v\frac{\partial F}{\partial y} + w\frac{\partial F}{\partial z} = 0 \quad , \qquad (4.11)$$

where, at the surface

$$F_s(x,y,z,t) = z - h(x,y,t)$$

and at the bottom

$$F_b(x,y,z,t=0) = z + h(x,y).$$

Equations (4.5), (4.6) reduce to

$$\frac{\partial \xi}{\partial t} + \frac{\partial(H\bar{u})}{\partial x} + \frac{\partial(H\bar{v})}{\partial y} = 0, \qquad (4.11)$$

$$\frac{\partial \bar{u}}{\partial t} + \bar{u}\frac{\partial \bar{u}}{\partial x} + \bar{v}\frac{\partial \bar{u}}{\partial y} - f\bar{v} + g\frac{\partial h}{\partial x} + \frac{\tau_b(x)}{H} = \frac{\tau_s(x)}{H} \qquad (4.12)$$

$$\frac{\partial \bar{v}}{\partial t} + \bar{u}\frac{\partial \bar{v}}{\partial x} + \bar{v}\frac{\partial \bar{v}}{\partial y} + f\bar{u} + g\frac{\partial h}{\partial y} + \frac{\tau_b(y)}{H} = \frac{\tau_s(y)}{H} \qquad (4.13)$$

where

$$H = \xi + h$$

$$\tau_b(x) = -\frac{Du\sqrt{u^2+v^2}}{H}$$

$$\tau_b(y) = -\frac{Dv\sqrt{u^2+v^2}}{H}$$

with bottom friction $D = g/c^2$

in which c is a Chezy coefficient giving D = 0.003 ,

$$\tau_s(x) = \lambda u\sqrt{u^2+v^2}\,,$$

$$\tau_s(y) = \lambda v\sqrt{u^2+v^2}\,,$$

with surface friction $\lambda = 3.2\times10^6$,

$$f = 2\,\omega\, Sin\Phi$$

in which ω is the Earth's angular velocity at latitude Φ ,

$$\bar{u} = \int_{-h}^{\xi} \frac{1}{H\bar{\rho}}\rho u\, dz \;,$$

$$\bar{\rho} = \int_{-h}^{\xi} \frac{1}{H}\rho\, dz$$

and

$$\bar{v} = \int_{-h}^{\xi} \frac{1}{H\bar{\rho}}\rho v dz \;.$$

4.3 BOUNDARY CONDITIONS

On the land boundary, the normal velocity component is taken as zero $(\eta.U=0)$, η being the outward directed normal. On certain open boundaries (river boundary in estuary models) the more appropriate boundary condition is to prescribe the flux of water across the boundary. Across open ocean boundaries, however, it is most appropriate to prescribe the water heights. In the present model at the open boundary (Strait of Harmouz) the radiation type conditions (Beckers (1985) , Flather (1976)) are applied.

We use a generalization of the linearized radiation condition successfully applied by John et. al. (1981). As well as allowing for the approximate outward radiation of an internally generated response from the analysis region, it also communicates the tides of the Gulf of Oman into the Strait of Harmouz. The condition has the form

$$u - \sqrt{\frac{g}{h}}\,\xi = 2A\sqrt{\frac{g}{h}}\,Cos\left(\frac{2\pi t}{T} - \Psi\right) \qquad \text{at } X = L \tag{4.15}$$

In (4.15), A and Ψ *de*note, respectively, the prescribed amplitude and phase of the tidal forcing and T is the period of the tidal constituents M_2, K_1, S_2 and O_1 under consideration.

If the tidal response entering the Strait of Harmouz across $X = L$ is in the form of a progressive wave with its crest parallel to $Y = L$, then

$$u = -\sqrt{\frac{g}{h}}\,\xi \tag{4.16}$$

and (4.15) reduces to equation (2.95), given by

$$\xi = A\,Cos\left(\frac{2\pi t}{T} - \Psi\right) \qquad \text{at } X = L \tag{4.17}$$

In this case A and Ψ correspond to amplitude and phase of the tidal elevation along $X = L$. A consequence of applying (4.15) rather than (4.17) is that the values of neither ξ nor u are prescribed separately along the open boundary of the model. Thus, during the solution process, the boundary values of both ξ and u may correlatively adjust subject only to (4.15). We anticipate that such a solution procedure, which is based on prescribing conditions on an incoming characteristic, will be superior to one using (4.17), especially if $X = L$ should coincide with a nodal line. Further generalization of (4.15) to a discrete spectrum of tidal constituents follows without difficulty.

The values of A, h and Ψ are taken from Admiralty Tide Tables (1988) . Flather (1973) noted that the application of the radiation condition in the numerical model may remove the unrealistically large currents and grid scale oscillations in the open boundary, which may be modelled by application of conventional open-sea boundary conditions.

4.4 INITIAL CONDITIONS

The initial conditions defined throughout the region are as follows:

$$\xi(x,y,t=0) \quad = \quad \xi_0(x,y) \tag{4.18a}$$

$$u(x,y,t=0) \quad = \quad u_0(x,y) \tag{4.18b}$$

$$v(x,y,t=0) \quad = \quad v_0(x,y) \tag{4.18c}$$

At the open boundary

$$\xi(x,y,t = 0) \quad = \quad A \tag{4.18d}$$

The values of ξ_0 , u_0 , v_0 are generally not known. The computation is started by assuming these values to be zero. Due to the frictional dissipation, the influence of initial conditions becomes negligible after some time and stable conditions are reached after a few cycles of the computation.

4.5 CHEZY COEFFICIENTS

The following formulae for the chezy coefficients mostly are mentioned in the literature;

i) Leendertsee (1967), Lardner et. al. (1982):

$$c \quad = \quad C_1 \ln\left(C_2 H + C_3 \right), \tag{4.19}$$

where C_1 , C_2 and C_3 are constants values depending on the nature of the bottom and H is total depth.

ii) Von Trapka (1968):

$$c = \frac{d}{H} \quad , \tag{4.20}$$

where d is a bottom friction.

iii) Wilders et. el. (1988), Falconer (1983);

$$c = \frac{H^{\frac{1}{6}}}{\eta} \tag{4.21}$$

where η denotes Manning's coefficient.

CHAPTER FIVE

THE EXPLICIT FINITE DIFFERENCE METHOD

5.0 INTRODUCTION

Two-dimensional hydrodynamical models are concerned with tides and storm-surge predictions.The increased interest recently in fisheries management, intensive oil traffic in the Gulf and pollution control has led to spectacular developments of mathematical modelling including residual circulation, dispersion of contaminants from coastal or off-shore releases, chemical and ecological dynamics.

One way of studying dynamic behaviour of the waters of the Gulf is to develop a numerical model which can predict and reproduce accurately the observed data for the tidal heights, phase lag, etc. of the main dominant tidal constituents. Most numerical models being used for simulation of tidal flows are based on shallow water equations. For the present study, in its attempt to simulate tidal flow in the Arabian Gulf, an efficient explicit method has been designed to solve the shallow water equations (SWE).

Starting from the hydrodynamic equations for shallow waters, this chapter proceeds by presenting a review of the method, boundary conditions, stability, and boundary identifications.

In the first section 5.1 a few general aspects of nonlinear shallow water equations are discussed.

In section 5.2 an explicit finite difference method (EFDM) for the numerical approximation of (5.1) is proposed. The approximation of each term of (5.1) at inner points is discussed separately. Use of staggered grids is also discussed in detail.

Sections 5.3 and 5.4 deal with the numerical approximations of (5.1) near the boundaries. The boundary approximations are based upon a heuristic principal described in section 5.3. This section also describes the boundary treatment near closed boundaries. Section 5.4 is devoted to open

boundaries.

In section 5.5 the numerical treatment of tidal flats is discussed. Section 5.6 deals with the topography of the Arabian Gulf bottom. In section 5.7 the method of grid identification is explained. Section 5.8 deals with the stability analysis of explicit finite difference scheme and finally, in section 5.9 we discuss the stopping criteria and convergence.

5.1 SHALLOW WATER EQUATIONS

The hydrodynamic non-linear equations used in this study are the shallow water equations as described in Chapter 4.

$$\frac{\partial \xi}{\partial t} + \frac{\partial (H\bar{u})}{\partial x} + \frac{\partial (H\bar{v})}{\partial y} = 0 \qquad (5.1a)$$

$$\frac{\partial \bar{u}}{\partial t} + \bar{u}\frac{\partial \bar{u}}{\partial x} + \bar{v}\frac{\partial \bar{u}}{\partial y} - f\bar{v} + g\frac{\partial \xi}{\partial x} + g\bar{u}\frac{\sqrt{\bar{u}^2+\bar{v}^2}}{c^2 H} + \lambda\bar{v}\frac{\sqrt{\bar{u}^2+\bar{v}^2}}{H} - \nu\left(\frac{\partial^2 \bar{u}}{\partial x^2} + \frac{\partial^2 \bar{v}}{\partial y^2}\right) = F^{(x)} \qquad (5.1b)$$

$$\frac{\partial \bar{v}}{\partial t} + \bar{u}\frac{\partial v}{\partial x} + \bar{v}\frac{\partial \bar{v}}{\partial y} + f\bar{u} + g\frac{\partial \xi}{\partial x} + g\bar{v}\frac{\sqrt{\bar{u}^2+\bar{v}^2}}{c^2 H} - \lambda\bar{v}\frac{\sqrt{\bar{u}^2+\bar{v}^2}}{H} - \nu\left(\frac{\partial^2 \bar{u}}{\partial x^2} + \frac{\partial^2 \bar{v}}{\partial y^2}\right) = F^{(y)}, \qquad (5.1c)$$

where

u = velocity in x direction,

v = velocity in y direction,

ξ = water elevation above some plane of reference,

h = waterdepth below some plane of reference,

$H = h + \xi$ = total waterdepth,

f = coriolis parameter,

g = acceleration due to gravity,

c = Chezy coefficient for bottom roughness,

λ = surface friction,

$F^{(x)}, F^{(y)}$ = external forcing functions of wind stress or barometric pressure in x and y directions,

ν = viscosity constant,

and

t = time.

In order to make a choice for an EFDM, we adopt the following criteria:

1. The numerical solution should be sufficiently accurate. Hence, the method should be consistent and stable. According to practical experience, second-order accuracy is satisfactory. It is also necessary that the numerical solution is not greatly influenced by spurious solutions and rounding errors.
2. The method should be robust. In our case this means that the method should be applicable to a wide range of practical 2-D flow problems in civil engineering such as tidal problems in coastal seas and estuaries with tidal flats, model problems in tidal flumes, or steady-state problems in rivers.
3. The method should be computationally efficient. Efficiency should not be obtained at the cost of robustness, so robustness has a high priority.
4. The numerical treatment of boundary conditions should be such that the overall accuracy and efficiency are not greatly decreased.

5.2 EXPLICIT FINITE DIFFERENCE SCHEME

5.2.1 EFDM SCHEME AT INNER POINTS

In this section we propose a nonlinear shallow water equations (SWE) for the approximation. We will describe each term of our EFDM separately and we will elucidate each approximation. For convenience we repeat (5.1)-(5.3), omitting the non-homogeneous part and taking $\nu = 0$.

$$\frac{\partial \xi}{\partial t} + \frac{\partial(H\bar{u})}{\partial x} + \frac{\partial(H\bar{v})}{\partial y} = 0 \qquad (5.2a)$$

$$\frac{\partial \bar{u}}{\partial t} + \bar{u}\frac{\partial \bar{u}}{\partial x} + \bar{v}\frac{\partial \bar{u}}{\partial y} - f\bar{v} + g\frac{\partial \xi}{\partial x} + g\,\bar{u}\,\frac{\sqrt{\bar{u}^2+\bar{v}^2}}{c^2 H} - \lambda\,\bar{u}\frac{\sqrt{\bar{u}^2+\bar{v}^2}}{H} = 0 \qquad (5.2b)$$

$$\frac{\partial \bar{v}}{\partial t} + \bar{u}\frac{\partial \bar{v}}{\partial x} + \bar{v}\frac{\partial \bar{v}}{\partial y} + f\bar{u} + g\frac{\partial \xi}{\partial y} + g\,\bar{v}\,\frac{\sqrt{\bar{u}^2+\bar{v}^2}}{c^2 H} - \lambda\,\bar{v}\frac{\sqrt{\bar{u}^2+\bar{v}^2}}{H} = 0 \qquad (5.2c)$$

5.2.2 STAGGERED GRIDS

The finite difference model is based on staggered grids (Beckers et al (1985), Hansen (1962)) given in Figure 5.1. The scheme is applied with mesh sizes of Δx and Δy in the x and y directions respectively at wet points with timestep Δt. The geography of the Arabian Gulf is given in Figure 4.1. The grid arrangement is shown in Figures 5.1 and 5.2. The variables are regarded as specified at different points in the grid as follows:

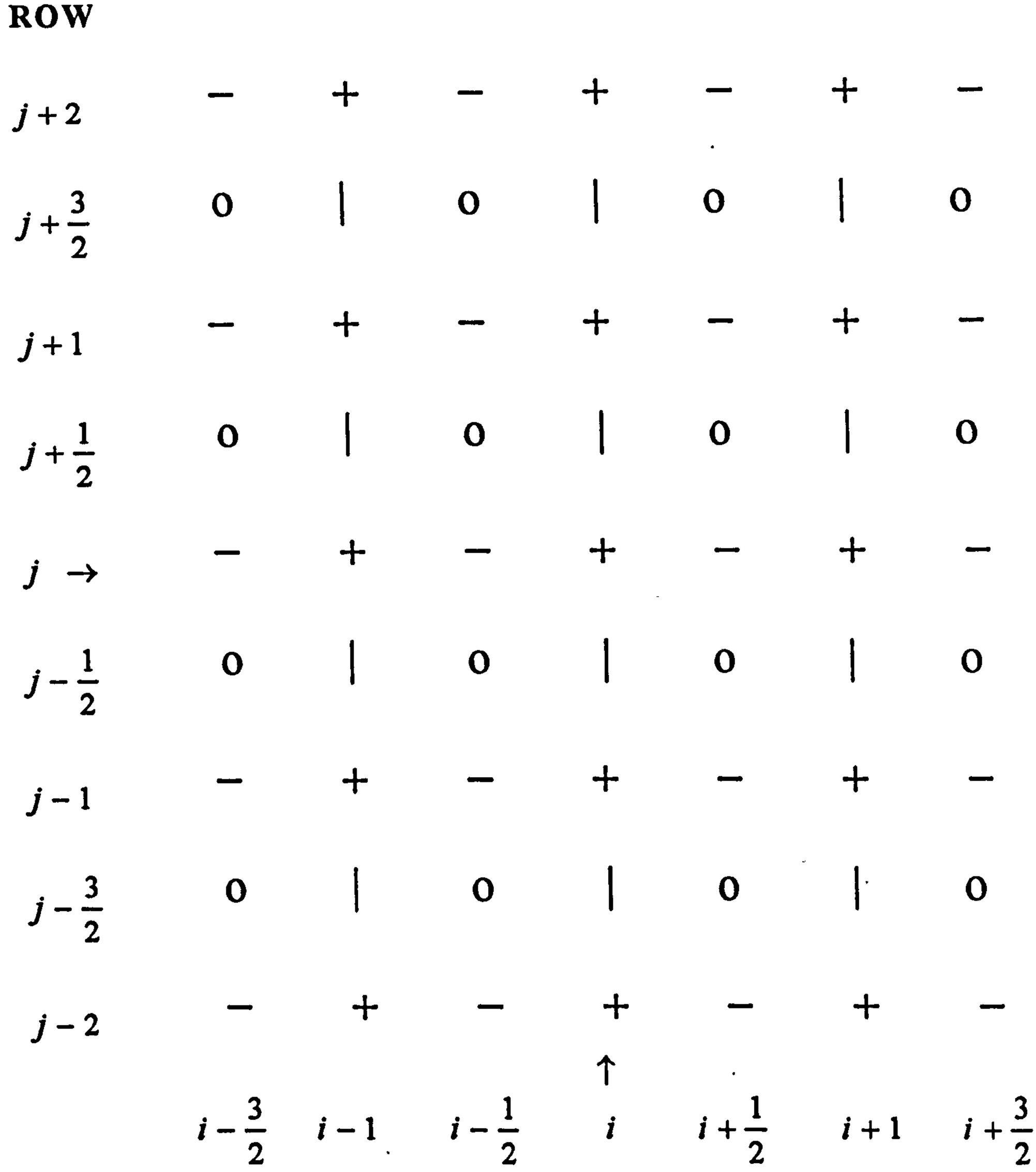

Figure 5.1 Staggered spatial grid

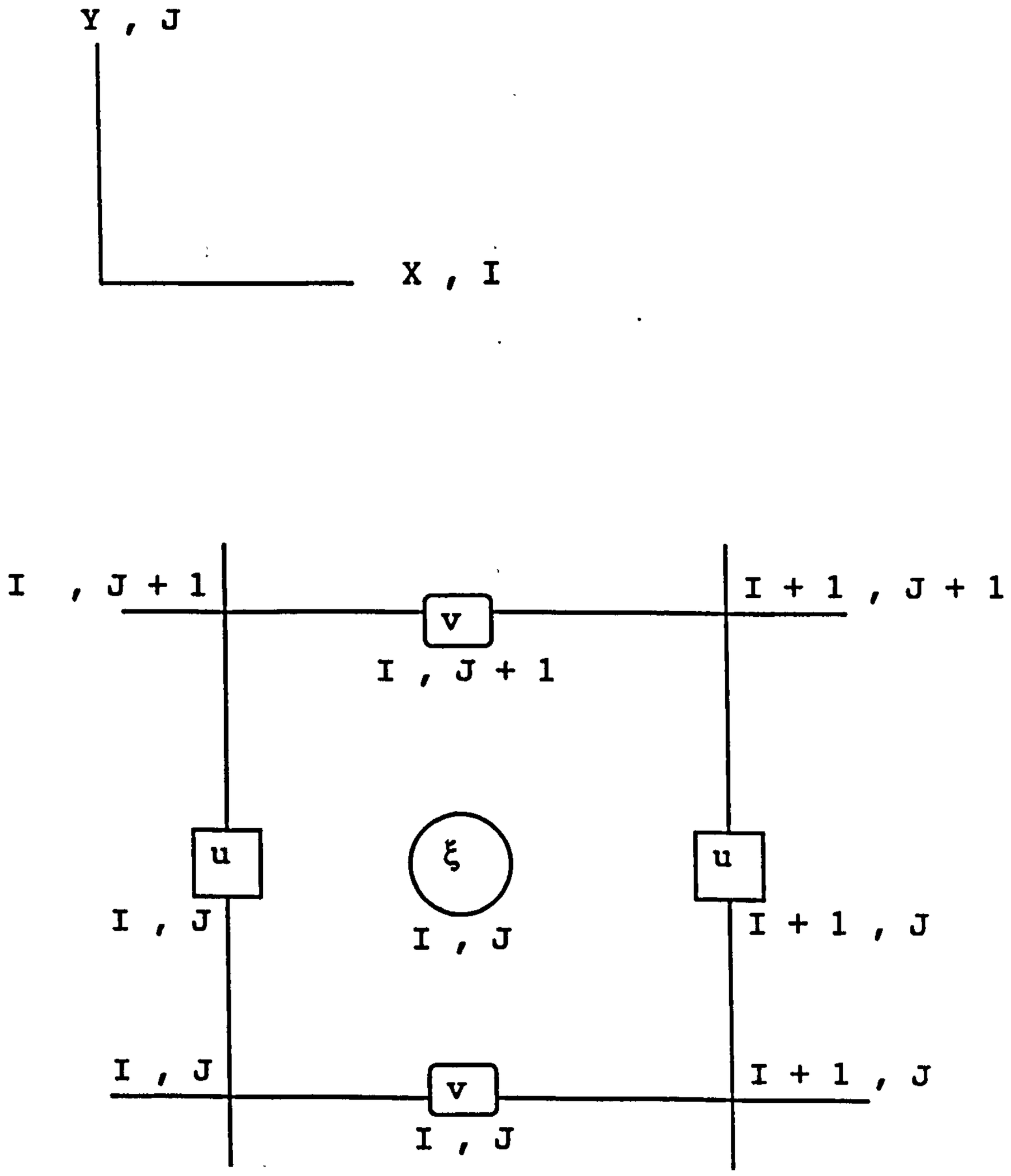

Figure 5.2 Indexing system in the horizontal plane

i) The water height ξ is specified at the grid points (i,j) themselves, marked + in the figure.

(ii) The x-component of velocity u is specified at the points $\left(i-\frac{1}{2}, j \right)$, marked — in the figure.

(iii) The y-component v is specified at the points $\left(i, j-\frac{1}{2} \right)$ marked | .

(iv) The h is specified at the points $\left(i-\frac{1}{2}, j-\frac{1}{2} \right)$ marked O

At the inner points of the grid, the details of the approximation of the explicit finite difference scheme are as follows:

$$\frac{\xi_{i,j}^{k+1} - \xi_{i,j}^{k}}{\Delta t} =$$

$$- \frac{\left[\left(h_{i+\frac{1}{2},j} + \xi^{k}_{i+\frac{1}{2},j} \right) \overline{u}^{k}_{i+\frac{1}{2},j} - \left(h_{i-\frac{1}{2},j} + \xi^{k}_{i-\frac{1}{2},j} \right) \overline{u}^{k}_{i-\frac{1}{2},j} \right]}{\Delta x}$$

$$- \frac{\left[\left(h_{i,j+\frac{1}{2}} + \xi^{k}_{i,j+\frac{1}{2}} \right) \overline{v}^{k}_{i,j+\frac{1}{2}} - \left(h_{i,j-\frac{1}{2}} + \xi^{k}_{i,j-\frac{1}{2}} \right) \overline{v}^{k}_{i,j-\frac{1}{2}} \right]}{\Delta y} \qquad (5.3a)$$

$$\frac{\bar{u}^{k+1}_{i-\frac{1}{2},j} - \bar{u}^{k}_{i-\frac{1}{2},j}}{\Delta t} =$$

$$- \frac{\bar{u}^{k}_{i-\frac{1}{2},j}\left(\bar{u}^{k}_{i+\frac{1}{2},j} - \bar{u}^{k}_{i-\frac{1}{2},j} \right)}{\Delta x} - \frac{g\left(\xi^{k+1}_{i,j} - \xi^{k+1}_{i-1,j} \right)}{\Delta x}$$

$$+ f\bar{v}^{k}_{i+\frac{1}{2},j} - \frac{g\bar{u}^{k}_{i-\frac{1}{2},j}\sqrt{\left(\bar{u}^{k}_{i-\frac{1}{2},j} \right)^2 + \left(v'_{i,j-\frac{1}{2}} \right)^2}}{c^2\left(h_{i+\frac{1}{2},j} + \xi^{k}_{i+\frac{1}{2},j} \right)}$$

$$- \frac{\lambda\bar{u}^{k}_{i-\frac{1}{2},j}\sqrt{\left(\bar{u}^{k}_{i-\frac{1}{2},j} \right)^2 + \left(v'_{i,j-\frac{1}{2}} \right)^2}}{\left(h_{i+\frac{1}{2},j} + \xi^{k}_{i+\frac{1}{2},j} \right)} -$$

$$-v'_{i,j-\frac{1}{2}} \begin{cases} \dfrac{\left(3\bar{u}^{k}_{i-\frac{1}{2},j} - 4\bar{u}^{k}_{i-\frac{1}{2},j-1} + \bar{u}^{k}_{i-\frac{1}{2},j-2} \right)}{2\Delta y} & v'_{i,j-\frac{1}{2}} > 0 \\ \dfrac{\left(-3\bar{u}^{k}_{i-\frac{1}{2},j} + 4\bar{u}^{k}_{i-\frac{1}{2},j+1} - \bar{u}^{k}_{i-\frac{1}{2},j+2} \right)}{2\Delta y} & v'_{i,j-\frac{1}{2}} \leq 0 \end{cases} \qquad (5.3b)$$

$$\frac{\bar{v}^{k+1}_{i,j-\frac{1}{2}} - \bar{v}^{k}_{i,j-\frac{1}{2}}}{\Delta t} =$$

$$- \frac{\bar{v}^{k}_{i,j-\frac{1}{2}}\left(\bar{v}^{k}_{i,j+\frac{1}{2}} - \bar{v}^{k}_{i,j-\frac{1}{2}} \right)}{\Delta y} - \frac{g\left(\xi^{k}_{i,j} - \xi^{k}_{i,j-1} \right)}{\Delta y}$$

$$+ \quad f\,\bar{u}^{\,k+1}_{i-\frac{1}{2},j} - \frac{g\bar{v}^{\,k}_{i,j-\frac{1}{2}}\sqrt{\left(\bar{u}^{\,k}_{i-\frac{1}{2},j}\right)^2+\left(\bar{v}^{\,k}_{i,j-\frac{1}{2}}\right)^2}}{c^2\left(h_{i,j+\frac{1}{2}}+\xi^{k}_{i,j+\frac{1}{2}}\right)}$$

$$+ \quad \frac{\lambda\bar{v}^{\,k}_{i,j-\frac{1}{2}}\sqrt{\left(\bar{u}^{\,k}_{i-\frac{1}{2},j}\right)^2+\left(\bar{v}^{\,k}_{i,j-\frac{1}{2}}\right)^2}}{\left(h_{i,j+\frac{1}{2}}+\xi^{k}_{i,j+\frac{1}{2}}\right)}$$

$$-u'_{i-\frac{1}{2},j}\begin{cases}\dfrac{\left(3\bar{v}^{\,k}_{i,j-\frac{1}{2}}-4\bar{v}^{\,k}_{i-1,j-\frac{1}{2}}+\bar{v}^{\,k}_{i-2,j-\frac{1}{2}}\right)}{2\Delta x} & u'_{i-\frac{1}{2},j} > 0\\[2ex] \dfrac{\left(-3\bar{v}^{\,k}_{i,j-\frac{1}{2}}+4\bar{v}^{\,k}_{i+1,j-\frac{1}{2}}-\bar{v}^{\,k}_{i+2,j-\frac{1}{2}}\right)}{2\Delta x} & u'_{i-\frac{1}{2},j} \le 0\end{cases} \tag{5.3c}$$

where

$$h_{i,j+\frac{1}{2}} = \frac{1}{2}\left(h_{i+\frac{1}{2},j+\frac{1}{2}}+h_{i-\frac{1}{2},j+\frac{1}{2}}\right) \tag{5.4a}$$

$$\xi_{i+\frac{1}{2},j} = \frac{1}{2}\left(\xi_{i,j}+\xi_{i+1,j}\right) \tag{5.4b}$$

$$h_{i-\frac{1}{2},j} = \frac{1}{2}\left(h_{i-\frac{1}{2},j+\frac{1}{2}}+h_{i-\frac{1}{2},j-\frac{1}{2}}\right) \tag{5.4c}$$

$$\xi_{i-\frac{1}{2},j} = \frac{1}{2}\left(\xi_{i,j}+\xi_{i-1,j}\right) \tag{5.4d}$$

$$h_{i+\frac{1}{2},j} = \frac{1}{2}\left(h_{i+\frac{1}{2},j+\frac{1}{2}}+h_{i+\frac{1}{2},j-\frac{1}{2}}\right) \tag{5.4e}$$

$$\xi_{i,j+\frac{1}{2}} = \frac{1}{2}\left(\xi_{i,j} + \xi_{i,j+1} \right) \tag{5.4f}$$

$$h_{i,j-\frac{1}{2}} = \frac{1}{2}\left(h_{i-\frac{1}{2},j-\frac{1}{2}} + h_{i+\frac{1}{2},j-\frac{1}{2}} \right) \tag{5.4g}$$

$$\xi_{i,j-\frac{1}{2}} = \frac{1}{2}\left(\xi_{i,j} + \xi_{i,j-1} \right) \tag{5.4h}$$

$$u'_{i-\frac{1}{2},j} = \frac{1}{4}\left(\overline{u}^{k+1}_{i-\frac{1}{2},j-1} + \overline{u}^{k+1}_{i-\frac{1}{2},j} + \overline{u}^{k+1}_{i+\frac{1}{2},j} + \overline{u}^{k+1}_{i+\frac{1}{2},j-1} \right)$$

(5.5a)

and

$$v'_{i,j-\frac{1}{2}} = \frac{1}{4}\left(\overline{v}^{k}_{i-1,j-\frac{1}{2}} + \overline{v}^{k}_{i,j-\frac{1}{2}} + \overline{v}^{k}_{i,j+\frac{1}{2}} + \overline{v}^{k}_{i-1,j+\frac{1}{2}} \right)$$

(5.5b)

It is also convenient from a programming point of view to make certain changes of notation which remove the half indices. The necessary changes are

$$h_{i-\frac{1}{2},j-\frac{1}{2}} \rightarrow h_{i,j} \tag{5.6a}$$

$$u_{i-\frac{1}{2},j} \rightarrow u_{i,j} \tag{5.6b}$$

$$v_{i,j-\frac{1}{2}} \rightarrow v_{i,j} \tag{5.6c}$$

(dropping the overbars also.) The difference equations then take the following form:

$$\frac{\xi_{i,j}^{k+1} - \xi_{i,j}^{k}}{\Delta t} = \frac{\left[h_{i+1,j+1} + h_{i+1,j} + \xi_{i+1,j}^{k} + \xi_{i,j}^{k} \right] u_{i+1,j}^{k}}{2\Delta x}$$

$$- \frac{\left[h_{i,j+1} + h_{i,j} + \xi_{i-1,j}^{k} + \xi_{i,j}^{k} \right] u_{i,j}^{k}}{2\Delta x}$$

$$- \frac{\left[h_{i,j+1} + h_{i+1,j+1} + \xi_{i+1,j}^{k} + \xi_{i,j}^{k} \right] v_{i,j+1}^{k}}{2\Delta y}$$

$$- \frac{\left[h_{i,j} + h_{i+1,j} + \xi_{i,j-1}^{k} + \xi_{i,j}^{k} \right] v_{i,j}^{k}}{2\Delta y} \qquad (5.7a)$$

$$\frac{u_{i,j}^{k+1} - u_{i,j}^{k}}{\Delta t} = - \frac{u_{i,j}^{k}\left(u_{i+1,j}^{k} - u_{i,j}^{k} \right)}{\Delta x} - \frac{g\left(\xi_{i,j}^{k+1} - \xi_{i-1,j}^{k+1} \right)}{\Delta x}$$

$$+ f v_{i,j}' - \frac{2 g u_{i,j}^{k} \sqrt{\left(u_{i,j}^{k} \right)^2 + \left(v_{i,j}' \right)^2}}{c^2\left(h_{i+1,j} + h_{i+1,j+1} + \xi_{i+1,j}^{k} + \xi_{i,j}^{k} \right)}$$

$$+ \frac{2 \lambda u_{i,j}^{k} \sqrt{\left(u_{i,j}^{k} \right)^2 + \left(v_{i,j}' \right)^2}}{\left(h_{i+1,j} + h_{i+1,j+1} + \xi_{i+1,j}^{k} + \xi_{i,j}^{k} \right)}$$

$$- v_{i,j}' \begin{cases} \dfrac{\left(3 u_{i,j}^{k} - 4 u_{i,j-1}^{k} + u_{i,j-2}^{k} \right)}{2\Delta y} & v_{i,j}' > 0 \\ \dfrac{\left(-3 u_{i,j}^{k} + 4 u_{i,j+1}^{k} - u_{i,j+2}^{k} \right)}{2\Delta y} & v'_{i,j} \leq 0 \end{cases} \qquad (5.7b)$$

where

$$v'_{i,j} = \frac{1}{4}\left(v^k_{i-1,j} + v^k_{i,j} + v^k_{i,j-1} + v^k_{i-1,j+1} \right) \tag{5.7c}$$

$$\frac{v^{k+1}_{i,j} - v^k_{i,j}}{\Delta t} = - \frac{v^k_{i,j}\left(v^k_{i,j+1} - v^k_{i,j} \right)}{\Delta y} - \frac{g\left(\xi^k_{i,j} - \xi^k_{i-1,j} \right)}{\Delta y}$$

$$+ f u^{k+1}_{i,j} - \frac{2 g v^k_{i,j} \sqrt{\left(u'_{i,j} \right)^2 + \left(v^k_{i,j} \right)^2}}{c^2\left(h_{i,j+1,} + h_{i+1,j+1} + \xi^k_{i,j+1,} + \xi^k_{i,j} \right)}$$

$$+ \frac{2 \lambda v^k_{i,j} \sqrt{\left(u'_{i,j} \right)^2 + \left(v^k_{i,j} \right)^2}}{\left(h_{i,j+1,} + h_{i+1,j+1} + \xi^k_{i,j+1,} + \xi^k_{i,j} \right)}$$

$$- u'_{i,j} \begin{cases} \dfrac{\left(3v^k_{i,j} - 4v^k_{i-1,j} + v^k_{i-2,j} \right)}{2\Delta x} & u'_{i,j} > 0 \\ \dfrac{\left(-3v^k_{i,j} + v^k_{i+1,j} - v^k_{i+2,j} \right)}{2\Delta x} & u'_{i,j} \leq 0 \end{cases} \tag{5.7d}$$

where

$$u'_{i,j} = \frac{1}{4}\left(u^{k+1}_{i-1,j} + u^{k+1}_{i,j} + u^{k+1}_{i,j+1} + u^{k+1}_{i-1,j+1} \right) \tag{5.7e}$$

5.3 BOUNDARY CONDITIONS

5.3.1 CLOSED BOUNDARIES

The SWE given by (5.3) are of course incomplete without boundary conditions. In general, two types of boundary conditions are to be distinguished: closed and open. Closed boundaries are land-water boundaries; they are physical because they relate to a really existing boundary. Open boundaries are

mathematical; they are introduced to restrict the size of the domain of the problem. This section describes the numerical treatment of closed boundaries.

At a closed boundary, one boundary condition is to be prescribed if $\nu = 0$ in (5.1) ; then the equations are hyperbolic. If $\nu \neq 0$, two boundary conditions are to be prescribed. In that case the equations are " incompletely parabolic ", see Oliger and Sundstorm (1978).

At closed boundaries the following boundary conditions are given:

$$u_{\perp} = 0, \tag{5.8a}$$

$$(1-\alpha)\, u_{//} \;+\; \Delta\, \alpha \frac{\partial}{\partial n} u_{//} \;=\; 0 \tag{5.8b}$$

where $u_{\perp}$ denotes the velocity normal to the boundary, $u_{//}$ denotes the velocity parallel to the boundary and $\frac{\partial}{\partial n}$ denotes the derivative normal to the boundary. If $\alpha = 1$ then (5.8b) describes a " perfect slip " boundary condition but if $\alpha = 0$ then (5.8b) represents a " no slip " boundary condition. In general $\alpha = 1$; Δ equals Δx or Δy.

For the EFDM (5.7), closed boundaries are represented by zero velocities in either the x-direction or the y direction. In our model, the east-west separation distance Δx between points at which the elevation is computed is 5′ latitude (approximately 8.7 km). The north-south distance Δy between computational points is 5′ longitude (approximately 9 km). The grid-point arrangement is staggered in such a way that ξ is computed at the centre of a grid cell while u and v are computed at the mid-points of its y-directed and x-directed sides respectively. The vanishing of the normal component of velocity at a coastline is then readily achieved by an appropriate stair-step representation of the boundary.The use of staggered grids is found to be very efficient for the discretization of shallow water equations. The number of grid points however has been reduced by a factor of 4. Moreover, the use of staggered grids reduces the possibility of spurious " $2\Delta x$ waves".

For some geometries this yields the typical " zig-zag " lines of which an example is Figure 5.3.

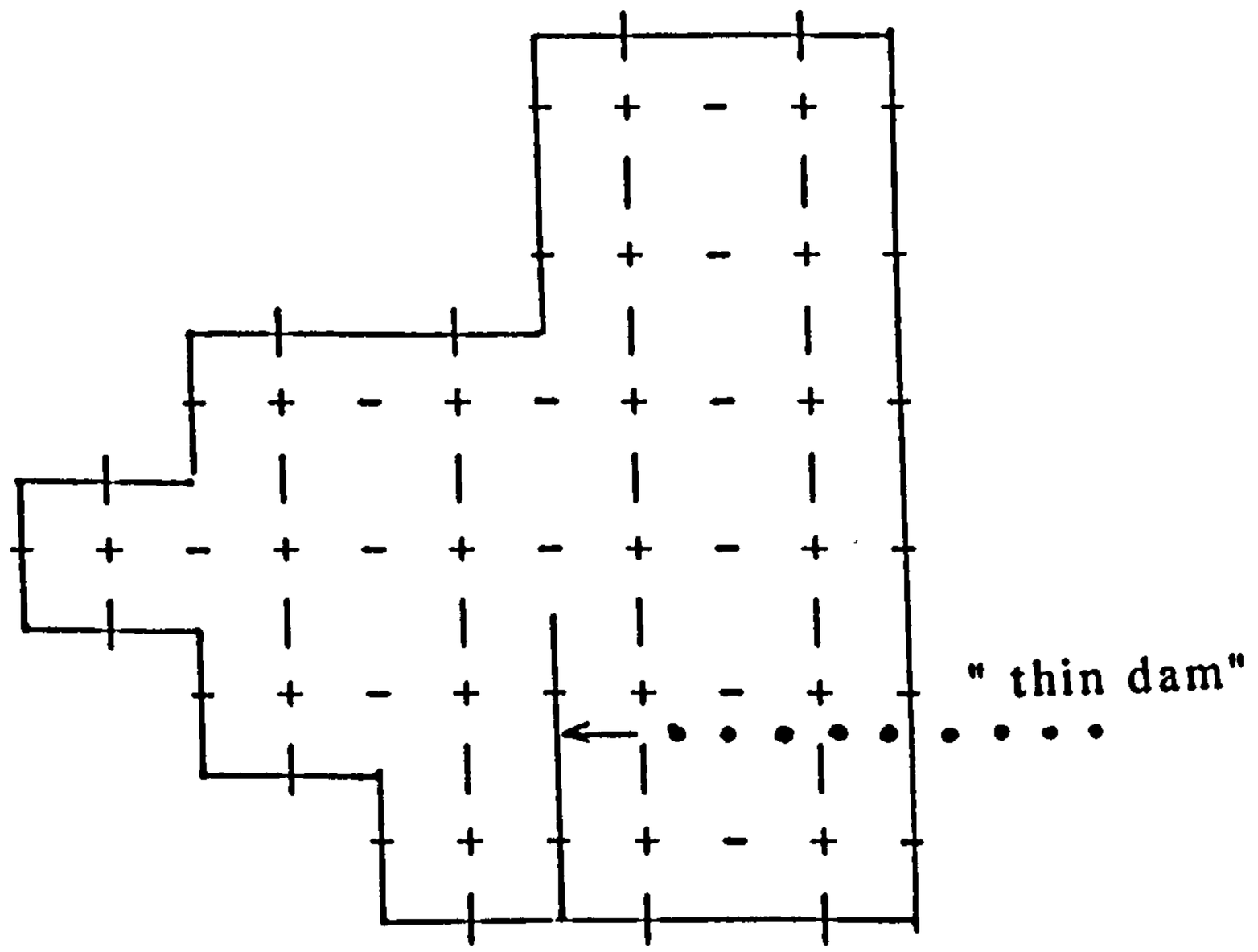

Figure 5.3 Example of closed boundaries as represented by the staggered grid.

The staggered grid allows a simple treatment of the boundary conditions. At a closed boundary only one dependant variable is to be calculated. Because this variable equals zero, no special boundary scheme is needed at the boundary itself. Near closed boundaries, however, the discretizations of section (5.2) cannot always be applied. This problem concerns only the discretizations of the momentum equations. For the descretization of the continuity equation, special boundary schemes are not necessary.

We will describe the boundary schemes for the momentum equation in the x-direction. The boundary treatment of the momentum equation in the y-direction is similar.

We will give a separate description of the discretization of the momentum equation for each term that needs a special

boundary treatment. It is to be noted that $\frac{\partial u}{\partial t}$, $\frac{\partial v}{\partial t}$, $g\frac{\partial \xi}{\partial x}$ and $g\frac{\partial \xi}{\partial y}$ never need special discretization. This is an important advantage because these are in general the most important terms of the momentum equation. In fact the special boundary discretizations are only necessary for the advection terms, which only have limited influence in case of some applications, see Verboom (1982) or Stelling (1984).

5.3.2 NEAR THE CLOSED BOUNDARIES

The boundary treatment, near closed boundaries, for the advection terms is as follows:

5.3.2a $u\frac{\partial u}{\partial \xi}$

For the inner points the discretization of this term is given in (5.7b) as

$$\frac{u^k_{i,j}\left(u^k_{i+1,j} - u^k_{i,j} \right)}{\Delta x} \qquad (5.9a)$$

which is second-order accurate in space. If we look at the point depicted in Figure 5.4 then it seems that

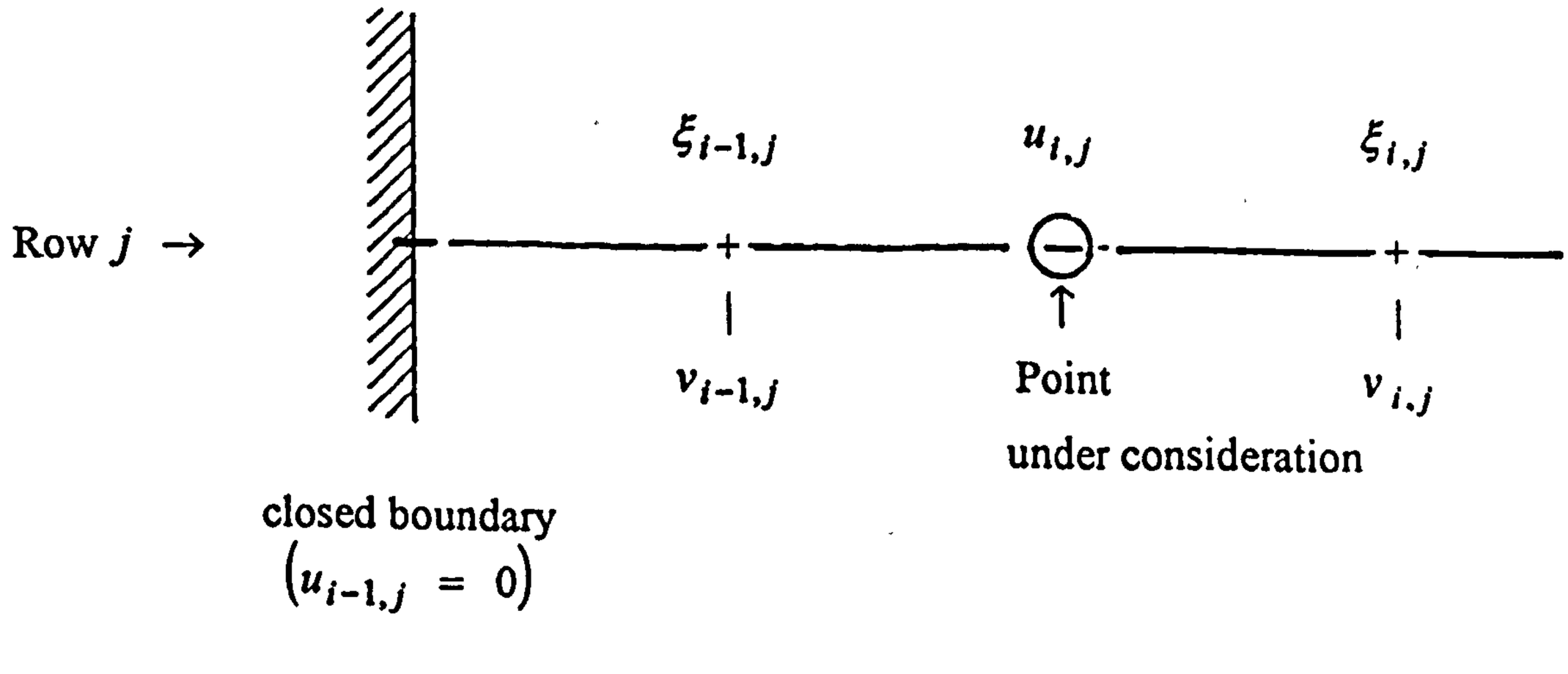

Figure 5.4

for $u\frac{\partial u}{\partial x}$ a special boundary discretization is not necessary.

Theoretically this is true. But for practical applications when (5.9a) is applied near boundaries, it can produce instability or artificial boundary layers. Consider for example the situation of Figure 5.5.

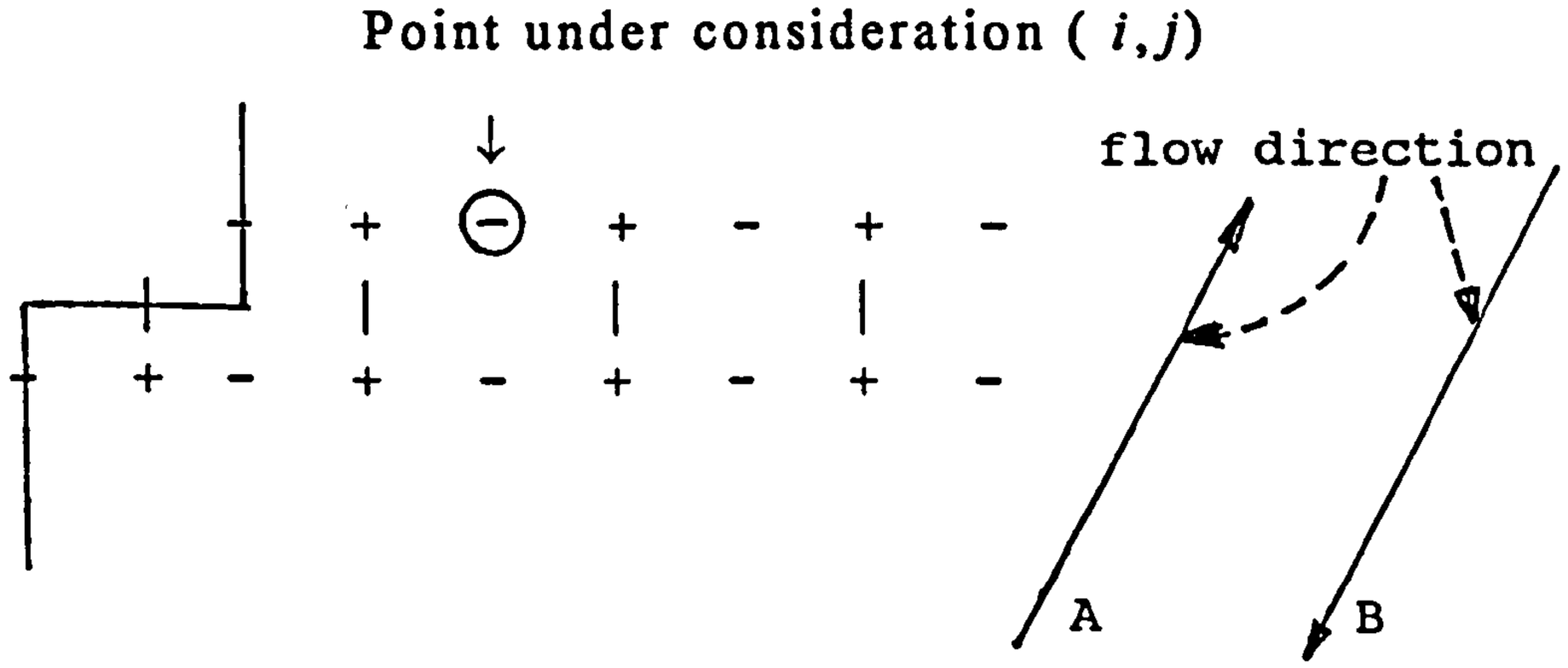

Figure 5.5

Application of (5.9a) for the discretization of the advection term at the point under consideration yields:

$$\left(u\frac{\partial u}{\partial x} \right)_{i,j} = u_{i,j}\,\frac{(u_{i+1,j} - 0)}{2\Delta x} \qquad (5.9b)$$

In practical applications the velocity in the point under consideration can be quite large. In case of flow direction A i.e, $u > 0$ (5.9b) acts as an artificial bottom friction term, yielding a large local water level gradient and an artificial boundary layer. In case of flow direction B, (5.9b) might act as a destablizing term as has been confirmed by numerical experiments.

To avoid too-large dissipative discretizations near the boundary or unstable discretizations, we adopt the following procedure for the situation of Figure 5.5:

$$u\frac{\partial u}{\partial x} = \begin{cases} 0 & u_{i,j} > 0 \\ u_{i,j}\dfrac{u_{i+1,j} - u_{i,j}}{\Delta x} & u_{i,j} \le 0 \end{cases} \qquad (5.9c)$$

This approximation is only first-order accurate, but does not appear to affect second-order convergence because this approximation is applied only near the boundary, see also Stelling (1984).

The discretization (5.9c) turns out to give satisfactory results for a large variety of geometries. By practical experience we found that, in general, satisfactory discretizations for advection terms near boundaries are generated by taking into account the following principles:

i) Always avoid negative diffusion in the truncation error of the discretization.

ii) If the discretization formula contains the boundary value $u = 0$ then try to avoid this by using a discretization that needs fewer grid points, or by upwind differencing. If it is not possible to avoid the boundary value $u = 0$ in the discretization formula, then the advection term has to be approximated by a zero value.

By using (i) instabilities are avoided while (ii) suppresses artificial boundary layers.

Summarizing, for the discretization of $u\frac{\partial u}{\partial x}$ we adopt the following procedure for the situations of Figures 5.6 and 5.7:

Case (1a)

Closed boundary at left end at $(i-1,j)$. In this case the boundary condition is $u_{i-1,j} = 0$.

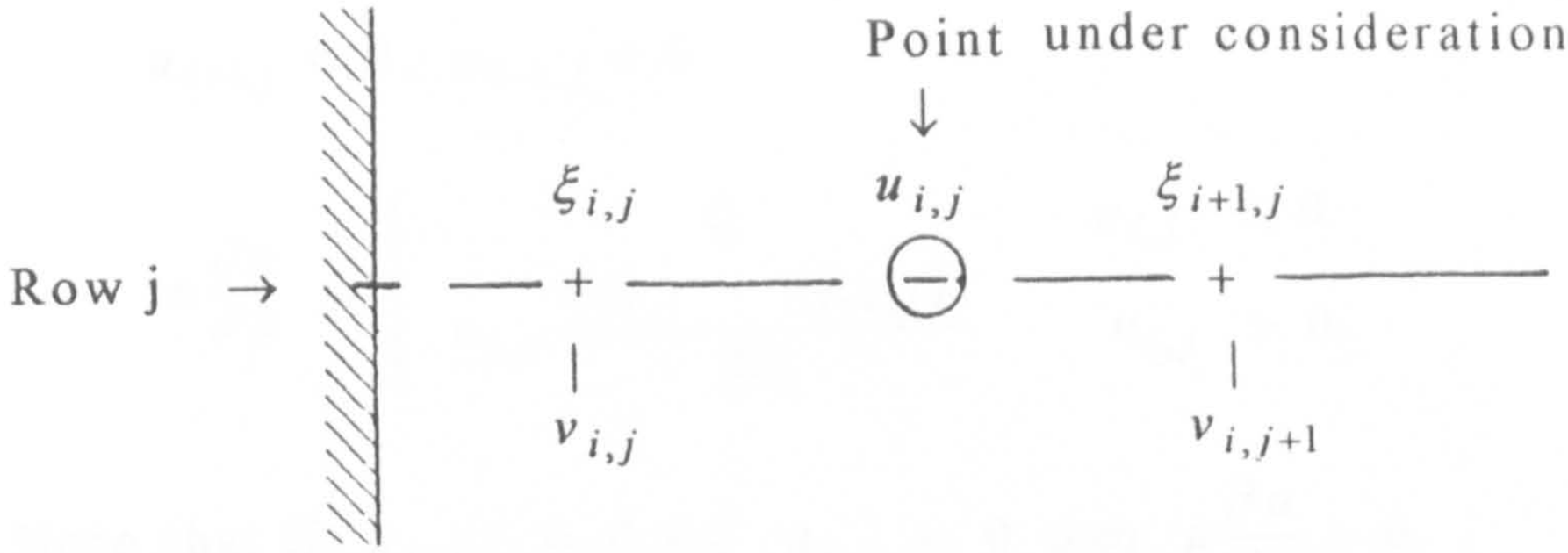

Figure 5.6

$$u_{i-1,j} = 0\,, \quad u_{i+1,j} \neq 0$$

$$u\frac{\partial u}{\partial x} = \begin{cases} 0 & u_{i,j} \geq 0 \\ u_{i,j}\,\dfrac{(u_{i+1,j} - u_{i,j})}{\Delta x} & u_{i,j} < 0 \end{cases} \qquad (5.9\text{d})$$

Note that if $u_{i-1,j} = 0$ and $u_{i,j} = 0$ then $u\dfrac{\partial u}{\partial x} = 0$.

The discretization of $v\dfrac{\partial v}{\partial y}$ is the same as is shown in (5.7d).

CASE (1b)

Closed boundary at right end at $(i+1, j)$. In this case the boundary condition is $u_{i+1,j} = 0$.

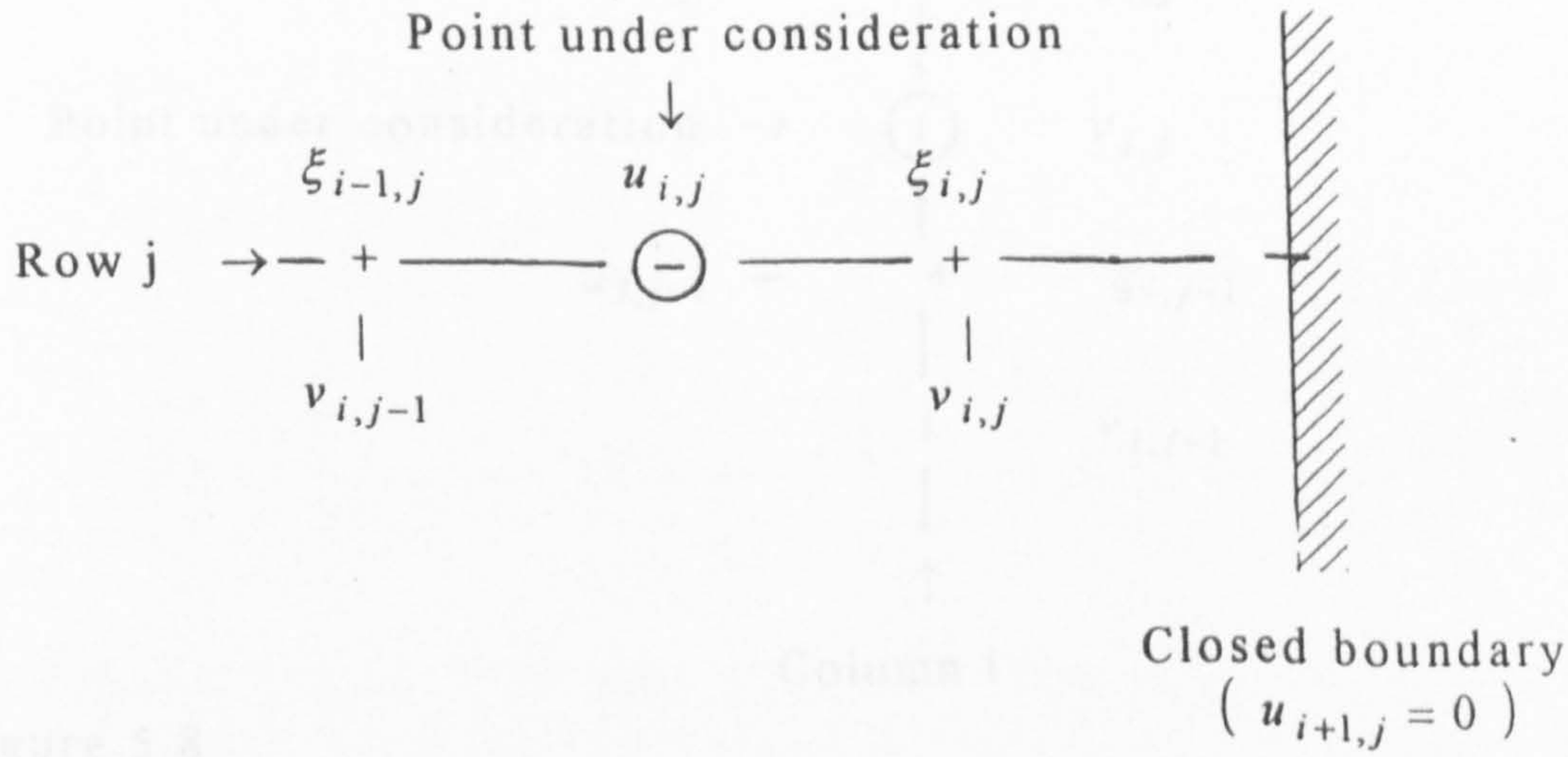

Figure 5.7

$$u_{i+1,j} = 0\,,\ u_{i-1,j} \neq 0$$

$$u\frac{\partial u}{\partial x} = \begin{cases} 0 & u_{i,j} \leq 0 \\ u_{i,j}\,\dfrac{(u_{i,j} - u_{i-1,j})}{\Delta x} & u_{i,j} > 0 \end{cases} \qquad (5.9e)$$

Note that if $u_{i-1,j} = 0$ and $u_{i,j} = 0$ then $u\dfrac{\partial u}{\partial x} = 0$.

Discretization of $v\dfrac{\partial v}{\partial y}$ in case (1a) and case (1b) is similar, as shown in (5.7d).

5.3.2b $v\dfrac{\partial v}{\partial y}$

The discretizations of $v\dfrac{\partial v}{\partial y}$ near boundaries are similar to those of $u\dfrac{\partial u}{\partial x}$.

CASE (2a)

Closed end at top at $(i, j+1)$. The boundary condition is $v_{i,j+1} = 0$

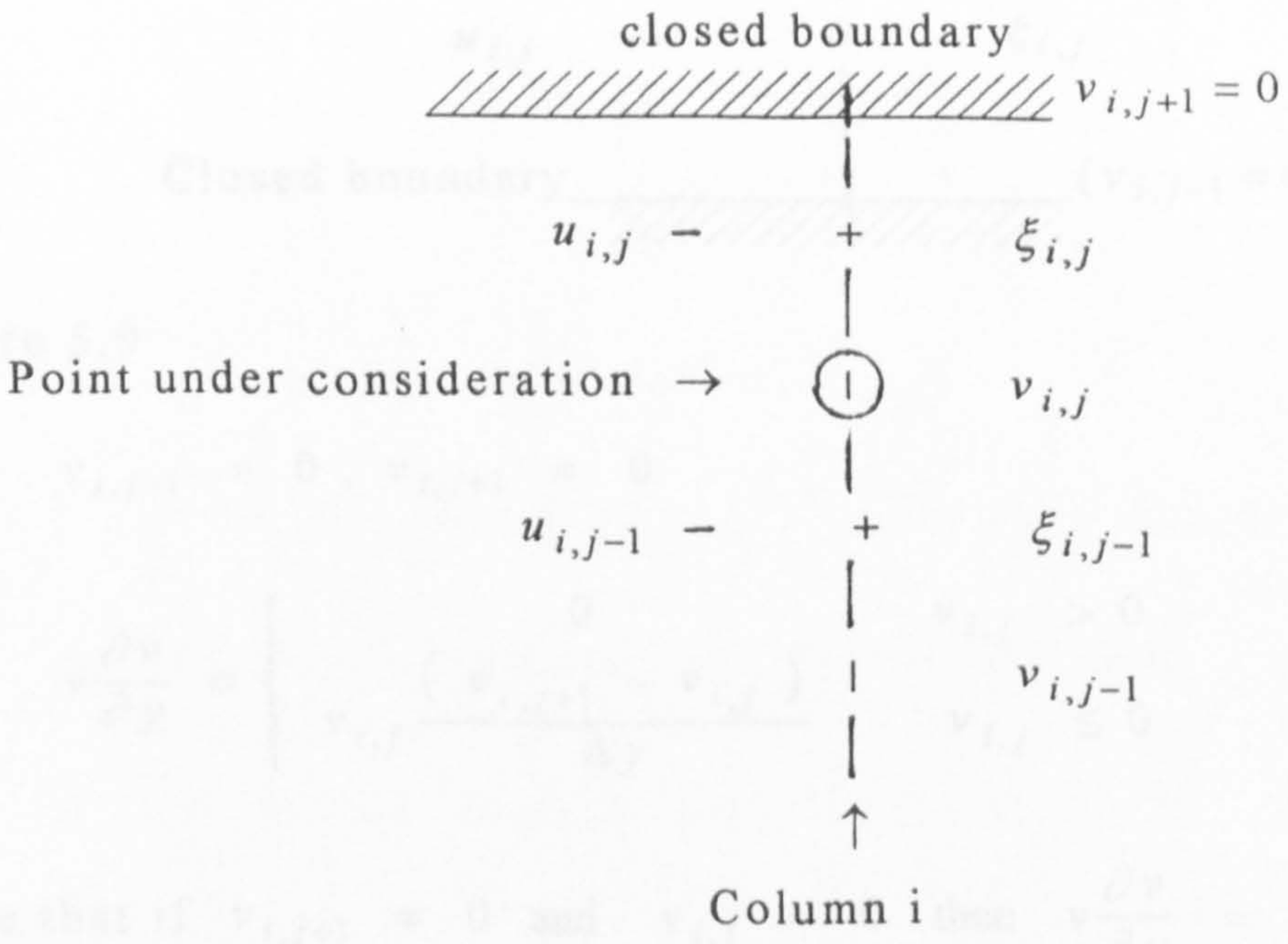

Figure 5.8

$$v_{i,j+1} = 0, \quad v_{i,j-1} \neq 0$$

$$v\frac{\partial v}{\partial y} = \begin{cases} 0 & v_{i,j} \leq 0 \\ v_{i,j}\dfrac{(v_{i,j} - v_{i,j-1})}{\Delta y} & v_{i,j} > 0 \end{cases} \qquad (5.10a)$$

Note if $v_{i,j+1} = 0$ and $v_{i,j} = 0$ then $v\dfrac{\partial v}{\partial y} = 0$

CASE (2b)

Closed boundary at the bottom end at $(i, j-1)$. The boundary condition is $v_{i,j-1} = 0$.

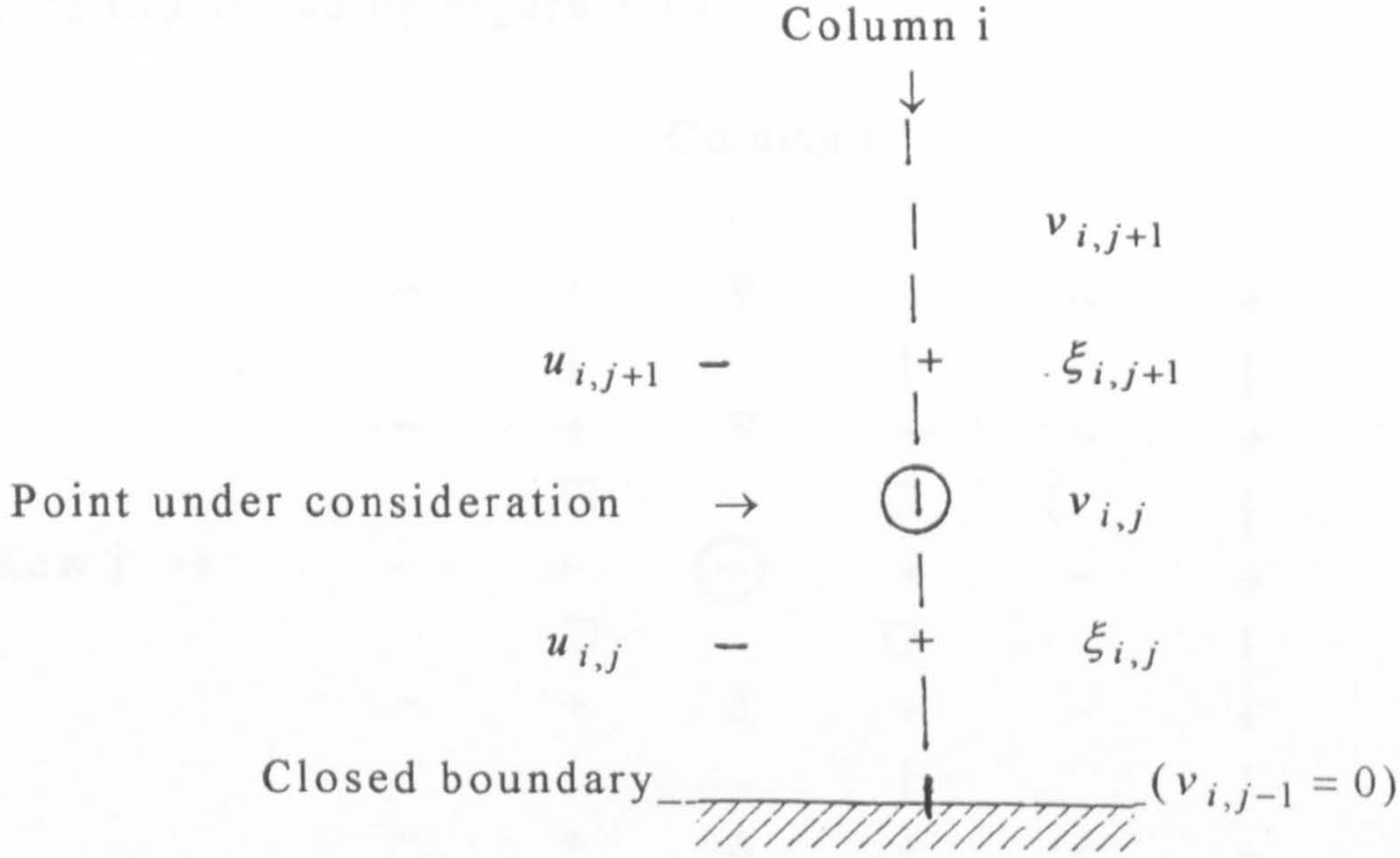

Figure 5.9

$$v_{i,j-1} = 0, \quad v_{i,j+1} = 0$$

$$v\frac{\partial v}{\partial y} = \begin{cases} 0 & v_{i,j} > 0 \\ v_{i,j}\dfrac{(v_{i,j+1} - v_{i,j})}{\Delta y} & v_{i,j} \leq 0 \end{cases} \qquad (5.10b)$$

Note that if $v_{i,j+1} = 0$ and $v_{i,j} = 0$ then $v\dfrac{\partial v}{\partial y} = 0$

The discretization of $u\frac{\partial u}{\partial x}$ in case (2a) and case (2b) is similar as shown in (5.7b).

5.3.2c $v\frac{\partial u}{\partial y}$

For the discretization of $v\frac{\partial u}{\partial y}$ we take into account the principals that were used for $u\frac{\partial u}{\partial x}$. Also for this case first-order accuracy at the boundary is assumed not to affect overall second-order convergence. For $v\frac{\partial u}{\partial y}$ the boundary procedure is more complex, which stems from the fact that the "full" discretization at the inner points as given by (5.7b) involves more grid points, as is illustrated by Figure 5.10.

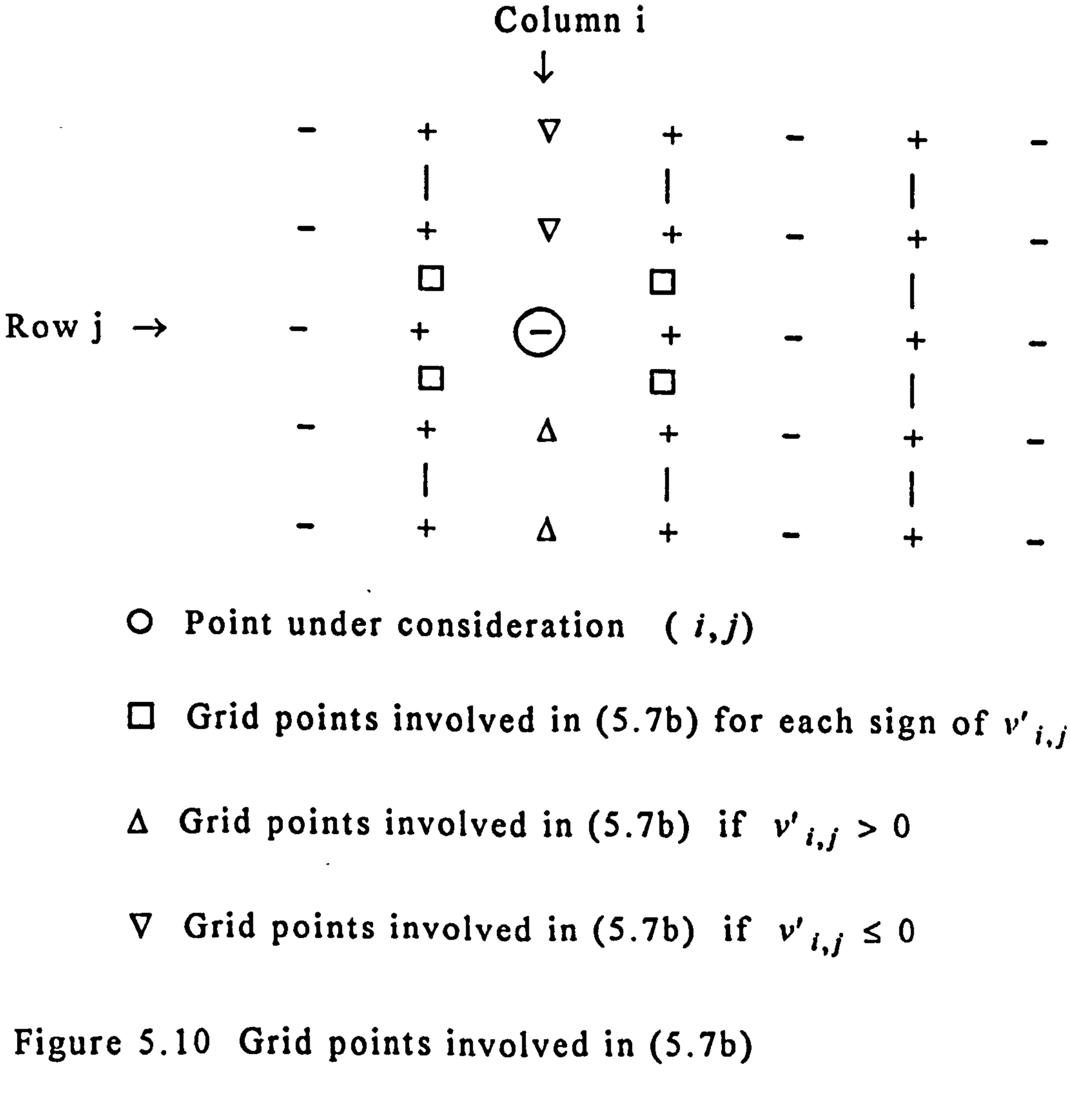

Figure 5.10 Grid points involved in (5.7b)

Because of the large number of grid points involved in Figure 5.10 there are many possibilities that might cause a considerable amount of computational overhead. To reduce the overhead we consider only the following situations of Figures 5.11 - 5.14:

CASE (3a)

Closed boundary at top end at ($i,j+1$). The boundary condition is $u_{i,j+1} = 0$

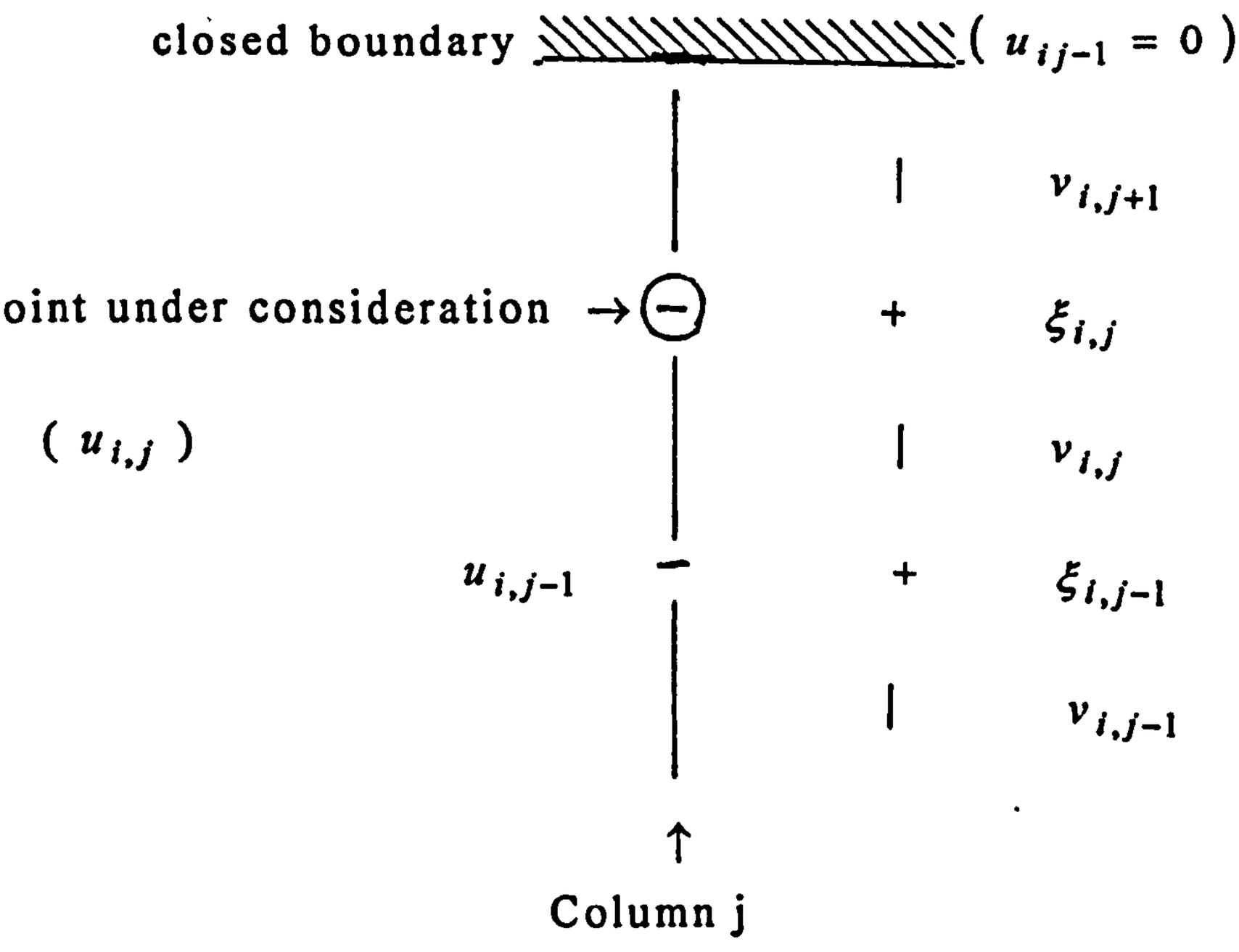

Figure 5.11

$u_{i,j+1} = 0, \quad u_{i,j-1} \neq 0$

$$v\frac{\partial u}{\partial y} = \begin{cases} 0 & v'_{i,j} \leq 0 \\ v'_{i,j}\dfrac{(u_{i,j} - u_{i,j-1})}{\Delta y} & v'_{i,j} > 0 \end{cases} \qquad (5.11a)$$

Note that if $u_{i,j+1} = 0$ and $u_{i,j} = 0$ then $v\dfrac{\partial u}{\partial y} = 0$

CASE (3b)

Closed boundary at the top end at $(i, j+2)$. The boundary condition is $u_{i,j+2} = 0$

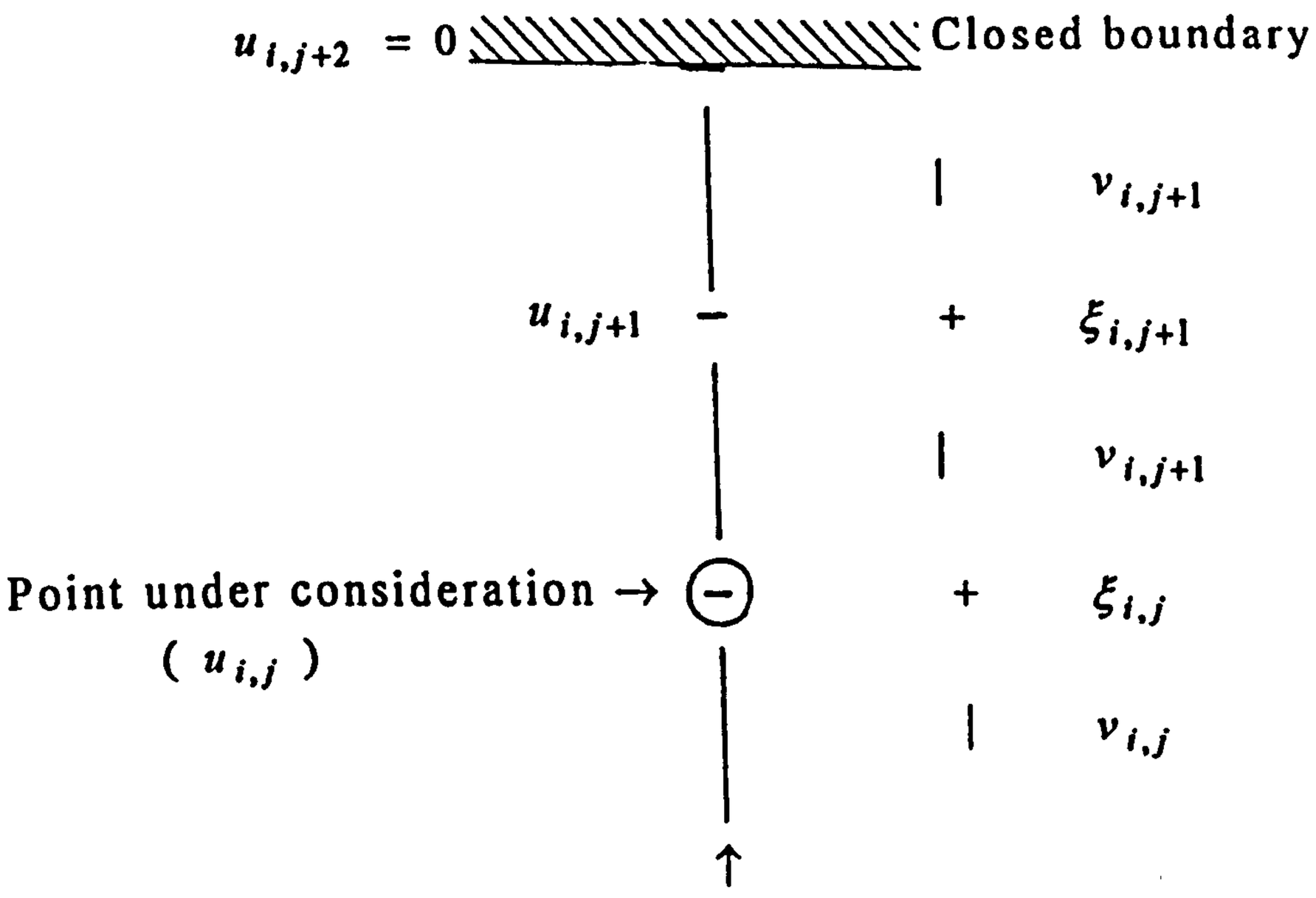

Figure 5.12

$u_{i,j+2} = 0$, $u_{i,j+1} \neq 0$ and $u_{i,j-1} \neq 0$

$$v\frac{\partial u}{\partial y} = \begin{cases} v'_{i,j}\dfrac{(u_{i,j+1} - u_{i,j})}{\Delta y} & v'_{i,j} \leq 0 \\ v'_{i,j}\dfrac{(u_{i,j} - u_{i,j-1})}{\Delta y} & v'_{i,j} > 0 \end{cases} \qquad (5.11b)$$

Note that if $u_{i,j+2} = 0$, $u_{i,j+1} = 0$ and / or $u_{i,j} = 0$ then

$$v\frac{\partial u}{\partial y} = 0$$

In case (3a) and (3b) the discretization of $u\frac{\partial u}{\partial x}$ is the same as shown in (5.7d).

CASE (3c)

Closed boundary at the bottom end at $(i,j-1)$ and boundary condition is $u_{i,j-1} = 0$.

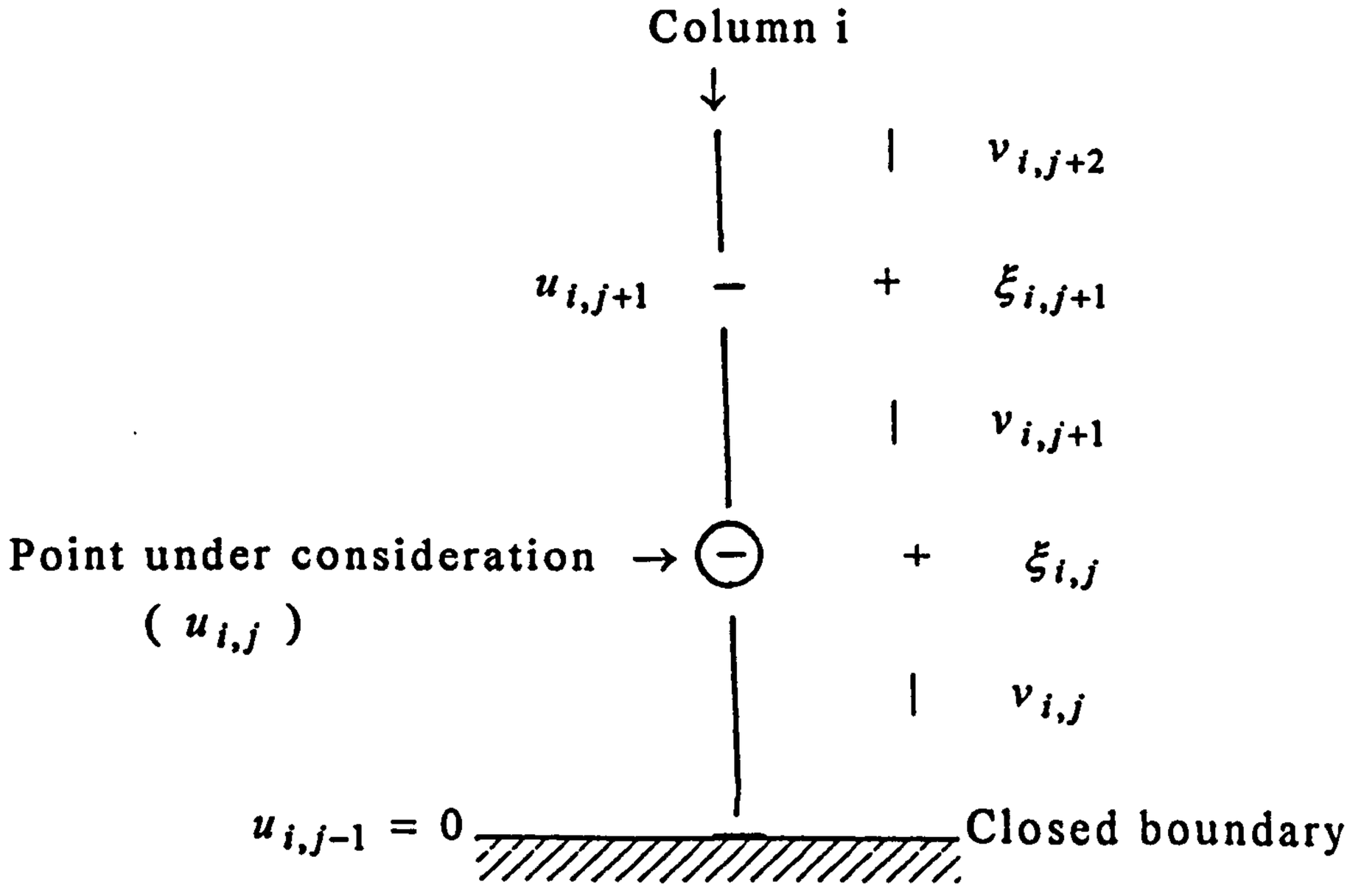

Figure 5.13

$$u_{i,j-1} = 0, \quad u_{i,j+1} \neq 0$$

$$v\frac{\partial u}{\partial y} = \begin{cases} 0 & v'_{i,j} \geq 0 \\ v'_{i,j}\dfrac{(u_{i,j+1} - u_{i,j})}{\Delta y} & v'_{i,j} < 0 \end{cases} \qquad (5.11c)$$

Note that if $u_{i,j-1} = 0$ and $u_{i,j} = 0$ then $v\dfrac{\partial u}{\partial y} = 0$

CASE (3d)

Closed boundary at bottom end at $(i,j-2)$. The boundary condition is $u_{i,j-2} = 0$

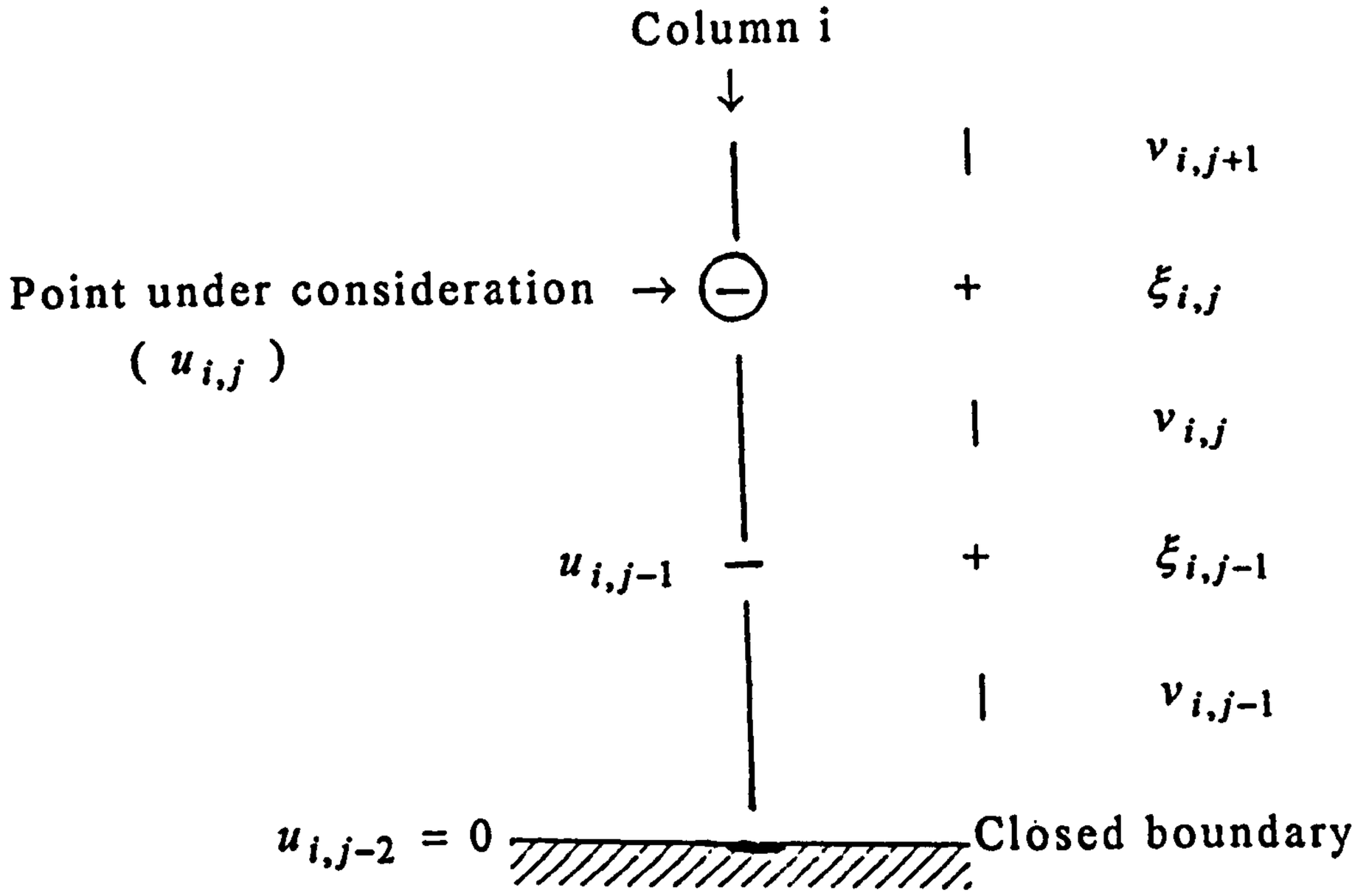

Figure 5.14

$u_{i,j-2} = 0$, $u_{i,j-1} \neq 0$ and $u_{i,j+1} \neq 0$

$$v\frac{\partial u}{\partial y} = \begin{cases} v'_{i,j}\dfrac{(u_{i,j+1} - u_{i,j})}{\Delta y} & v'_{i,j} > 0 \\ v'_{i,j}\dfrac{(u_{i,j} - u_{i,j-1})}{\Delta y} & v'_{i,j} \leq 0 \end{cases} \qquad (5.11d)$$

Note that if $u_{i,j-2} = 0$, $u_{i,j-1} = 0$ and / or $u_{i,j+1} = 0$ then

$$v\frac{\partial u}{\partial y} = 0$$

In case (3c) and (3d) $u\frac{\partial v}{\partial x}$ is similar as shown in (5.7d).

5.3.2d $u\frac{\partial v}{\partial x}$

The discretizations of $u\frac{\partial v}{\partial x}$ near boundaries are similar to those of $v\frac{\partial u}{\partial y}$. The " full " discretization at the inner points as given by (5.7d) involves more grid points, as illustrated by Figure 5.15

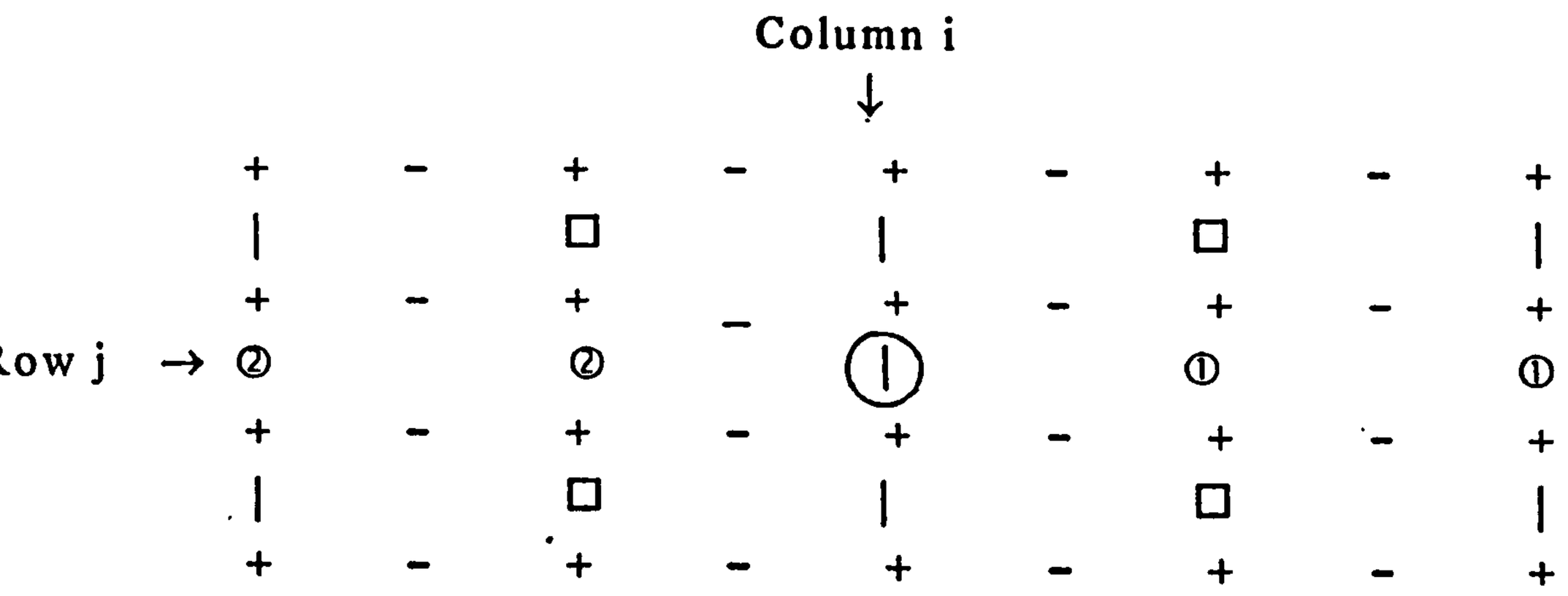

Figure 5.15 Grid points involved in (5.7d)

CASE (4a)

Closed boundary at right end at ($i-1,j$). The boundary condition is $v_{i-1,j} = 0$.

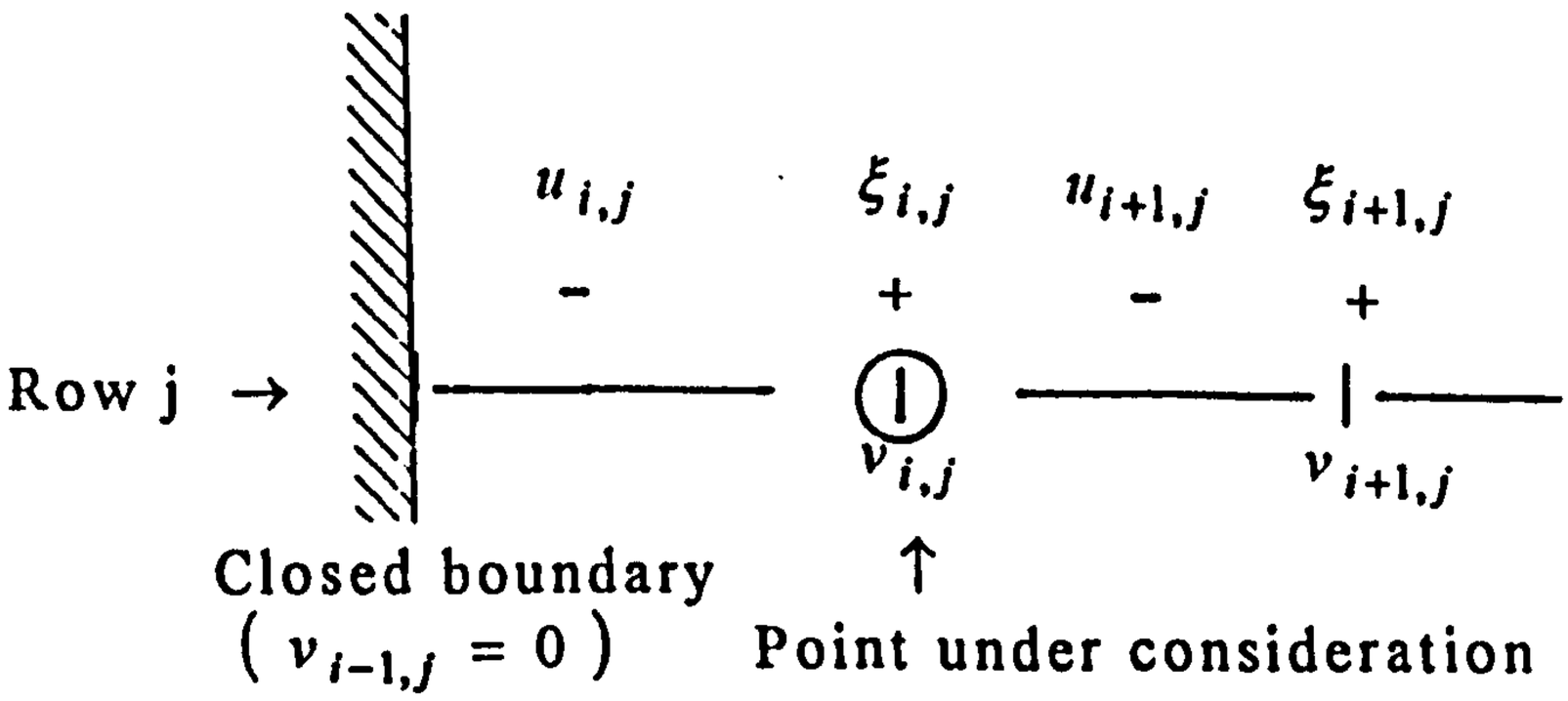

Figure 5.16

$$v_{i-1,j} = 0 \quad v_{i+1,j} \neq 0$$

$$u\frac{\partial v}{\partial x} = \begin{cases} 0 & u'_{i,j} > 0 \\ u'_{i,j}\dfrac{(\,v_{i+1,j} - v_{i,j}\,)}{\Delta x} & u'_{i,j} \leq 0 \end{cases} \qquad (5.12a)$$

Note that if $v_{i-1,j} = 0$ and $v_{i,j} = 0$ then $u\dfrac{\partial v}{\partial x} = 0$

CASE (4b)

Closed boundary at right end $(i-2,j)$ and $v_{i-2,j} = 0$.

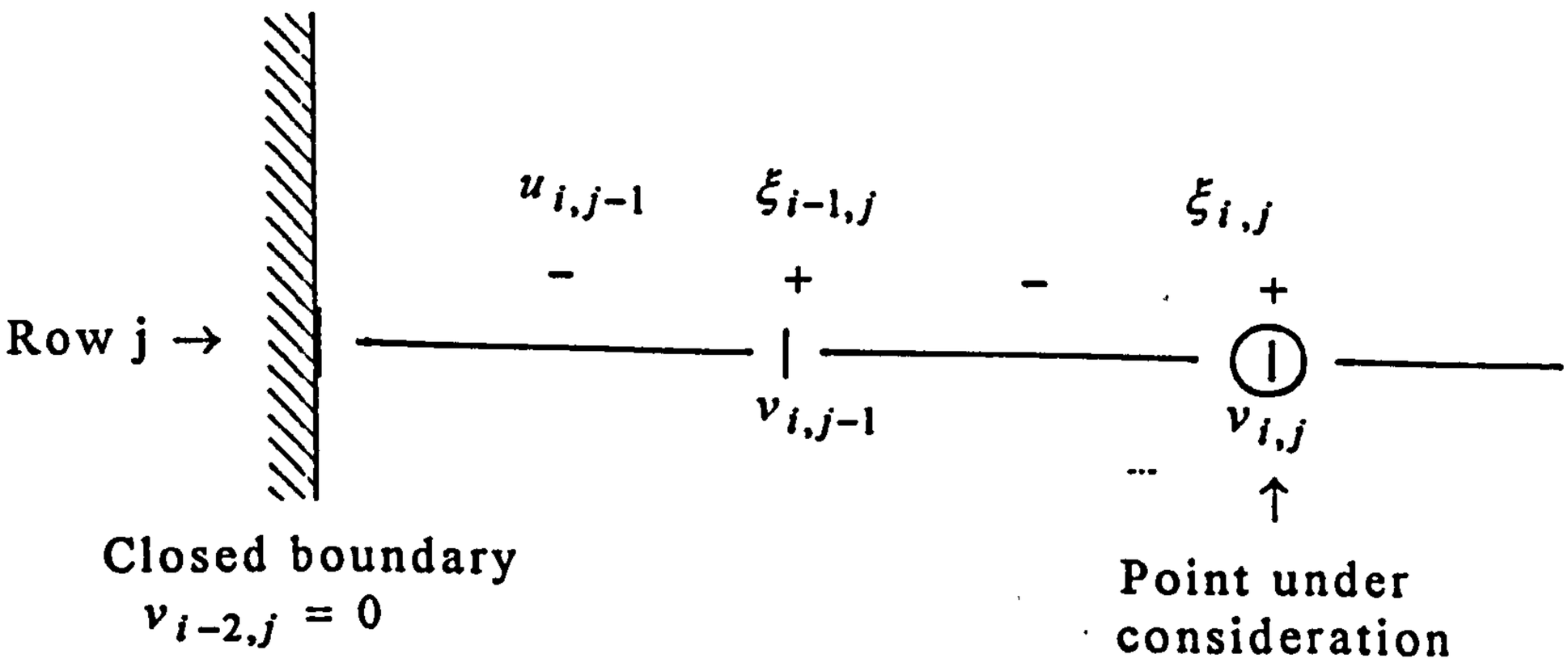

Figure 5.17

$$v_{i-2,j} = 0\,,\ v_{i-1,j} \neq 0 \quad \text{and} \quad v_{i+1,j} = 0$$

$$u\frac{\partial v}{\partial x} = \begin{cases} u'_{i,j}\dfrac{(\,v_{i+1,j} - v_{i,j}\,)}{\Delta x} & u'_{i,j} > 0 \\ u'_{i,j}\dfrac{(\,v_{i,j} - v_{i-1,j}\,)}{\Delta x} & u'_{i,j} \leq 0 \end{cases} \qquad (5.12b)$$

Note that if $v_{i-2,j} = 0\,,\ v_{i-1,j} = 0$ and / or $v_{i,j} = 0$ then $u\dfrac{\partial v}{\partial x} = 0$

CASE (4c)

Closed boundary at right end at $(i+1,j)$. The boundary condition is $v_{i+1,j} = 0$.

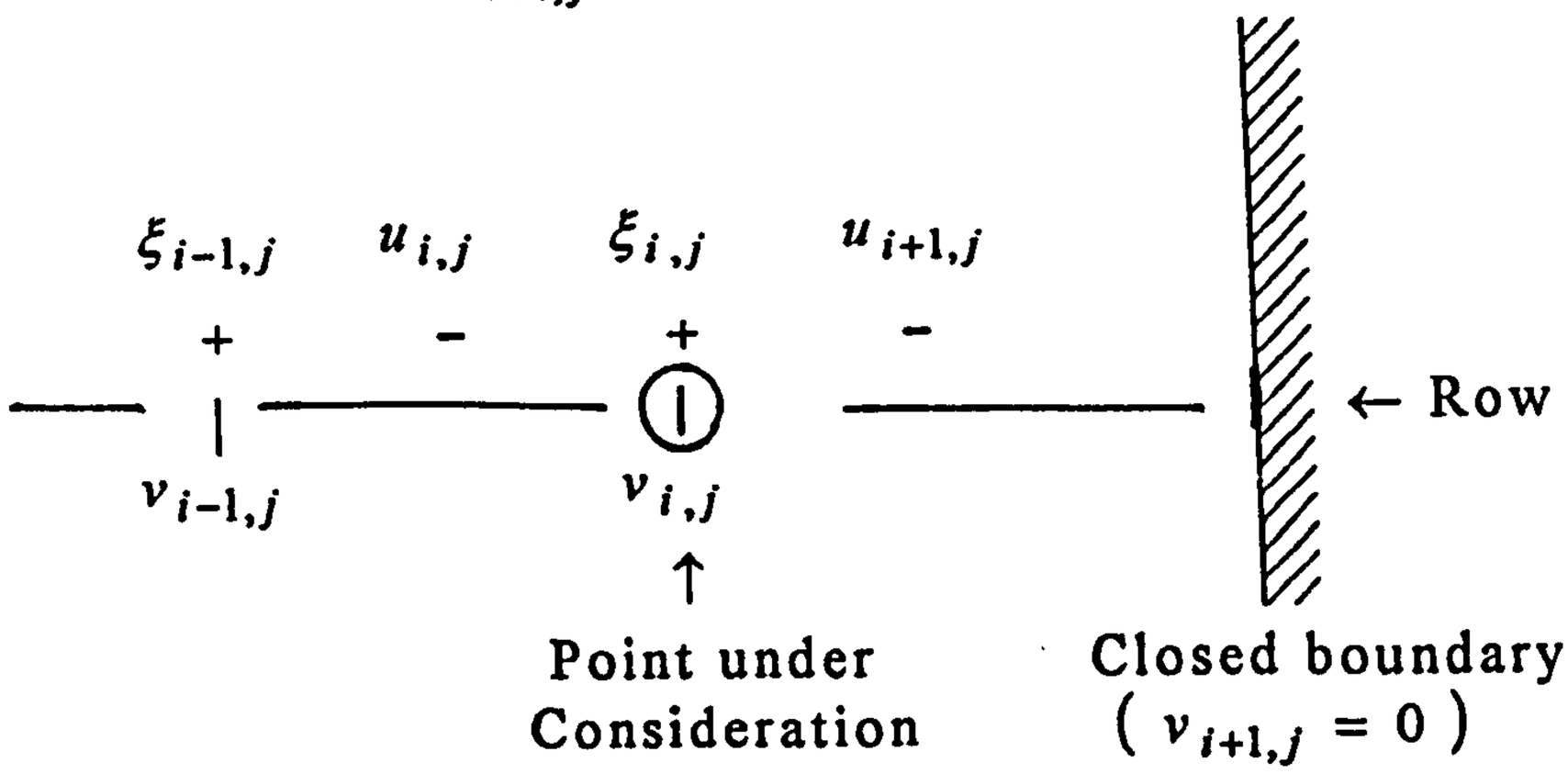

Figure 5.18

$$v_{i+1,j} = 0 \qquad v_{i-1,j} \neq 0$$

$$u\frac{\partial v}{\partial x} = \begin{cases} 0 & u'_{i,j} \leq 0 \\ u'_{i,j}\dfrac{(v_{i,j} - v_{i-1,j})}{\Delta x} & u'_{i,j} > 0 \end{cases} \qquad (5.12c)$$

Note that if $v_{i+1,j} = 0$ and $v_{i,j} = 0$ then $u\dfrac{\partial v}{\partial x} = 0$

CASE (4d)

Close boundary at right end at $(i+2,j)$. The boundary condition is $v_{i+2,j} = 0$.

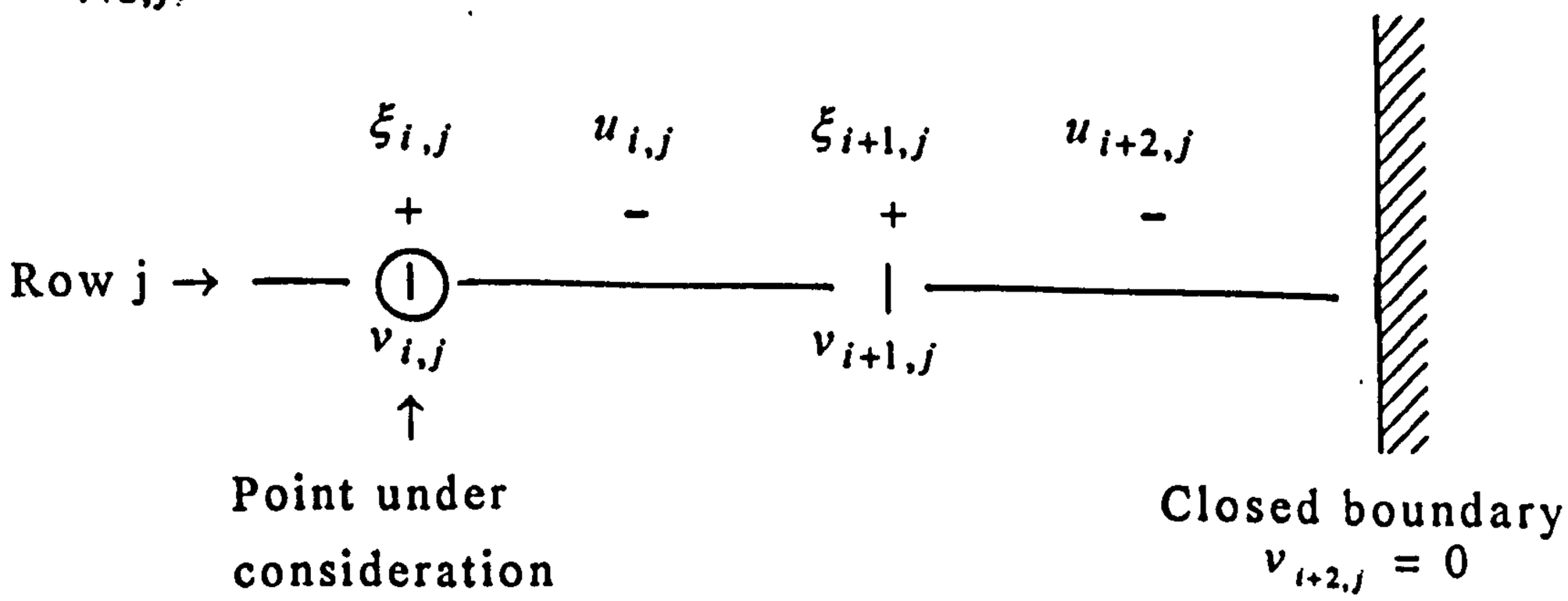

Figure 5.19

$$v_{i+2,j} = 0 \, , \; v_{i+1,j} \neq 0 \quad \text{and} \quad v_{i-1,j} = 0$$

$$u \frac{\partial v}{\partial x} = \begin{cases} u'_{i,j} \dfrac{(v_{i+1,j} - v_{i,j})}{\Delta x} & u'_{i,j} \leq 0 \\ u'_{i,j} \dfrac{(v_{i,j} - v_{i-1,j})}{\Delta x} & u'_{i,j} > 0 \end{cases} \qquad (5.12d)$$

Note that if $v_{i-2,j} = 0$, $v_{i-1,j} = 0$ and / or $v_{i,j} = 0$ then $u \frac{\partial v}{\partial x} = 0$

In cases (4a),(4b),(4c) and (4d) the discretization of $v \frac{\partial u}{\partial y}$ is similar to that shown in (5.7d).

5.4 BOUNDARY CONDITIONS, OPEN BOUNDARIES

As already mentioned, open boundaries are artificial water-water boundaries that have been arbitrarily drawn somewhere across a wider flow field to restrict the domain of the problem. Computational fluid dynamicists, as well as numerical analysts are quite active in the subject of open boundary approximation, see, e.g., Kreiss (1970), Kreiss and Gustafsson (1979), Oliger and Sundstrom (1978), Verboom et al. (1982), Gottlieb et al. (1982).

This section describes the numerical boundary condition procedures for the following boundary conditions at open boundaries.

5.4.1a VELOCITY BOUNDARY CONDITIONS

Velocity boundary conditions given by:

$$u_{\perp} = f^{u}(t) \qquad (5.13a)$$

$$u_{//} = 0 \qquad (5.13b)$$

$$\frac{\partial}{\partial n} u_{//} = 0, \text{ if } \nu \neq 0 \qquad (5.13c)$$

5.4.1b WATER LEVEL BOUNDARY CONDITIONS

Water level boundary conditions given by:

$$\xi = f^{\xi}(t) \tag{5.14a}$$

$$u_{//} = 0 \tag{5.14b}$$

$$\frac{\partial}{\partial n} u_{//} = 0, \text{ if } \nu \neq 0, \tag{5.14c}$$

where (5.13b) and (5.14b) are prescribed only at inflow, i.e , if $u_{\perp}$ is directed from outside the domain of the problem to inside. The well-posedness of (5.13) and (5.14) is treated by Verboom et al. (1981) and (1982).

The conditions (5.13) and (5.14) are often applied to practical flow problems in civil engineering because the prescribed quantities can be measured.

Because of the staggered grid , the special boundary procedures are necessary only because of the advection terms. Various extrapolation procedures were tested as proposed, for example, by Elvius and Sundstrom (1973). When applied to our grid structure these procedures were not satisfactory for inflow boundaries. At inflow, extrapolation procedures are sensitive to instabilities as was found by practical experience. It seems that boundary extrapolation methods are stable only if they are based upon extrapolation of quantities that reach the boundary from inside, like the outgoing " Riemann invariants ", see Gottlieb et al. (1982). For relevant applications in civil engineering it was also found by practical experience that the order of consistency of the advection discretization near the open boundary is hardly important. This means that the solution at the inner points is not greatly influenced by the order of the advection discretization near the open boundary. This observation was also made by Leendertse as suggested in Stelling (1984). It is important that the boundary procedure be stable. We found that the heuristic principles of the preceding section are also applicable for the construction of open boundary procedures. For the descretization of (5.13) and (5.14) we propose the following procedures:

5.4.2a VELOCITY BOUNDARY CONDITIONS:

For velocity boundary conditions we assume a geometry as given by Figure 5.20

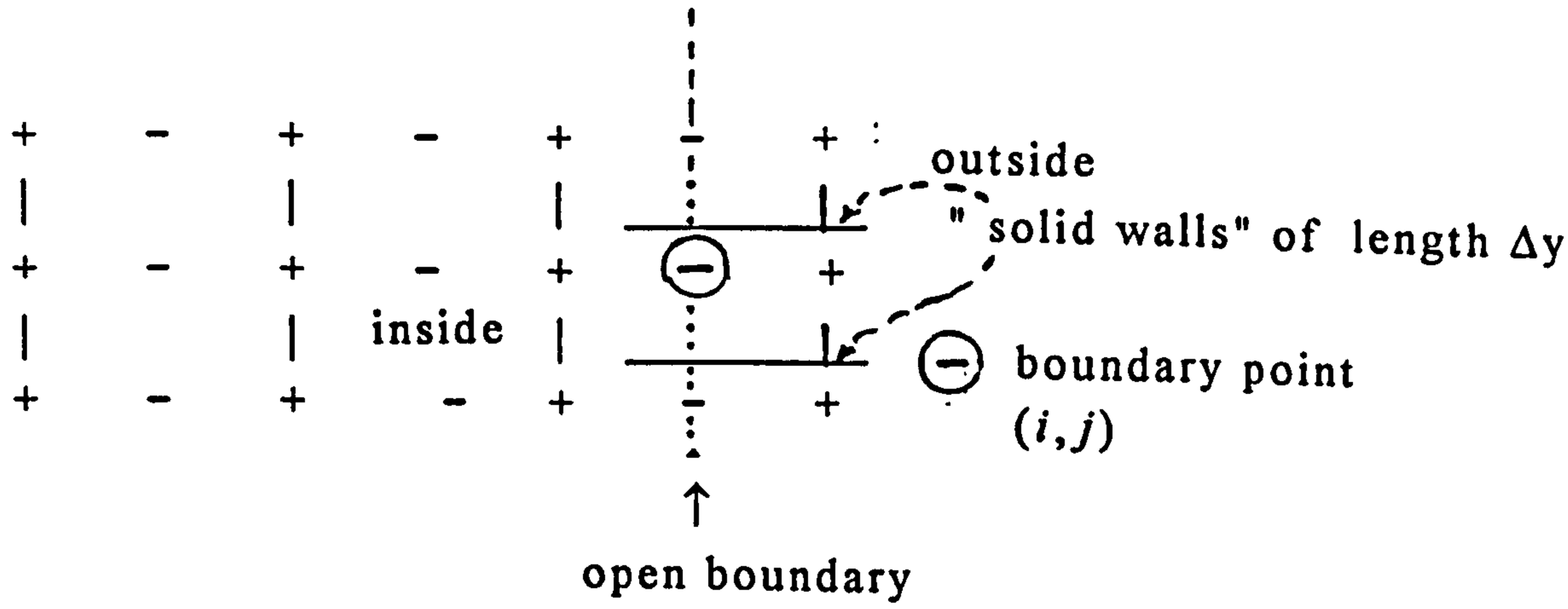

Figure 5.20 Open velocity boundary

The following discretizations are used:

$$u^k = f^u(k\tau), \text{ at } (i,j) \tag{5.15a}$$

$$v^k = 0, \text{ at } \left(i+\frac{1}{2},j+\frac{1}{2}\right) \text{ and } \left(i+\frac{1}{2},j-\frac{1}{2}\right) \tag{5.15b}$$

$$\xi^k_{i+\frac{1}{2},j} = \xi^k_{i-\frac{1}{2},j} \tag{5.15c}$$

5.4.2b NEAR THE OPEN BOUNDARY

Near the open boundary at (i,j), $u\frac{\partial u}{\partial x}$ is approximated by

$$u\frac{\partial u}{\partial x} = \begin{cases} u_{i,j}\dfrac{(u_{i+1,j}-u_{i,j})}{\Delta x} & u_{i,j} \leq 0 \\ u_{i,j}\dfrac{(u_{i,j}-u_{i-1,j})}{\Delta x} & u_{i,j} > 0 \end{cases} \tag{5.16a}$$

This procedure is consistent with (5.13). The condition given by (5.15a) is consistent with (5.13a). Because of the procedures for the discretizations of $u\frac{\partial u}{\partial x}$ and $v\frac{\partial v}{\partial y}$ near a closed boundary as described in section 5.3, (5.15b) is consistent with (5.13b) and (5.13c). Because of (5.15c) at point (i,j) of Figure 5.20, the continuity equation is approximated with zero-order consistency. According to Gustafsson (1975) or Beam et al. (1982), this is sufficient to maintain convergence. Experiments with extrapolations of a higher order did not greatly change the results at the inner points or become unstable. Boundary conditions in the x and y direction are treated similarly.

5.4.3a WATER LEVEL BOUNDARY CONDITIONS

For water level boundary conditions we assume a geometry as given by Figure 5.20.

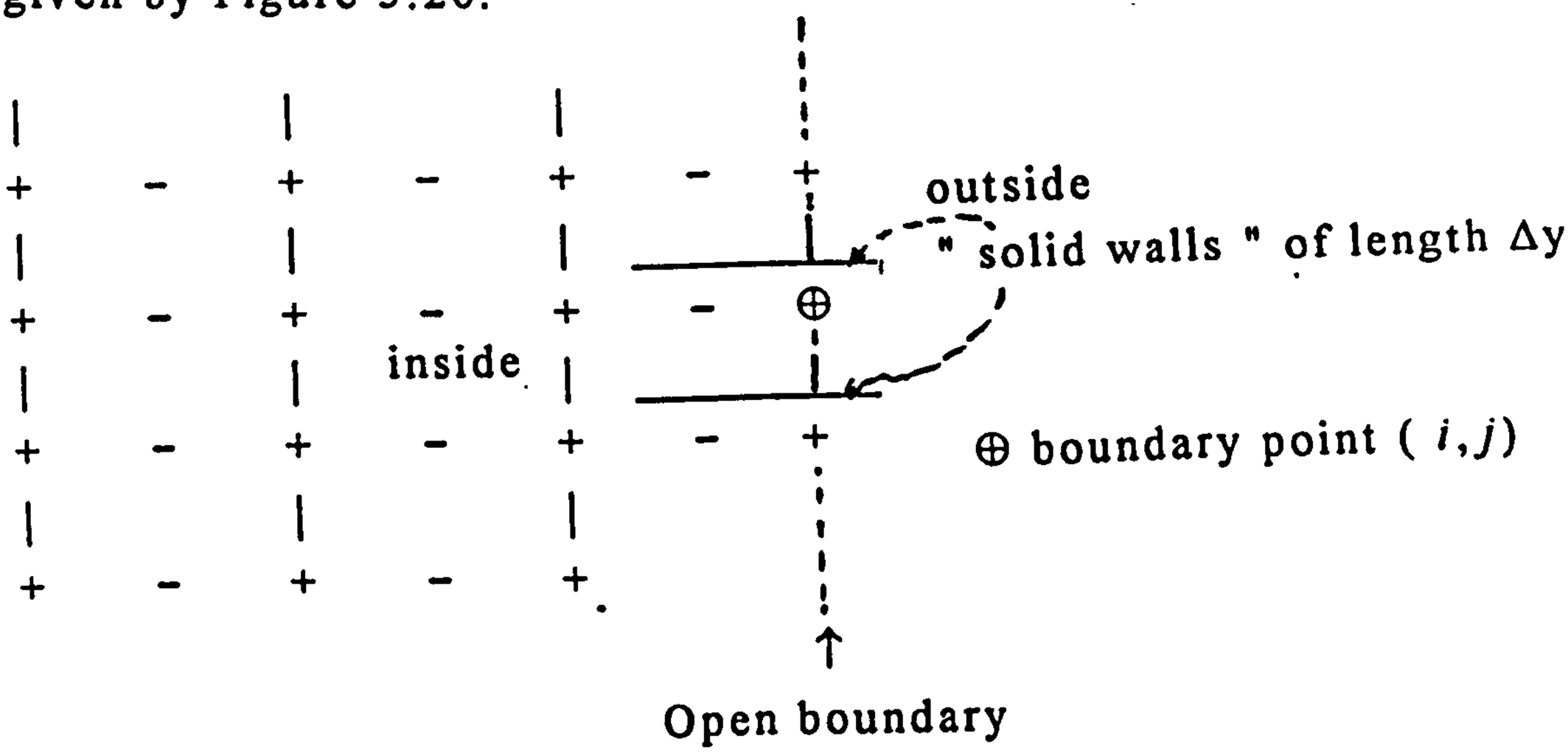

Figure 5.21 Open water level boundary

The following discretizations are proposed:

$$\xi^k = f^{\xi}(k\tau), \quad \text{at } (i,j) \tag{5.17a}$$

$$v^k = 0 \quad , \quad \text{at } \left(i,j+\frac{1}{2}\right) \text{ and } \left(i,j-\frac{1}{2}\right) \tag{5.17b}$$

Discretization of $u\frac{\partial u}{\partial x}$ Near the open boundary is as follows:

At $\left(i-\frac{1}{2},j \right)$

$$u\frac{\partial u}{\partial x} = \begin{cases} 0 & u_{i,j} \leq 0 \\ u_{i,j}\dfrac{\left(u_{i,j} - u_{i-1,j} \right)}{\Delta x} & u_{i,j} > 0 \end{cases} \qquad (5.18a)$$

At $\left(i-\frac{3}{2},j \right)$

$$u\frac{\partial u}{\partial x} = \begin{cases} u_{i,j}\dfrac{\left(u_{i+1,j} - u_{i,j} \right)}{\Delta x} & u_{i,j} \leq 0 \\ u_{i,j}\dfrac{\left(u_{i,j} - u_{i-1,j} \right)}{\Delta x} & u_{i,j} > 0 \end{cases} \qquad (5.18b)$$

This discretization is a consistent approximation of (5.14).

Note that at inflow $u\frac{\partial u}{\partial x}$ is approximated by a zero value at $\left(i-\frac{1}{2},j \right)$. This yields a zero-order consistent approximation of the momentum equation at $\left(i-\frac{1}{2},j \right)$. Again this yields only first-order convergence from a theoretical point of view. Yet the influence on the inner points of this approximation is negligible as was found in numerical experiments. The only noticeable effect of approximations of a higher order is that sometimes they became unstable. Consider for example the following extrapolation formula for a " virtual " u value at $\left(i+\frac{1}{2},j \right)$:

$$u^{k}_{i+\frac{1}{2},j} = 2u^{k}_{i-\frac{1}{2},j} - u^{k}_{i-\frac{3}{2},j} \qquad (5.19)$$

where the boundary procedures as proposed by Elvius and Sundstrom (1973) are based upon similar extrapolation formulae.

Equation (5.18) may be written at the point $\left(i+\frac{1}{2}, j \right)$.

$$u \frac{\partial u}{\partial x} = u_{i,j} \frac{\left(u_{i,j} - u_{i-1,j} \right)}{\Delta x} \tag{5.20}$$

If we calculate the truncation error of spatial discretization of (5.20), we obtain

$$u(x,y,t)\left[u(x,y,t) \right]_x$$

$$= u(x,y,t)\left[u(x,y,t) \right]_x$$

$$- \frac{\Delta x}{2} u(x,y,t)\left[u(x,y,t) \right]_{xx} + O\left(\Delta x^2 \right) \tag{5.21}$$

If $u < 0$, then the truncation error of (5.20) contains negative diffusion as follows from (5.21). This is probably the reason for the observed instabilities.

A stabilizing effect is often experienced as a result of the prescription of Riemann invariants at the open boundaries, see, e.g., Oliger and Sundstrom (1978) . In this case we obtain the following boundary conditions; we use

$$u_{\perp} \pm 2\left(gH \right)^{\frac{1}{2}} = f^R(t), \tag{5.22}$$

$$u_{//} = 0 \tag{5.22b}$$

$$\frac{\partial}{\partial n} u_{//} = 0, \text{ if } \nu \neq 0 \tag{5.22c}$$

As mentioned before, Riemann invariants are quantities that are not measured in nature. In order to profit from the stabilizing effect of Riemann invariants, while velocities are still prescribed as boundary conditions, we propose the following boundary conditions;

$$u_{\perp} + \varepsilon \frac{\partial}{\partial t}\left[u \pm 2(gH)^{\frac{1}{2}}\right] = f^{u}(t)\,, \tag{5.23a}$$

$$u_{//} = 0 \tag{5.23b}$$

$$\frac{\partial}{\partial n} u_{//} = 0\,, \text{ if } \nu \neq 0 \tag{5.23c}$$

For sufficiently small values of ε , (5.23a) is an accurate approximation of (5.13a). Yet with respect to very short wave lengths, which are produced for example by nonlinear effects inside the domain of the initial boundary-value problem, (5.23a) acts as a non- reflective boundary condition.

Numerical experiments carried out by the author confirmed this conjecture.

The Arabian Gulf has only one open boundary at its eastern side, at Strait of Harmouz. Summarizing, for the discretization at and near the open boundaries we adopt the following procedure for the situation of Figures 5.22 and 5.23:

CASE (5a) Open boundary at (i,j)

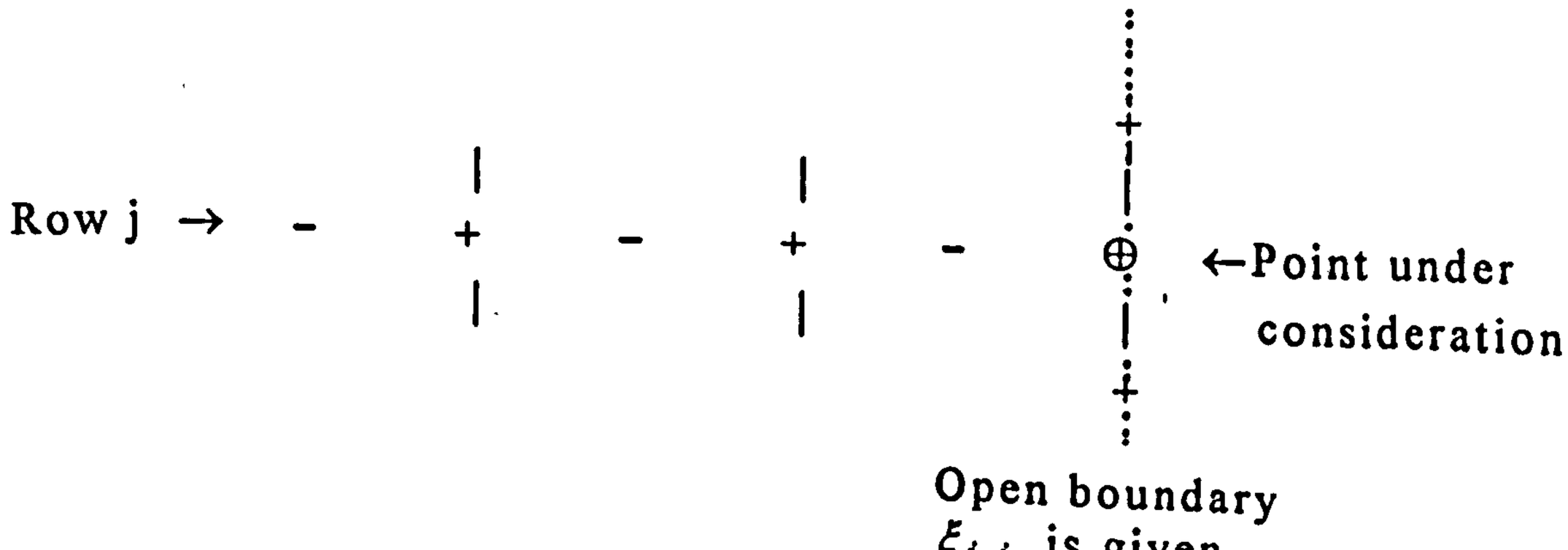

Figure 5.22

$$\xi_{i,j} = A_{TC} \cos\left(\frac{2\pi t}{T} - \Psi_{TC} \right) \qquad (5.24a)$$

$$u_{i,j} = -\gamma \xi_{i,j} \sqrt{\frac{g}{h}} \qquad (5.24b)$$

$$v_{i,j} = 0 \qquad (5.24c)$$

where

A_{TC} = The amplitude of the tidal constituent at Strait of Harmouz,

Ψ_{TC} = Phase of the tidal constituent Strait of Harmouz,

T = Period of the tidal constituent,

γ = Correction factor.

CASE (5b) Discritization of $u \frac{\partial u}{\partial x}$ close and near to the open boundary.

Open boundary at Strait of Harmouz at (i,j). The boundary condition is $\xi_{i,j}$ is prescribed and $v_{i,j} = 0$.

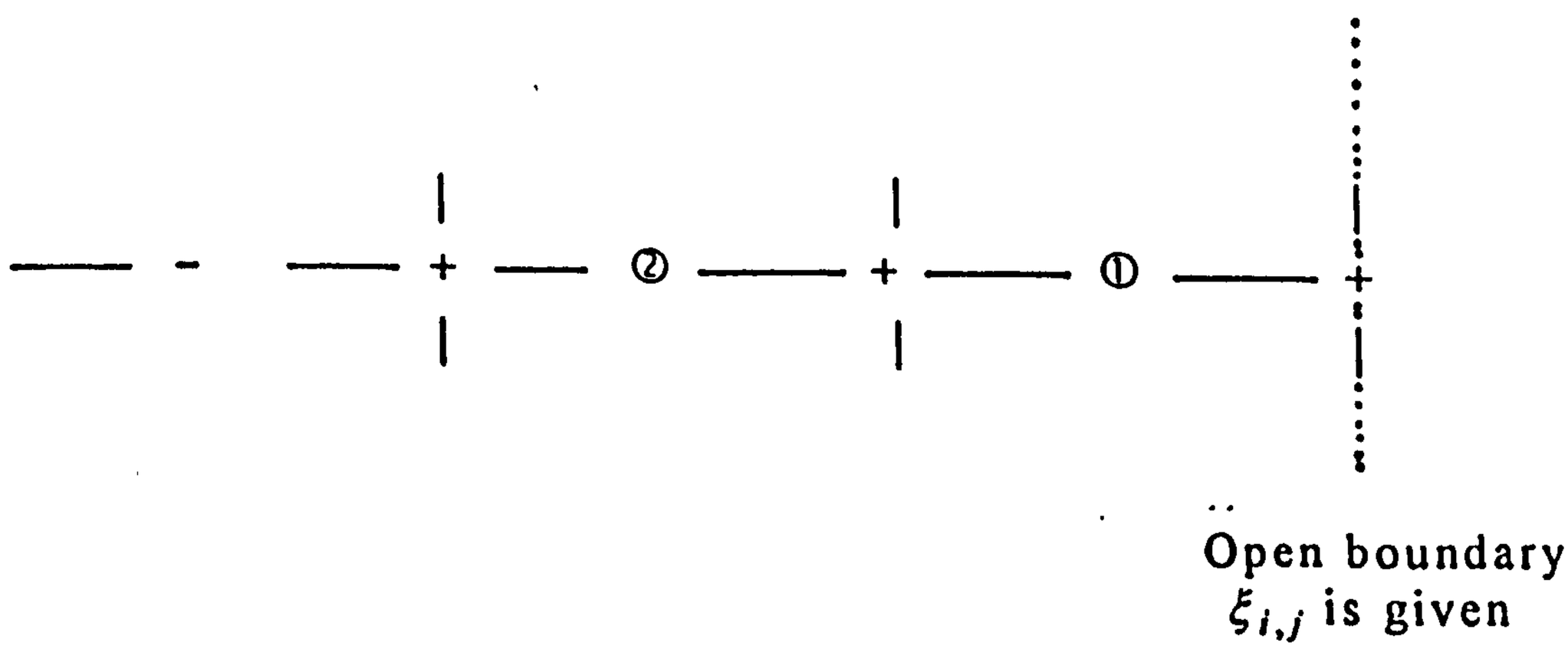

Figure 5.23

Discretization at ①

$$u\frac{\partial u}{\partial x} = \begin{cases} 0 & u_{i,j} \leq 0 \\ u_{i,j}\dfrac{(\,u_{i,j} - u_{i-1,j}\,)}{\Delta x} & u_{i,j} > 0 \end{cases}$$

and at ②

$$u\frac{\partial u}{\partial x} = \begin{cases} u_{i,j}\dfrac{(\,u_{i+1,j} - u_{i,j}\,)}{\Delta x} & u_{i,j} \leq 0 \\ u_{i,j}\dfrac{(\,u_{i,j} - u_{i-1,j}\,)}{\Delta x} & u_{i,j} > 0 \end{cases}$$

5.5 TIDAL FLATS

In this section we describe the treatment of land-water boundaries for which the location is a function of water level. The location of these boundaries is given implicitly by the following relation:

$$\xi + h = 0 \qquad (5.24)$$

If ξ (x,y t) varies as a function of time then the location of tidal flat boundaries varies as well, depending on the shape of the bottom profile, see e.g Figure 5.24.

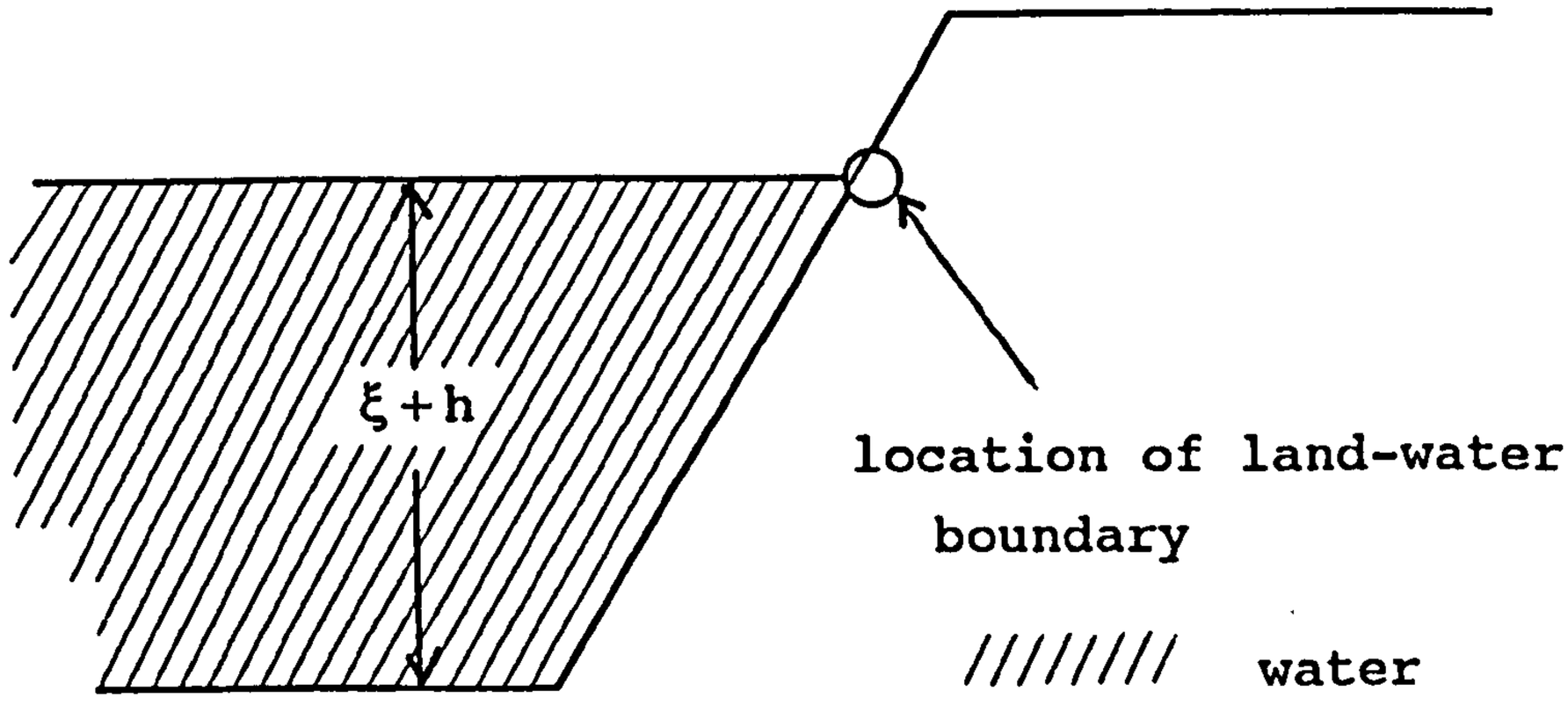

Figure 5.24 1 D Bottom profile with varying land-water boundary

For the fixed one-dimensional grid of Figure 5.24 a continuously varying position of the boundary is not possible. As discretization for the situation of Figure 5.22 the bottom profile of Figure 5.23 is assumed.

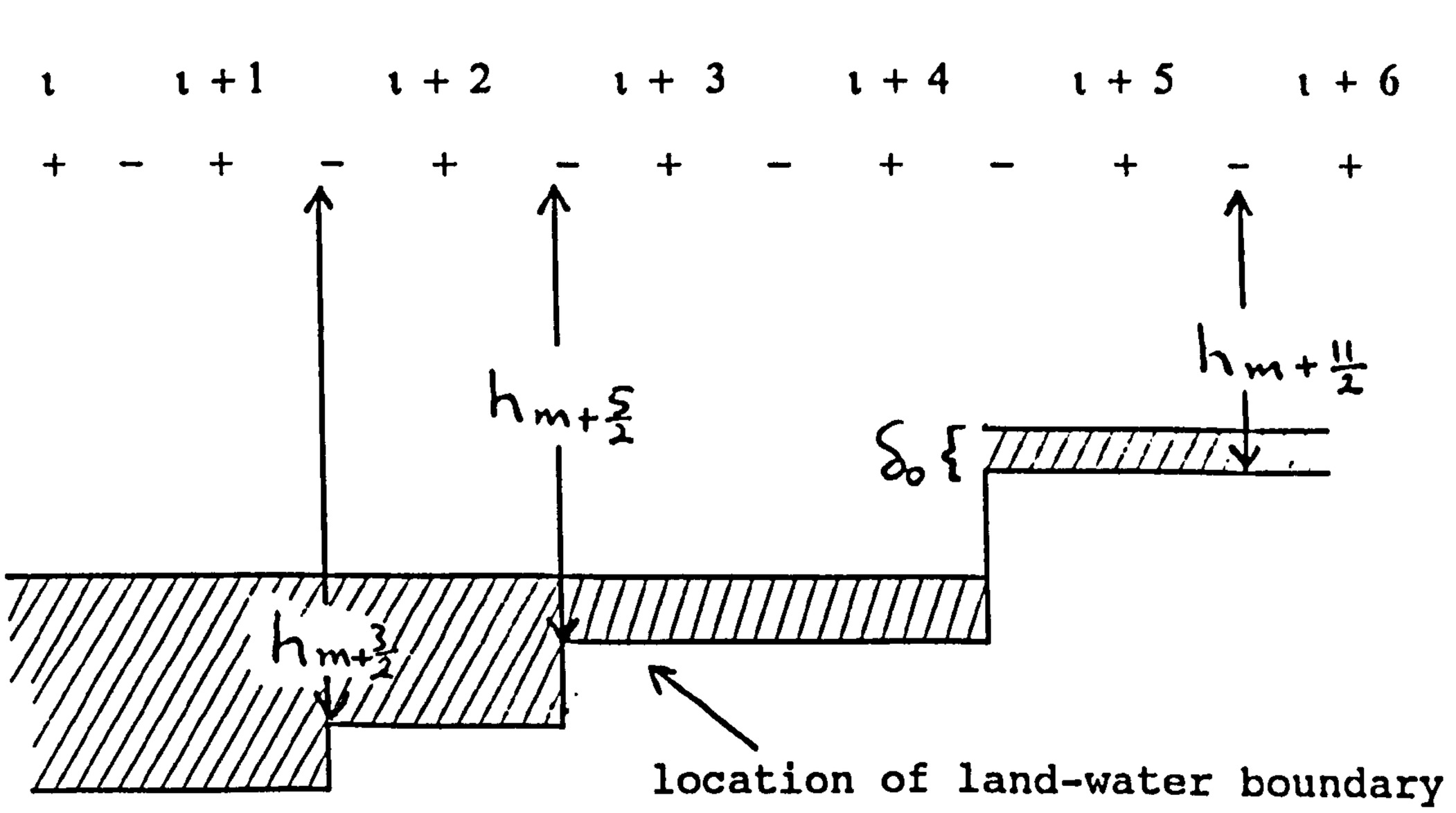

Figure 5.25 Discretized 1-D bottom profile

For the bottom profile of Figure 5.25 the boundary conditions are given by

$$u_{i+\frac{1}{2},j} = 0, \quad \text{if } h_{i+\frac{1}{2},j} + \frac{1}{2}\left(\xi_{i,j} + \xi_{i+1,j} \right) \leq \delta_0$$

where $h_{i+\frac{1}{2},j}$ denotes the bottom depth below some plane of reference.

For the two-dimensional grid, the boundary conditions are given by:

$$u_{i+\frac{1}{2},j} = 0, \quad \text{if} \quad H_{i+\frac{1}{2},j} \leq \delta_0$$

$$v_{i,j+\frac{1}{2}} = 0, \quad \text{if} \quad H_{i,j+\frac{1}{2}} \leq \delta_0$$

These equations assume intrinsically a bottom profile as given by Stelling (1984).

In very shallow regions there are several sources that might destabilize an EFDM . Examples of destabilizing sources are given by:

(i) Singularities due to the intersection characteristics. See Abbott (1975) for a discussion on characteristics and Liggett (1975) for a discussion on flow stability, roll waves, critical flow, etc.

(ii) Singularity of the bottom friction term if $H \rightarrow 0$. It is questionable if the numerical representation of the bottom friction term remains stable in this limiting case.

(iii) The numerical flooding and drying procedure induces disturbances by suddenly changing the status of a velocity point from flowing, i.e $u,v \neq 0$, to dry, i.e., $u, v = 0$ and vice versa.

In general the flow distribution of the shallow regions is not very important for the flow distribution of the deep regions. Considered as a storage basin, however, the shallow regions may be important. Therefore δ_0 should be chosen as small as possible. Very small values of H facilitate the onset of instabilities, however. Moreover it is questionable whether at

very shallow regions the water movement is described accurately by EFDM, especially if one takes into account the bottom friction law that has been applied . In order to control the instabilities while maintaining the storage capacity of the shallow region we propose the application of a strongly dissipative EFDM for regions characterized by the following relation

$$\delta_0 < H < \delta_1$$

Where δ_0 and δ_1 are some prescribed small values.

5.6 THE TOPOGRAPHY OF THE ARABIAN GULF BOTTOM

The Arabian Gulf topography was based on the data from the following two charts:

(i) Admiralty Chart No 2858, published by Hydrographic of the Navy U.K. (1985).

(ii) Bahrain Coastguard Directorate (depth) Chart. Muharraq, Bahrain. (1963).

(i) contains about five hundred soundings and (ii) about three thousand five hundred soundings. The average observed depth in a square of 5 minutes in Mercator coordinates around a grid point was taken as the initial value of depth for a point. In this way the depth at about half the number of the grid points was determined. The depth at points on the coast was derived on the basis of the bottom slopes in the neighbouring oceanic points. There remained blank areas where the depth was interpolated, on the basis of the depth at the boundaries of the area, through the scheme

$$h_{i,j} = \frac{1}{4}\left[h_{i-1,j} + h_{i,j-1} + h_{i+1,j} + h_{i,j+1} \right]$$

This procedure yielded a rough bythemetry. These initial data were then subjected to a smoothing operation by taking for each point the weighted average depth of the neighbouring points

according to the weighting scheme:

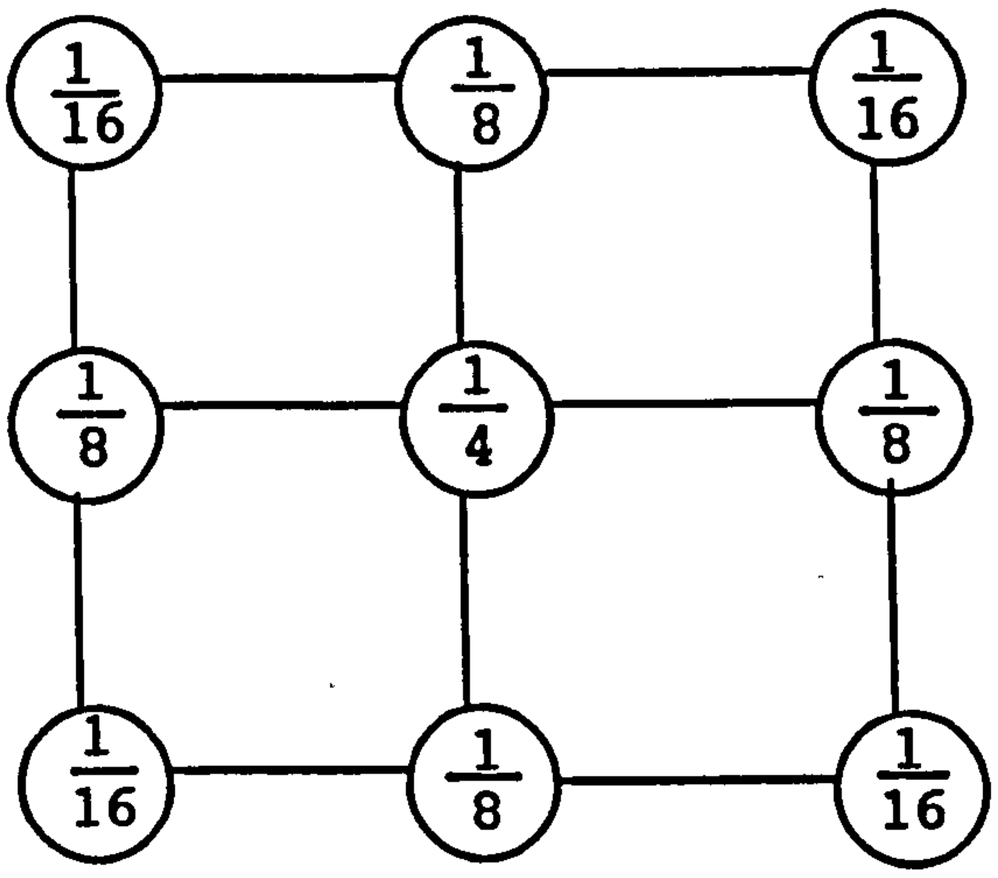

Figure 5.26

Five smoothing operations were applied for the basic 5 minutes map. It gives the depth-contours in metres. The representations in the model of very shallow region in the Gulf was particularly difficult. Here a lower limit to the depth of 1 km was imposed.

5.7 GRID IDENTIFICATION

The method of solution in EFDM involves solving for dependent variables in each grid cell. The computation is performed row by row proceeding from the first cell to the last. Three types of grid cell occur in the solution domain : land, water, and boundary cells. The land cells are characterized by their zero depths. In the computation, if the depth of a cell is zero, velocity and water elevation in that cell are set to be zero. In the water cells velocity and water elevation are computed. If the side of a water cell is contigious to a land cell, normal velocity there is set to be zero. At the boundary cells either velocity or water elevation is specified.

5.8 STABILITY

For the explicit finite difference scheme (EFDM) proposed in this thesis, the following condition is necessary for stability

$$Cf < 1 , \qquad (5.25)$$

where Cf is the Courant number. This is the well-known CFL condition, see Courant, Friedrichs and Lewy (1928).
The Courant- Freiedrichs-Lewy (CFL) condition for first-order hyperbolic equations implies that the characteristic through the advanced point of an explicit difference scheme (EFDM) must intersect the line through the points used by the scheme at the base time level within the range of these points. If the CFL condition is not satisfied, convergence cannot be guaranteed, see for example, Mitchell and Griffiths (1980) and Twizell (1984). The Courant number Cf for two-dimensional shallow water equations is defined as follows (see Stelling (1984))

$$Cf = \Delta t \sqrt{g\, h_{max}} \left(\frac{1}{\Delta x^2} + \frac{1}{\Delta y^2} \right)^{\frac{1}{2}} \qquad (5.26)$$

Using the stability condition (5.25) in equation (5.26) the following stability criterion is obtained for the optimal time-step (see also Leendertse (1967))

$$\Delta t \leq \frac{\Delta x \, \Delta y}{\sqrt{g\, h_{max} (\Delta x^2 + \Delta y^2)}} \qquad (5.27)$$

where

Δx = the cell's width in the x direction.
Δy = the cell's width in the y direction.
h_{max} = the maximum depth in the cell
Δt = time step

5.9 STOPPING CRITERIA

The explicit finite difference scheme (EFDM) with specified initial and boundary conditions, is implemented on the whole Arabian Gulf region with staggered grid . It took about 100 hours to reach the steady state with time-step τ = 180 seconds. The stopping criterion thus used is $\varepsilon = 10^{-6}$, such that

$$\left\| \underline{w}^{(k+1)} - \underline{w}^{(k)} \right\|_{\infty} \leq \varepsilon$$

where $\underline{w} = [u, v, \xi]^T$, T denoting the transpose.

CHAPTER SIX

6 NUMERICAL EXPERIMENT AND DISCUSSION

6.1 APPLICATIONS TO ARABIAN GULF

Having designed a numerical model it was obviously necessary to validate its accuracy. The computation of amplitudes and phases of tidal constituents M_2, S_2, K_1 and O_1 in the Arabian Gulf were chosen as an appropriate means of testing the algorithm described in Chapter 5.

In the Arabian Gulf two dominant types of tide exist; diurnal and semi-diurnal. Two of each types of these dominant tides, M_2, S_2, K_1 and O_1 , respectively, were selected for the model to reproduce amplitudes and phases. The results were then compared with the British Admiralty co-tidal charts (1976). We also compared the results with those obtained earlier by Lardner et al. (1982), Evans-Roberts (1979) and Von Trepka (1968).

The diurnal and semi-diurnal tides in the Gulf mentioned above, have an interesting structure. The diurnal components, O_1 and K_1, have a single amphidromic point while the semi-diurnal components, M_2 and S_2 have two such points. In addition, the open boundary across the Strait of Harmouz is very narrow, providing greater accuracy for specifying the boundary values and so fewer points need to be prescribed reasonably accurately. These reasons make this region a good test-bed for tidal models.

The model covers an area along the y-axis between 47° 50′ E and 56° 30′ E longitude and along x-axis 24° 00′ N and 30° 10′ N latitude shown in Figure 6.1. The grid is shown in Figure 6.2a. The grid-spacing is 5 minutes latitude (approx 8.7 km) and 5 minutes longitude (approx 9 km) which leads to a total grid-size of 74x104 . The total number of grids at wet and boundary points is 3044.

The only open ocean boundary occurs at the Strait of Harmouz. The tide height ξ is prescribed at this boundary. The computational procedure at each time step is to calculate the new

values of ξ and velocity components u and v using the given heights at Strait of Harmouz as driving force.

In each case the model was started from initially flat conditions. Open boundary conditions in the Strait of Harmouz were taken from the Admiralty co-tidal chart (1976) for the Gulf for each tidal component.

It takes approximately 12 hours of real time for the disturbance at Harmouz to propagate to the head of the Gulf and considerably longer for steady conditions to be reached. Therefore the computations needed to be carried out for a period of 90 hours of real time. When the computation was extended to 125 hours very little change was found in the calculated tidal amplitudes, phase and velocity components; thus 100 hours was considered sufficient. The length of the time-step τ was chosen so that these were 240 steps per tide-cycle for the semi-diurnal components M_2 and S_2 and 480 steps per cycle for the diurnal components O_1 and K_1.

The depth has been read from two navigational charts of the Arabian Gulf; British Admiralty Chart (1988) and the Bahrain Coastguard Directorate (depth) Chart (1963). The readings on the British Admiralty chart are in metres and the depth values obtained tended to be underestimates of the actual depths. This was, firstly, because the charted values are given with reference to the highest high water rather than mean water level and, secondly, because a navigational chart, by its nature, must be conservative.

For these reasons the depths were corrected by subtracting a quantity h_{mean} which is mean to all depths. This correction was treated as a tuning parameter and it was found that a value in the region of 1/15 metres gave the best results.

British Admiralty Chart (1988), with its readings in metres has only 400 readings while Bahrain Coastguard Directorate (depth) Chart (1963) measures in fathoms, which were converted to metres. The second chart has nearly 3500 readings and was thus found to be very useful.

The following output has been obtained from the EFDM so far,

a) the values of the velocity components and tide heights for the whole region at certain selected time intervals. Typically, these have been obtained at intervals of one quarter of tide cycle (for every 5 time-steps for semi-diurnal and 10 time-steps for diurnal tide).

b) The values of the tidal amplitudes and phases for the whole region and for each tidal component.The amplitude-values are computed as an average of all the maximum and minimum values of $|\xi|$ during the last 500 time-steps (25 hours) of each run for M_2 and S_2. tidal constituents and 800 time steps (40 hours) of each run for tidal constituents K_1 and O_1.

c) The phase values are computed from the time of the last maximum of ξ and are converted to degrees of phase lag (for M_2 12.42 hours = 360 degrees, S_2 12 hours = 360°, K_1 23.93 hours = 360° and O_1 25.82 hours = 360°) behind the input at the Strait of Harmouz. Since the amplitude and phase values have been the main tool in tuning the model these results will be given in detail below.

d) At 112 tidal stations the tide heights were recorded for each component. After the steady-state had been reached it was run for 25 hours for M_2 and S_2 and 40 hours for K_1 and O_1. The phase values were then calculated, as described in (c).

e) Eighteen tidal stations were then chosen and for each component the tide heights were recorded. Again, after the steady-state had been reached , recordings were made for 25 hours for M_2 and S_2 and for 40 hours for K_1 and O_1. The tide heights being computed every 15 minutes.

From the results obtained in (d), four table were made, representing each of the tidal components (Tables 6.1 - 6.4). The tables for M_2 and K_1 covered 73 tidal stations while those for O_1 and S_2 covered 74 stations. The computed values obtained for

amplitudes and phase are shown in the tables, along with the observed data from the Admiralty Tide Tables (1988).

For the tidal stations mentioned in (e) graphs were constructed for each of the four components and the tide heights were simulated alongside the observed data shown in Figures (6.15-6.18). The observed data are not based on hourly readings (as they are not available at these tidal stations) but only on the graph for high and low tide heights which are available from British Admiralty Tide Tables (1988).

From Tables 6.1-6.4 errors in amplitudes, percentage errors in amplitude, phase errors and percentage phase errors, for each of the tides were calculated . All these errors are further quantified in Figures 6.19-6.26, which show their distribution according to magnitude (represented as bar charts). An analysis of these errors was carried out and tabulated results can be seen in Tables 6.5-6.8.

Finally, the results from the numerical model were compared with those obtained by Lardner (1982) (Figures 6.27-6.28), Von Trepka (1969), Figure 6.29, and Evans-Robert (1979), Figure 6.30.

The Admiralty co-tidal charts (1976) for the dominant constituents in the Arabian Gulf M_2 , S_2 , K_1 and O_1 are shown in Figures 6.3-6.6 respectively. These charts are constructed from experimental observations of tide heights and contain lines of equal amplitude (in metres) and equal phase (in degrees) for each component. The offshore data contained in this chart have been inferred from data obtained at coastal sites, islands and some oil rigs.

The computed amplitudes are presented in Figures 6.7-6.10 and the computed contours of phases are represented in Figures 6.11-6.14. The contour lines in these figures were drawn using SURFACE IV plotting program (1992) using the Minicurve method.

In comparing model results and observations, 112 tidal stations were selected in the Gulf area and at each station tidal heights and phases were computed for each of the four tides M_2 , S_2 , K_1 and O_1. The model grid points closest to each of these

stations and the complete comparison of amplitudes and phases of the four tides are shown in Figure 6.2b.

6.2 CONCLUSION

Since the physical results for the component tides are largely known in the Arabian Gulf, the purpose here is to show that the numerical model EFDM is accurate for simulation of the tidal amplitude and phase as predicted by the theory.

The computed contours of equal amplitude are given in Figures 6.7-6.10 while the computed contours of equal phase are given in Figures 6.11-6.14. A comparison between observed and calculated data shows excellent agreement with the correct amphidromic systems being produced. There are, however, some slight differences in detail which require examination. Each of the four tidal constituents will be examined below.

Looking at the graphs for Figures 6.15-6.18 it can be seen that the observed and computed results are very close. The observed data in the graphs has been constructed using only the high and low tides heights and matching the phase lag of computed data. If at a future date hourly recordings of tide heights at the tidal stations becomes available it might show that this author's results are very close to observed data where at present there is some difference.

6.2.1 CONSTITUENT M_2

The dominant feature of the M_2 tide is the existence of the two amphihydromic points. From the British Admiralty Chart (1976), Figure 6.3, it can be seen that tides have relatively high amplitudes at the head of the Gulf, the Strait of Harmouz, near Bandar Abbas on the Iranian coast and in the region between Saudi Arabia and Qatar around the northern tip of Bahrain. It can be seen in Figure 6.7 that these observed features have been reproduced extremely well by our numerical model.

The computed amplitudes are quite low in the UAE areas of Jabal Az Zannah, Khawr al Udayd, Ajman, Dubay, Mina Zayed and Umm al Qaywayn. The north east coast of Qatar near Musay'id, Ad Dawhah, Jezirat Sharaiwah and Khawr Shaqiq also shows quite low amplitudes as does the Bahrain area of Sitra and mina Salman.

There are, similarly, slightly low amplitudes in the central Gulf near the Saudi Arabian eastern coast, Ras Tannurah, Al Jubayl, Abu Saa'fah and Fasht Ghribah and in the Iranian coastal areas of Basaidu.

Computed amplitudes are slightly higher than the observed data occur in the upper Gulf near Kuwait at Mina Saud, Jazirat Qaruh and Ras al Khafgi, on the Iranian coast at Lavar, Bushehr and Halileh and at the end of the Gulf near the Iraqi coast at Al Faw and Khor Musa region in Iran. Also, along the Saudi Arabian coast higher amplitudes were computed at Bandar Mish'ab, Ras as Saffaniyah. The amplitude computed at the Shat al Arab was very high. It is interesting to note that in this high-amplitude region there is a small area of low amplitudes at Warba Spit on Bubian island and Doha Harbour near the eastern coast of Kuwait.

In the lower Gulf the computed data showed quite high amplitudes in the Gulf of Salwa, in the vicinity of Bahrain at Zellaq, Um Jalid and Jabal Ali and in the Dhukan area of the Saudi Arabian coast.

The computed phases in Figure 6.10 are in reasonable agreement with the co-tidal lines shown in Figure 6.3. The results are slightly higher at the head of the Gulf from Kuwait round to the Iraqi coast. Low phases were recorded at Ad Damman and Al Jubayl on the north-east coast of Saudi Arabia, in the Strait of Harmouz at Jazireh ye Hangam and on the tip of Oman at Khawar al Quway and Khawr Khesab.

6.2.2 CONSTITUENT S_2

Again, the observed data in Figure 6.4, showing the same qualitative features of two amphidromic points with high amplitude at the end of the Gulf and off the northern tip of Bahrain, are reproduced well by the EFDM model. The results can

be seen in Figure 6.8. The results computed by our numerical model also show quite high amplitudes in the upper Gulf region but also in the north-west coast of Emirates, Qatar and the south tip of Bahrain.

In particular, at the head of the Gulf, quite high amplitudes were recorded off the Iraqi coast at Al Faw, Khor Musa, Shat al Arab and Bandar Deylam and at Halileh, Lavar, Bushehr and Jazireh ye Khark along the Iranian coast. In the Kuwait region at Warba Spit, The Mina Saud and Mina Al Ahmadi areas were high as were readings around Manifah and Bandar Mish'ab on the Saudi Arabian coast.

Along the Emirates coast quite high amplitudes occur at Ras Abu Qumayyis, Umm al Hatab and Jazir Ghaghah. High amplitudes were recorded at Ad Dawhah, Musa'yid, Al-wakrah, Zikirt and Al Khrajj, north-west region of Qatar. Also, there are high amplitudes around the lower coast of Bahrain although other lower parts of Gulf of Salwa, Jabal al Fuwayrit, Ras Ushayriq and Ras Laffan, shared lower amplitudes than the observed data. It was seen from the numerical model that the amphidromic point has moved slightly towards the end of the Gulf. Also, the areas of Mina Rashid, Ash Shariqah and Dubay in the UAE region recorded low amplitudes.

Computed phases can be seen in Figure 6.12. Slightly high computed phases were recorded on the north-east coast of Saudi Arabia at Ad Damman, Ras Tannurah and Dawhat at Tarut and at Zellaq and Sitra on Bahrain's northeast coast. The region where north-east Qatar joins with the UAE coast also showed high phases, at Ras Abu Qumayyis, Musa'yid and Al-Wakrah and on the west UAE coast close to Umm an Nar and Mina Zayed. Slightly low phases were recorded close to the Strait of Harmouz. It should be noted that the Amphidromic point has moved slightly towards the coast of UAE.

6.2.3 CONSTITUENT K_1

The dominant features of the diurnal components are the existence of a single amphidromic point north of Bahrain with the highest

amplitudes at the head of the Gulf and off the eastern Qatar and southern Emirates coast (Figure 6.5). These features are reproduced very well by the numerical model EFDM and can be seen in Figure 6.9. The computed amplitudes are in good agreement with observation except for the occurrence of a region of low amplitude along UAE coast.

High amplitudes occur at the head of the Gulf in the regions of Al Faw, Khor Musa , Bandar Deylam and Shat al Arab. Similarly, high amplitudes were also recorded along Saudi Arabia's north-east coast at Ad Damman, Al Jubayl, Al Khrajj, Ras Tannurah and Bandar Mish'ab. High amplitudes were recorded in the Gulf of Salwa which includes the area around Bahrain, north-west of Qatar and the Saudi Arabian coast in the central Gulf. High amplitudes were also recorded across the Gulf at Bandar Abbas on the Iranian coast.

Low amplitudes were computed for the lower Gulf region in the UAE coastal areas of Jazair al Yasat, Jazirat Dalma, Sir Bani Yas, Dubay and Ajman with a particularly low amplitude being computed at Jazair Ghaghah.

It is clear from the Figure 6.13 that the computed phases have a good agreement with the observed data in most areas of the Gulf except that the computed phases were found to be slightly higher at the north-west coast of Qatar in the areas of Ras Abu Qumayyis, Musa'yid, Ad Dawhah and Ras Laffan. High phases were recorded at the head of the Gulf and the area around Kuwait.

Low phases were computed in the region closer to Emirate coast at Dubay, Ajman, Bukha and Mina Saqr

6.2.4 CONSTITUENT O_1

In this component observed amplitudes can be seen in Figure 6.6 which shows high amplitudes at the head of the Gulf and on the south coast of Iran. There is only one amphidromic point. These features are reproduced (Figure 6.10) excellently by the EFDM model. The computed amplitudes are in good agreement all over the Gulf but some differences were found in a few regions of

the Gulf.

High amplitudes were found at the upper end of the Gulf starting from Ad Damman and Al Jubayl on the Saudi Arabian coast to Shat al Arab, Al Faw, Khor Musa and Bandar Deylam near the Iraqi and Iranian coast. High amplitudes were also found around the north of Bahrain, north-west of Qatar (Musa'yid and Ad Dawhah) and close to the Emirate coast at Khawr Zubayyah, Mina Zayed and Khwar Ghanadeh.

Low amplitudes were found in the two Emirates regions, one containing Dubay, Ajman and Ras al Khaymah and the other including Jazireh Dalma, Sir Bani Yas and Ruwais.

Figure 6.14 contains computed contours of equal phases. Comparing with the observed data they are again found to be in good agreement but some differences also can be noticed, like low phases along the north-east coast of Bahrain, Emirates' coast near Khawr Zubayyah, Mina Zayed and Mina Saqr and close to the Iranian coast at Bushehr and Jazireh ye Khark.

In comparing model results and observations, 112 tidal stations were selected in the Gulf area and at each station the tidal amplitudes and phases were computed for each of the four tides M_2 , S_2 , K_1 and O_1.

The model grid points closest to each of these stations are shown Figure 6.2a. Tables 6.1-6.4 were drawn up to show the values obtained and the results were compared with data from the Admiralty chart. The computed results are shown to be quite close to the observed data.

An average of 18 tidal stations were chosen for each component tide and both the computed and observed height were simulated. Figures 6.15-6.19 show a very close comparison between computed amplitudes and observed data and can be seen as a further justification of the results detailed above.

Figures 6.15a-o show computed and observed amplitudes for tide M_2 . The computed amplitudes are very close at Bandar Asalu (Iran), Khawr al Quway (Oman) and Dawaht al Tarout (Saudi Arabia). High amplitudes are shown at Umais (Bahrain), Mina Saud (Kuwait) and Sir Bani Yas (UAE). Slightly low amplitudes occur at Basidu (Iran), Al Jubail (Saudi Arabia) and Khawr Khasab (Oman).

Figures 6.16a-r show that the computed and observed results for S_2 are very close at Bandar Abbas (Iran), Mina Zayed (UAE) and Khawr khesab (Oman). At Musay'd (Qatar), Marjan Oilfield (Kuwait) and Ad Damman (Saudi Arabia) computed results are high. The computed result are slightly low at Basaidu (Iran), Umm Al Qaywayn (UAE) and Umais (Bahrain).

Analysing Figures 6.17a-p for tide K_1 it can be seen that results are very close at Khawr al Quway (Oman), Ad Dawhah (Qatar) and Bushehr (Iran). The computed results are slightly higher at Shat al Arab (Iraq), Bandar Asalu (Iran) and Jazirat Siri (UAE).

Finally for O_1, from Figures 6.18a-r it can be seen that computed and observed amplitudes are very close at Khawr al Quway (Oman), Khor musa (Iran) and Zirku Terminal (UAE). Higher amplitudes occur at Ad Dawhah (Qatar), Mina Al Ahmadi (Kuwait) and Bushehr (Iran) while low amplitudes can be seen at Jazirat Sirri (Iran), Umm Al Hatab (UAE) and Bukha (Oman).

6.3 ERROR ANALYSIS

Errors in amplitude, percentage errors in amplitude, phase errors and percentage phase errors were calculated for each of the four tides and the results are given in Tables 6.1-6.4. These tables contain the computed and observed values of phase and amplitude of 74 tidal stations for each tide.

The errors were calculated and further quantified in Figures 6.19-6.23, which show their distribution according to magnitude. Typical errors from these figures are of the order of 5 cm in amplitude and 5 degrees in phase. The asymmetry in distribution of errors suggests a slight tendency to underestimate amplitudes and to overestimate phases.

6.4 COMPARISON OF THE RESULTS WITH OTHER NUMERICAL MODELS OF THE ARABIAN GULF.

6.4.1 LARDNER ET AL. MODEL (LBC)

LBC model is based on a split implicit method developed by Leenderstee (1967). LBC developed a multi-block technique consisting of a coarse mesh (20 km) for the whole Gulf and 10 km for the shallow water area. They studied the different constituents separately by forcing them at the open boundary and carried out a simulation during 75 hours of real time considering that the dynamics have reached equilibrium after a spin-up phase of about two days. He produced co-tidal maps for M_2 , S_2 and K_1 for both amplitudes and phases . In the LBC model at the authors introduce a more complex formulation to calculate the bottom friction parameters, following Leendertsee (1967)

$$c = \frac{\rho g}{k^2} \quad \text{with} \quad k = c_1 \ln(c_2 h + c_3)$$

The solution looks quite good. However, from an analysis of the M_2 solution it appears that the amplitudes are too small in the centre part of the Gulf between Bahrain and the Iranian coast; similarly for K_1 between Qatar and UAE coast.

6.4.2 EVANS-ROBERTS (ER) MODEL

ER used a spherical polar system and a mesh size of 10 minutes of latitude and longitude. He took an area from $24^\circ N$ to $30^\circ N$. Evans-Roberts also did a simulation in which he approximated the tidal forcing at the Strait of Harmouz. He developed a low cost method to reproduce the M_2 and K_1 interaction by simulating the M_2 constituent together with an artificial diurnal tide (AM1) having the amplitude and phase of K_1, but with the period of exactly twice M_2. This produces a tide cycle which is repeated at intervals of 24.8 hours.

The economy is evident; the main features of the tides can thus be studied without the need to generate and analyse vast quantities of results. However, the method does not allow study of

other constituents of the tides such as S_2 and O_1, or the non linear interaction. The co-tidal map of M_2 produced by Evans-Roberts is presented in Figure 6.29. The amplitudes generated for M_2 tended to be lower than those observed in situ and those on the Admiralty co-tidal charts. This may be due to the fairly coarse grid used.

6.4.3 VON TREPKA (VT) MODEL

VT used the well known Hansen scheme. In his model the equation was written in Cartesian co-ordinates. He used a mesh size of 14 km and used a friction coefficient inversely proportional to the depth of the water column

$$c = r/(h + \xi).$$

He first investigated M_2 and K_1, his M_2 solution is presented in Figure 6.30. Globally the amplitude seems to be better in the centre of the basin, even in the Bahrain area of the Arabian Gulf with its complicated coast line and shallow waters Von Trepka's solution is very good. However an examination of that solution shows that the M_2 wave is too strong all along the eastern coast of Qatar and the southern coast of UAE; the discrepancies reached 20% in this area.

He did a simulation in which he approximated the tidal forcing at the Strait of Harmouz. Simulation was carried out for 75 hours of real time. In order to save computational effort the shallow water equation was sometimes linearized. Such a simplification is largely justified when the area modelled is not shallow.

6.4.4 EFDM MODEL

The numerical results indicate that amplitudes and phase are in good agreement with the observed values. A detailed study of all possible tidal stations reveals that the numerical model has produced reasonably good results in shallow as well as deep waters. Comparing the values of computed amplitudes and phases

with the other models it is noticed that the EFDM model gives better results than those of Lardner et al. (1982) (Figure 6.27-6.28), Evans-Roberts (1979) (Figure 6.29) and Evans-Roberts (1979) (Figure 6.30). The semi-implicit scheme proposed by Lardner et al. uses a sufficiently large time step to give a good computing economy but damping and phase error limit the time step in computing the solution. Moreover, it involves the simultaneous solution of coupled non-linear equations. The proposed explicit schemes differ considerably from those of Lardner et al. and Von Trepka in the way the tidal forcing term, closed and open boundary conditions are applied at the Strait of Harmouz. Another important feature is the simplicity and the economy of the scheme. Due to the explicit nature of the present model less CPU time is required than the LBC model. The model is thus computationally economical and efficient.

Several formulas for Chezy coefficients mentioned in Chapter 4 are being utilized in the experiment. However the Chezy coefficient

$$D = \frac{g}{c^2} = 2.5 \times 10^{-3} \quad \text{(D is a bottom friction)}$$

is seen to be performing reasonably well in the EFDM model and was considered to be the best.

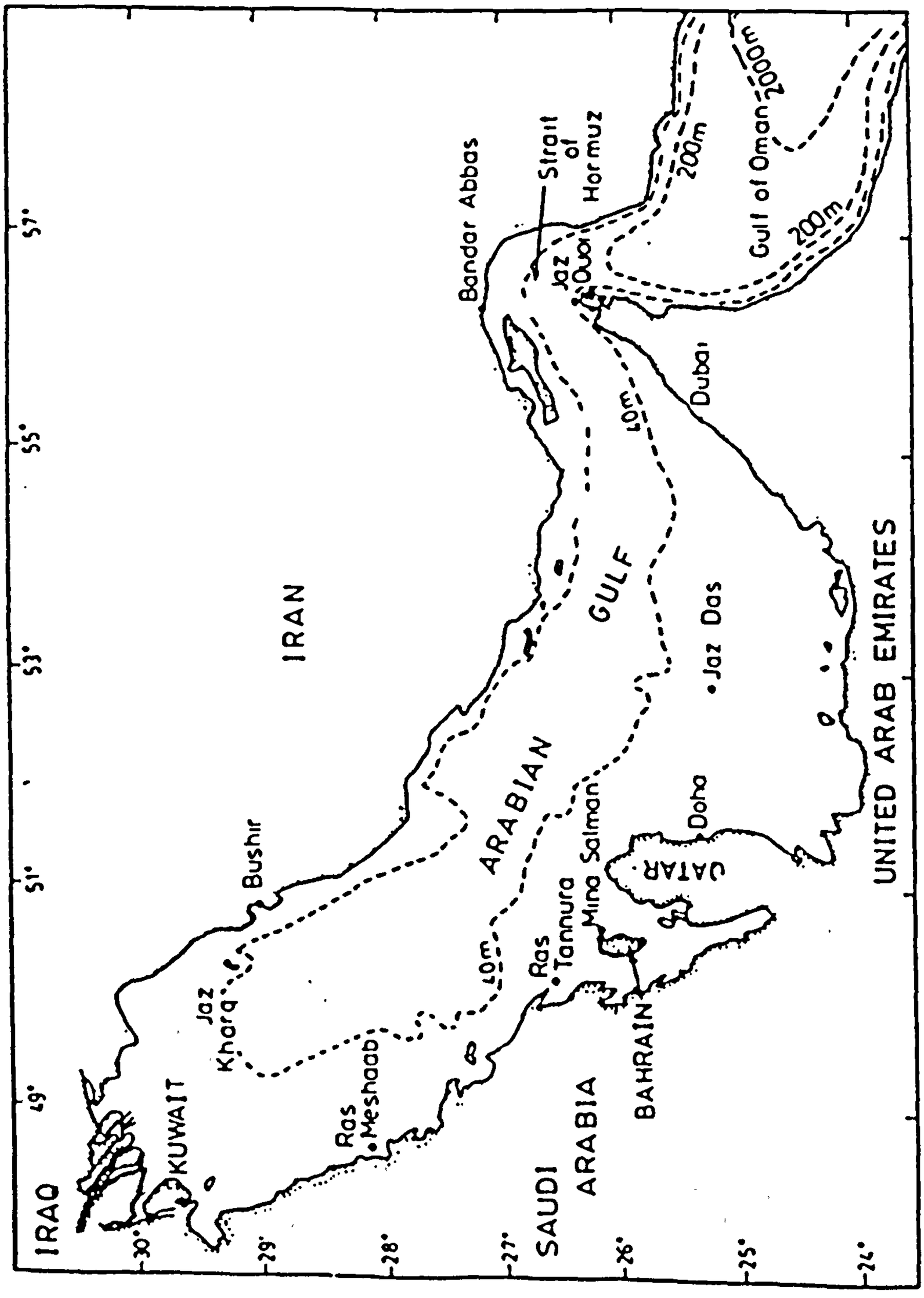

Topography of Arabian Gulf.

Figure 6.1

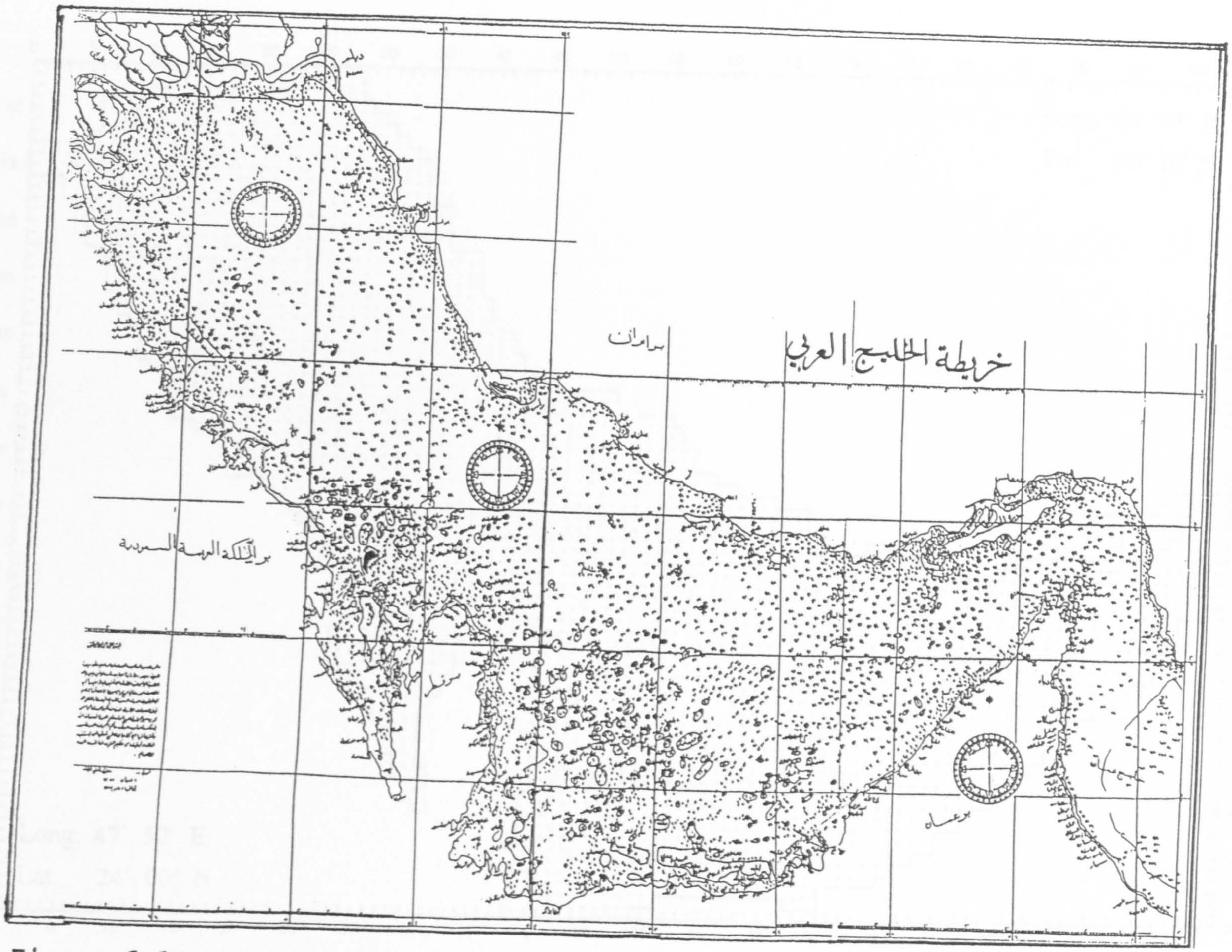

Figure 6.1(a) Bahrain Coast Guard Directorate (depth) Chart, Muharraq Bahrain.

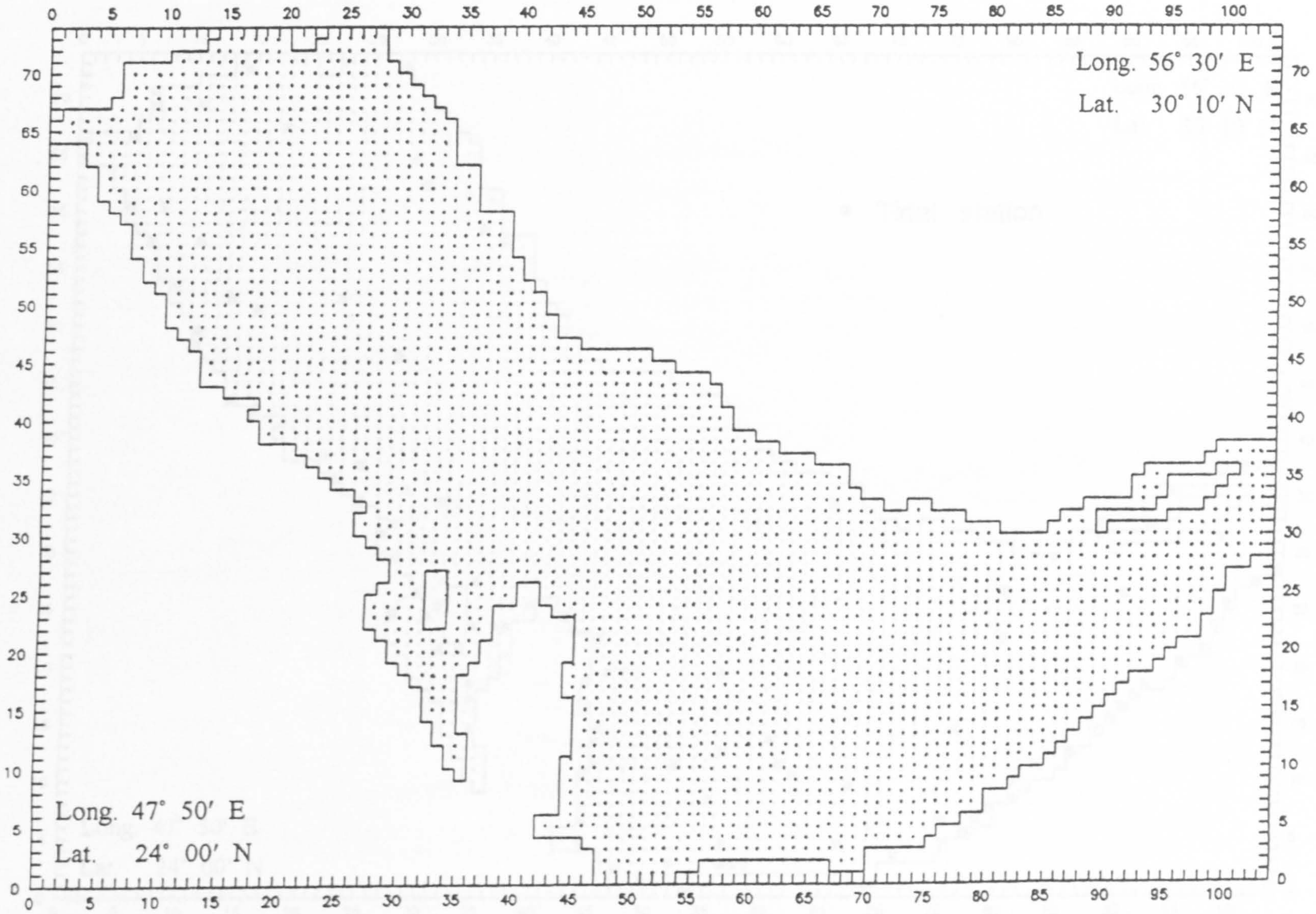

Figure 6.2a Grids for Arabian Gulf.

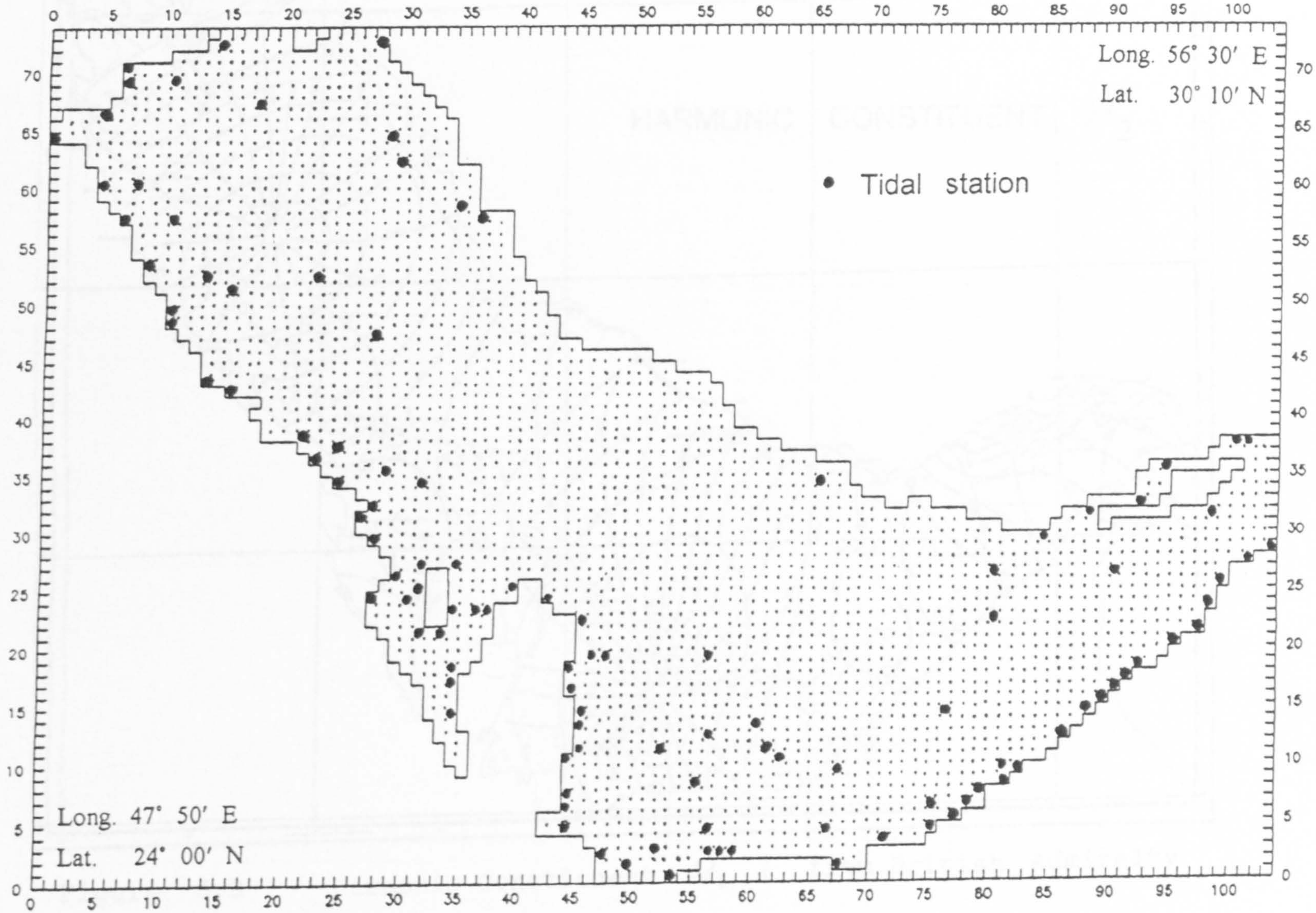

Figure 6.2b Location of tidal stations

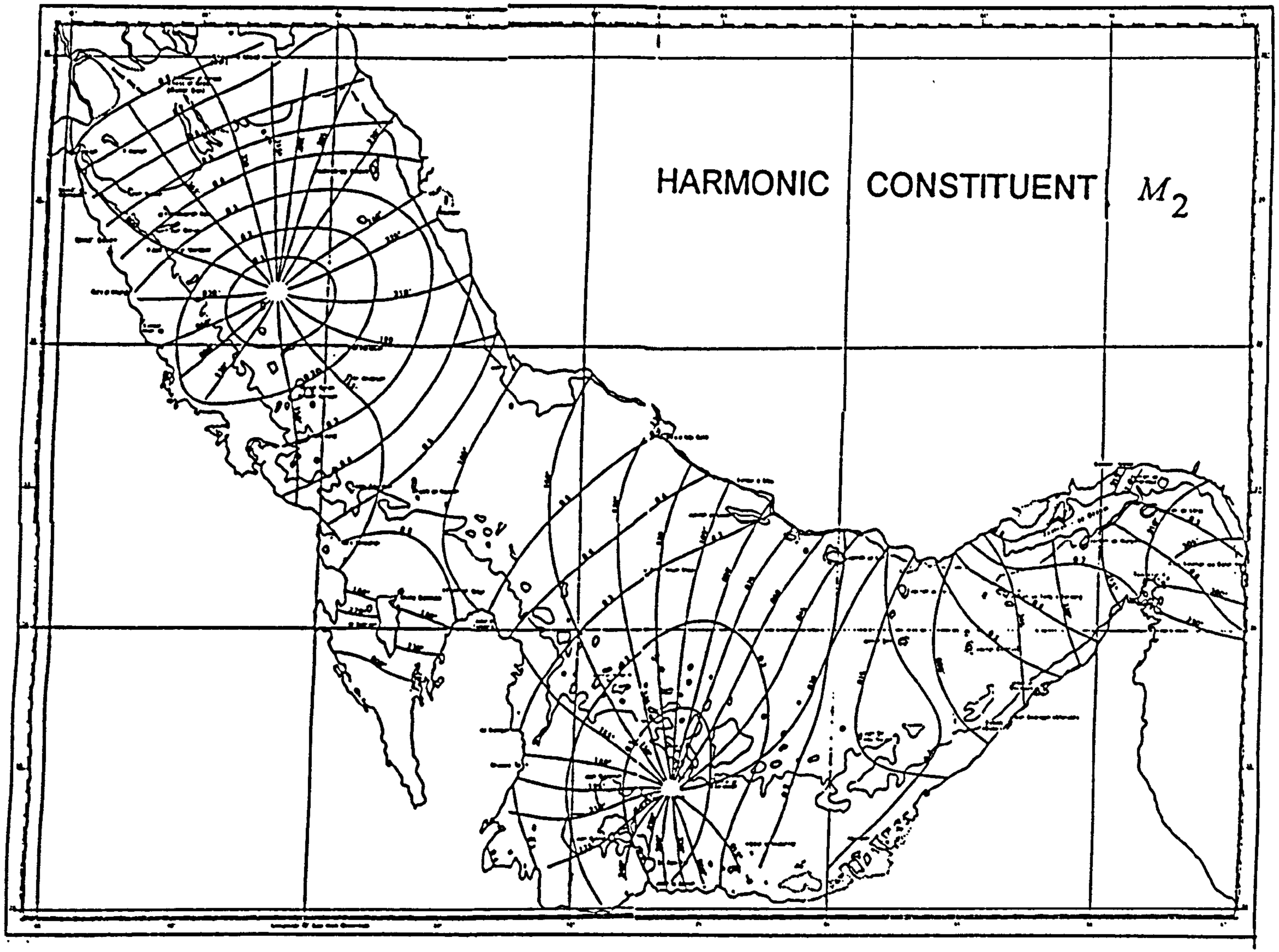

Figure 6.3 Harmonic Constituent M_2 (from British Admiralty)

g = time zone - 4 , H in metres.

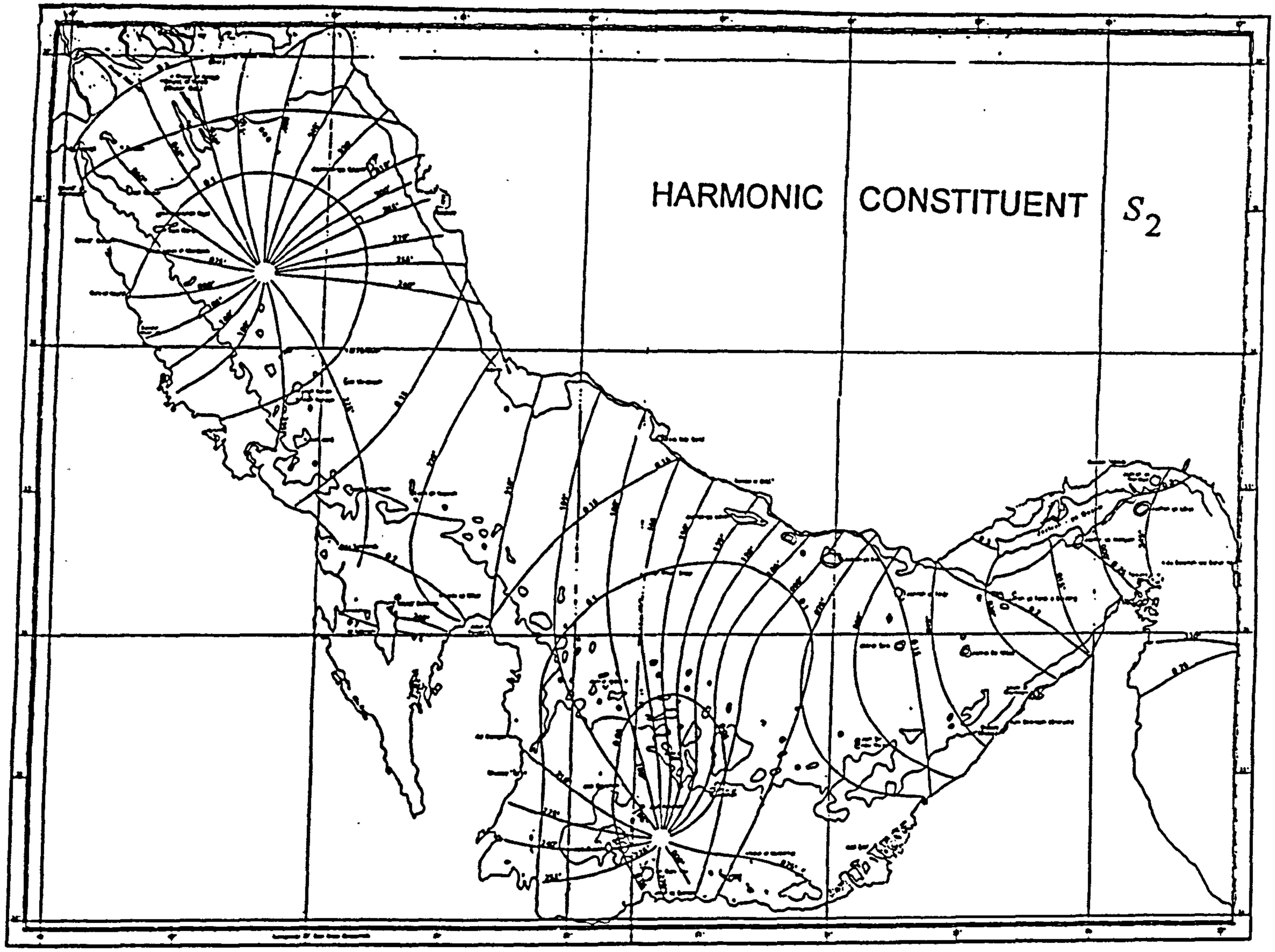

Figure 6.4 Harmonic Constituent S_2 (from British Admiralty)

g = time zone - 4 , H in metres.

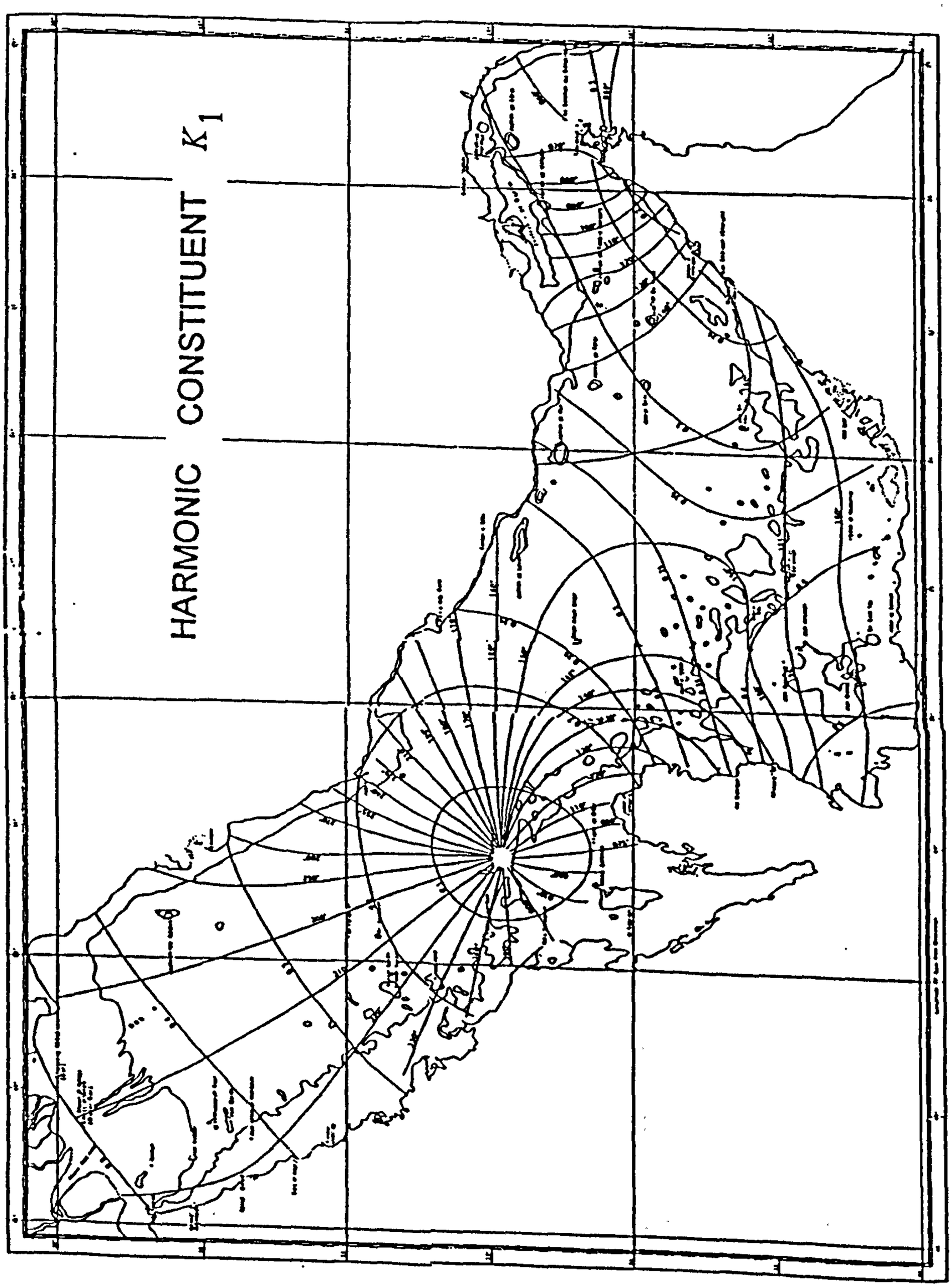

Figure 6.5 Harmonic Constituent K_1 (from British Admiralty)

g = time zone - 4 , H in metres.

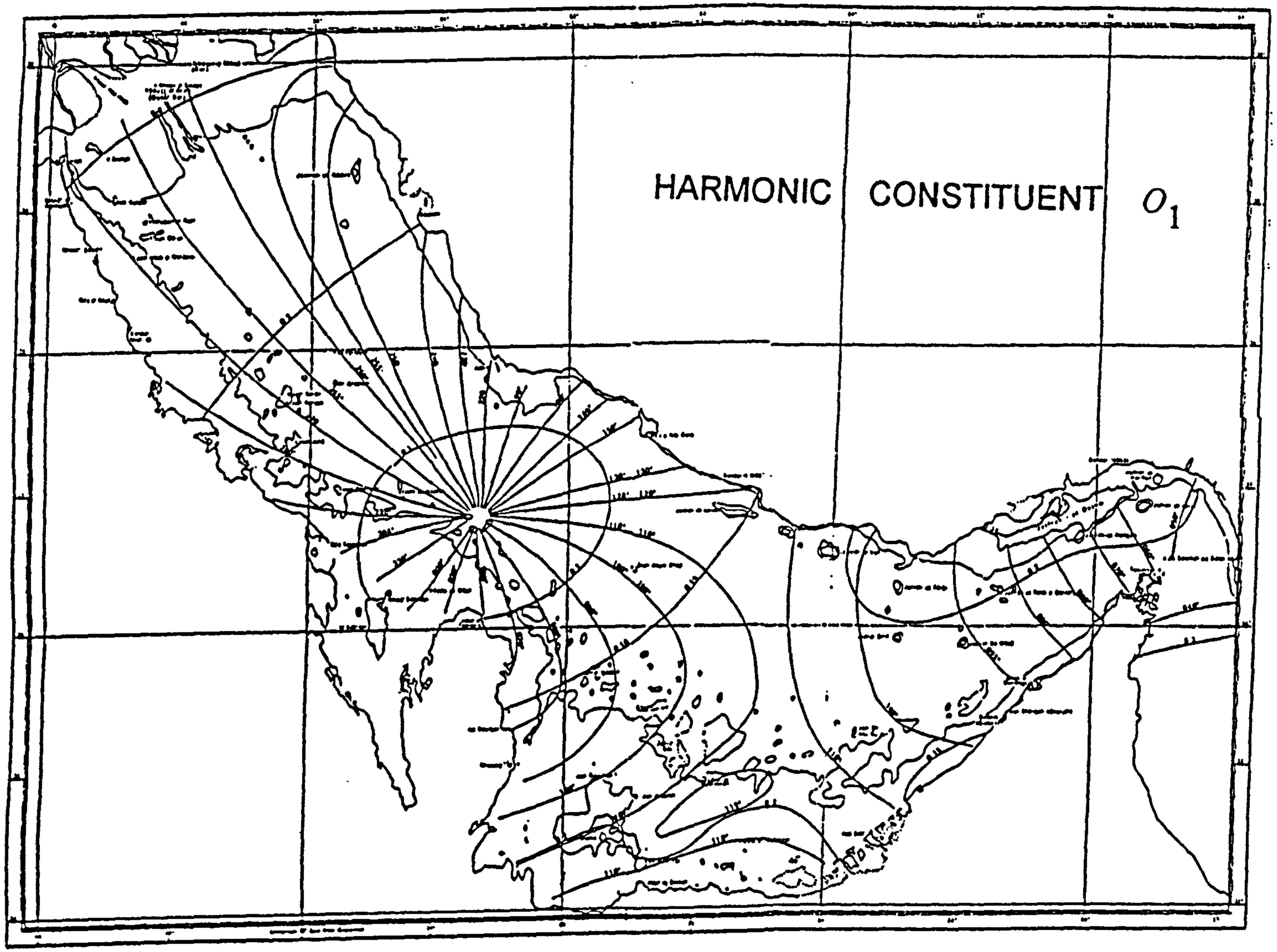

Figure 6.6 Harmonic Constituent O_1 (from British Admiralty)

g = time zone - 4 , H in metres.

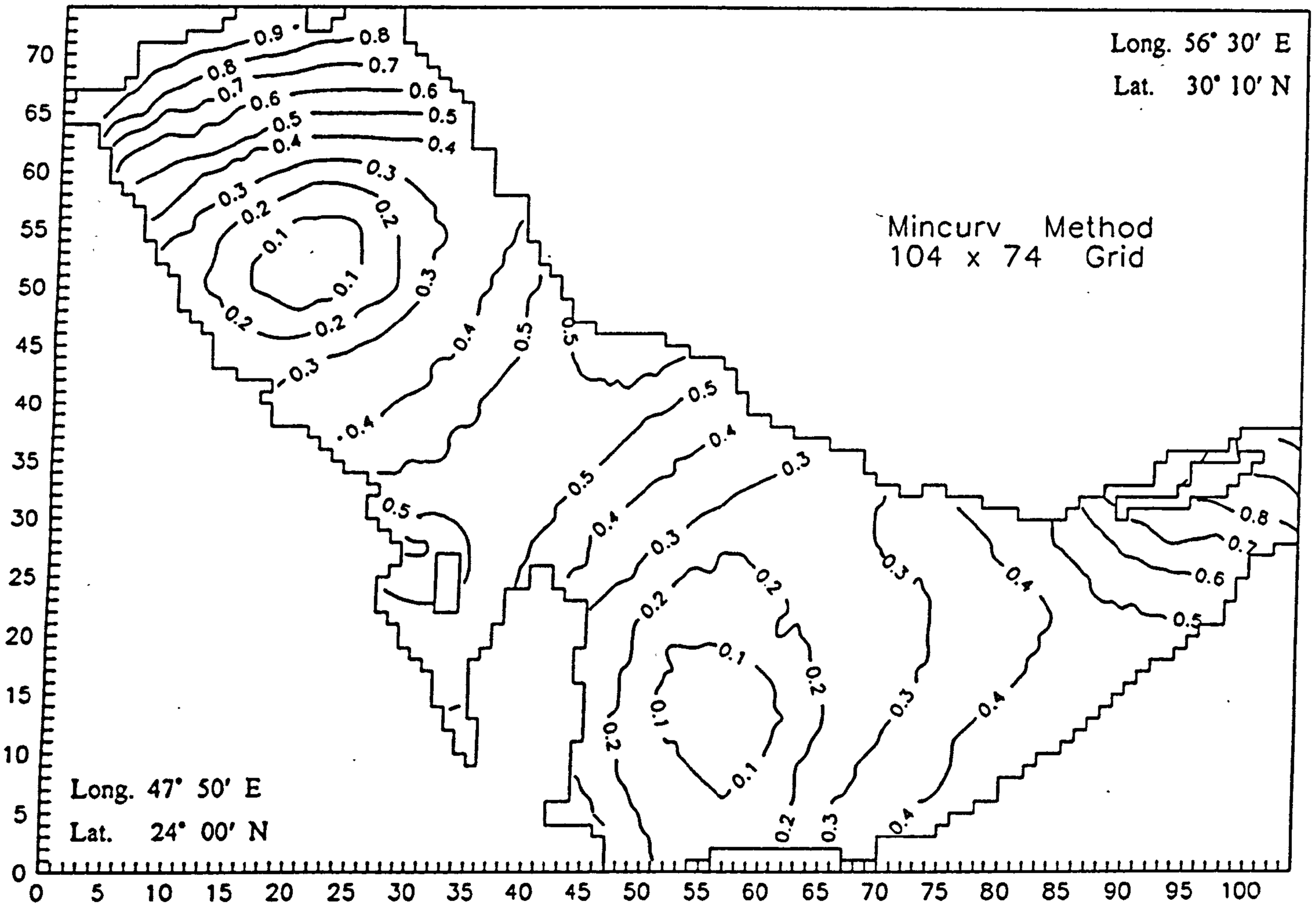

Figure 6.7 Contours of amplitude in metres for the M_2 tidal constituent computed from the EFDM model.

AMPLITUDE (metre) FOR TIDE S_2 IN ARABIAN GULF

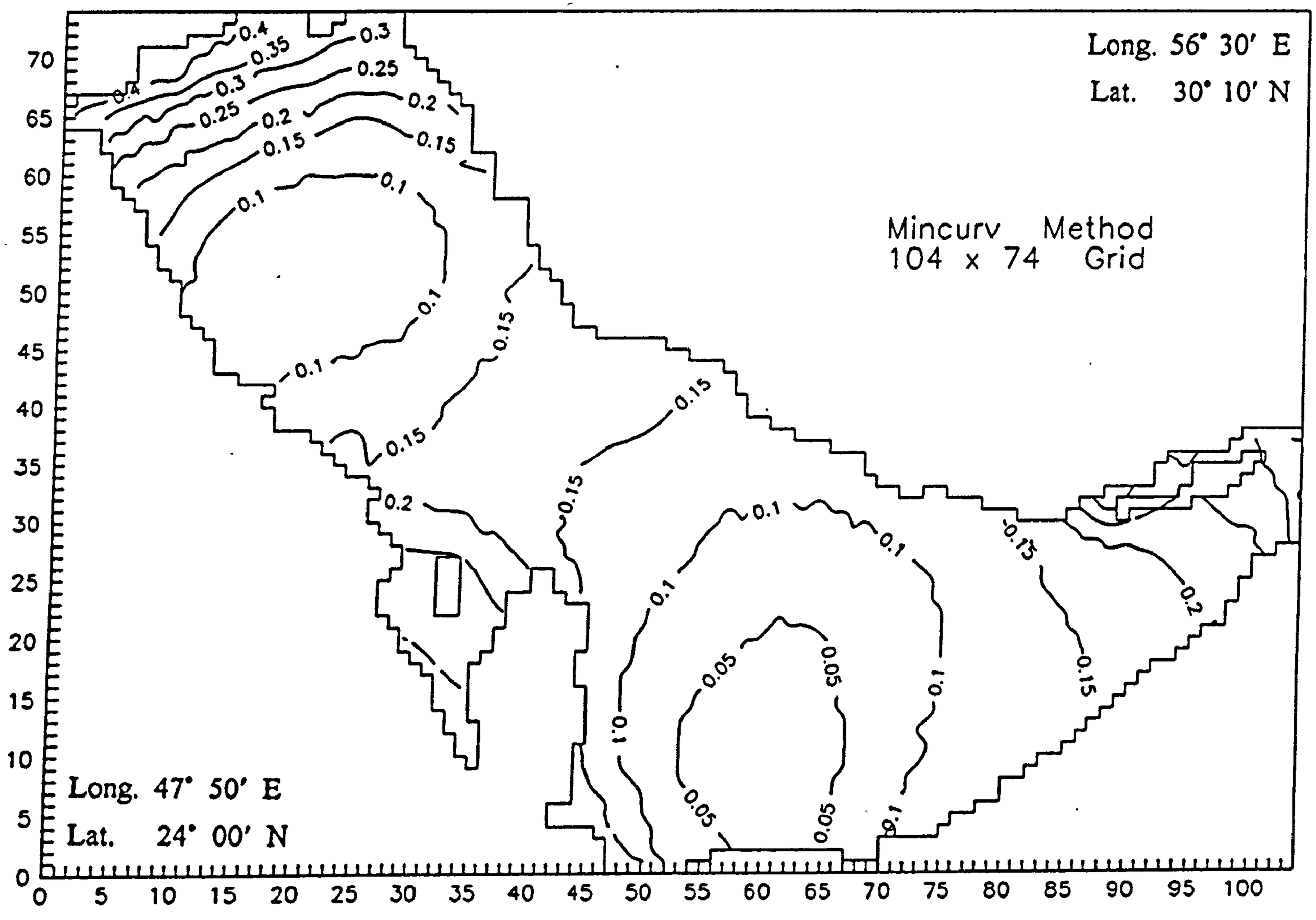

Figure 6.8 Contours of amplitude in metres for the S_2 tidal constituent computed from the EFDM model.

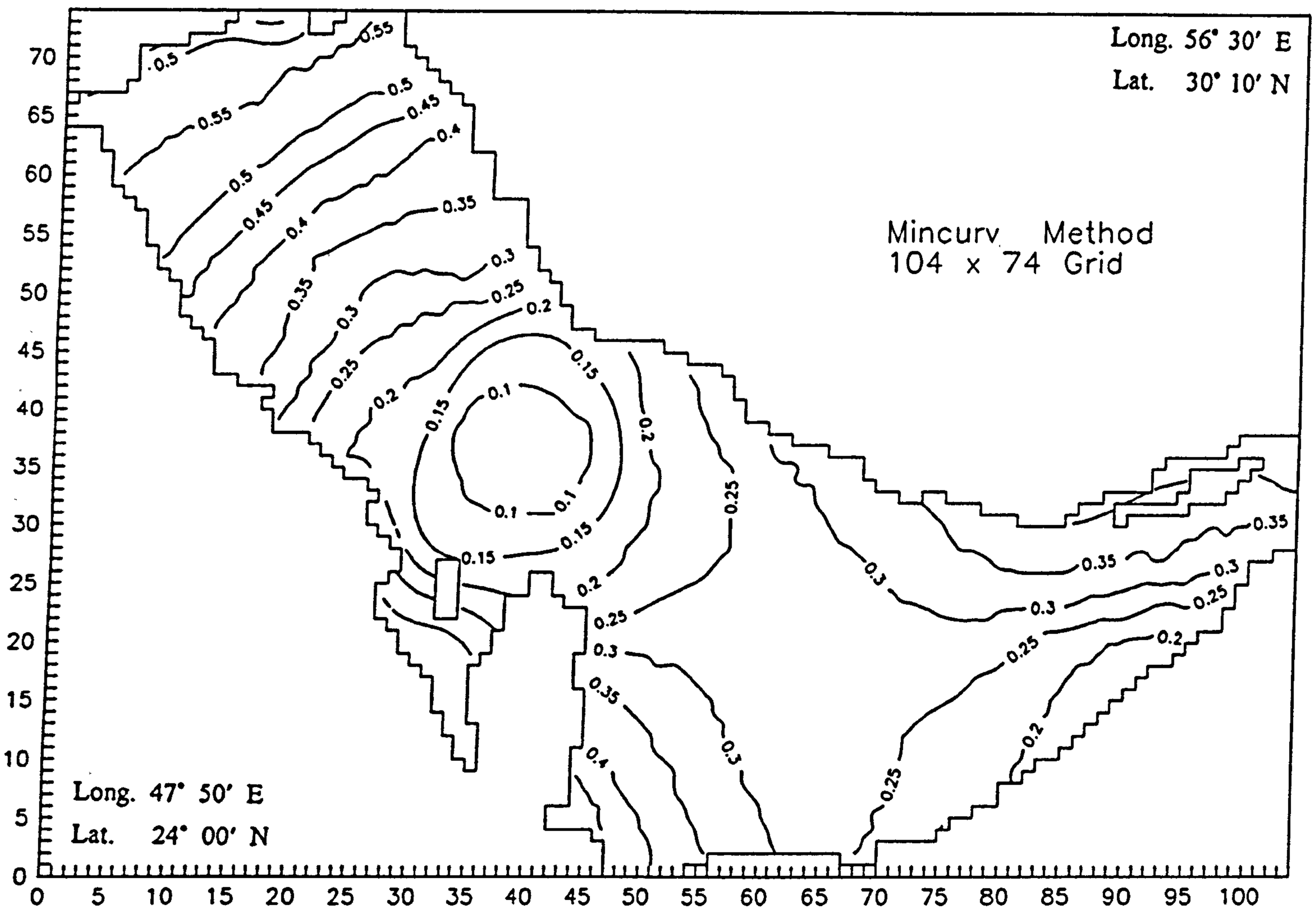

Figure 6.9 Contours of amplitude in metres for the K_1 tidal constituent computed from the EFDM model.

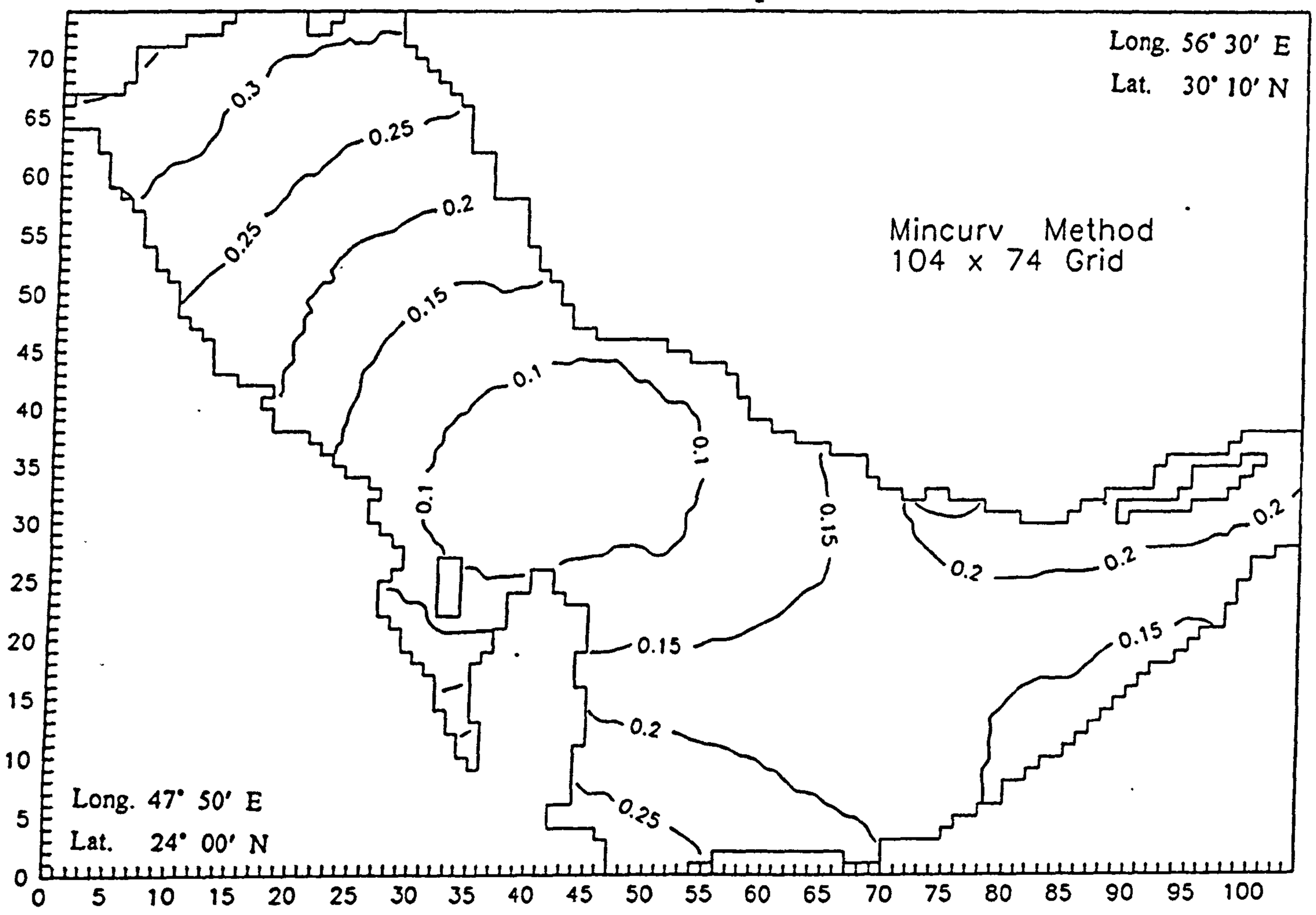

Figure 6.10 Contours of amplitude in metres for the O_1 tidal constituent computed from the EFDM model.

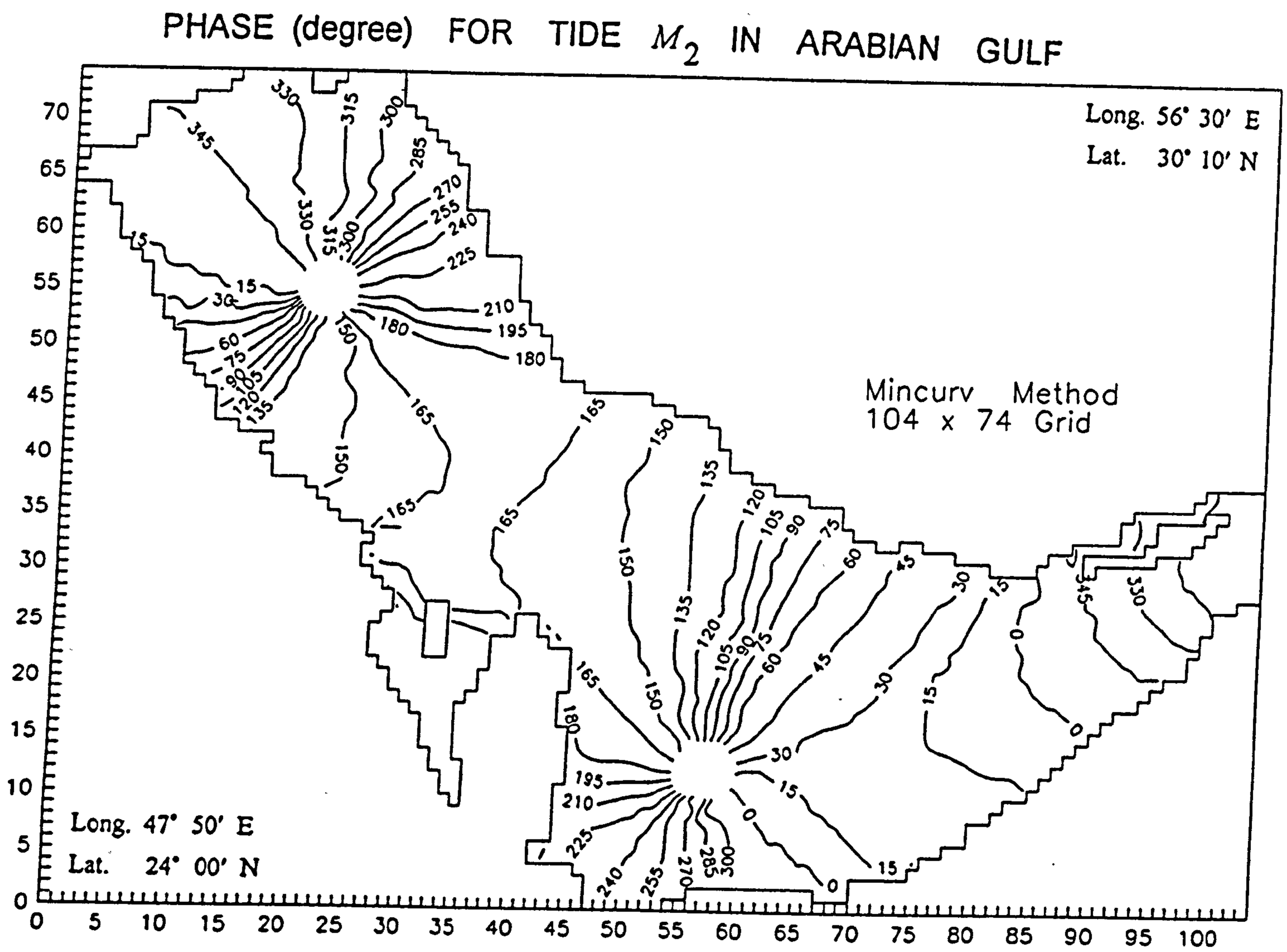

Figure 6.11 Contours of the phase in degrees for the M_2 tidal constituent computed from the EFDM model.

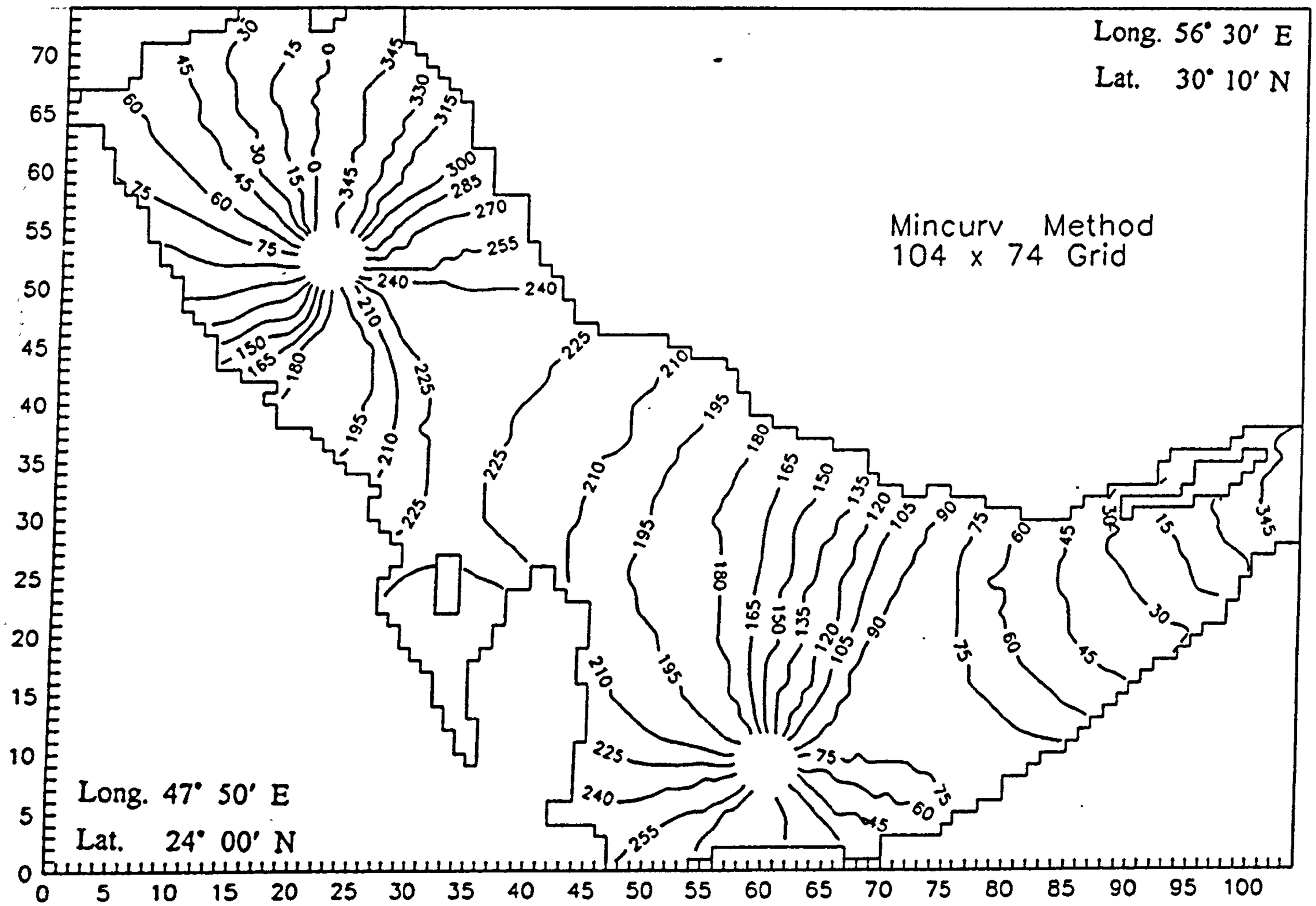

Figure 6.12 Contours of the phase in degrees for the S_2 tidal constituent computed from the EFDM model.

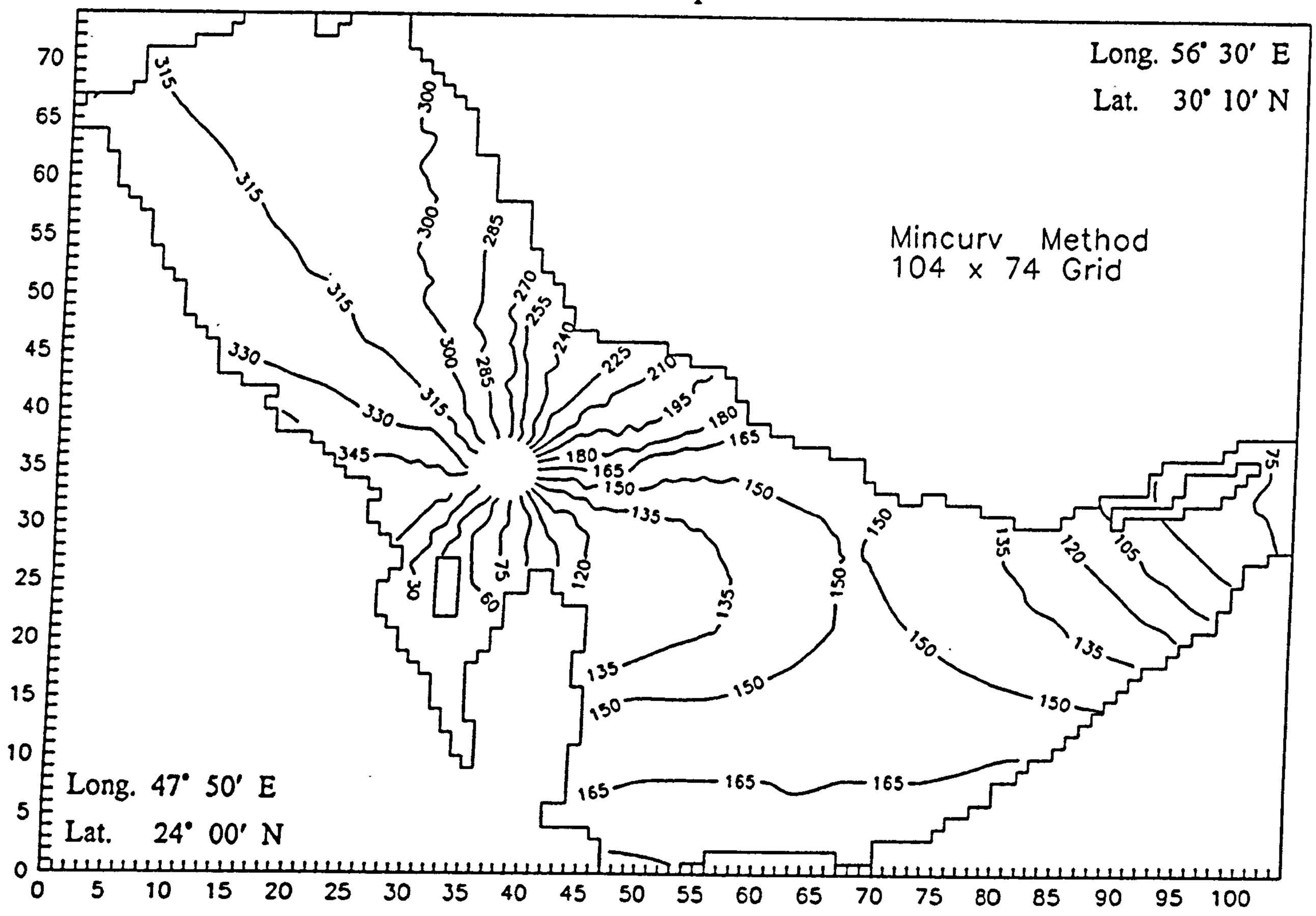

Figure 6.13 Contours of the phase in degrees for the K_1 tidal constituent computed from the EFDM model.

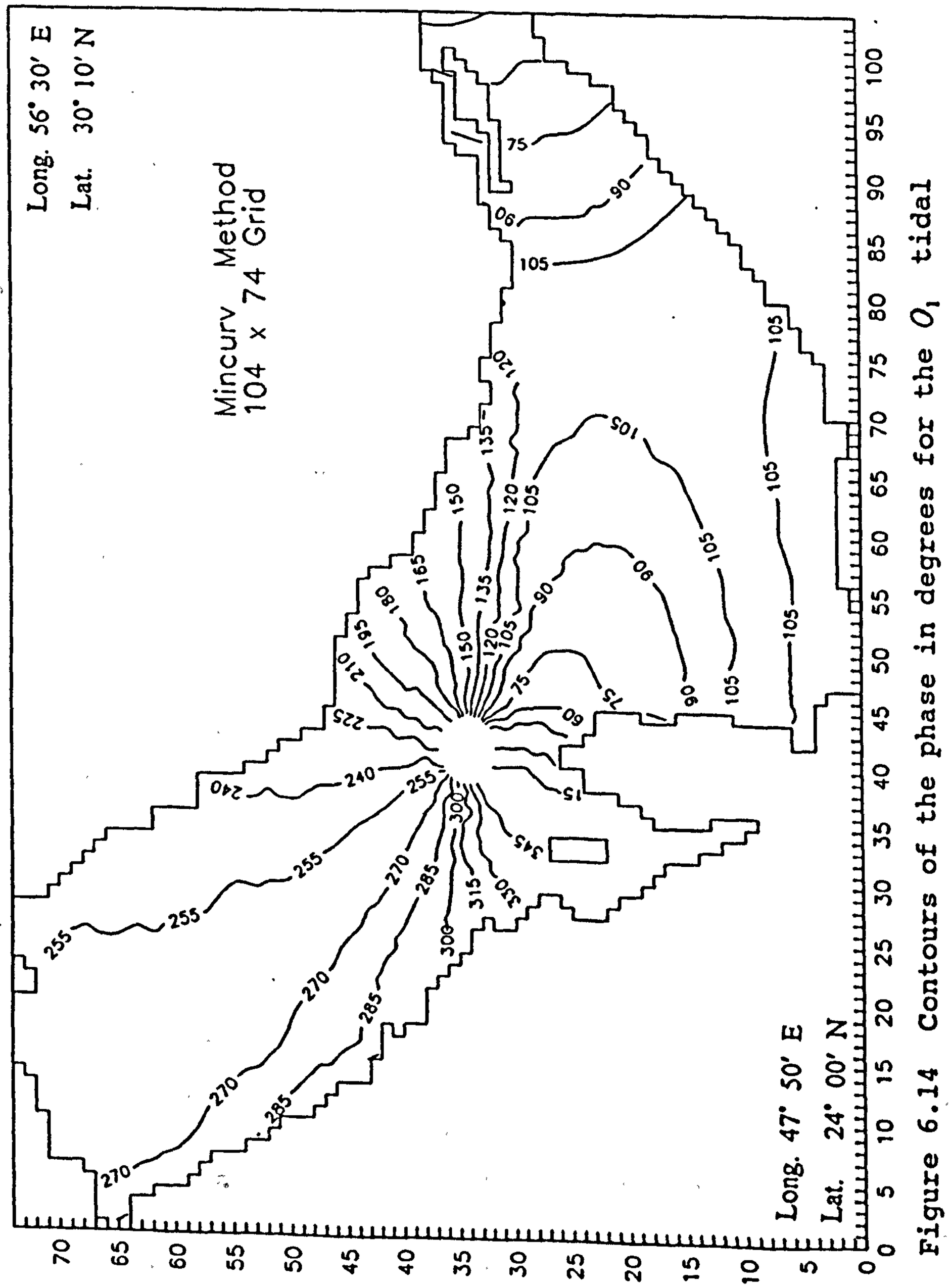

Figure 6.14 Contours of the phase in degrees for the O_1 tidal constituent computed from the EFDM model.

TABLE 6.1 Observed(O^*) and computed(C^*) amplitudes (cm) and phases(degree) of Tide M_2 in Arabian Gulf at Tidal stations shown in Figure 6.2b.

REF No.	Tidal Station	Lat.	Long.	Amplitude		Phase	
		N°	E°	O^*	C^*	O^*	C^*
4228	Jazirat Shawayhat	24 06	52 27	17	18	237	240
4230	Jazair al Yasat	24 10	52 00	21	22	230	231
4231	Umm al Hatab	24 13	51 52	23	24	224	228
4223	Sir Bani Yas	24 17	52 37	10	11	271	271
4222	Jabal az Zannah	24 11	52 38	22	19	272	272
4221b	Ruwais	24 08	52 44	09	07	292	297
4210c	Umm an Nar	24 26	54 30	25	27	079	077
4234	Jazair Ghaghah	24 24	51 33	34	28	219	225
4223a	Ghasha Light Bouy	24 26	52 34	13	07	245	251
4214	Halat al Mubarraz	24 27	53 22	28	20	017	012
4212	Khawr Zubayyah	24 20	54 10	37	29	045	043
4235	Ras Abu Qumayyis	24 34	51 30	25	22	185	195
4210b	Mina Zayed	24 31	54 23	25	25	027	029
4235a	Khawr al Udayd	24 42	51 27	30	26	179	178
4224	Jazirat Arzanah	24 47	52 34	05	06	227	239
4247e	Ghar al Buraid	24 48	50 52	23	22	280	280
4215	Zaqqum Oilfield	24 51	53 31	27	22	016	017
4237	Musay'id Harbour	24 57	51 35	26	26	173	187
4219	Jazirat Zarakkuh	24 53	53 05	11	15	022	020
4236	Musayid O. Channel	25 02	51 39	29	25	152	160
4226	Jazirat Sharaiwah	25 02	52 14	15	14	180	180
4216	Zirku Terminal	25 02	53 01	13	15	040	030
4221a	El Bunduq Oilfield	25 06	52 37	10	13	140	142
4238	Al-Wakrah	25 10	51 37	27	24	153	142
4221	Jazirat Das	25 10	52 53	10	14	070	060
4247b	Umm Bab	25 13	50 46	22	24	281	281
4239	Ad Dawhah	25 17	51 33	32	35	138	140
4239a	Jazirah al Aliyah	25 24	51 34	32	25	138	138
4247b	Dukhan	25 26	50 45	20	24	283	286
4247	Nagiyah	25 41	50 54	17	18	209	209

Table 6.1 (Continued)

REF No.	Tidal Station	Lat.	Long.	Amplitude		Phase	
		N°	E°	*O°*	*C°*	*O°*	*C°*
4227	Jazirat Halul	25 40	52 25	20	18	136	133
4202	Jazirat Al Hamra	25 43	55 47	40	40	209	209
4201	Ras al Khaymah	25 49	55 57	54	45	326	320
4296	Jazirat Sirri	25 54	54 33	39	33	351	350
4250b	Umm Jalid	26 02	50 43	27	27	193	195
4250c	Umais	25 59	50 53	17	23	172	176
4253a	Qurayah	25 53	50 07	16	18	256	260
4249	Az Zellaq	26 03	50 29	08	10	283	276
4253b	Al Khubar	26 17	50 13	31	25	146	155
4295	Jazireh-ye-Farur	26 15	54 31	42	40	357	003
4298	Jazir Tunb al Kubra	26 16	55 18	54	51	329	332
4199	Khawr Khasab	26 12	56 15	67	58	312	310
4198	Khawr al Quway	26 21	56 22	69	69	309	308
4253c	Ad Damman	26 27	50 05	65	58	132	144
4297	Bandar-e Lengeh	26 33	54 53	60	55	346	354
4253d	Dawhat at Tarut	26 39	50 02	54	59	139	150
4299	Jazireh-ye Hangam	26 41	55 54	74	71	305	310
4254	Ras Tannurah	26 38	50 10	59	50	169	156
4260c	Ras al Kafji	28 25	48 31	33	42	342	357
4254c	Ras al Qualay'ah	26 51	49 54	48	45	123	140
4254a	Abu Sa'afah	26 56	50 30	51	43	144	150
4254b	Fasht Gharibah	26 59	50 13	51	44	131	141
4302	Laft	26 56	55 44	45	41	315	315
4255	Al Jubayl	27 04	49 39	47	43	119	135
4255b	Jazirat al Jurayd	27 12	49 57	41	42	124	137
4303a	Bandar Abbas	27 10	56 12	108	116	298	300
4255a	Dawhat Abu Ali	27 13	49 43	44	42	124	137
4288	Bandar Asalu	27 28	52 37	51	52	120	130
4256	Al Farisiyeh	28 00	50 10	22	26	146	150
4258	Ras as Saffaniyah	28 00	48 46	25	32	015	019
4259	Bandar Mish'ab	28 07	48 37	25	32	009	002
4260c	Zuluf Oilfield	28 22	49 10	10	12	340	331

Table 6.1 (Continued)

REF No.	Tidal Station	Lat.	Long.	Amplitude		Phase	
				---	---	---	---
		N°	E°	$O^{\bullet}$	$C^{\bullet}$	$O^{\bullet}$	$C^{\bullet}$
4285	Lavar	28 15	51 16	50	57	169	180
4260b	Saffaniyah Oilfield	28 25	49 00	17	23	342	350
4260	Marjan Oilfield	28 26	49 43	08	09	179	165
4260d	Jazirat Umm al	28 41	48 39	34	38	333	342
4261	Mina Saud	28 44	48 24	42	51	336	350
4261a	Jazirat Qaruh	28 49	48 47	37	43	323	330
4262	Mina Al-Ahmadi	29 04	48 10	65	65	334	335
4261b	Jazirat Kubbar	29 04	48 30	54	61	324	333
4263	Shuwaykh	29 21	47 55	95	101	343	340
4268	Shatt Al Arab	29 50	48 43	94	95	338	320
4269	Al Faw	29 58	48 29	82	90	337	337

$C^{\bullet}$ = Computed values.

$O^{\bullet}$ = Observed values are taken from Admirality chart (1988a).

TABLE 6.2 Observed(O^*) and computed(C^*) amplitudes (cm) and phases(degree) of Tide K_1 in Arabian Gulf at Tidal stations shown in Figure 6.2b.

Ref No.	Tidal Station	Lat.	Long.	Amplitude		Phase	
		N°	E°	O^*	C^*	O^*	C^*
4210c	Umm an Nar	24 26	54 30	22	22	211	210
4235	Ras Abu Qumayyis	24 34	51 30	47	40	141	155
4210b	Mina Zayed	24 31	54 23	27	22	166	170
4210	Khawr Sa'diyat	24 33	54 33	24	21	235	230
4208a	Khawr Ghurabi	24 49	54 43	26	20	164	164
4208	Khawr Ghanadah	24 50	54 46	27	19	165	165
4237	Musay'id Harbour	24 57	51 35	43	39	138	155
4219	Jazirat Zarakkuh	24 53	53 05	36	30	156	154
4216	Zirku Terminal	25 02	53 01	35	30	152	152
4221a	El Bunduq Oilfield	25 06	52 37	38	33	152	157
4207	Jabal Ali	25 03	55 05	24	18	157	156
4238	Al Wakrah	25 10	51 37	37	36	126	146
4221	Jazirat Das	25 13	52 53	36	30	146	150
4239	Ad Dawhah	25 17	51 33	36	34	118	135
4211	Jaz Sir Abu Nuayr	25 13	54 13	28	21	149	150
4206	Dubayy	22 15	55 19	17	14	167	155
4239a	Jazirat al Aliyah	25 24	51 34	34	32	118	125
4204	Ajman	25 25	55 26	17	13	163	145
4240	Sumaysimah	25 34	51 30	34	32	109	125
4203	Um al Qaywayn	25 35	55 35	20	13	134	129
4212	Khawr Zubayyah	24 20	54 10	30	25	180	180
4241	Khawr Shaqiq	25 41	51 31	35	31	119	125
4227	Jazirat Halul	25 40	52 25	29	26	140	145
4202	Jazirat al Hamra	25 43	55 47	13	12	115	115
4201	Ras al Khaymah	25 49	55 57	13	13	111	108
4242	Ras Laffan	25 54	51 35	25	20	098	110
4296	Jazirat Sirri	25 54	54 33	24	25	137	138
4200	Mina Saqr	25 58	56 03	17	18	110	106
4253a	Qurayah	25 53	50 07	07	08	149	136

Table 6.2 (continued)

Ref No.	Tidal Station	Lat.	Long.	Amplitude		Phase	
		N°	E°	*O°*	*C°*	*O°*	*C°*
4243	Jabal al Fuwayrit	26 03	51 22	20	18	099	100
4244	Ar Ru'ays	26 10	51 11	15	15	064	075
4253b	Al Khubar	26 17	50 13	08	10	015	017
4295	Jazireh-ye Farur	26 15	54 31	35	30	134	135
4298	Jaz. Tunb al Kubra	26 16	55 18	25	28	122	115
4250d	Bahrain App Bay	26 22	50 47	12	12	055	055
4199	Khawr Khesab	26 12	56 15	22	22	068	075
4198	Khawr al Quway	26 21	56 22	26	28	070	069
4253c	Ad Damman	26 27	50 05	15	18	332	353
4297	Bandar-e Lengeh	26 33	54 53	33	33	127	123
4301	Basa'idu	26 40	55 16	39	39	109	105
4299	Jazireh-ye Hangam	26 41	55 54	29	35	081	081
4254	Ras Taannurah	26 38	50 10	14	20	339	349
4254c	Ras al Qualay'ah	26 51	49 54	18	23	319	325
4254a	Abu Sa'afah	26 56	50 30	09	10	347	345
4290	Jazireh ye Laven	26 48	53 23	30	32	145	145
4254b	Fasht Gharibah	26 59	50 13	14	18	322	340
4302	Laft	26 56	55 44	44	45	085	083
4255	Al Jubayl	27 04	49 39	19	22	317	335
4255b	Jazirat al Jurayd	27 12	49 57	15	18	305	321
4255a	Dawhat Abu Ali	27 13	49 43	17	22	318	330
4288	Bandar Asalu	27 28	52 37	24	28	168	170
4257	Manifah	27 35	48 54	31	35	316	303
4256	Al Farisiyah	28 00	50 10	27	25	305	315
4258	Ras as Saffaniyah	28 00	48 46	39	45	311	320
4259	Bandar Mish'ab	28 07	48 37	38	42	304	318
4260a	Zulf Oilfield	28 22	49 10	36	38	296	315
4285	Lavar	28 15	51 16	25	29	262	265
4260b	Saffaniyah	28 25	49 00	36	38	303	316
4260	Marjan Oilfield	28 26	49 43	32	33	286	300
4260d	Jaz Umm al Maradim	28 41	48 39	41	46	310	318
4261	Mina Saud	28 44	48 24	43	43	305	313

Table 6.2 (continued)

Ref No.	Tidal Station	Lat.	Long.	Amplitude		Phase	
		N°	E°	O^*	C^*	O^*	C^*
4261a	Jazirat Qaruh	28 49	48 47	44	45	298	309
4283a	Halileh	28 49	50 53	32	32	268	268
4283	Bushehr	28 54	50 45	31	33	280	282
4262	Mina Al Ahmadi	29 04	48 10	47	51	306	316
4282	Jazireh ye Khark	29 16	50 20	38	41	296	311
4264	Doha Harbour	29 23	47 48	51	43	309	310
4266	Warba Spit	29 59	48 09	66	65	306	315
4276a	Khor Musa	29 42	49 24	45	49	298	310
4266a	Beacon No 12	29 56	48 02	65	65	311	315
4268	Shat Al Arab	29 50	48 43	50	55	295	300
4279	Khawr-e Musa Bar	30 00	49 03	53	56	314	308
4280	Bandar Daylam	30 04	50 06	35	40	290	301

O^* = Observed values are taken from Adm. chart (1988a).

C^* = Computed values.

TABLE 6.3 Observed(O^*) and computed(C^*) amplitudes (cm) and phases(degree) of Tide O_1 in Arabian Gulf at Tidal stations shown in Figure 6.2b.

REF No.	Tidal Stations	Lat.	Long.	Amplitude		Phase	
				---	---	---	---
		N°	E°	O^*	C^*	O^*	C^*
4228	Jazirat Shawayhat	24 06	52 27	19	22	108	108
4230	Jazair al Yasat	24 10	52 00	25	25	110	110
4229	Jazirat Dalma	24 28	52 19	24	20	122	120
4223	Sir Bani Yas	24 17	52 37	25	20	107	110
4231	Umm al Hatab	24 13	51 52	24	22	114	114
4222	Jabal az Zannah	24 11	52 38	22	19	108	110
4221b	Ruwais	24 08	52 44	24	20	105	110
4213	Abu al Abyad	24 15	53 49	22	16	102	105
4234	Jazair Ghaghah	24 24	51 33	18	23	106	105
4210c	Umm an Nar	24 26	54 30	12	16	120	110
4235	Ras Abu Qumayyis	24 34	51 30	25	22	090	089
4210a	Umm ad Dalkh	24 35	54 09	18	16	108	105
4210b	Mina Zayed	24 31	54 23	18	15	109	100
4235a	Khawr al Udayd	24 42	51 27	27	22	090	098
4224	Jazirat Arzanah	24 47	52 34	19	17	105	101
4247e	Ghar al Buraid	24 48	50 52	12	15	070	064
4208a	Khawr Ghurabi	24 49	54 43	13	14	112	115
4208	Khawr Ghanadah	24 50	54 46	15	21	088	098
4219	Jazirat Zarakkuh	24 53	53 05	16	17	117	110
4226	Jazirat Sharaiwah	25 02	52 14	19	18	097	102
4216	Zirku Terminal	25 02	53 01	17	17	099	107
4207	Jabal Ali	25 03	55 05	16	13	103	105
4221	Jazirat Das	25 10	52 53	17	17	107	104
4239	Ad Dawhah	25 17	51 33	17	19	069	085
4211	Jaz. Sir Abu Nuayr	25 13	54 13	17	16	103	107
4206a	Mina Rashid	25 15	55 16	16	13	097	102
4206	Dubayy	25 15	55 19	18	15	107	099
4239a	Jazirat al Aliyah	25 24	51 34	15	18	095	075
4205	Ash Shariqah	25 22	55 23	16	13	102	096
4204	Ajman	25 25	55 26	18	14	106	094

Table 6.3 (continued)

Ref No.	Tidal Station	Lat.	Long.	Amplitude		Phase	
		N°	E°	$O^{\bullet}$	$C^{\bullet}$	$O^{\bullet}$	$C^{\bullet}$
4240	Sumaysimah	25 34	51 30	15	17	059	072
4203	Umm al Qaywayn	25 35	55 35	17	11	089	089
4241	Khawr Shaqiq	25 41	51 31	16	16	054	044
4227	Jazirat Halul	25 40	52 25	15	15	090	086
4242	Ras Laffam	25 54	51 35	12	12	042	059
4296	Jazirat Sirri	25 54	54 33	18	17	087	106
4200	Mina Saqr	25 58	56 03	15	18	075	068
4253a	Qurayah	25 53	50 07	08	10	051	050
4243	Jabal al Fuwayrif	26 03	51 22	09	11	042	042
4119b	Bukha	26 09	56 08	13	11	082	064
4295	Jazireh-ye-Farur	26 15	54 31	20	19	096	103
4298	Jaz. Tunb al Kubra	26 16	55 18	20	18	078	084
4199	Khawr Khesab	26 12	56 15	16	13	071	060
4198	Khawr al Quway	26 21	56 22	16	18	067	052
4253c	Ad Damman	26 27	50 05	13	18	292	304
4251	Sitrah	26 07	50 38	06	07	306	315
4297	Bardar-e Lengeh	26 33	54 53	22	21	089	093
4301	Basaidu	26 40	55 16	25	24	101	090
4299	Jazireh-ye Hangam	26 41	55 54	20	19	063	064
4254	Ras Tannurah	26 38	50 10	12	17	290	297
4260c	Ras al Khafji	28 25	48 31	22	18	262	246
4254a	Abu Sa'afah	26 56	50 30	11	13	287	293
4254b	Fasht Gharibah	26 59	50 13	11	16	265	273
4303a	Bandar Abbas	27 10	56 12	25	25	053	053
4255c	Dawhat Abu Ali	27 13	49 43	14	18	269	290
4288	Bandar Asalu	27 28	52 37	12	14	168	165
4257	Manifah	27 35	48 54	21	25	267	287
4256	AL Farisiyah	28 00	50 10	20	18	260	258
4258	Ras as Saffaniyah	28 00	48 46	26	21	263	250
4285	Lavar	28 15	51 16	18	16	220	230
4260d	Jaz. Umm al Maraim	28 41	48 39	27	33	259	272
4261a	Jazirat Qaruh	28 49	48 47	31	31	254	260

Table 6.3 (continued)

Ref No.	Tidal Station	Lat.	Long.	Amplitude		Phase	
		N°	E°	$O^{\bullet}$	$C^{\bullet}$	$O^{\bullet}$	$C^{\bullet}$
4261	Mina Saud	28 44	48 24	27	32	259	273
4283a	Halileh	28 49	50 53	20	23	226	237
4262	Mina Al-Ahmadi	29 04	48 10	31	35	258	265
4261b	Jazirat Kubbar	29 04	48 30	28	33	249	260
4282	Jazirah ye Khark	29 16	50 20	25	27	241	241
4283	Bushehr	28 54	50 43	20	24	238	233
4264	Doha	29 23	47 48	33	27	267	250
4266	Warba Spit	29 59	48 09	31	37	254	264
4276a	Khor Musa	29 42	49 24	32	32	258	260
4279	Khawr-e Musa Bar	30 00	49 03	31	35	253	262
4268	Shatt al Arab	29 50	48 43	30	36	247	265
4280	Bandar Deylam	30 04	50 06	30	31	252	253

$C^{\bullet}$ = Computed values

$O^{\bullet}$ = Obseved values are taken from Admirality chart (1988a)

TABLE 6.4 Observed(O^*) and computed(C^*) amplitudes (cm) and phases(degree) of Tide S_2 in Arabian Gulf at Tidal stations shown in Figure 6.2b.

REF No.	Tidal station	Lat.		Long.		Amplitude		Phase	
		N°		E°		O^*	C^*	O^*	C^*
4228	Jazirat Shuwayhat	24	06	52	27	08	12	259	259
4230	Jazair al Yasat	24	10	52	00	09	13	260	260
4229	Jazirat Dalma	24	28	52	19	07	10	242	251
4231	Umm al Hatab	24	13	51	52	09	13	244	255
4223	Sir Bani Yas	24	17	52	37	05	06	240	250
4222	Jabal az Zannah	24	11	52	38	03	03	256	260
4221b	Ruwais	24	08	52	44	04	04	305	291
4213	Abu al Abyad	24	15	53	49	14	14	089	073
4234	Jazair Ghaghah	24	24	51	33	14	19	253	253
4223a	Ghasha Light Buoy	24	26	52	34	06	05	238	254
4214	Halat al Mubarraz	24	27	53	22	12	10	075	060
4212	Khawr Zubayyah	24	20	54	10	15	14	103	092
4235	Ras Abu Qumayyis	24	34	51	30	14	18	218	235
4210a	Umm Ad Dalkh	24	35	54	09	17	14	070	070
4210b	Mina Zayed	24	31	54	23	13	13	086	080
4235a	Khawr al Udayd	24	42	51	27	13	15	209	225
4210	Khawr Sa'Diyat	24	33	54	33	12	12	080	079
4224	Jazirat Arzanah	24	47	52	34	03	04	190	208
4208a	Khawr Ghurabi	24	49	54	43	14	12	072	072
4208	Khawr Ghanadah	24	50	54	46	15	10	078	075
4219	Jazirat Zarakkuh	24	53	53	05	04	05	097	090
4236	Musayid	25	02	51	39	11	13	184	201
4226	Jazirat Sharaiwah	25	02	52	14	06	05	200	205
4216	Zirku Terminal	24	02	53	01	05	06	090	099
4221a	El Bunduq Oil Field	25	06	52	37	05	06	181	181
4207	Jabal Ali	25	03	55	05	15	12	051	058
4221	Jazirat Das	25	10	52	53	05	04	129	130
4239	Ad Dawhah	25	17	51	33	11	13	171	156
4206a	Mina Rashid	25	15	55	16	16	10	041	048
4206	Dubayy	25	15	55	19	16	11	060	055

Table 6.4 (continued)

Ref No.	Tidal Station	Lat.	Long.	Amplitude		Phase	
		N°	E°	*O°*	*C°*	*O°*	*C°*
4211	Jazirat Sir Abu Nuayr	25 13	54 13	13	11	069	075
4239a	Al Jazirah Al Aliyah	25 24	51 34	10	12	163	151
4204	Ajman	25 25	55 26	13	11	061	046
4240	Sumaysimah	25 34	51 30	11	12	157	149
4203	Umm Al Qaywayn	25 35	55 35	15	12	027	030
4247	Nagiyah	25 41	50 54	06	07	271	270
4241	Khawr Shaqiq	25 41	51 31	09	09	198	199
4227	Jazirat Halul	25 40	52 25	07	06	165	179
4249a	Mutarid	25 47	50 43	04	04	289	275
4201	Ras al Khaymah	25 49	55 57	20	16	011	015
4242	Ras Laffan	25 54	51 35	11	11	166	181
4296	Jazirat Sirri	25 54	54 33	14	13	039	053
4250b	Umm Jalid	26 02	50 43	06	08	255	245
4250c	Umais	25 59	50 53	09	08	229	240
4246	Ras Ushayriq	25 59	51 00	11	09	218	229
4200	Mina Saqr	25 58	56 03	24	20	004	006
4249	Az Zellaq	26 03	50 29	04	05	003	004
4199b	Bukha	26 09	56 08	23	19	359	000
4253b	Al Khubar	26 17	50 13	10	12	190	200
4295	Jazireh-ye-Farur	26 15	54 31	14	16	042	055
4298	Jaz. Tunb al Kubra	26 16	55 18	20	20	017	025
4252	Mina Salman	26 13	50 36	22	18	213	215
4250d	Bahrain Approach buoy	26 22	50 47	20	16	192	205
4245	Fasht ad Dibal	26 17	50 59	18	15	218	230
4199	Khawr Khesab	26 12	56 15	22	22	359	350
4198	Khawr al Quway	26 21	56 22	25	27	347	340
4253c	Ad Damman	26 27	50 05	22	20	191	200
4297	Bandar-e Langeh	26 33	54 53	23	21	027	035
4301	Basaidu	26 40	55 16	33	28	031	031
4299	Jazireh-ye Hangam	26 41	55 54	25	26	352	358
4254	Ras Tannurah	26 38	50 10	20	24	198	210
4260c	Ras al Khafji	28 25	48 31	14	16	080	090

Table 6.4 (continued)

Ref No.	Tidal Station	Lat.	Long.	Amplitude		Phase	
		N°	E°	*O*°	*C*°	*O*°	*C*°
4254a	Abu Saafah	26 56	50 30	16	19	198	194
4290	Jazireh ye Laven	26 48	53 23	12	17	111	109
4254b	Fasht Gharibah	26 59	50 13	18	21	183	195
4255	Al Jubayl	27 04	49 39	17	20	184	186
4255b	Jazirat al Jurayd	27 12	49 57	16	19	184	187
4303a	Bandar Abbas	27 10	56 12	38	41	341	341
4255a	Dawhat Abu Ali	27 13	49 43	16	16	197	186
4288	Bandar Asalu	27 28	52 37	17	20	172	185
4257	Manifah	27 35	48 54	18	21	167	154
4256	Al Farisiyah	28 00	50 10	12	15	200	205
4285	Lavar	28 15	51 16	18	25	222	230
4260	Marjan Oilfield	28 26	49 43	05	06	226	225

C° = Computed values

O° = Observed values are taken from Admirality chart (1988a)

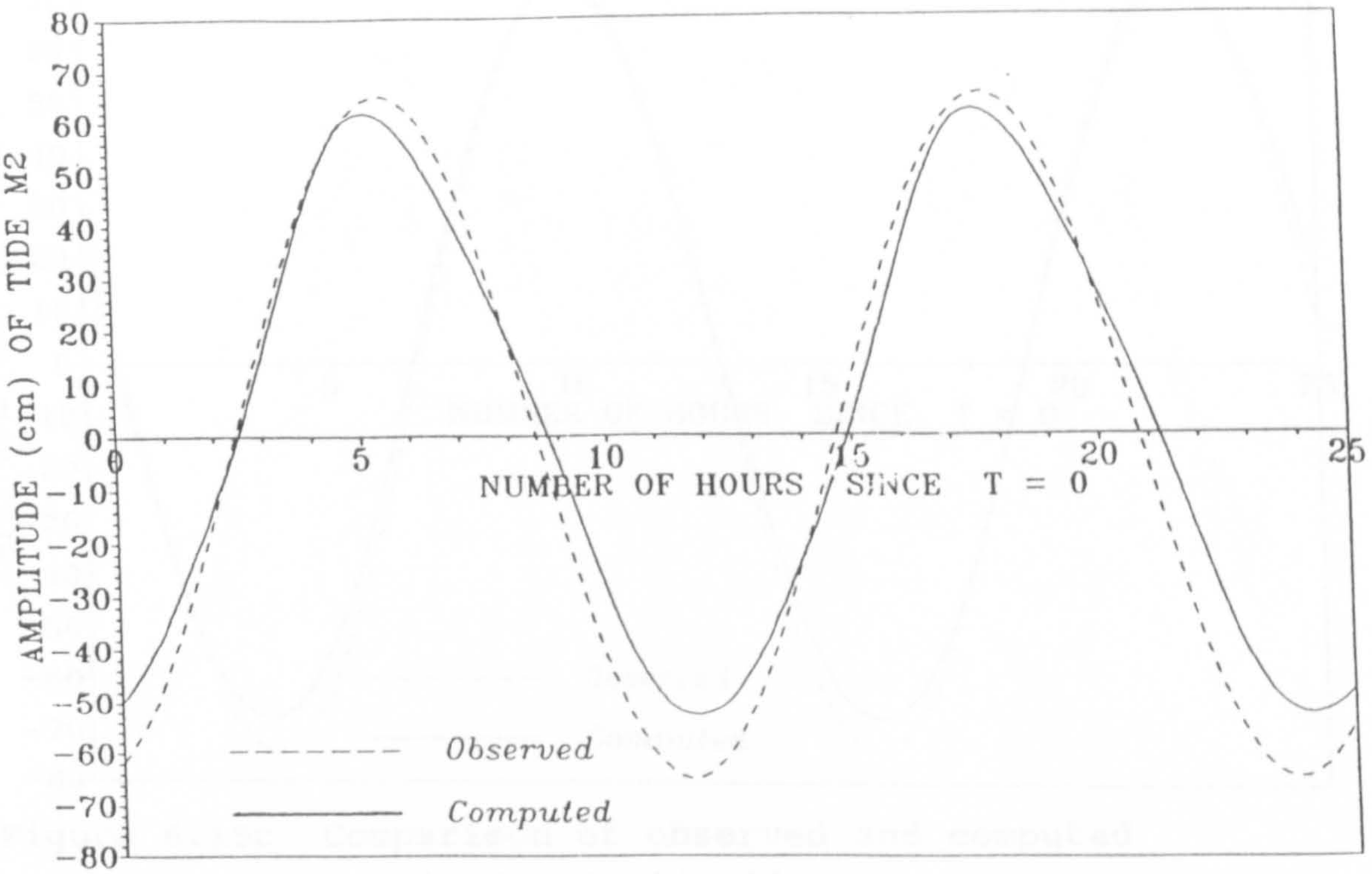

Figure 6.15a Comparison of observed and computed amplitude of tide M_2 at Ad Damman, S.Arabia

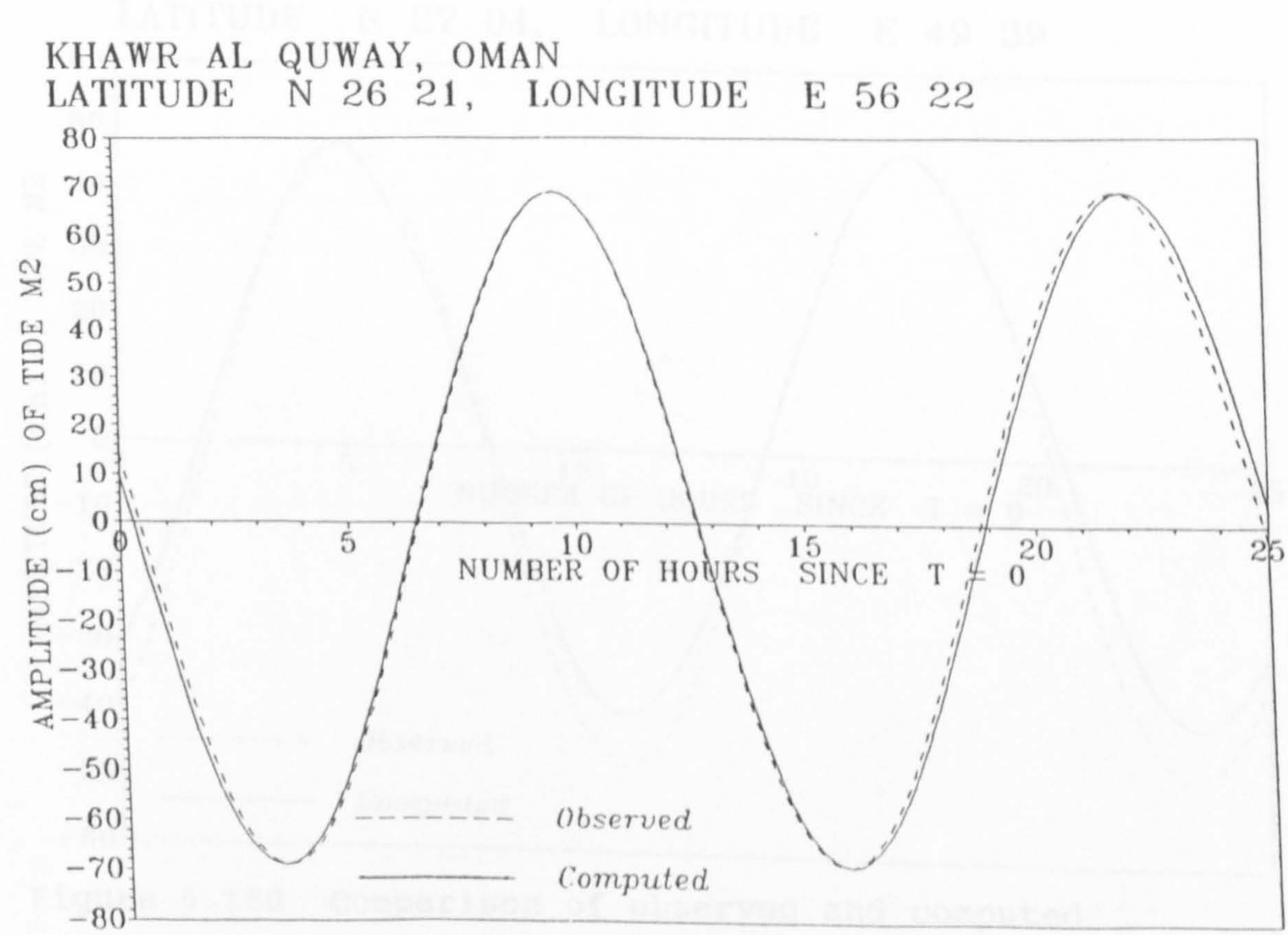

Figure 6.15b Comparison of observed and computed amplitude of tide M_2 at Khawr Al Quway, Oman

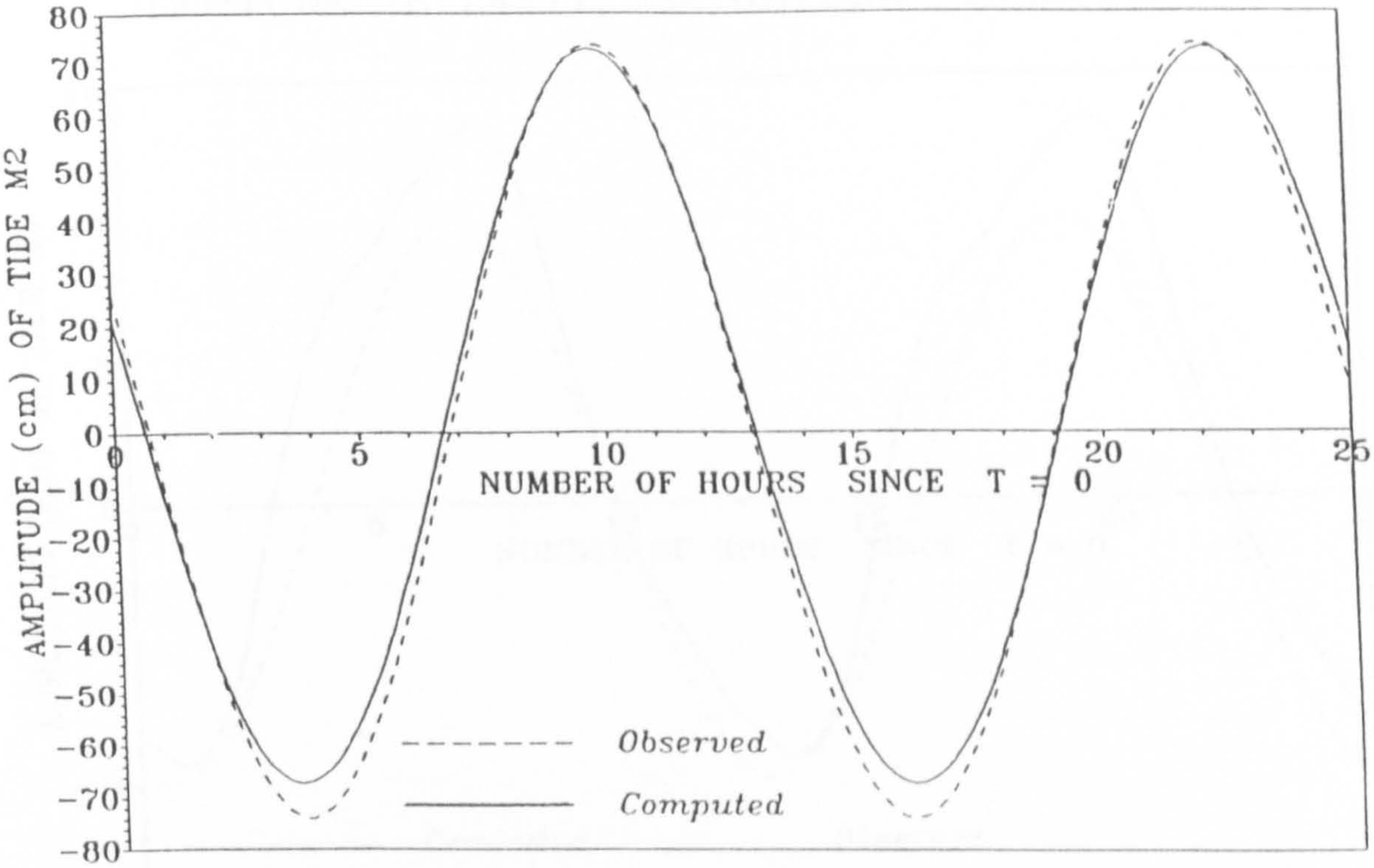

Figure 6.15c Comparison of observed and computed amplitude of tide M_2 at Jazireh-Ye Hangam, Iran

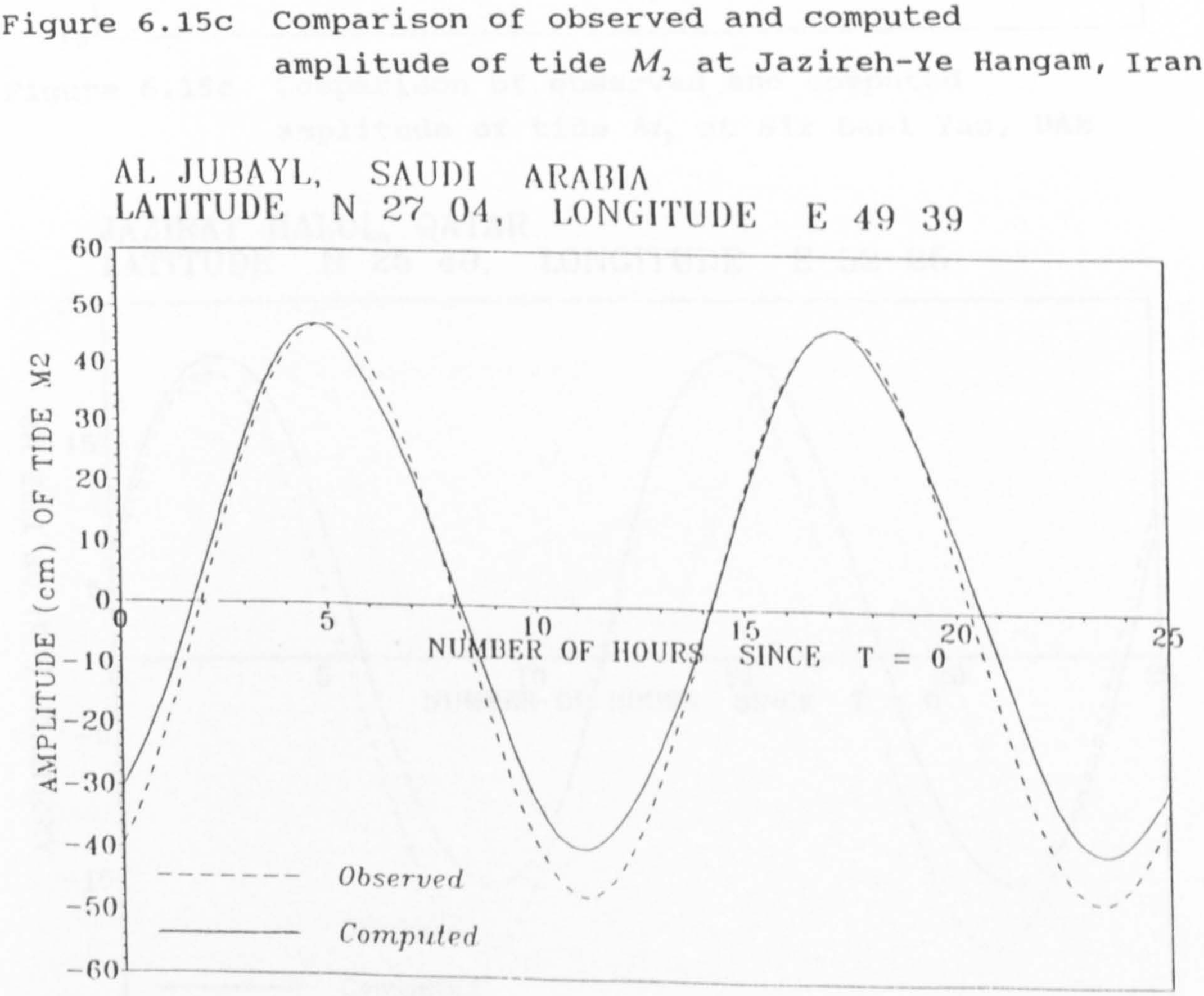

Figure 6.15d Comparison of observed and computed amplitude of tide M_2 at Al Jubayl, S. Arabia

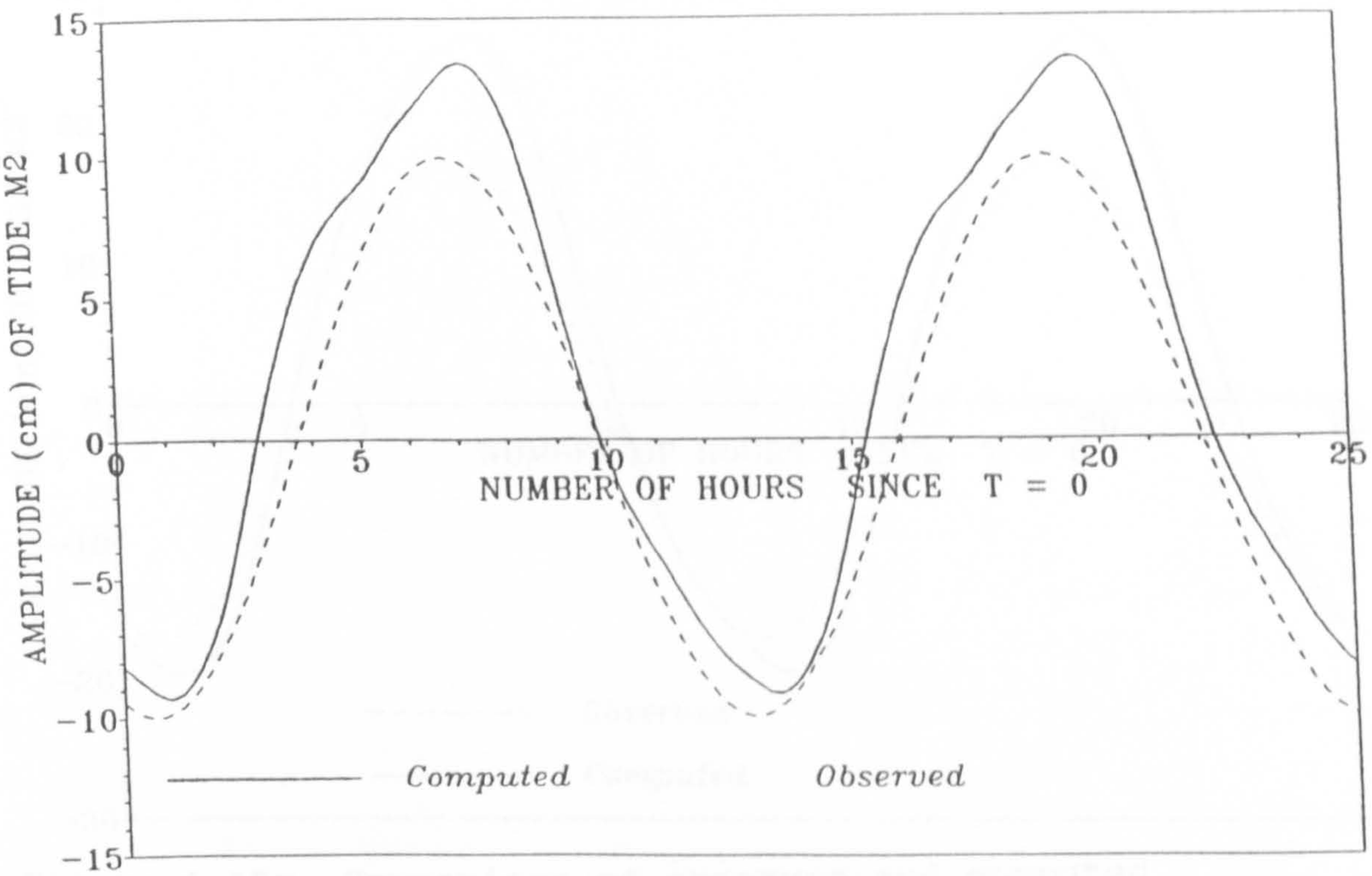

Figure 6.15e Comparison of observed and computed amplitude of tide M_2 at Sir Bani Yas, UAE

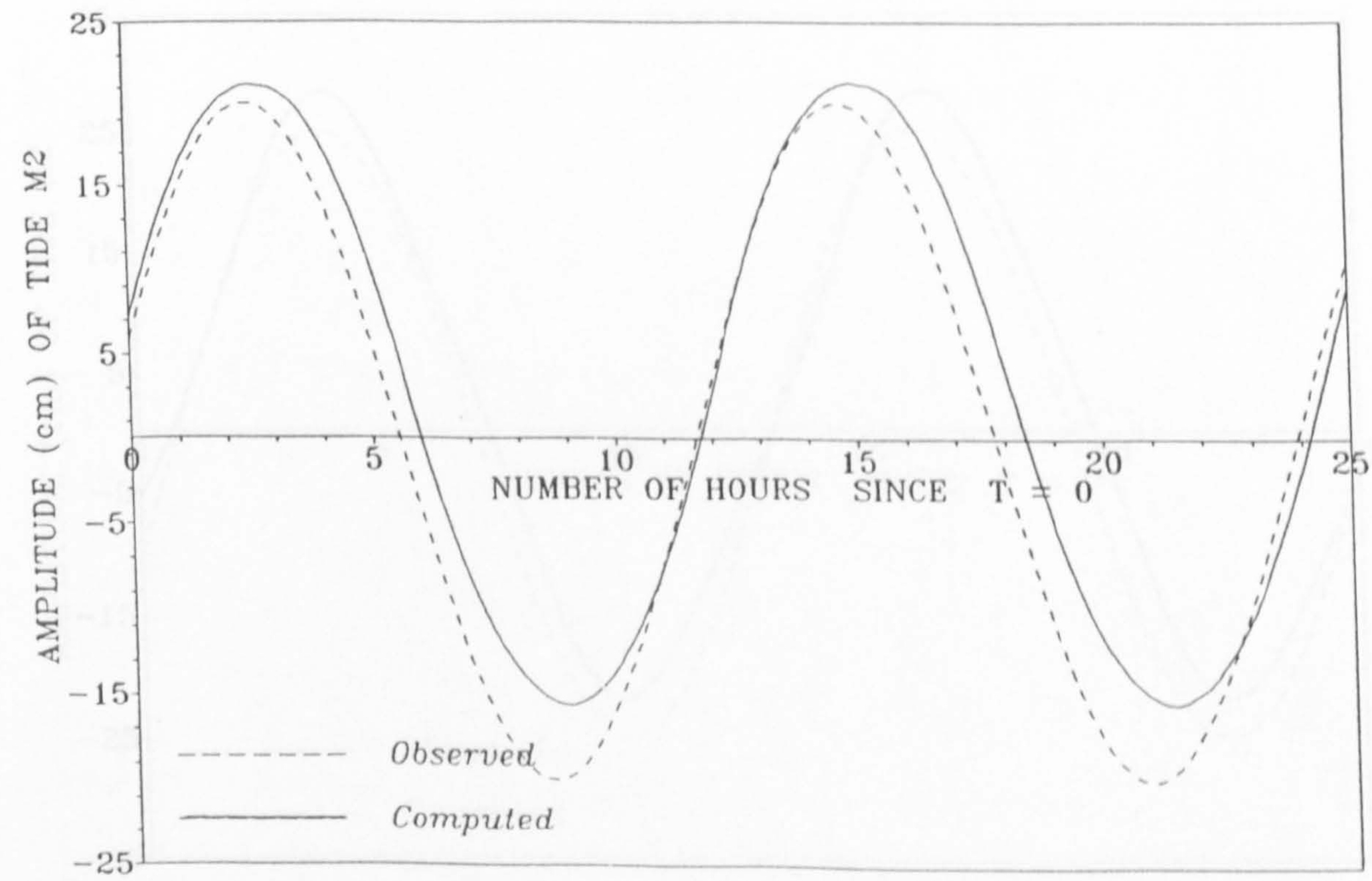

Figure 6.15f Comparison of observed and computed amplitude of tide M_2 at Jazirat Halul, Qatar

UMAIS, BAHRAIN.
LATITUDE N 25 59, LONGITUDE E 50 53

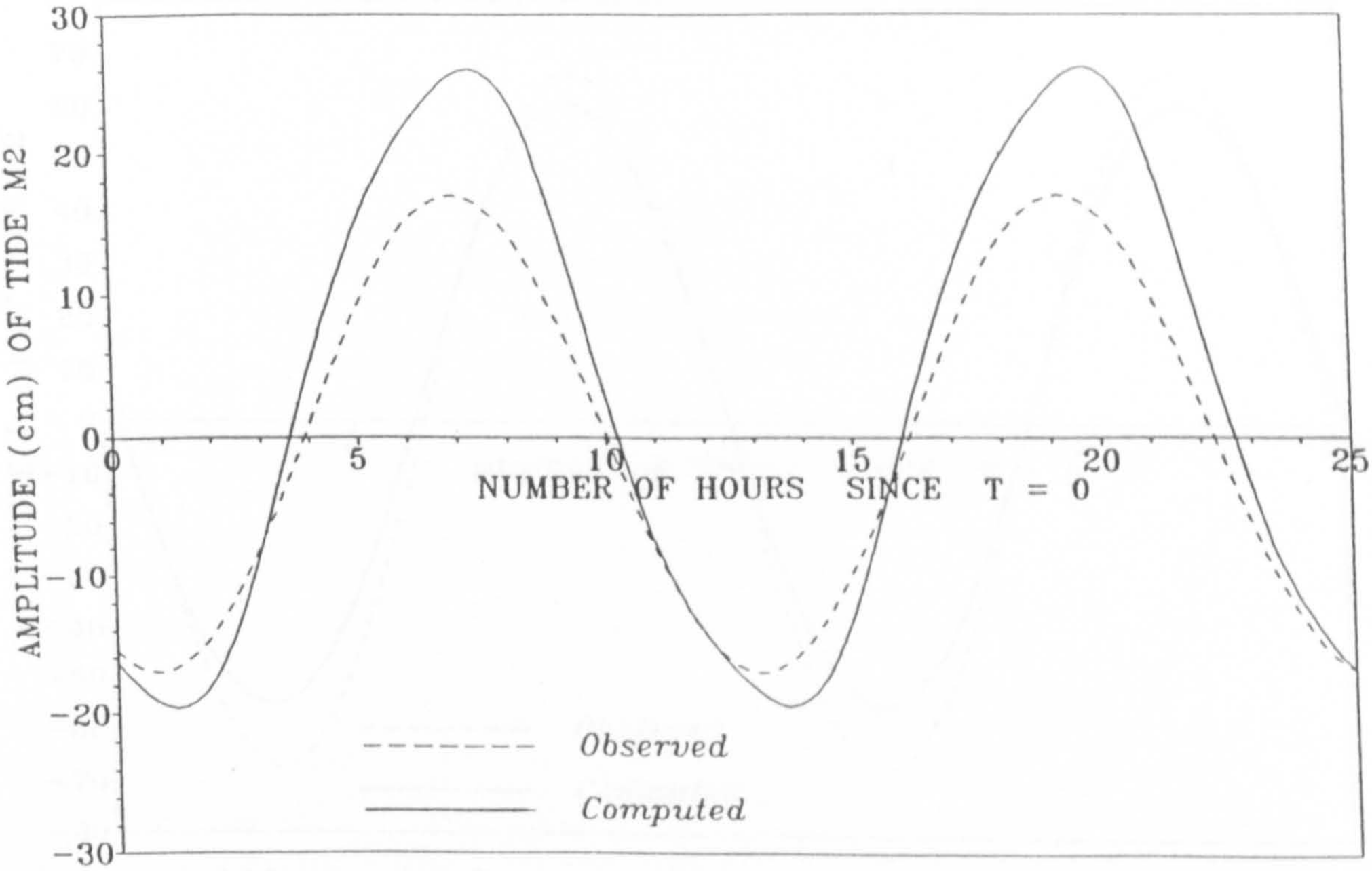

Figure 6.15g Comparison of observed and computed amplitude of tide M_2 at Umais, Bahrain

MUSAYID , QATAR.
LATITUDE N 25 02, LONGITUDE E 51 39

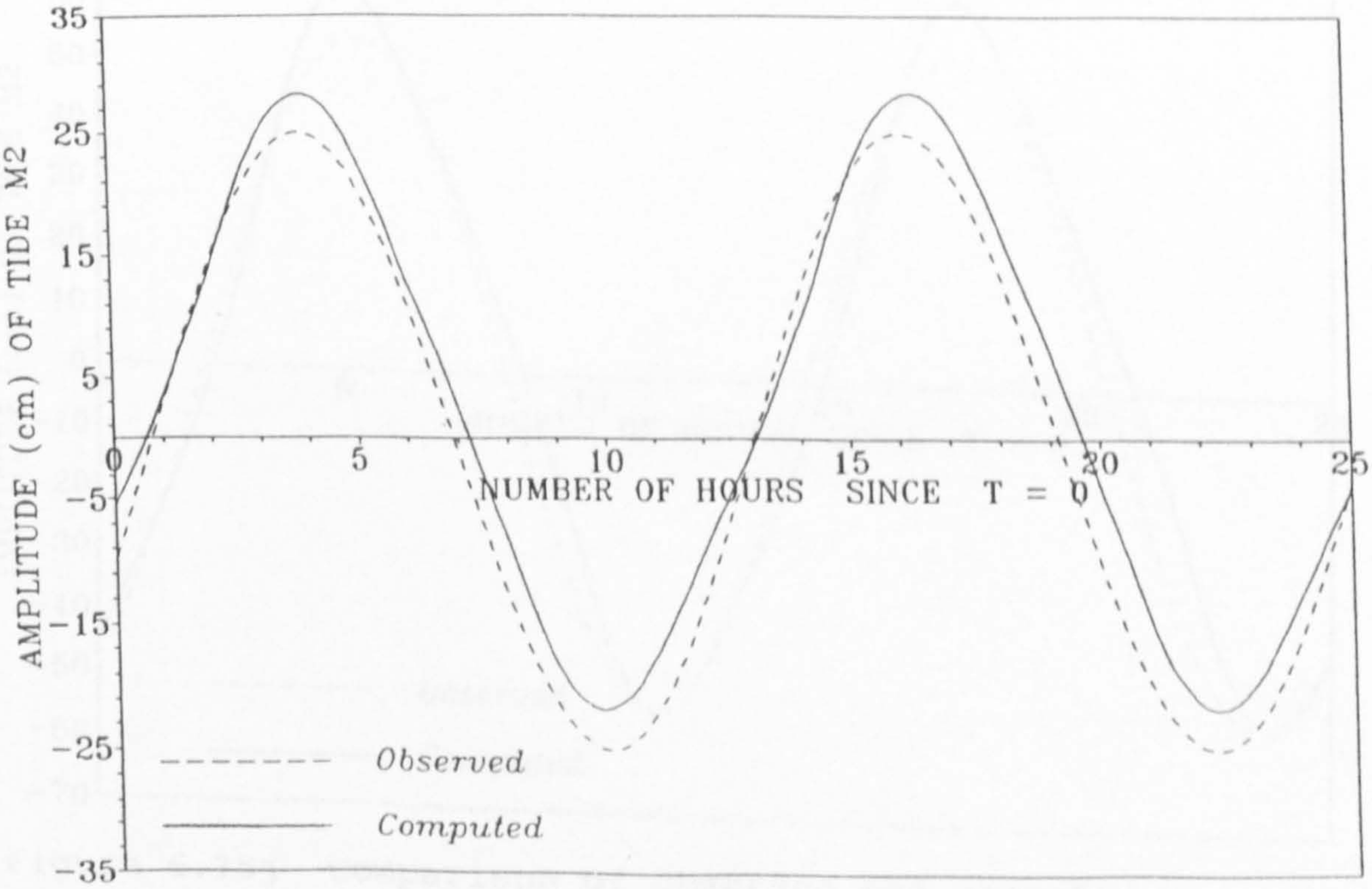

Figure 6.15h Comparison of observed and computed amplitude of tide M_2 at Musayid, Qatar

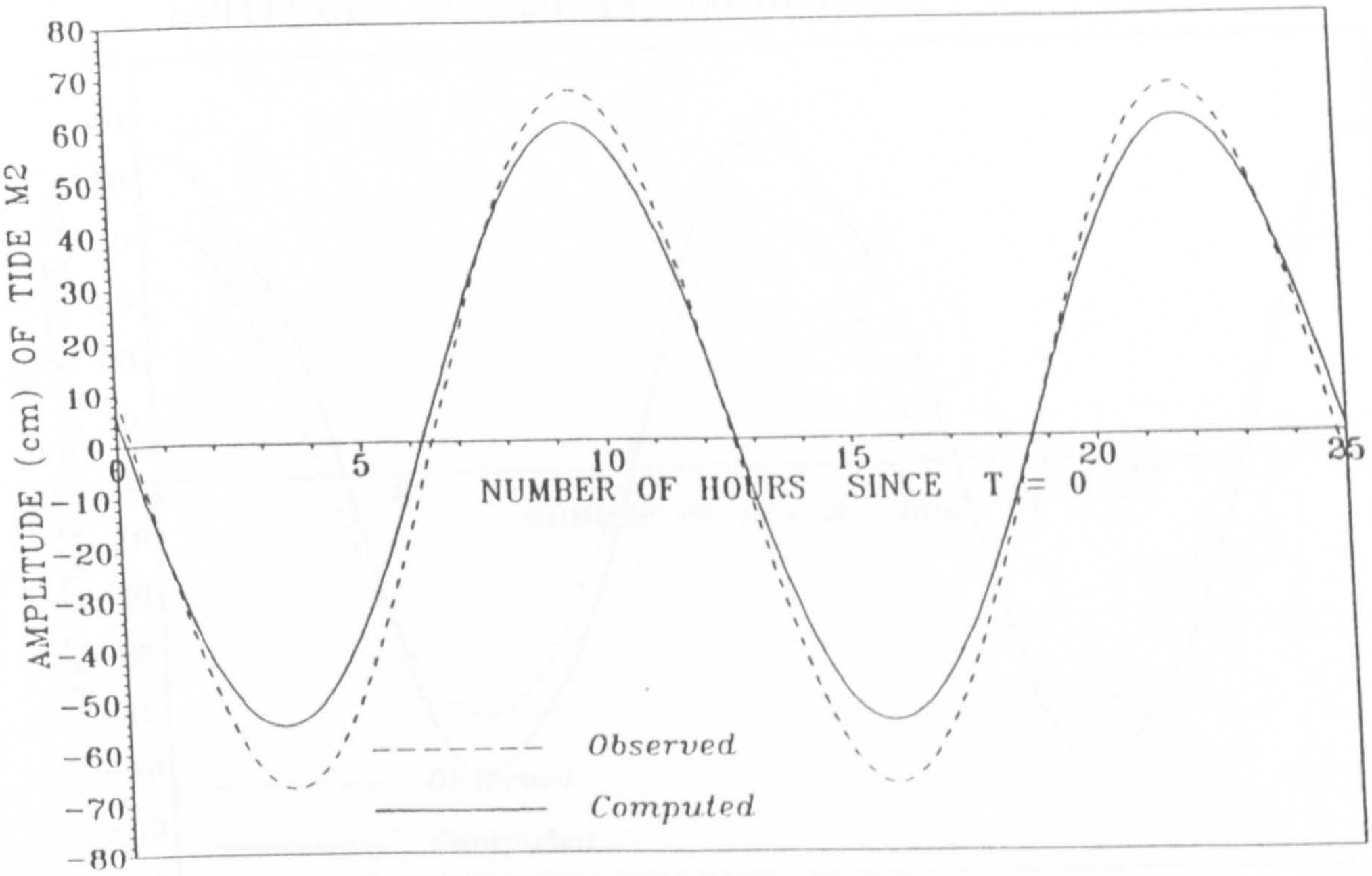

Figure 6.15i Comparison of observed and computed amplitude of tide M_2 at Khawar Khasab, Oman

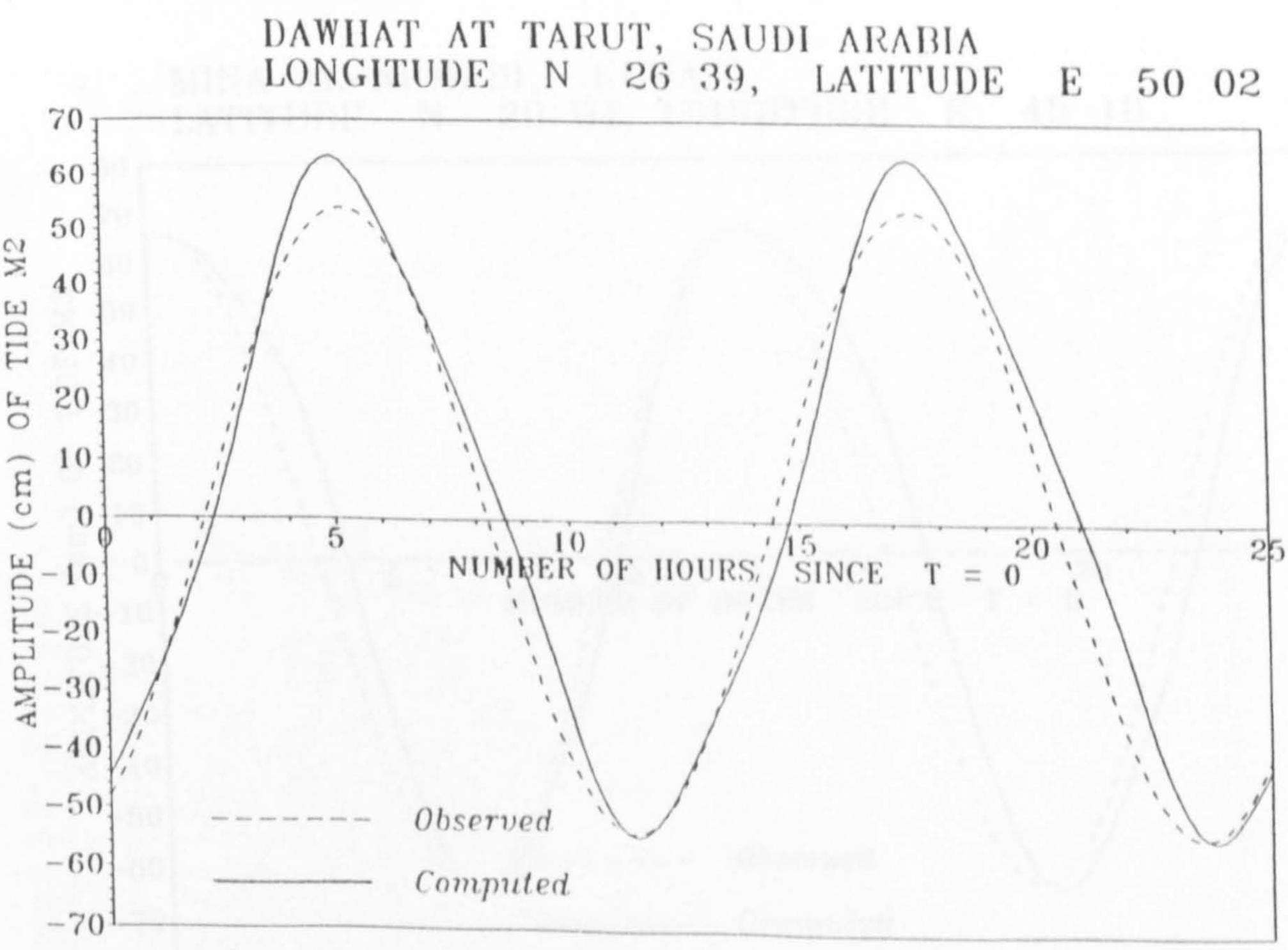

Figure 6.15j Comparison of observed and computed amplitude of tide M2 at Dawhat At Tarut, S. Arabia

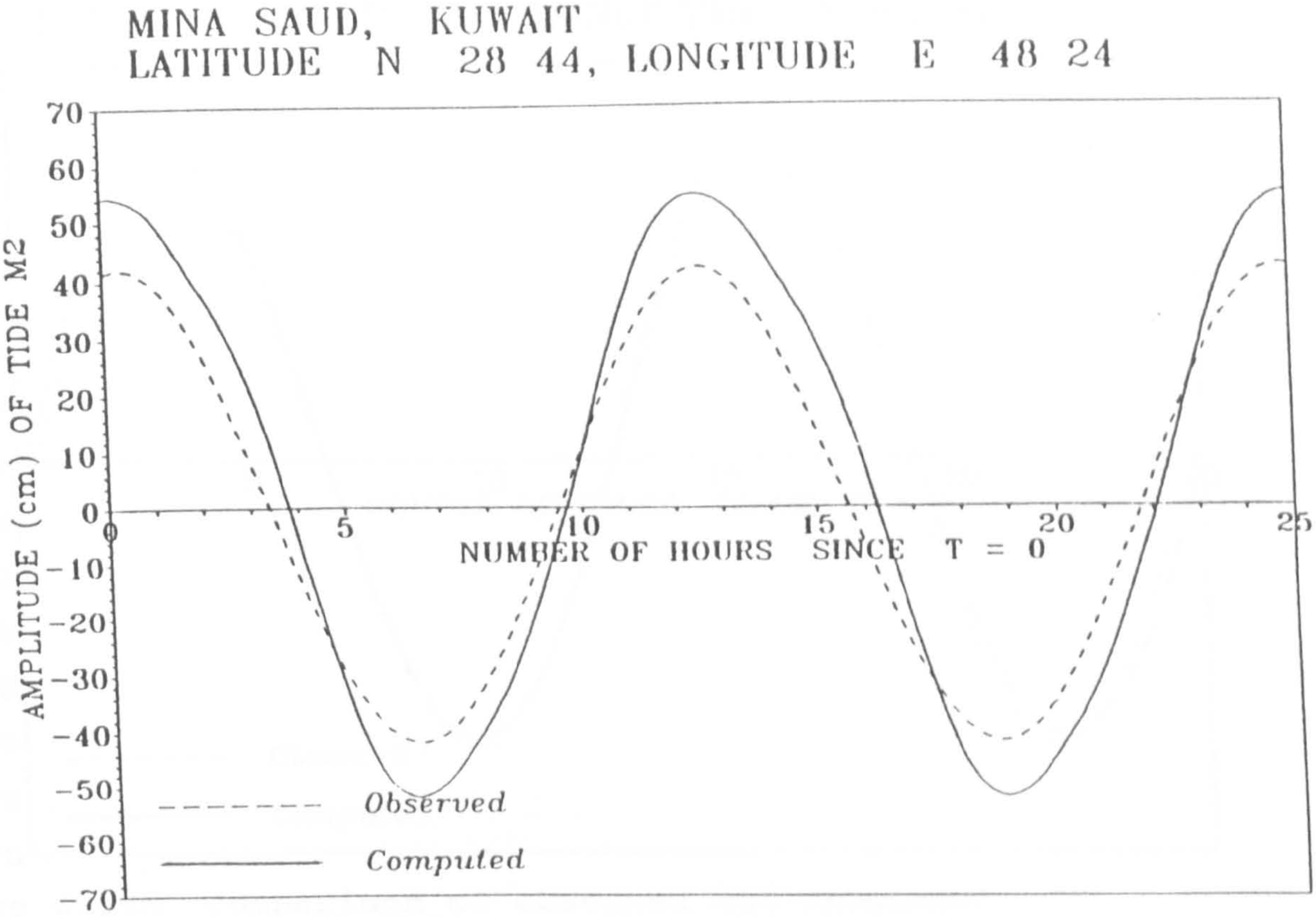

Figure 6.15k Comparison of observed and computed amplitude of tide M_2 at Mina Saud, Kuwait

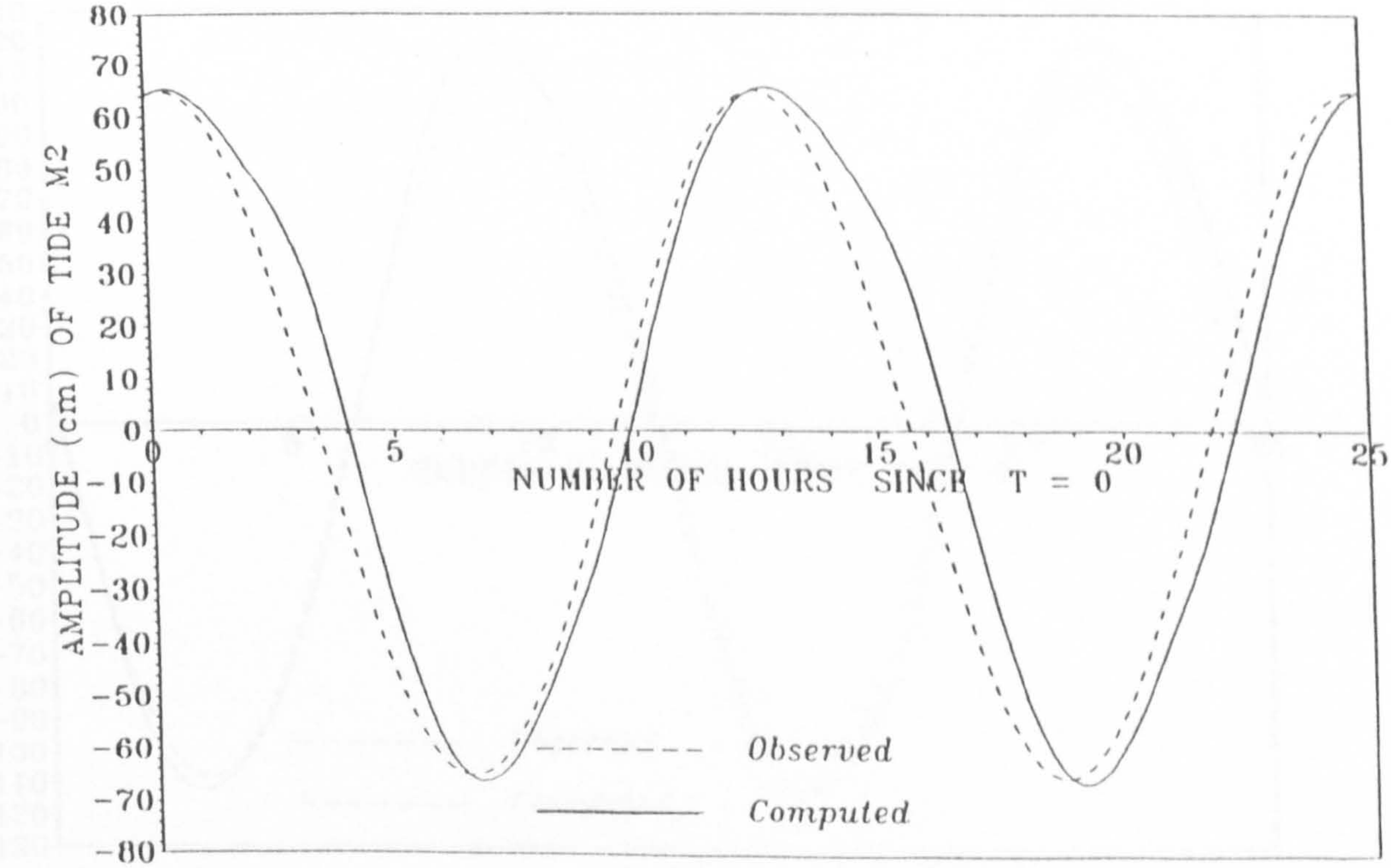

Figure 6.15l Comparison of observed and computed amplitude of tide M_2 at Mina Al-Ahmadi, Kuwait

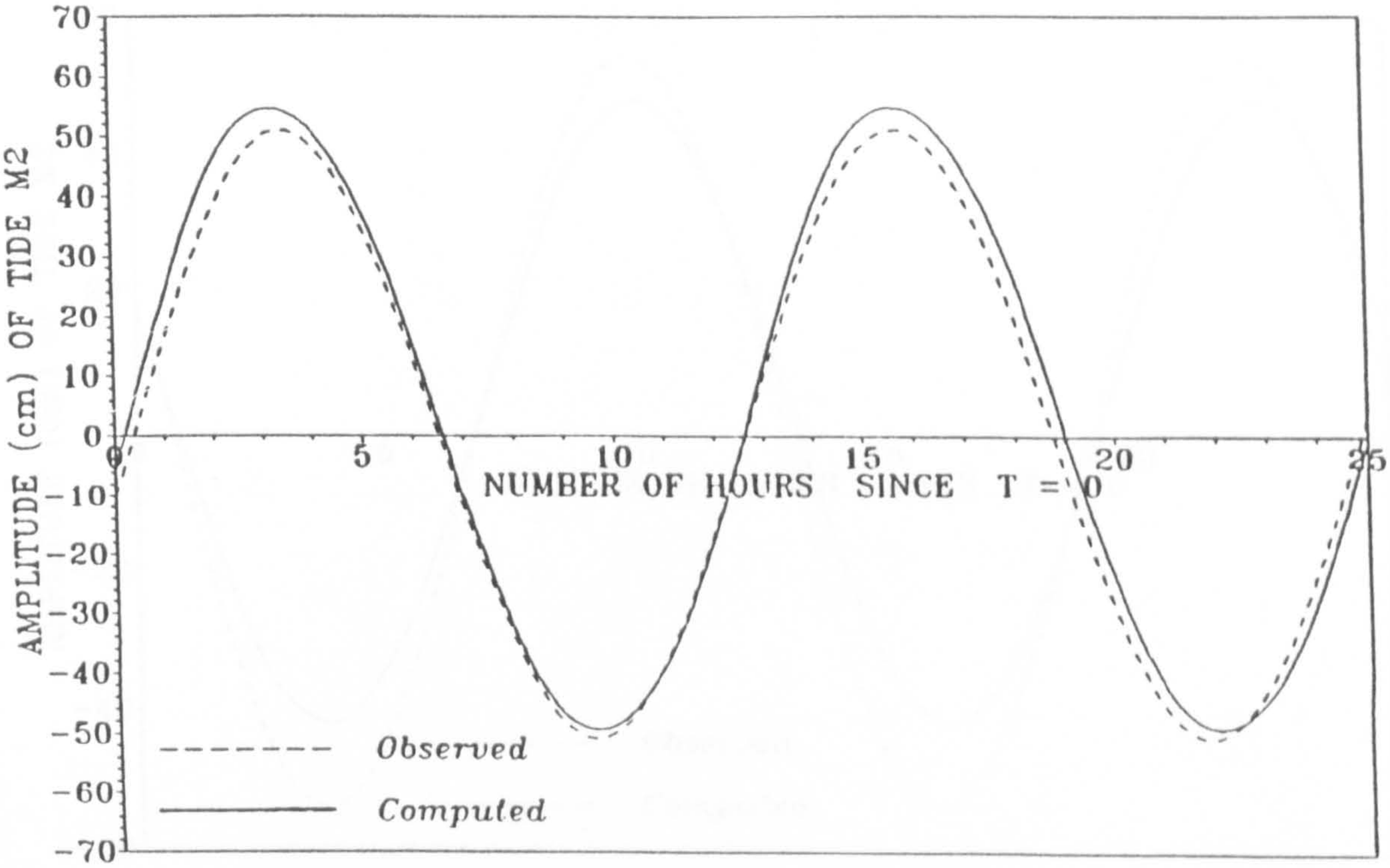

Figure 6.15m Comparison of observed and computed amplitude of tide M_2 at Bandar Asalu, Iran

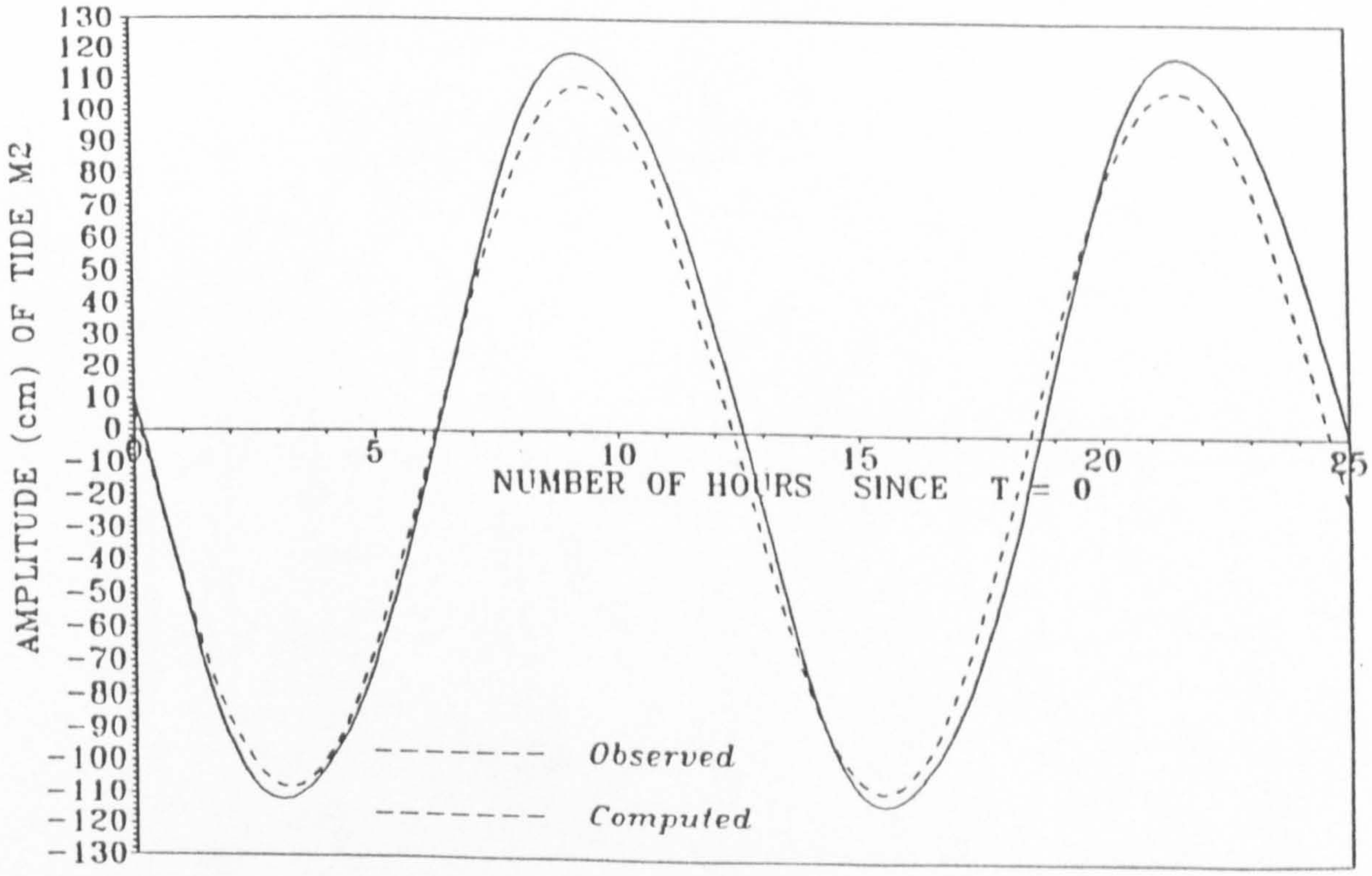

Figure 6.15n Comparison of observed and computed amplitude of tide M_2 at Bandar Abbas, Iran

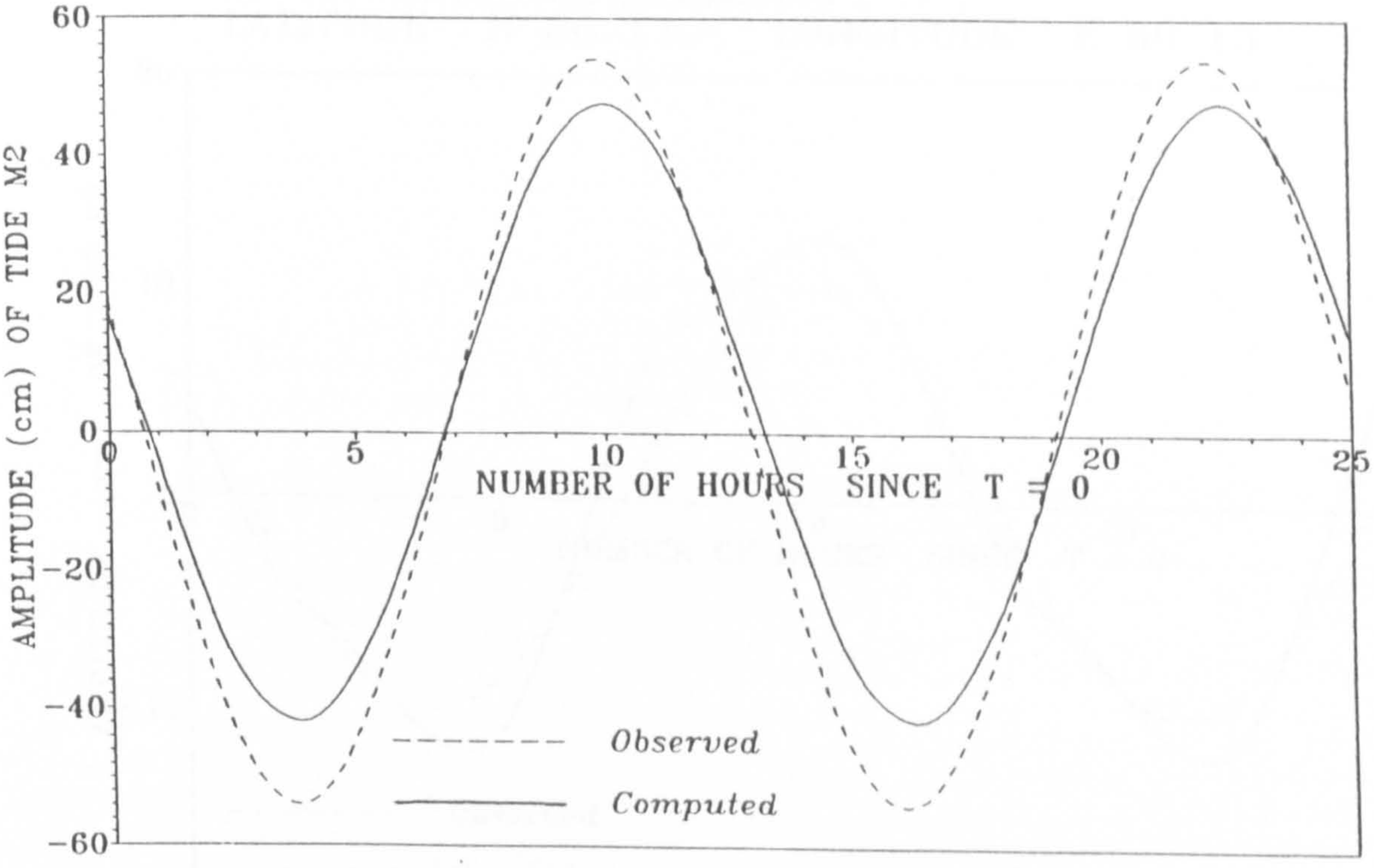

Figure 6.15o Comparison of observed and computed amplitude of tide M_2 at Ras Al Khaymah, UAE

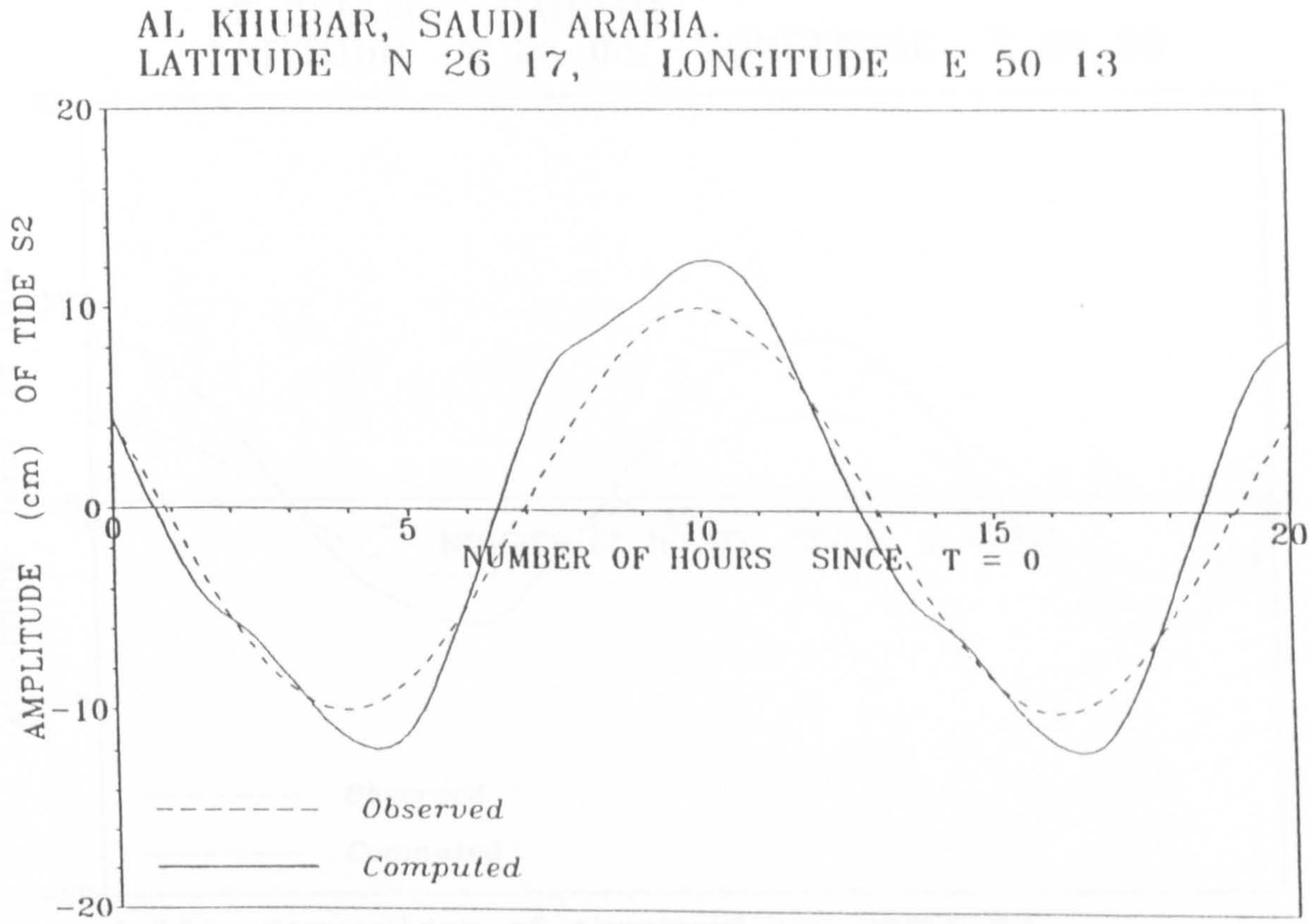

Figure 6.16a Comparison of observed and computed amplitude of tide S_2 at Al Khubar, S. Arabia

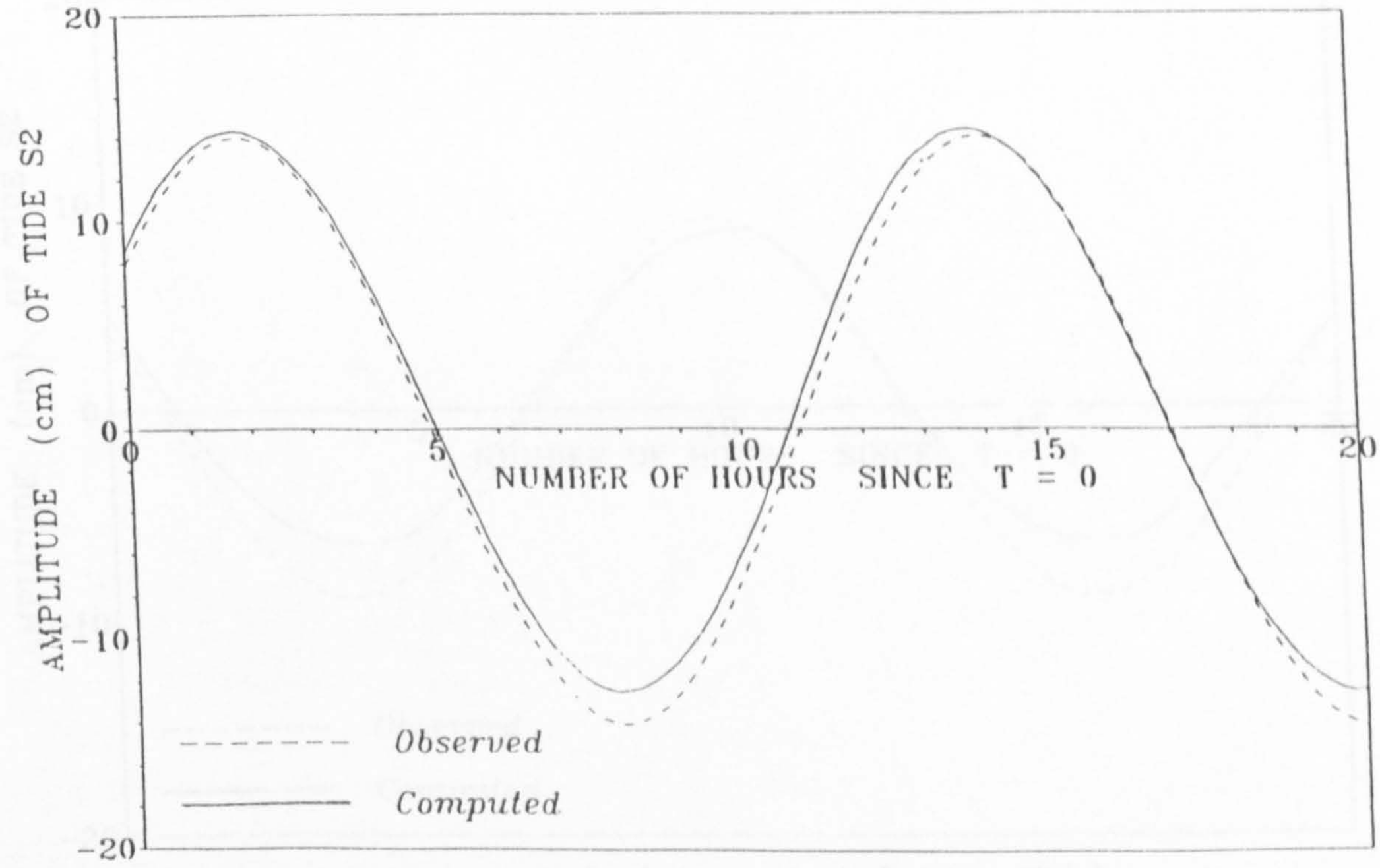

Figure 6.16b Comparison of observed and computed amplitude of tide S_2 at Jazirat Sirri, Iran

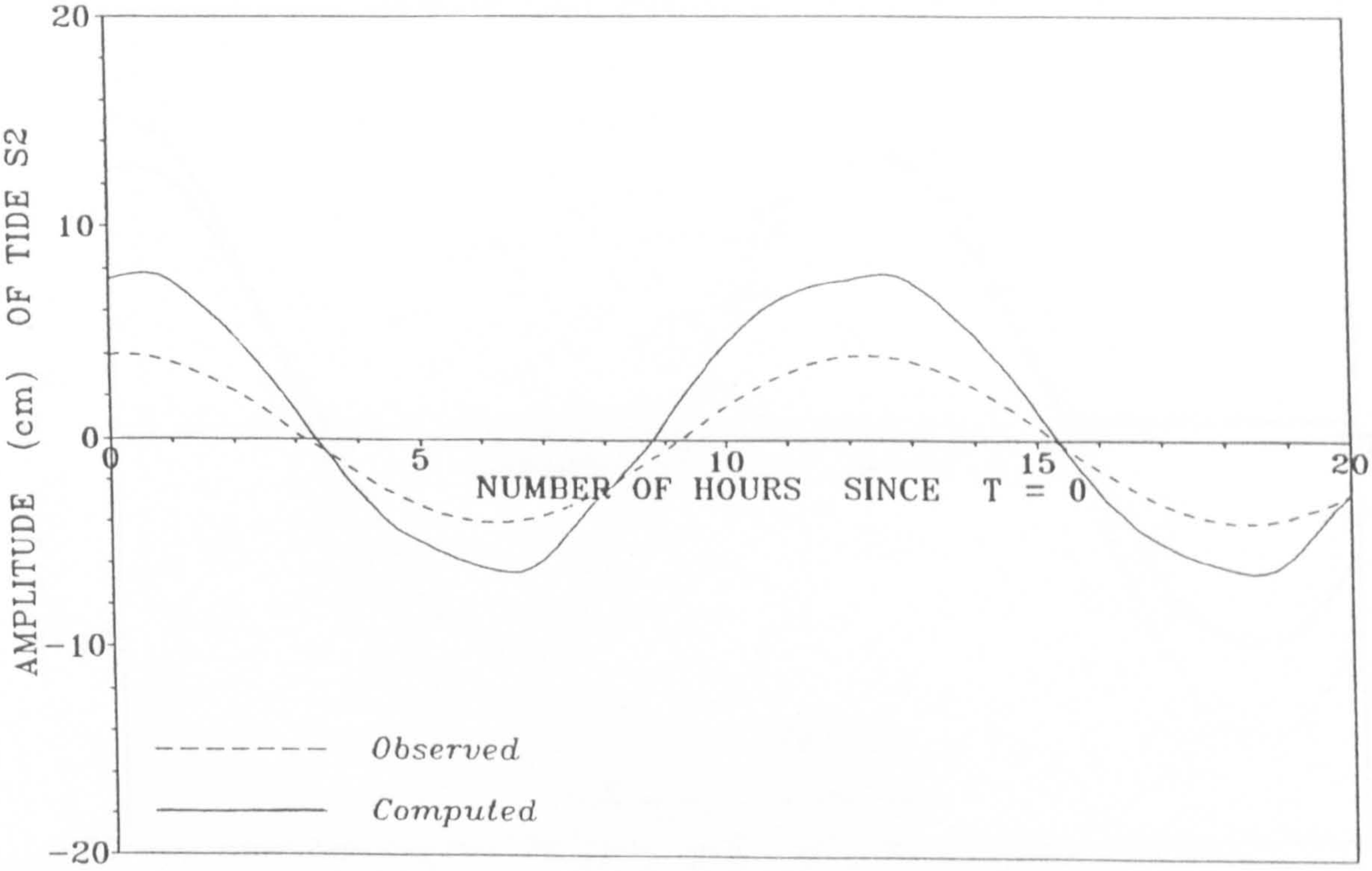

Figure 6.16c Comparison of observed and computed amplitude of tide S_2 at Az Zellaq, Bahrain

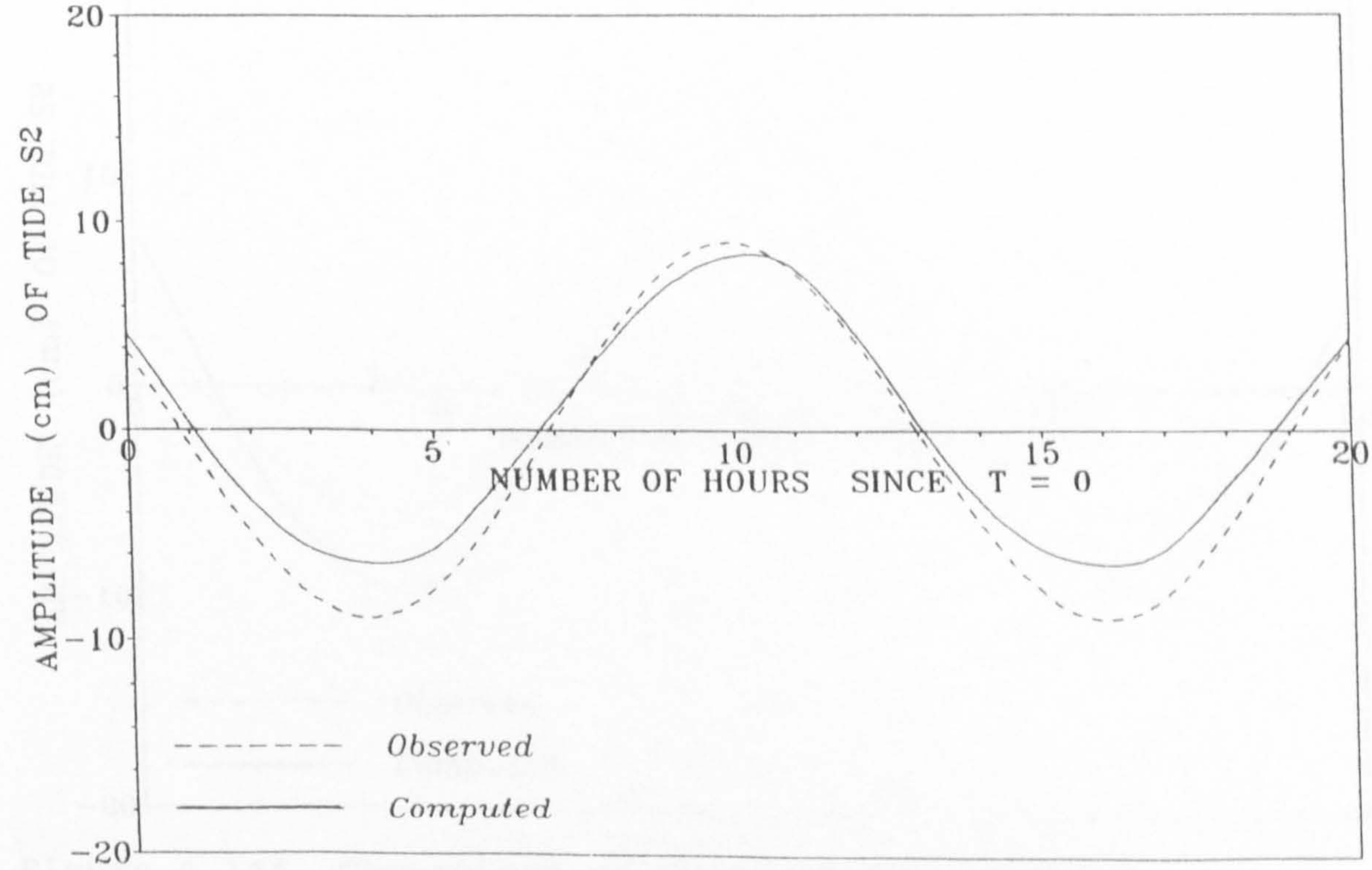

Figure 6.16d Comparison of observed and computed amplitude of tide S_2 at Umais, Bahrain

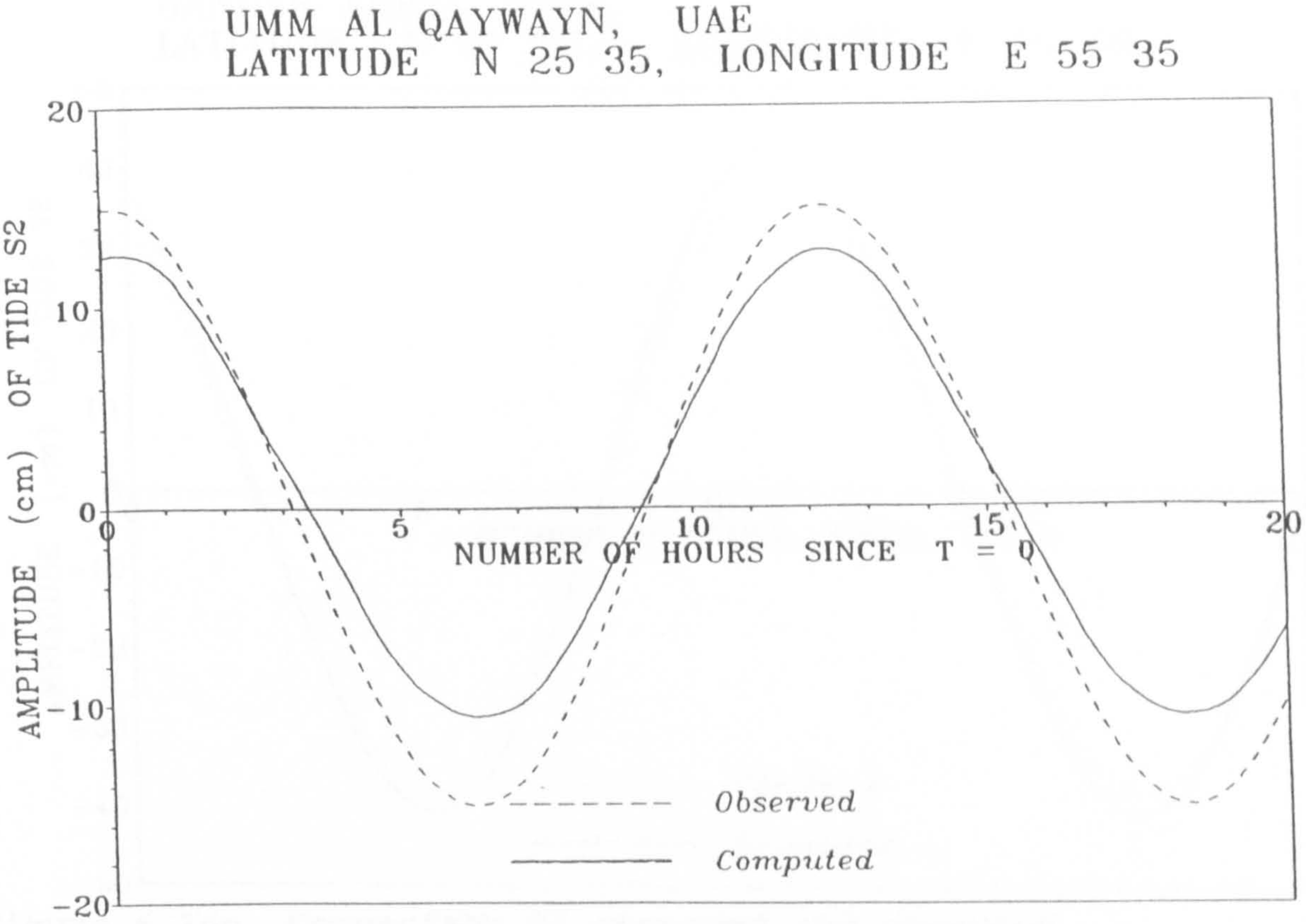

Figure 6.16e Comparison of observed and computed amplitude of tide S_2 at Umm Al Qaywayn, S. Arabia

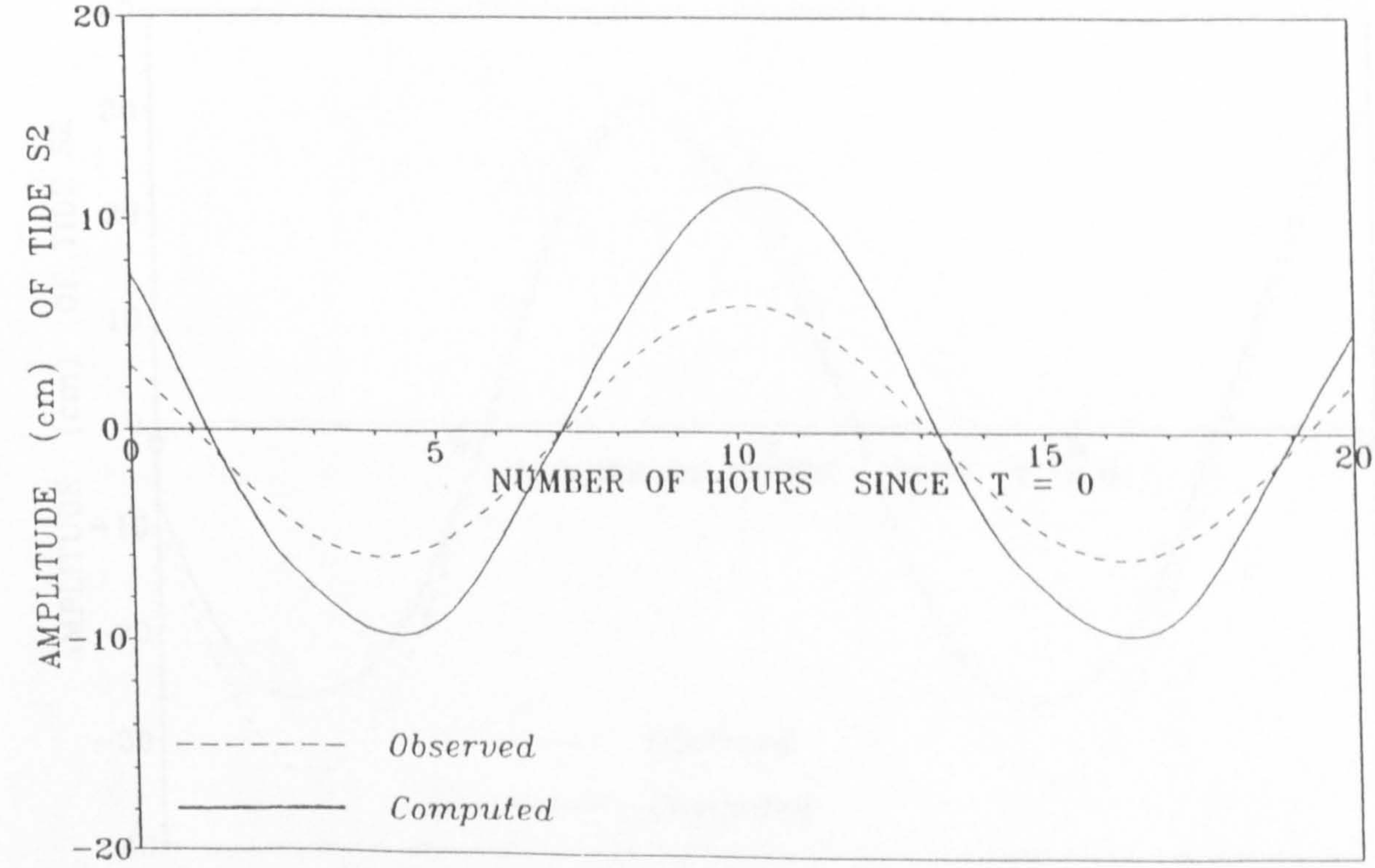

Figure 6.16f Comparison of observed and computed amplitude of tide S_2 at Umm Jalid, Bahrain

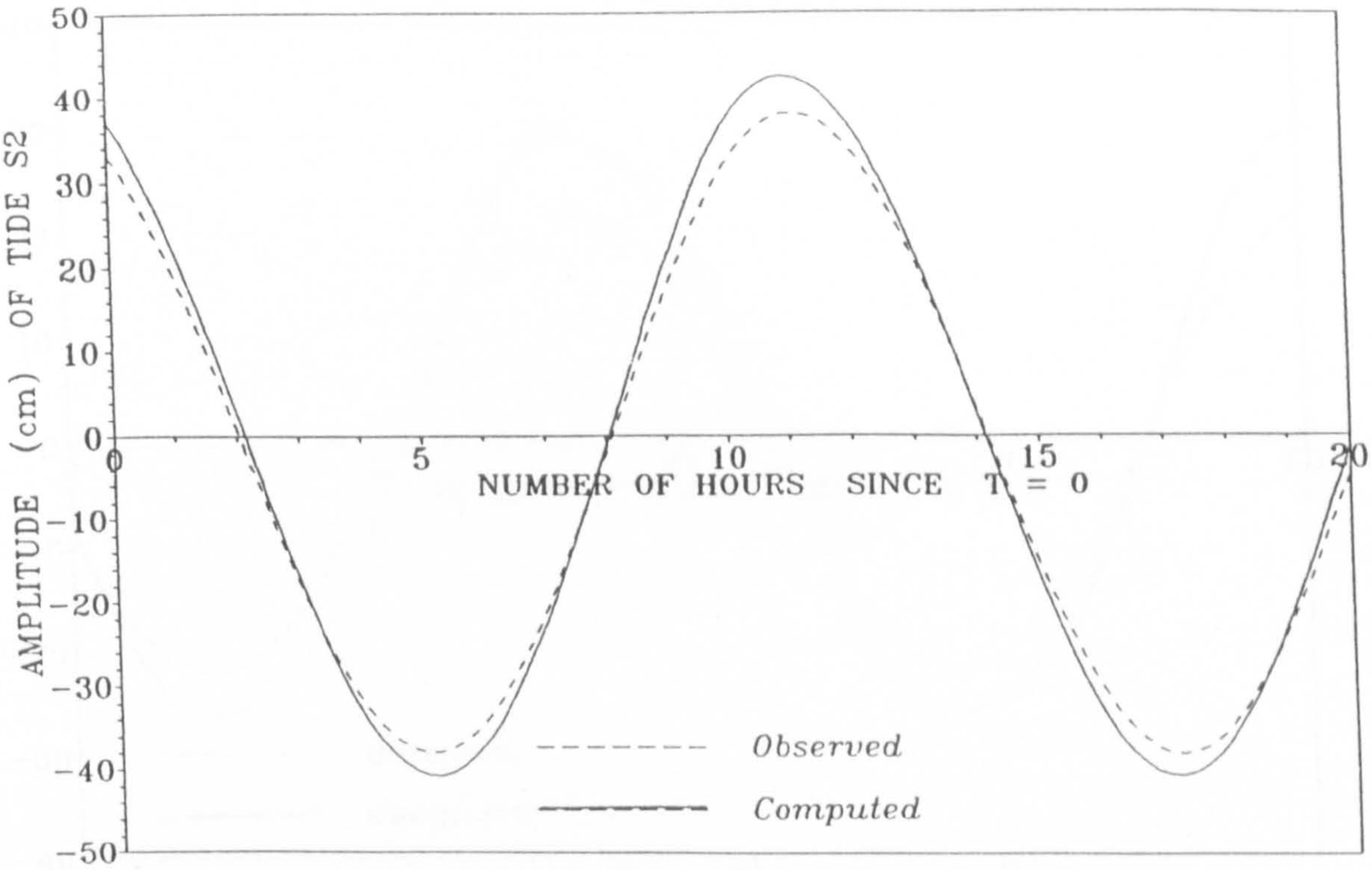

Figure 6.16g Comparison of observed and computed amplitude of tide S_2 at Bandar abbas, Iran

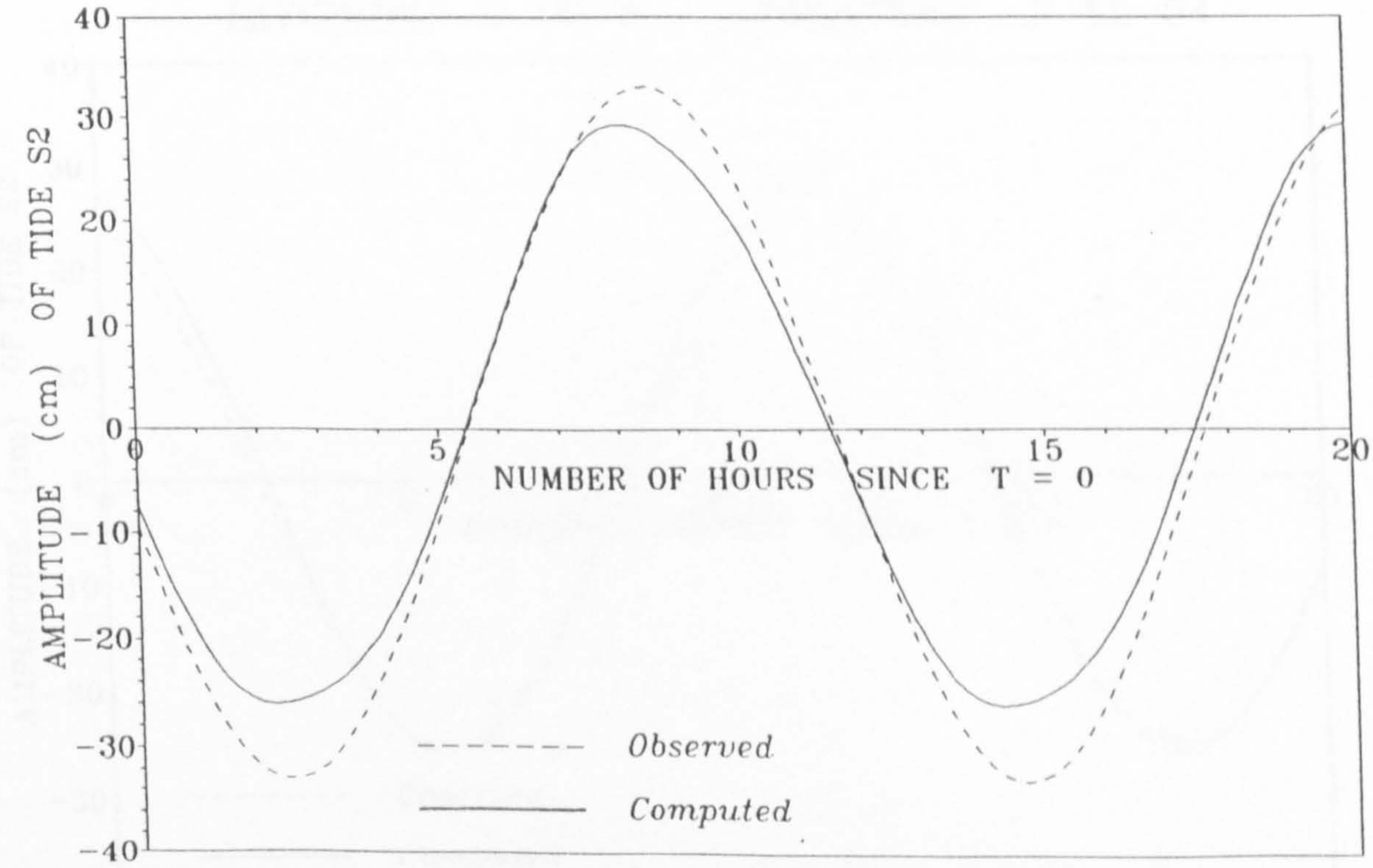

Figure 6.16h Comparison of observed and computed amplitude of tide S_2 at Basaidu, Iran

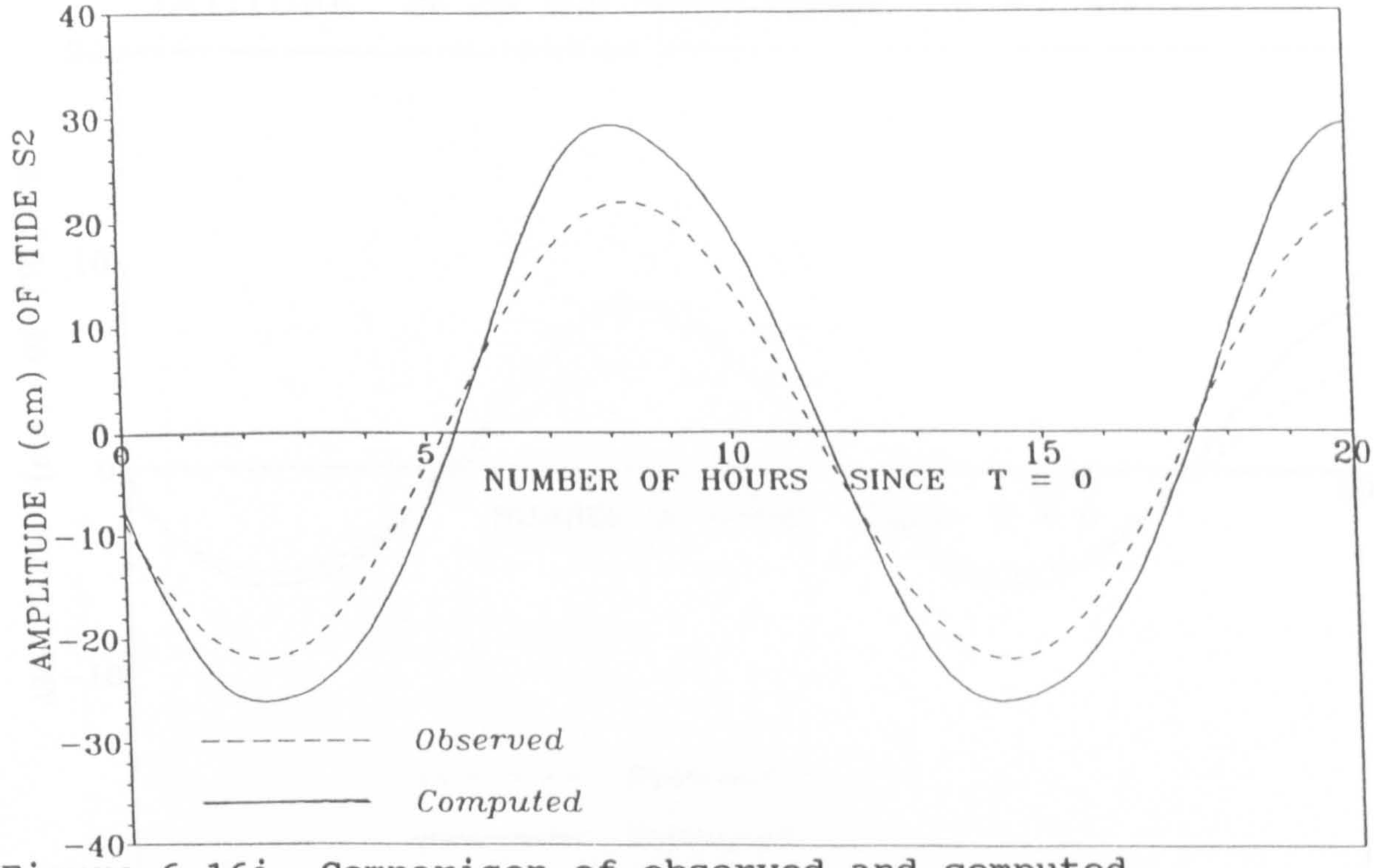

Figure 6.16i Comparison of observed and computed amplitude of tide S_2 at Ad Damman, S. Arabia

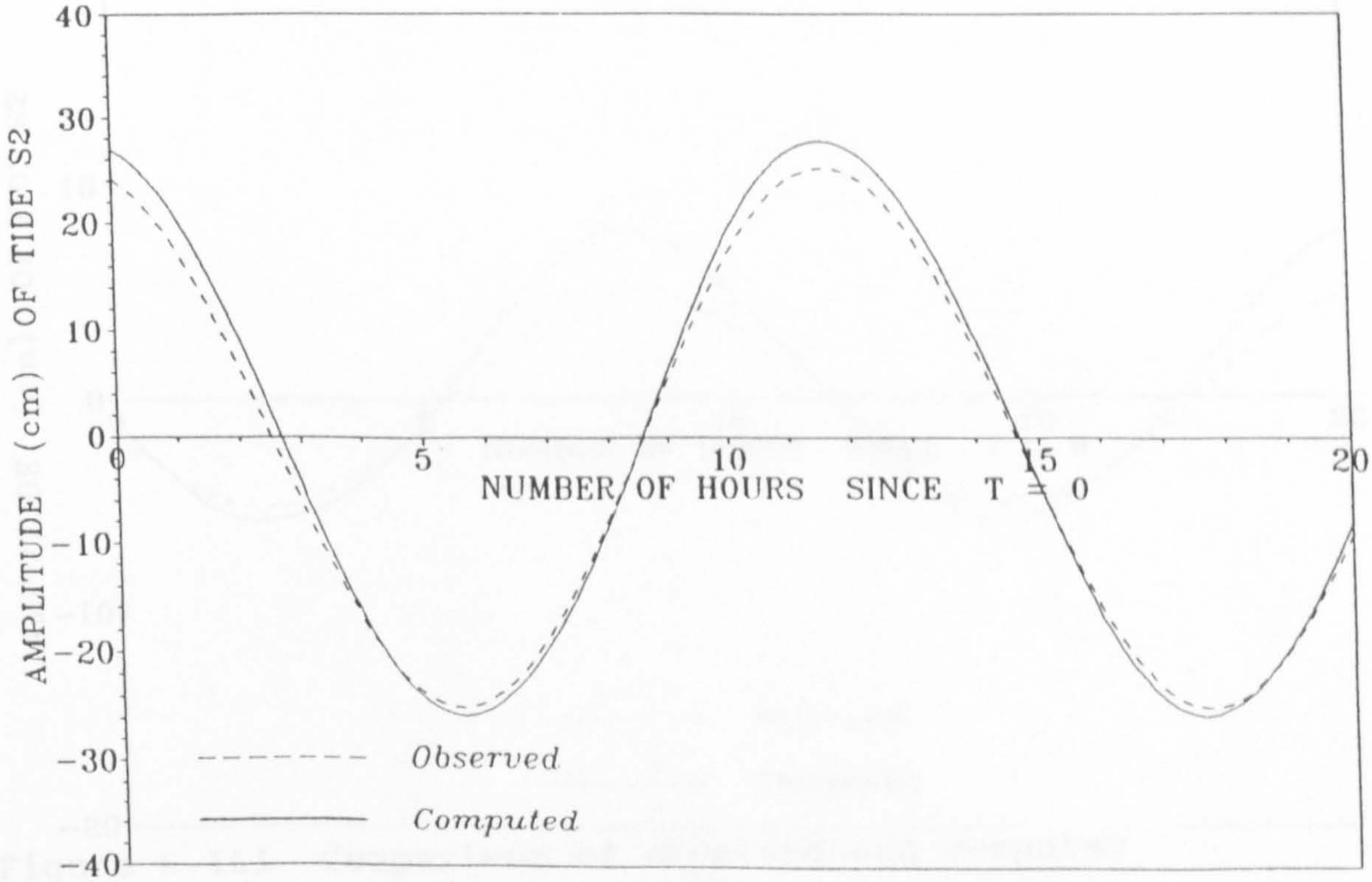

Figure 6.16j Comparison of observed and computed amplitude of tide S_2 at Jazireh-Ye Hangam, Iran

DOHA HARBOUR, KUWAIT.
LATITUDE N 29 23 LONGITUDE E 47 48

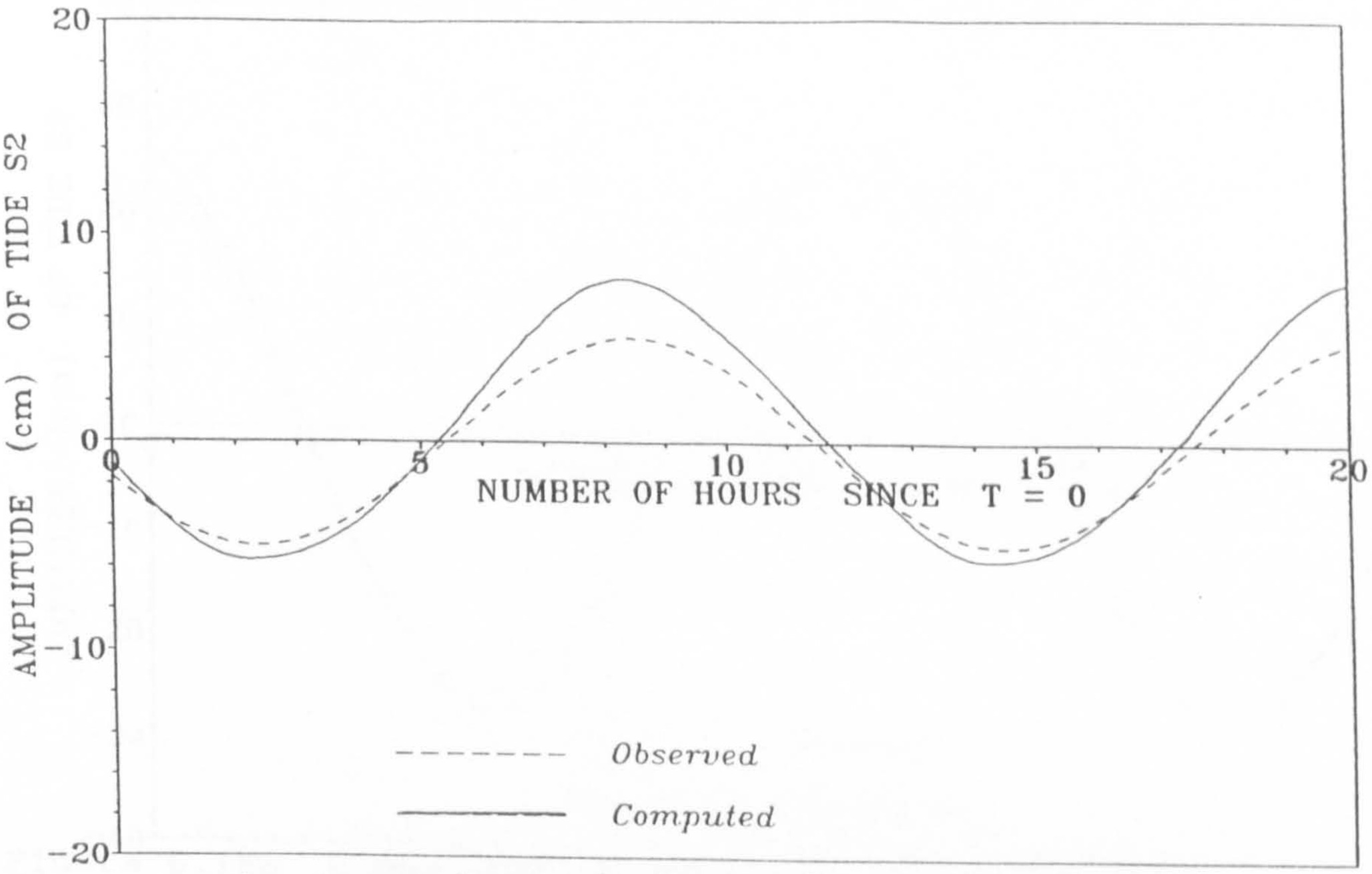

Figure 6.16k Comparison of observed and computed amplitude of tide S_2 at Doha Harbour, Kuwait

MARJAN OILFIELD, KUWAIT.
LATITUDE N 28 26, LONGITUDE E 49 43

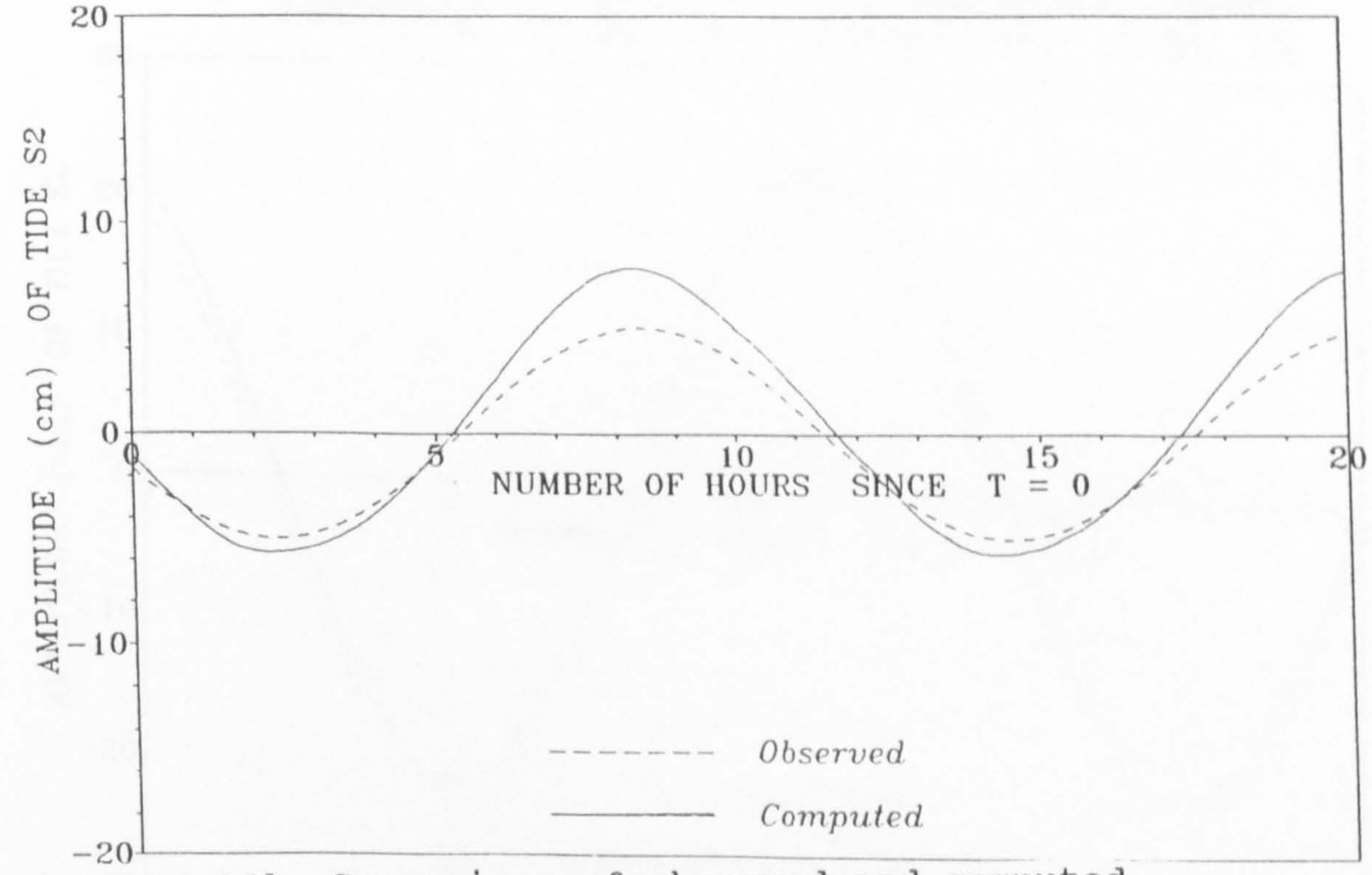

Figure 6.16l Comparison of observed and computed amplitude of tide S_2 at Marjan Oilfield, Kuwait

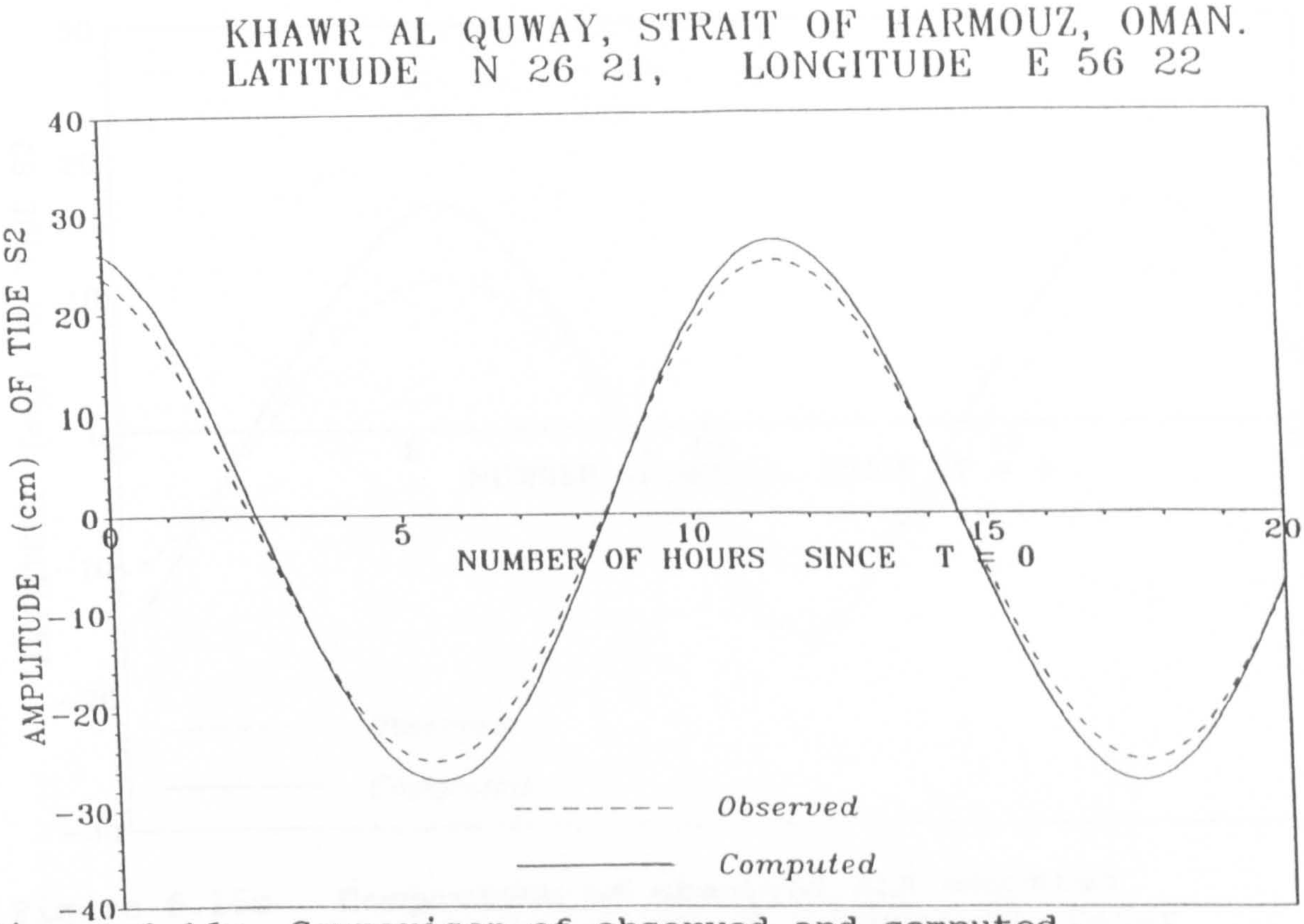

Figure 6.16m Comparison of observed and computed amplitude of tide S_2 at Khawr Al Quway, Strait of Harmouz, Oman

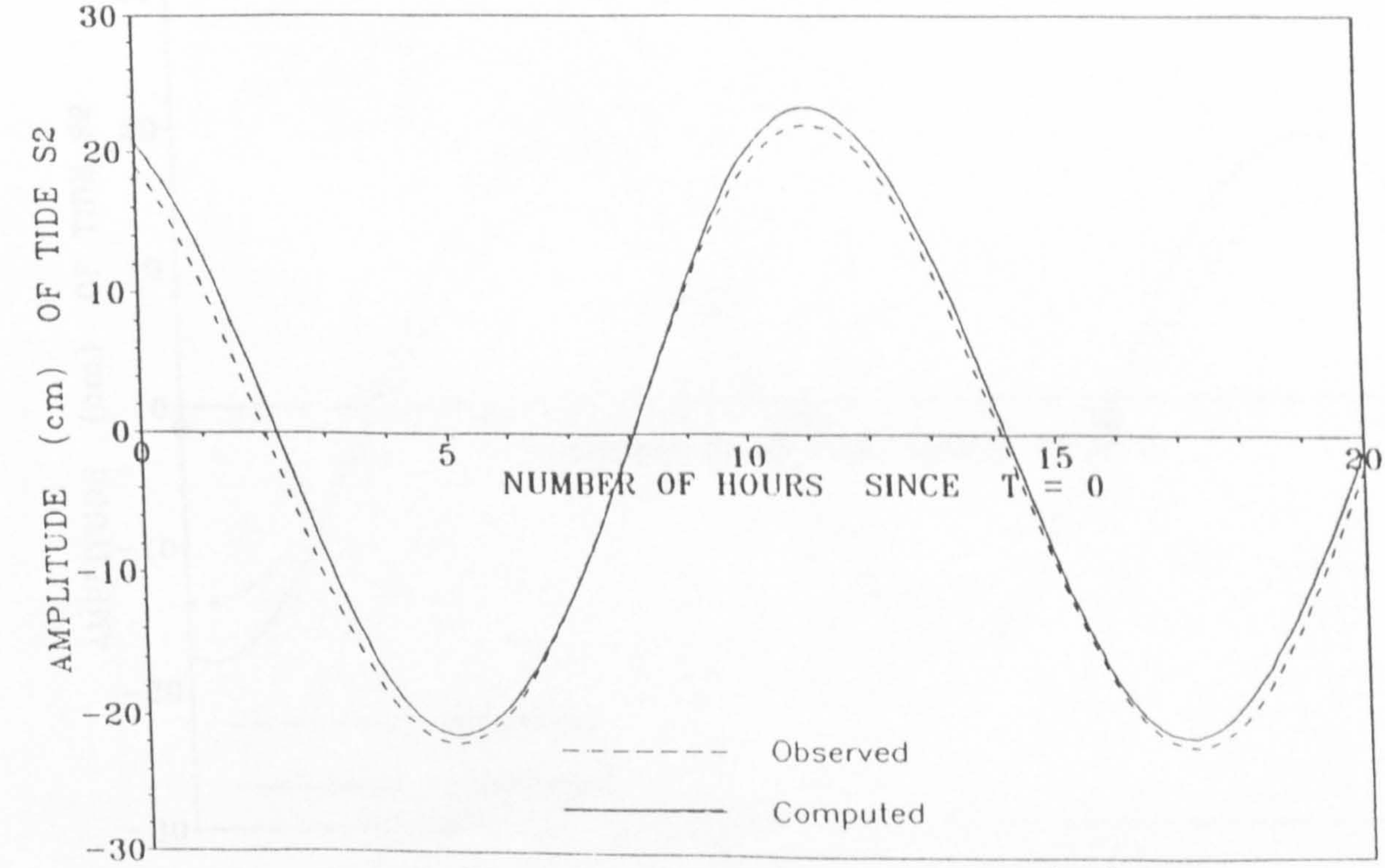

Figure 6.16n Comparison of observed and computed amplitude of tide S_2 at Khawr Khesab, Strait of Harmouz, Oman

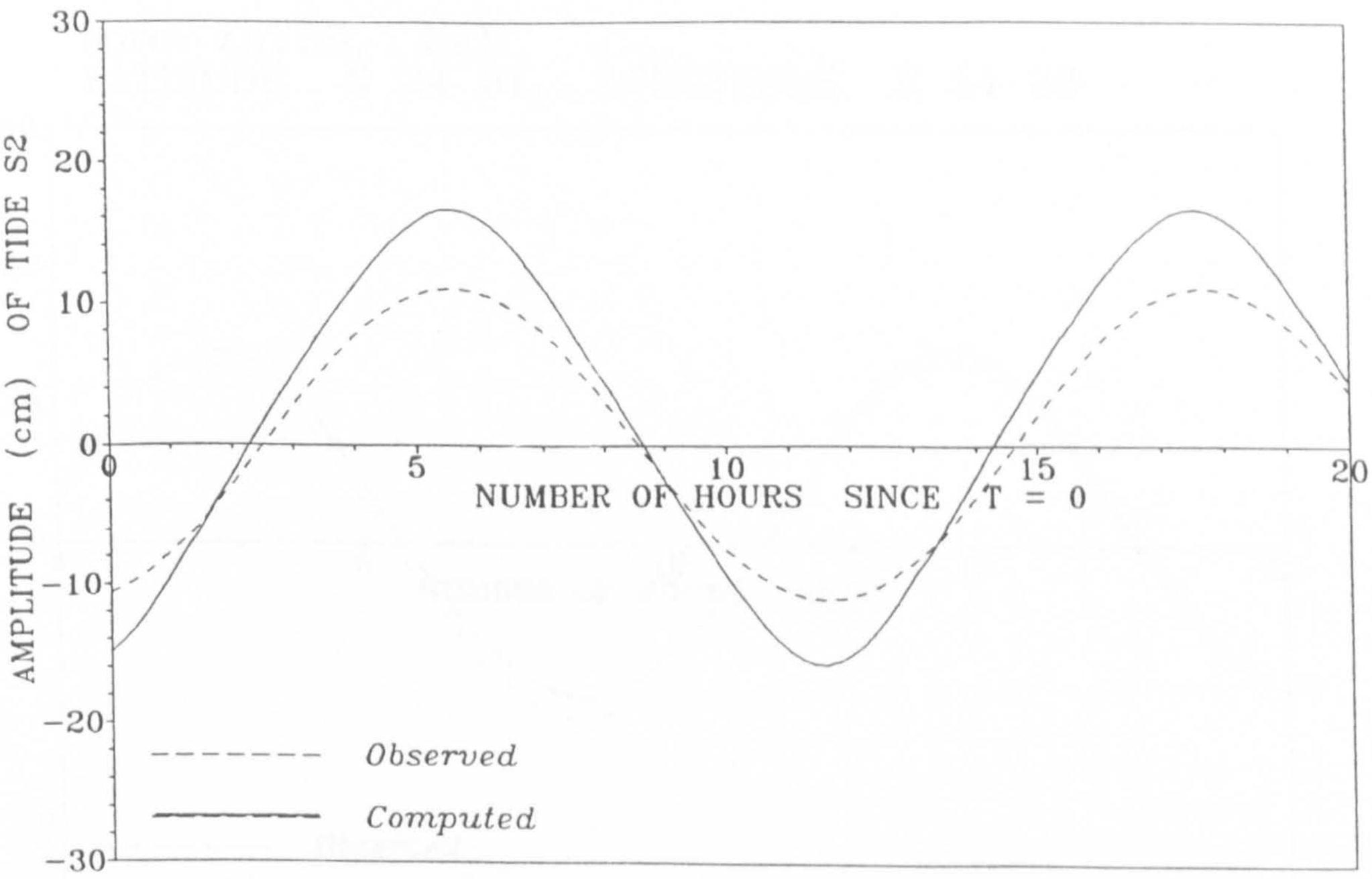

Figure 6.16o Comparison of observed and computed amplitude of tide S_2 at Musayid, Qatar

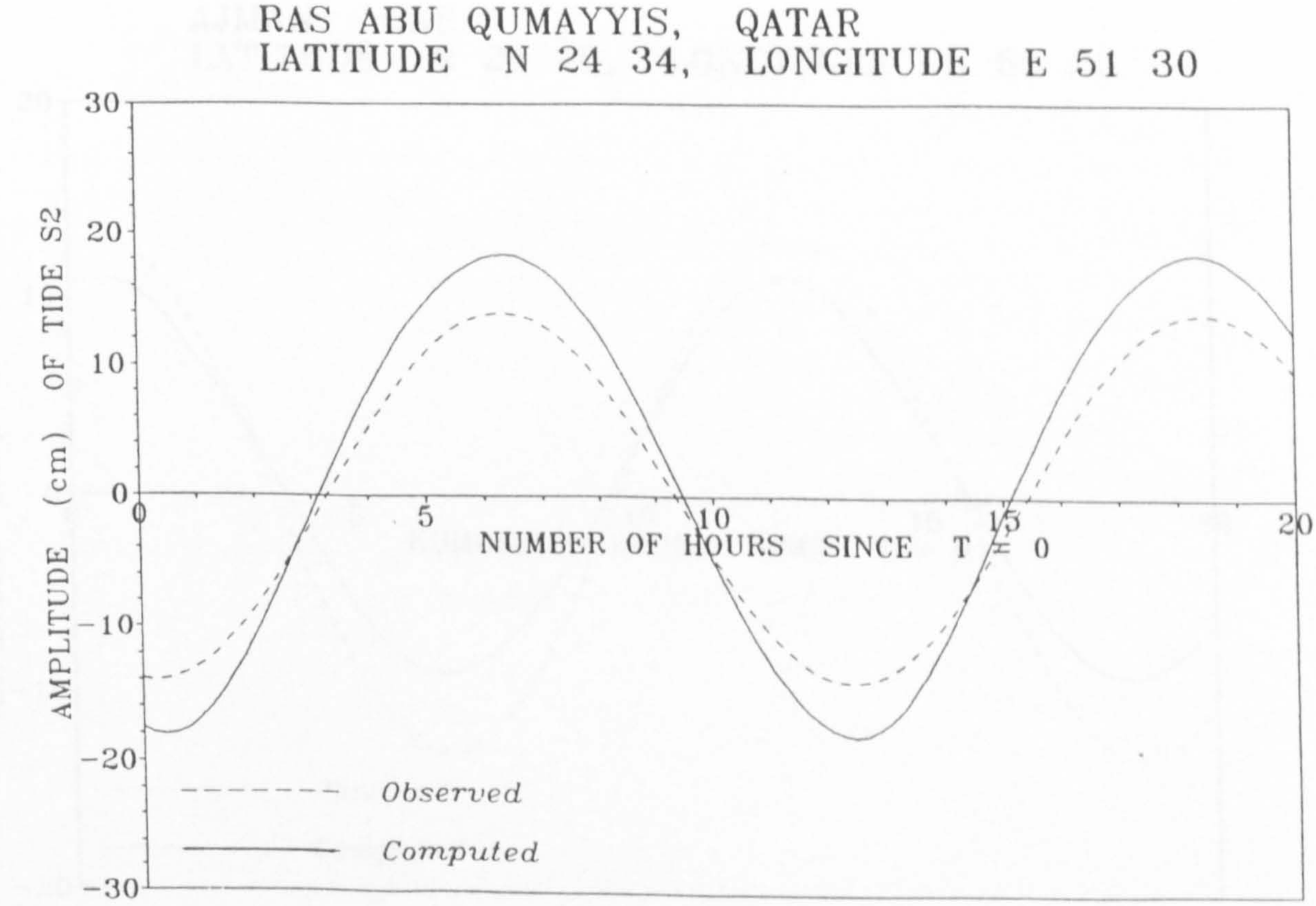

Figure 6.16p Comparison of observed and computed amplitude of tide S_2 at Ras Abu Qumayyis, Qatar

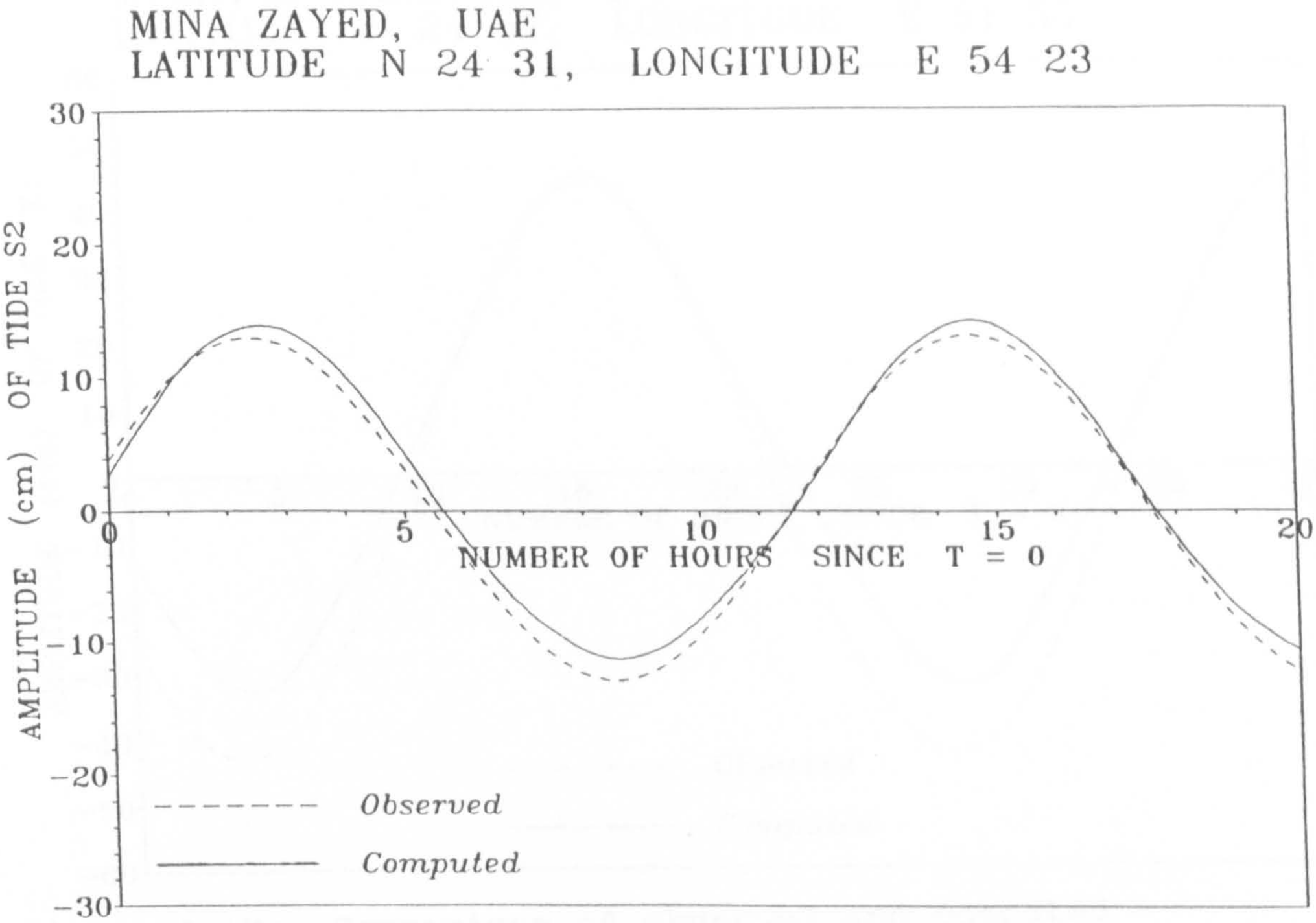

Figure 6.16q Comparison of observed and computed amplitude of tide S_2 at Mina Zayed, Uae

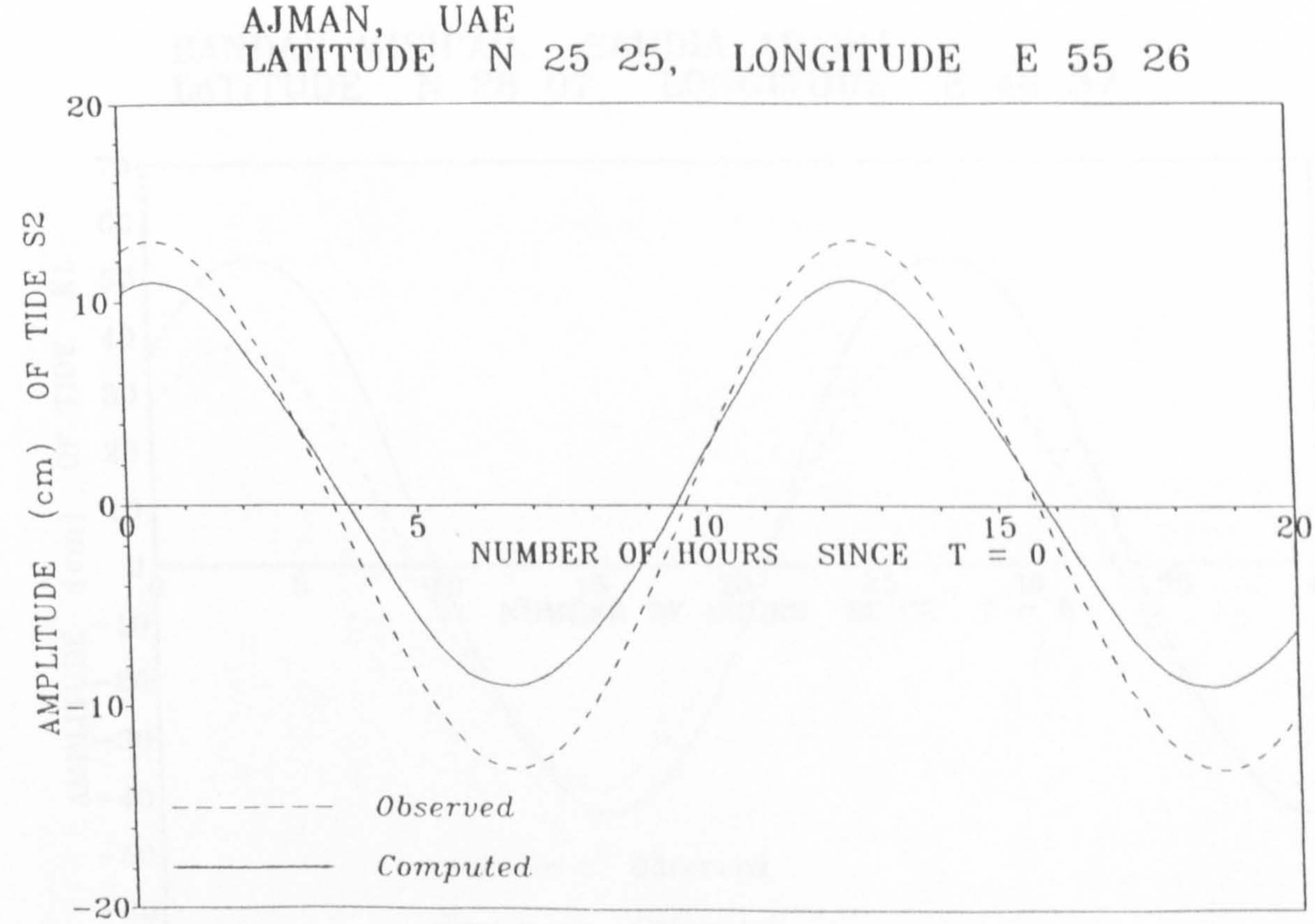

Figure 6.16r Comparison of observed and computed amplitude of tide S_2 at Ajman, UAE

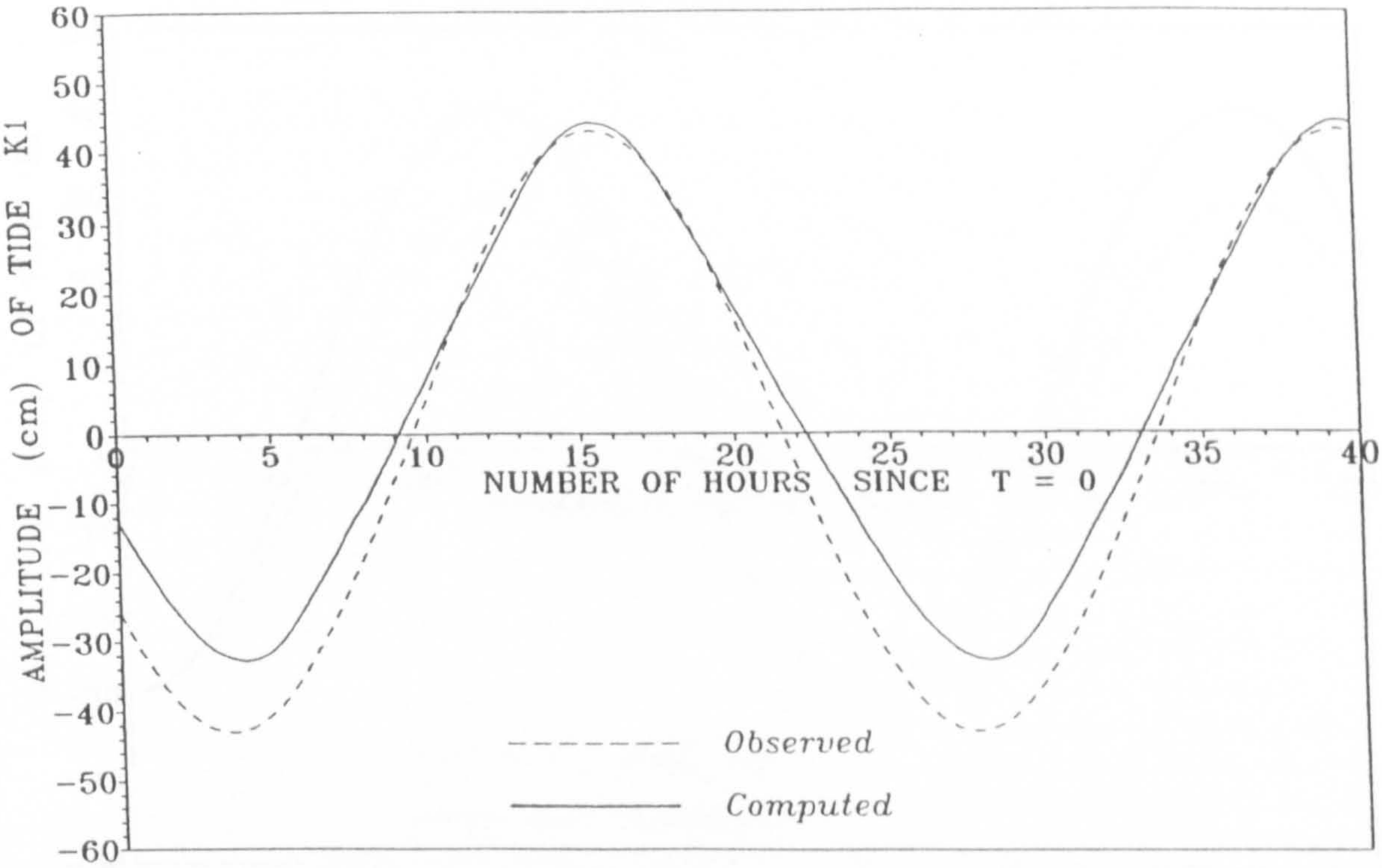

Figure 6.17a Comparison of observed and computed amplitude of tide K_1 at Musay'Id Harbour, Qatar

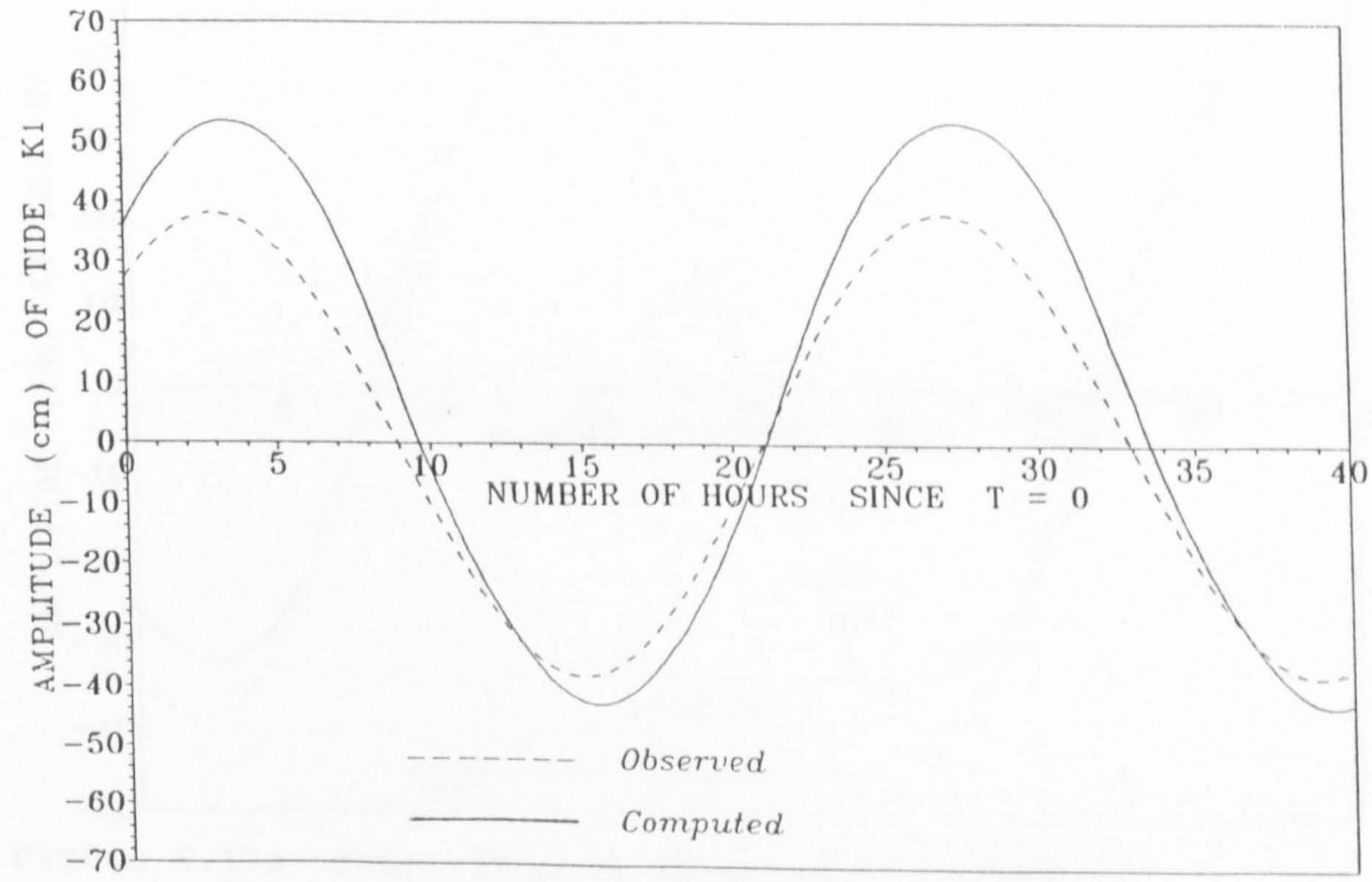

Figure 6.17b Comparison of observed and computed amplitude of tide K_1 at Bandar Mish'Ab, S. Arabia

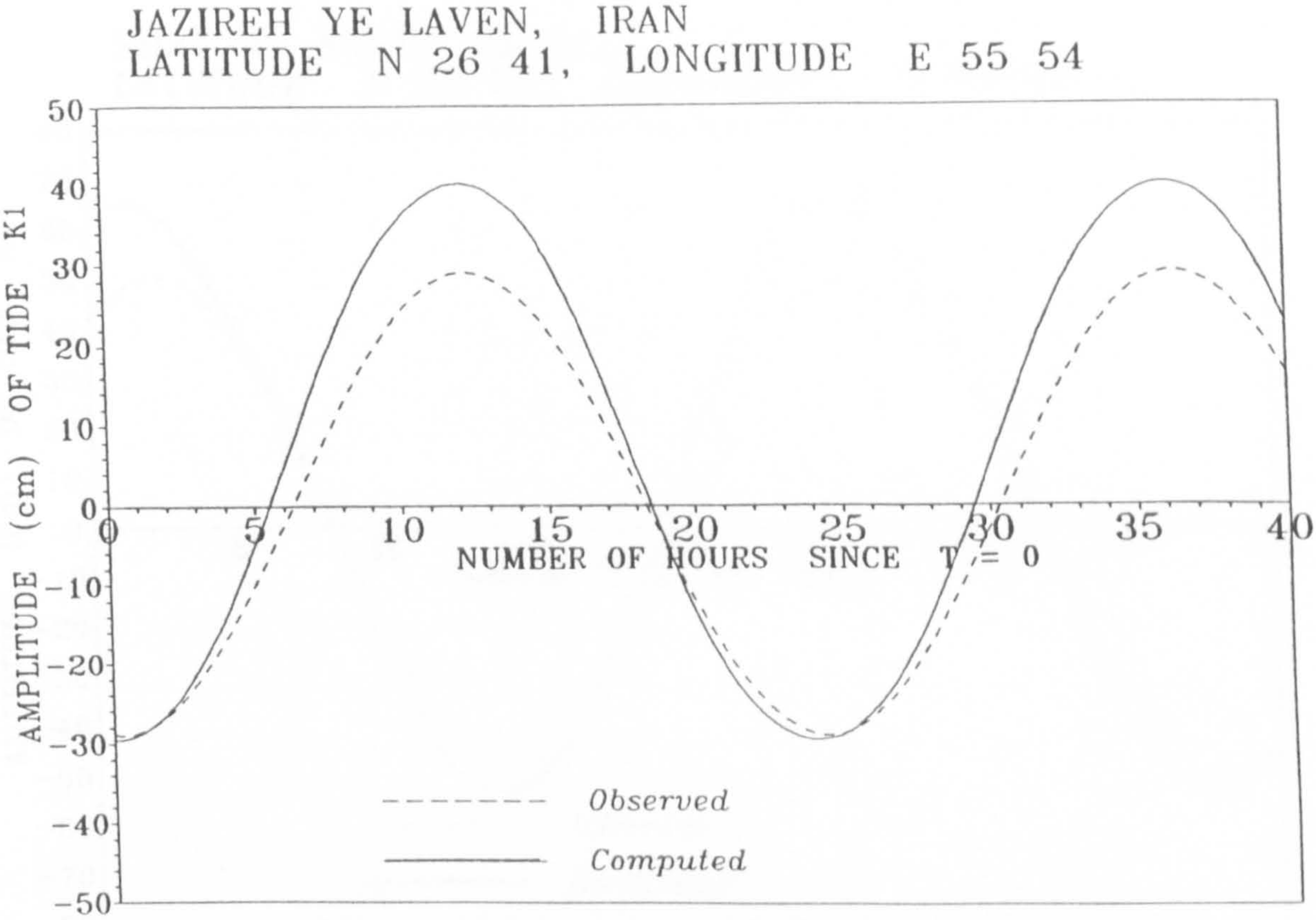

Figure 6.17c Comparison of observed and computed amplitude of tide K_1 at Jazireh Ye Laven, Iran

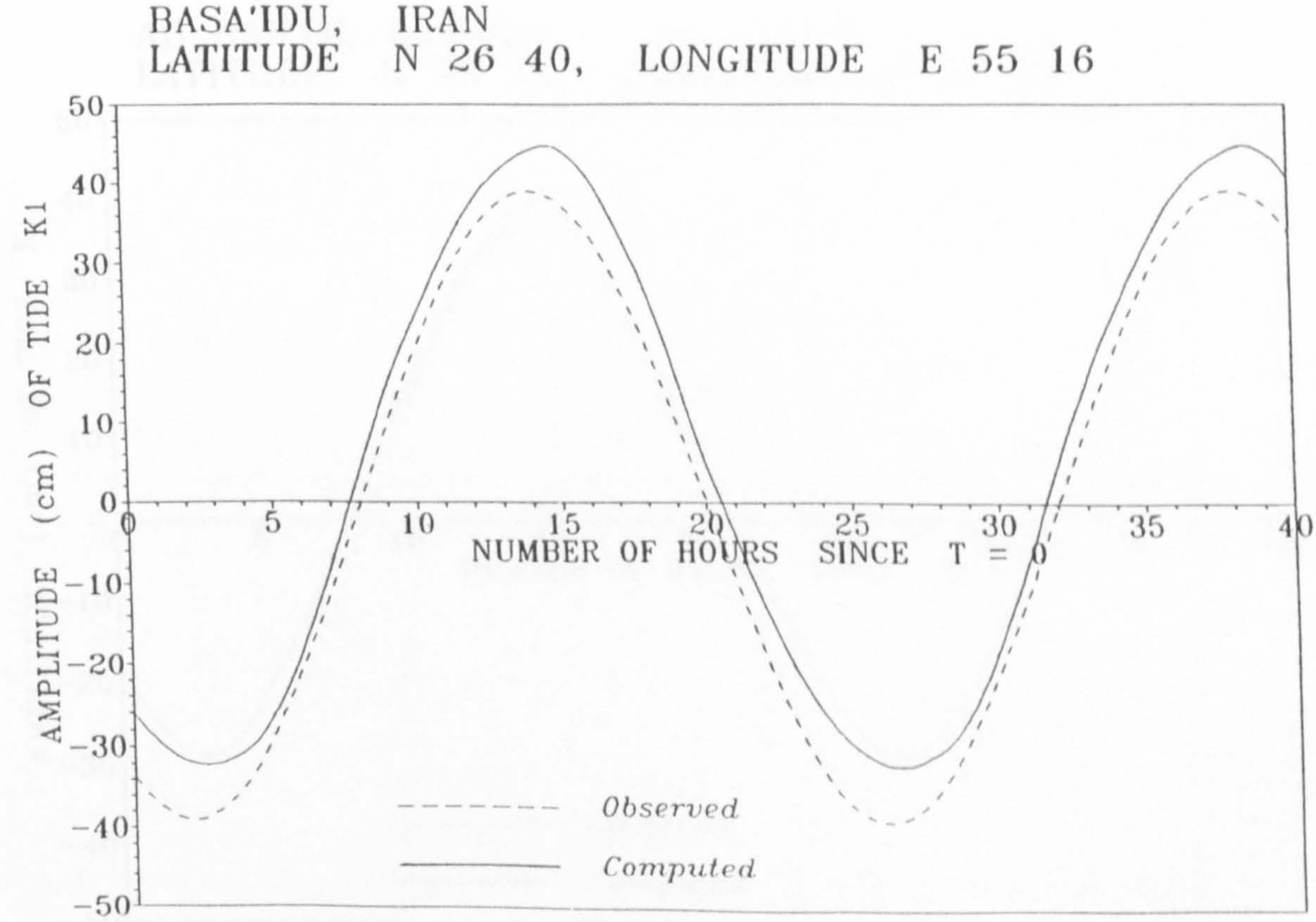

Figure 6.17d Comparison of observed and computed amplitude of tide K_1 at Basa'Idu, Iran

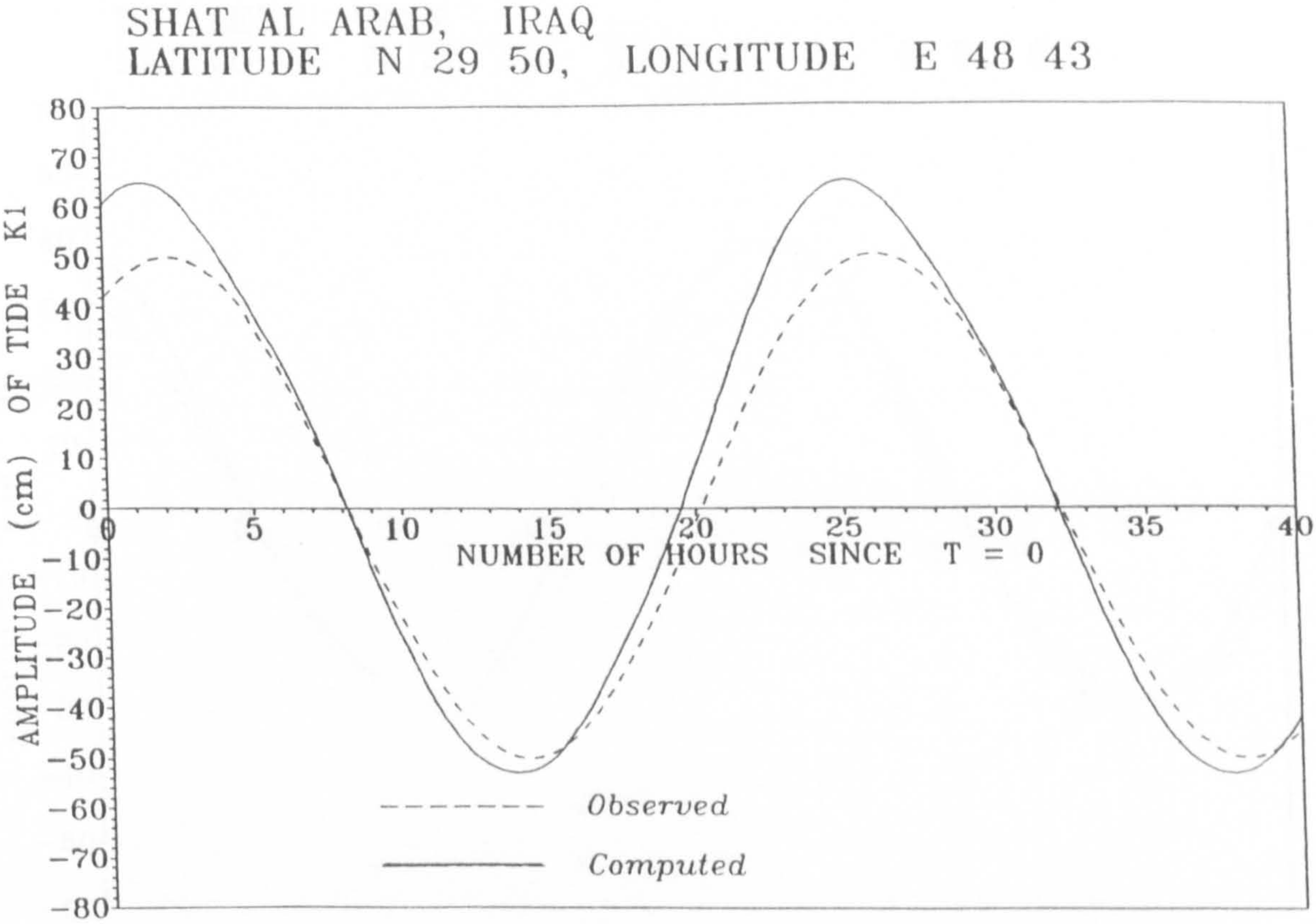

Figure 6.17e Comparison of observed and computed amplitude of tide K_1 at Shat Al Arab, Iraq

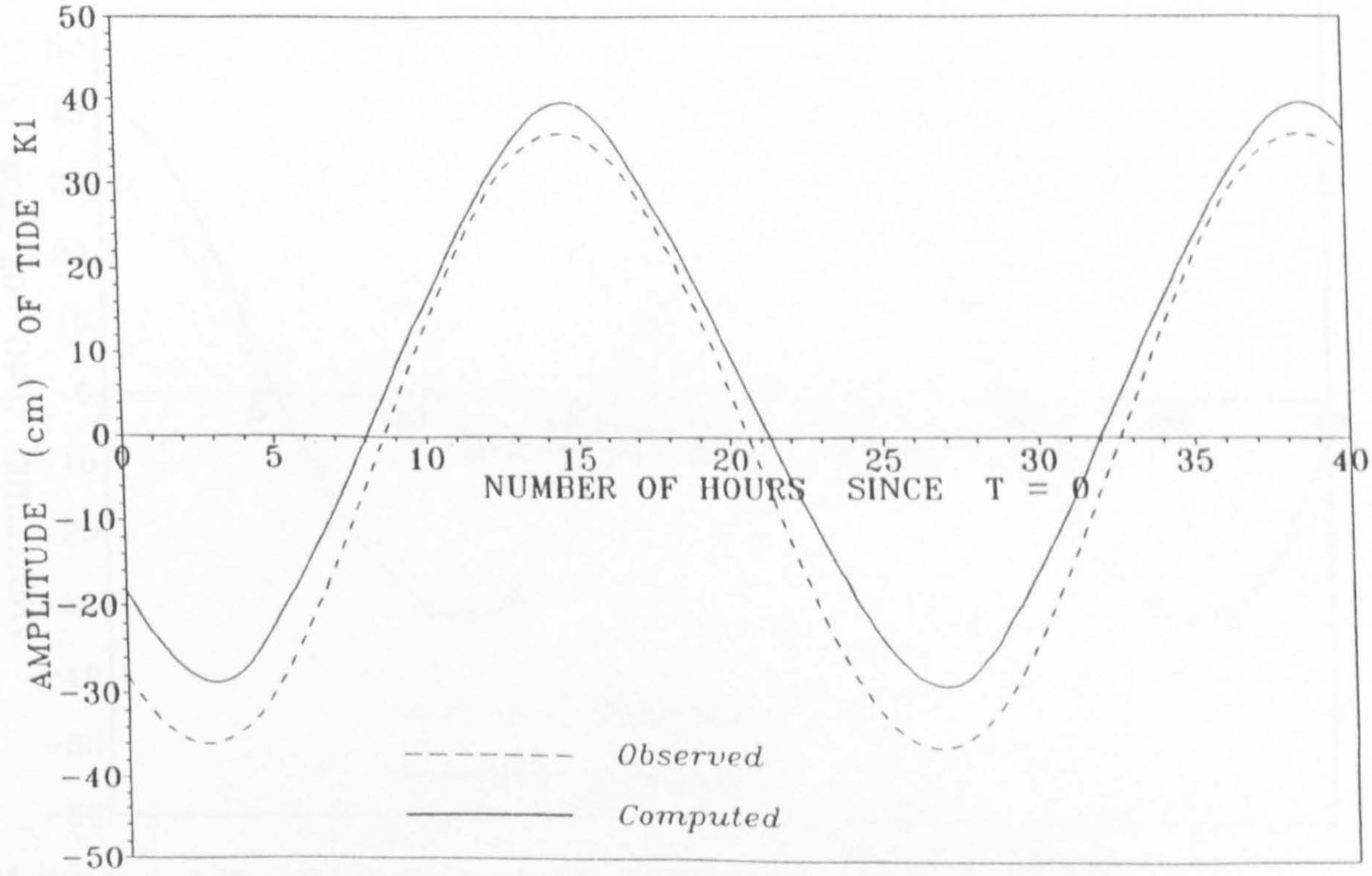

Figure 6.17f Comparison of observed and computed amplitude of tide K_1 at Ad Dawah, Qatar

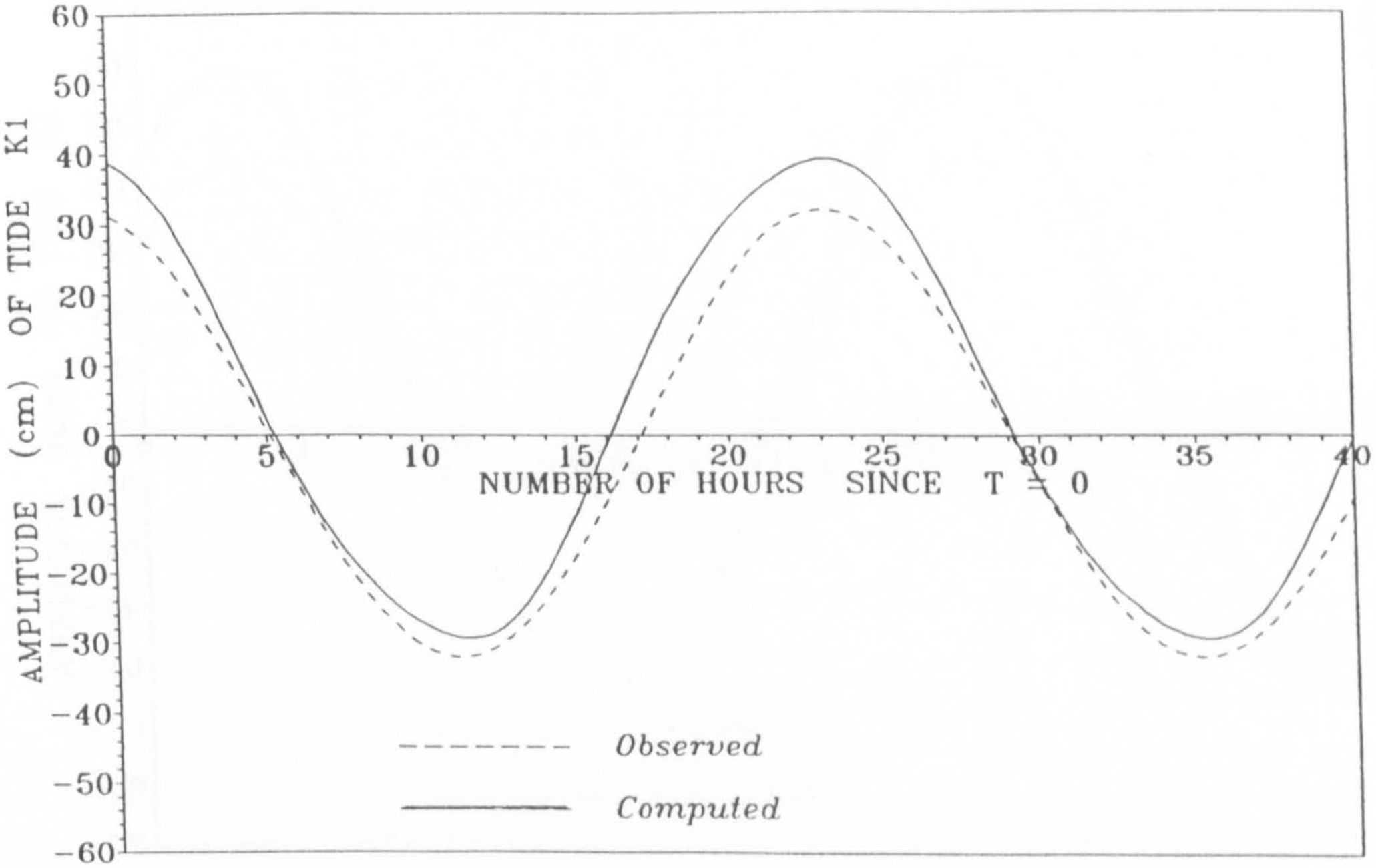

Figure 6.17g Comparison of observed and computed amplitude of tide K_1 at Halileh, Iran

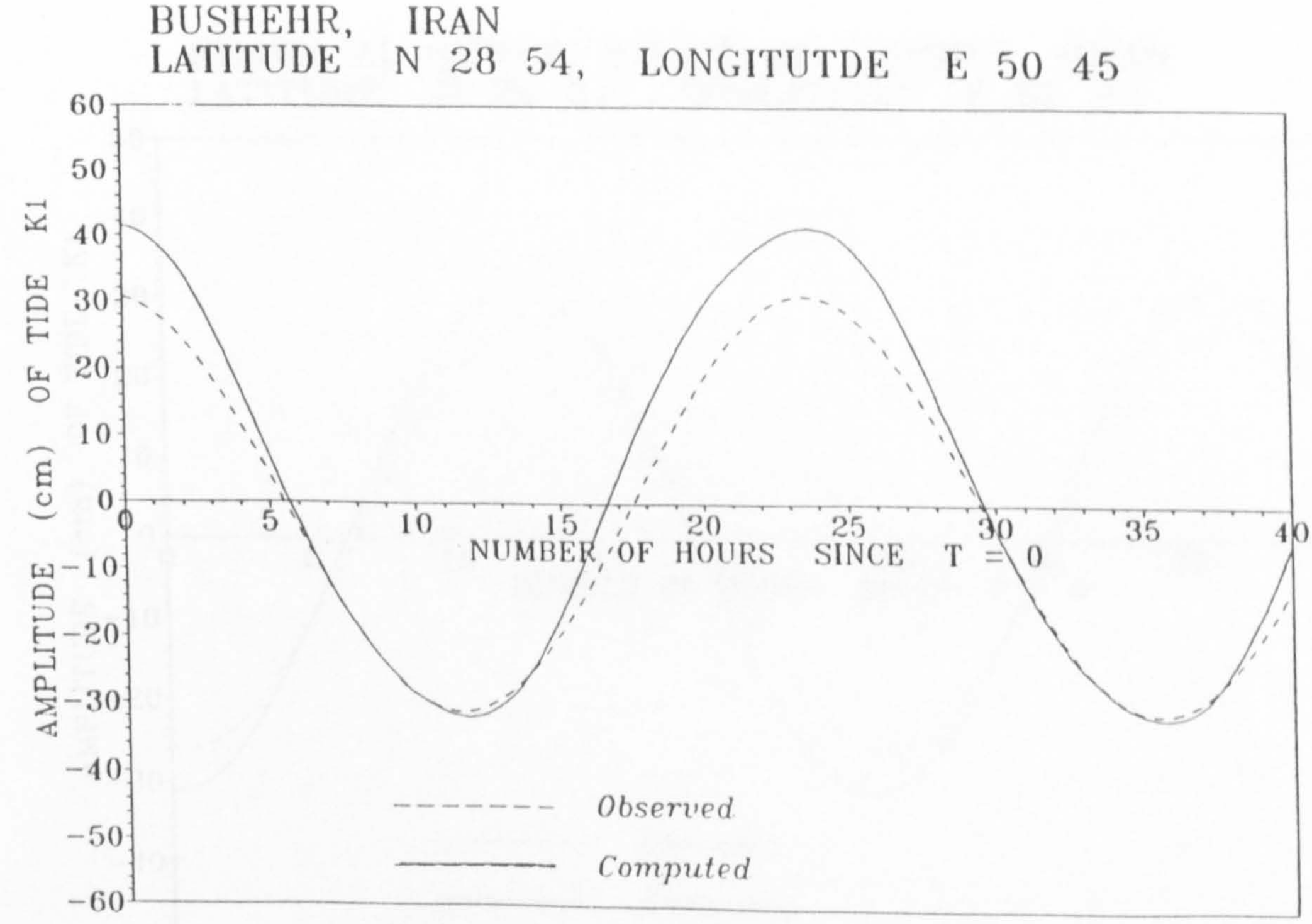

Figure 6.17h Comparison of observed and computed amplitude of tide K_1 at Bushehr, Iran

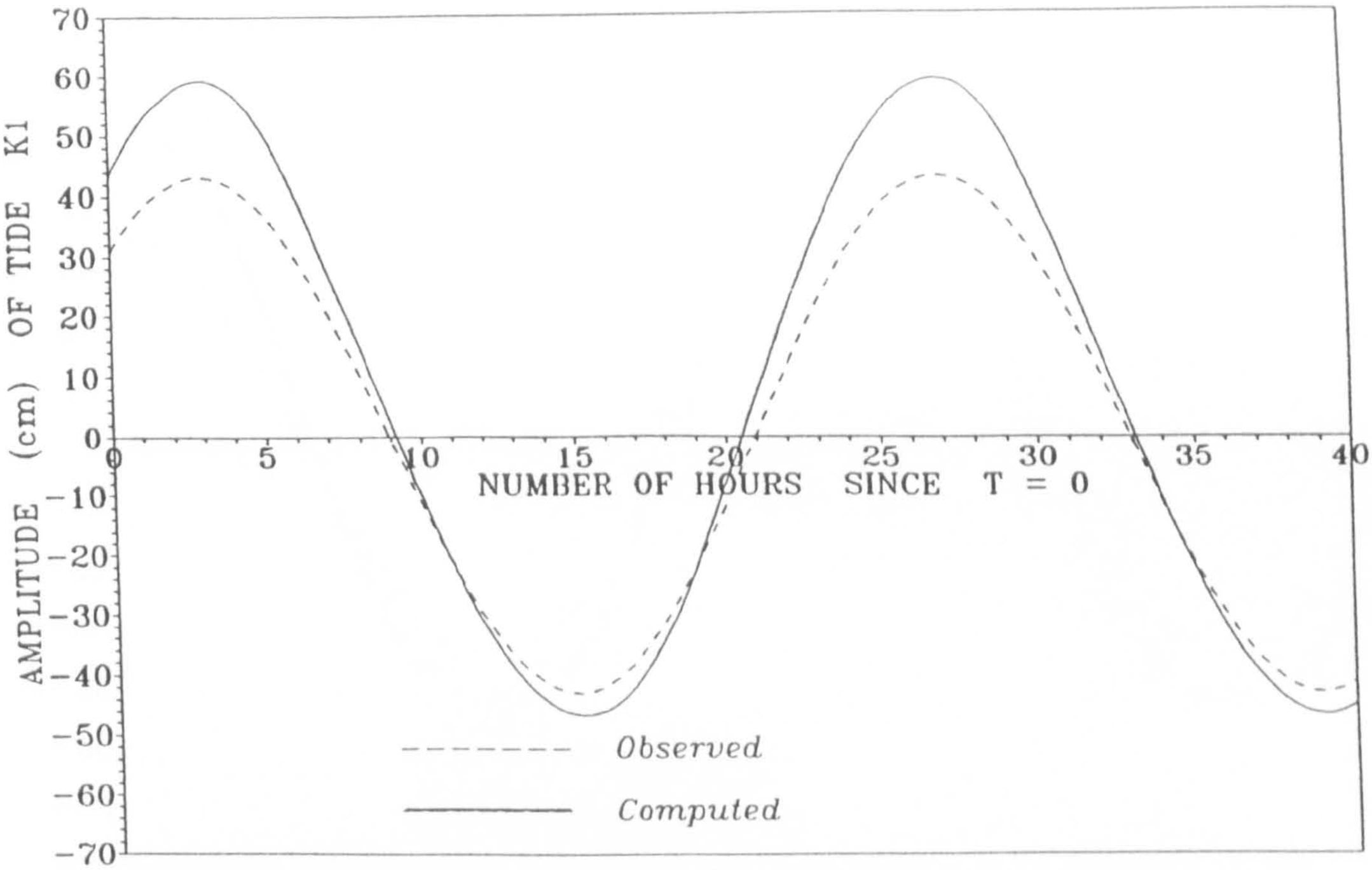

Figure 6.17i Comparison of observed and computed amplitude of tide K_1 at Mina Saud, Kuwait

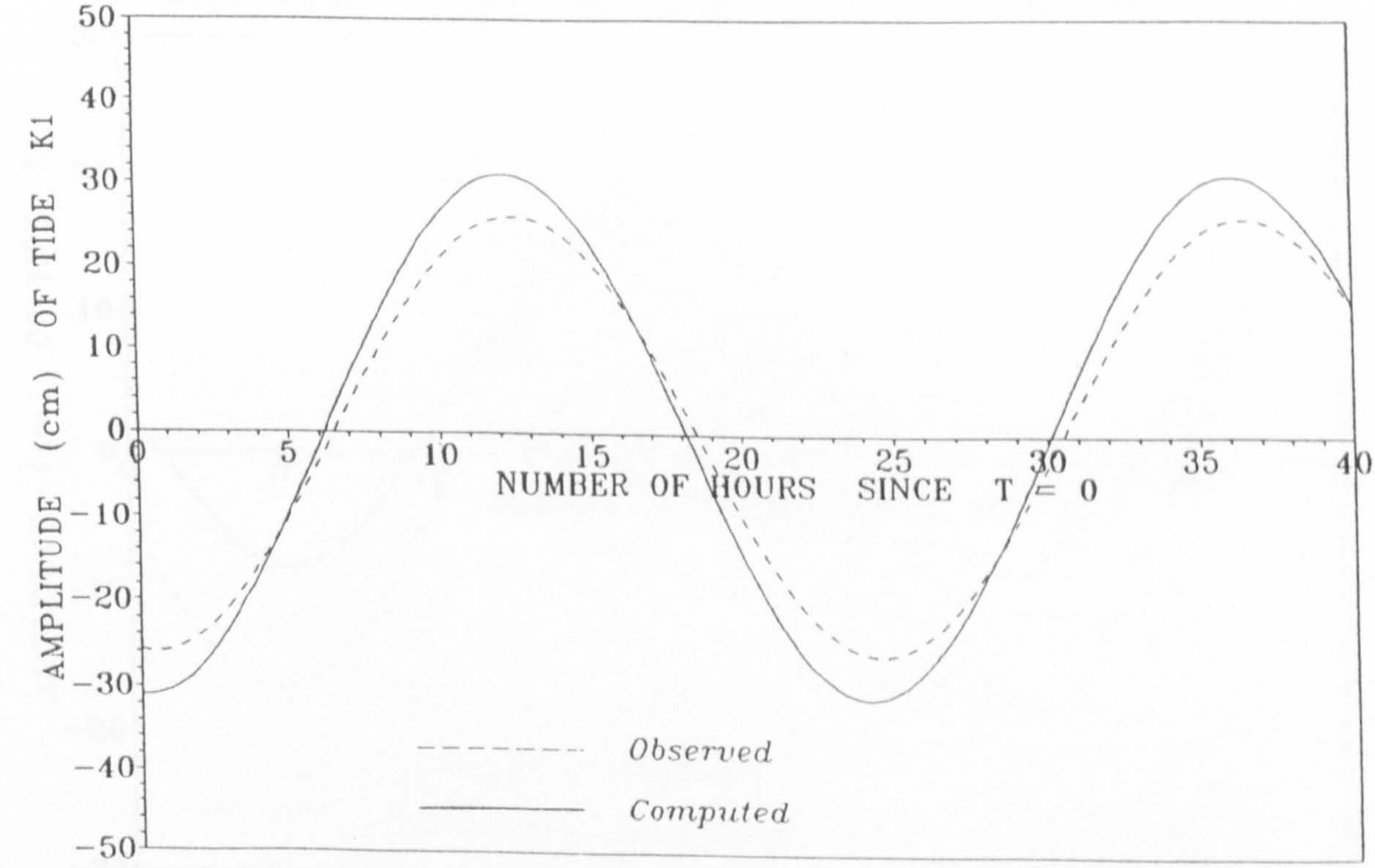

Figure 6.17j Comparison of observed and computed amplitude of tide K_1 at Khawr Al Quway, Strait Of Hormuz, Oman

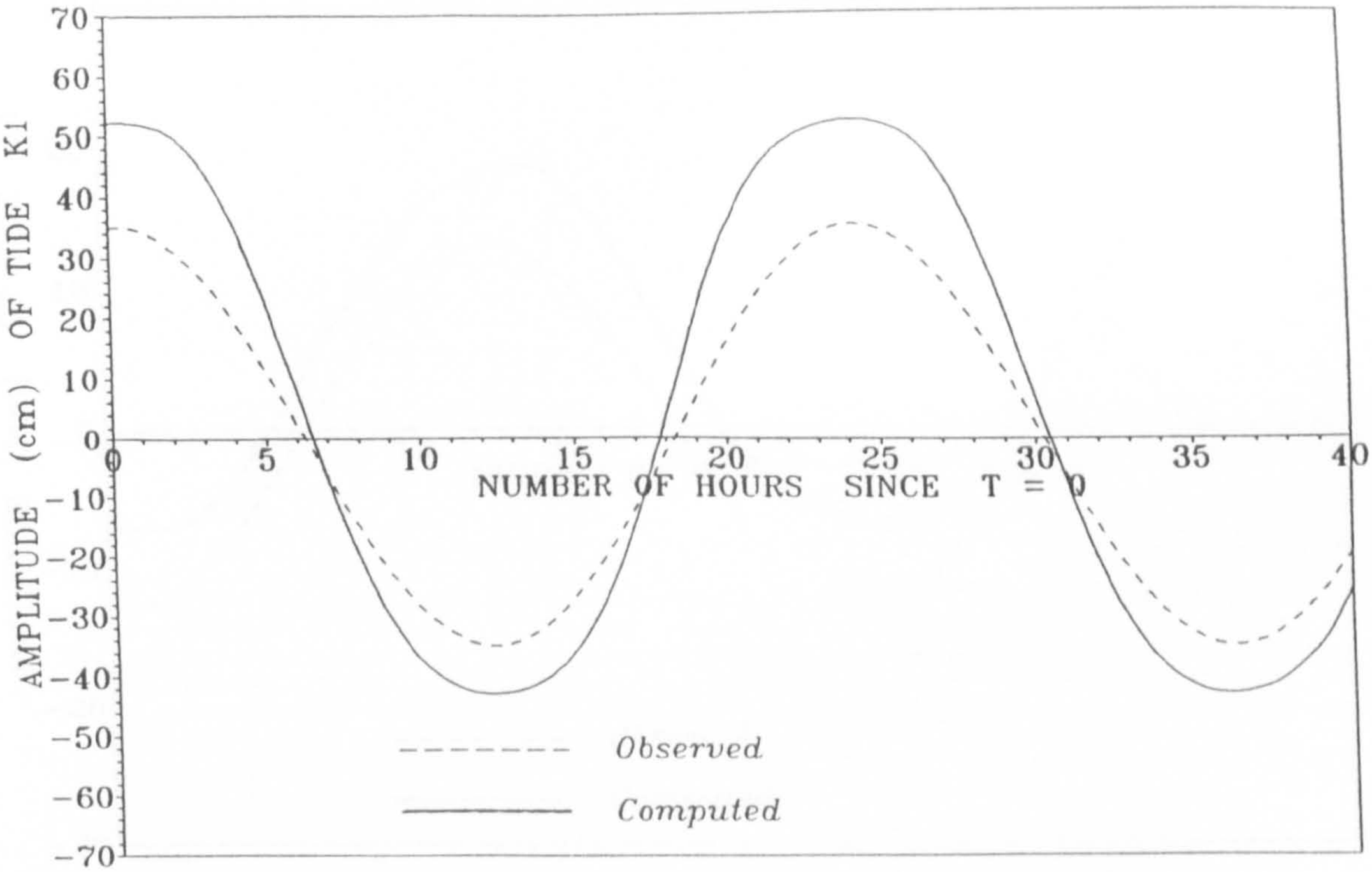

Figure 6.17k Comparison of observed and computed amplitude of tide K_1 at Bandar Daylam, Iran

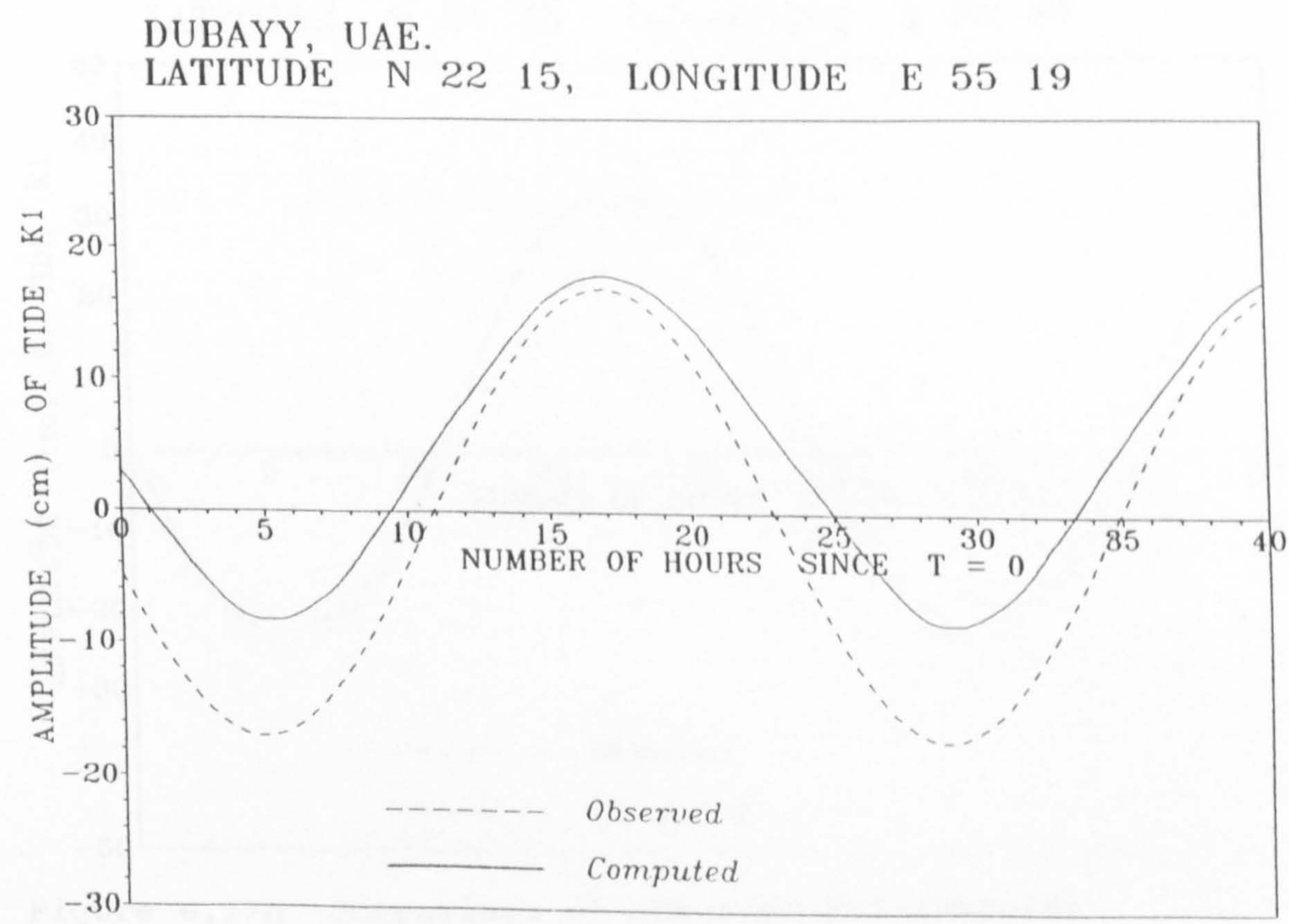

Figure 6.17l Comparison of observed and computed amplitude of tide K_1 at Dubayy, UAE

RAS AL KHAYMAH, UAE.
LATITUDE N 25 49, LONGITUDE E 55 57

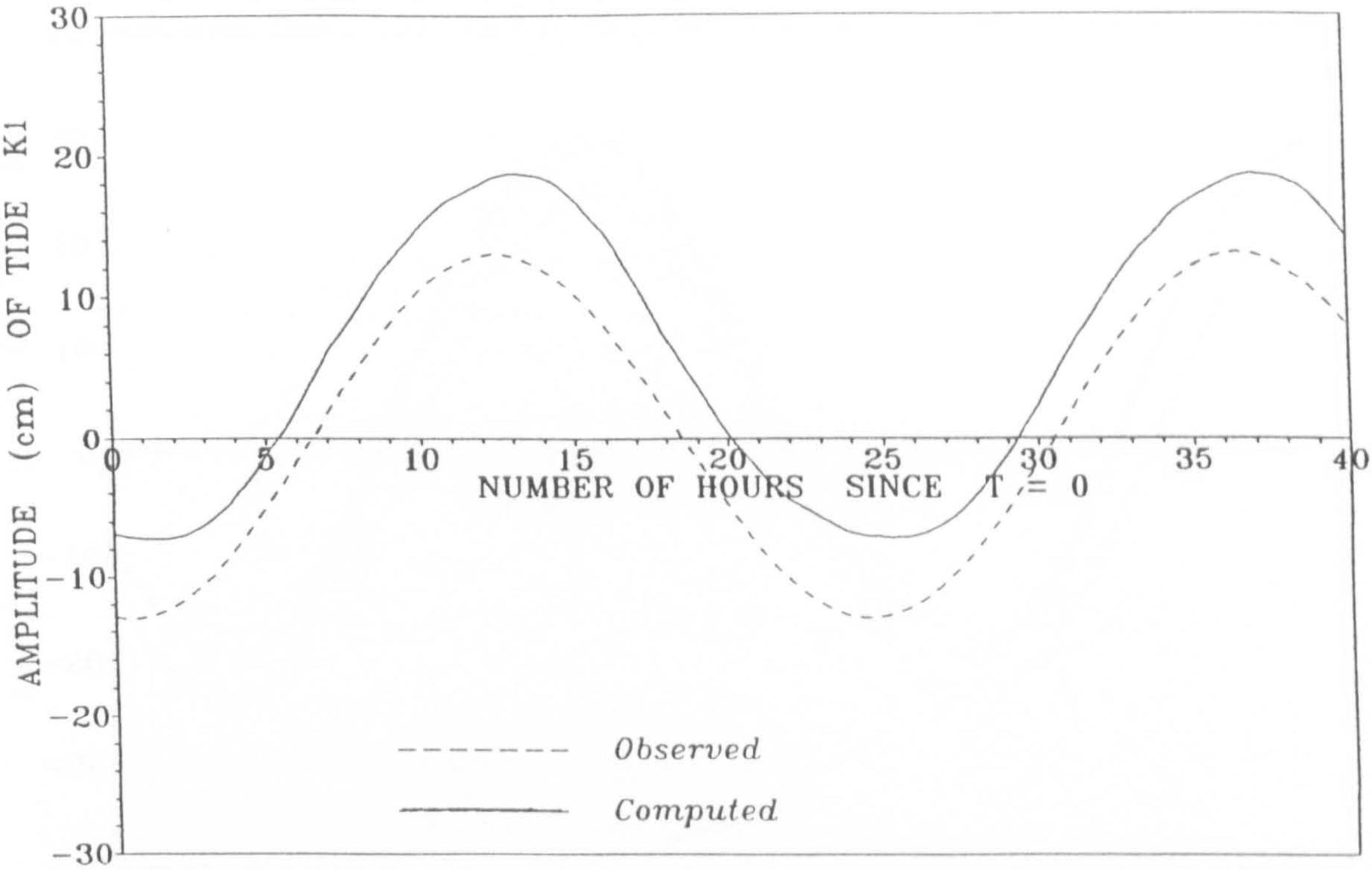

Figure 6.17m Comparison of observed and computed amplitude of tide K_1 at Ras Al Khaymah, UAE

BANDAR ASALU, IRAN
LATITUDE N 27 28, LONGITUDE E 52 37

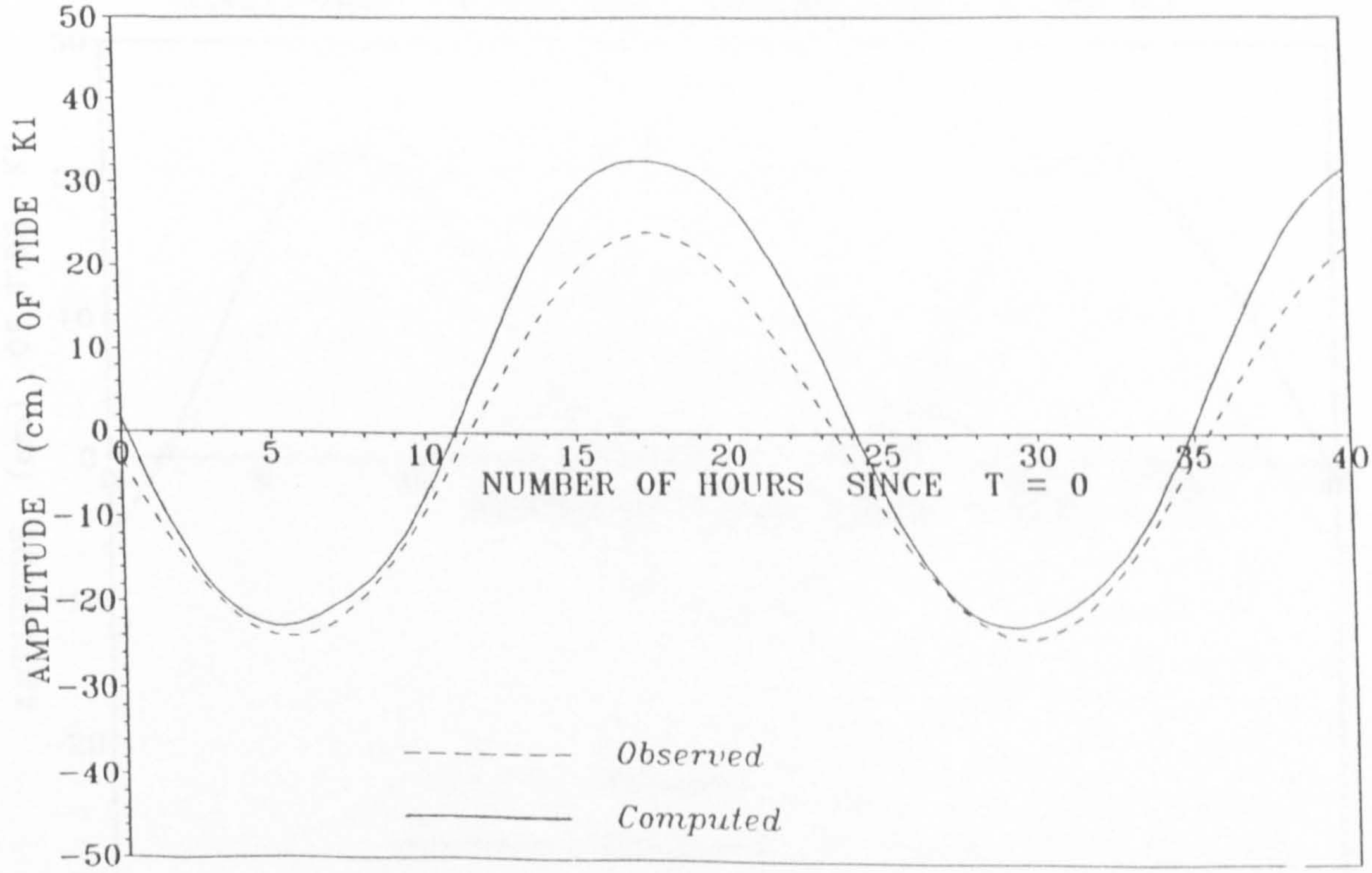

Figure 6.17n Comparison of observed and computed amplitude of tide K_1 at Bandar Asalu, Iran

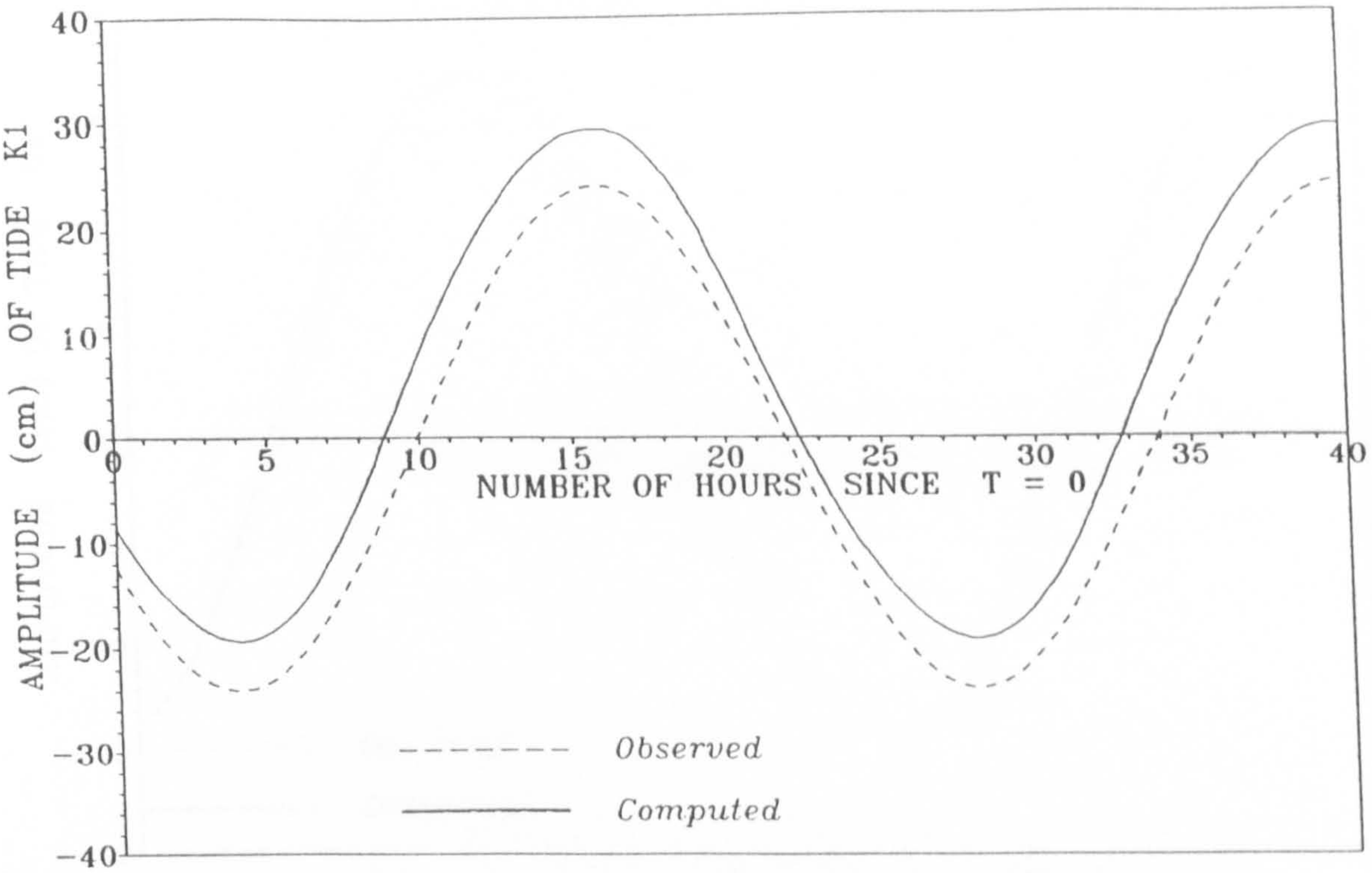

Figure 6.17o Comparison of observed and computed amplitude of tide K_1 at Jazirat Siri, UAE

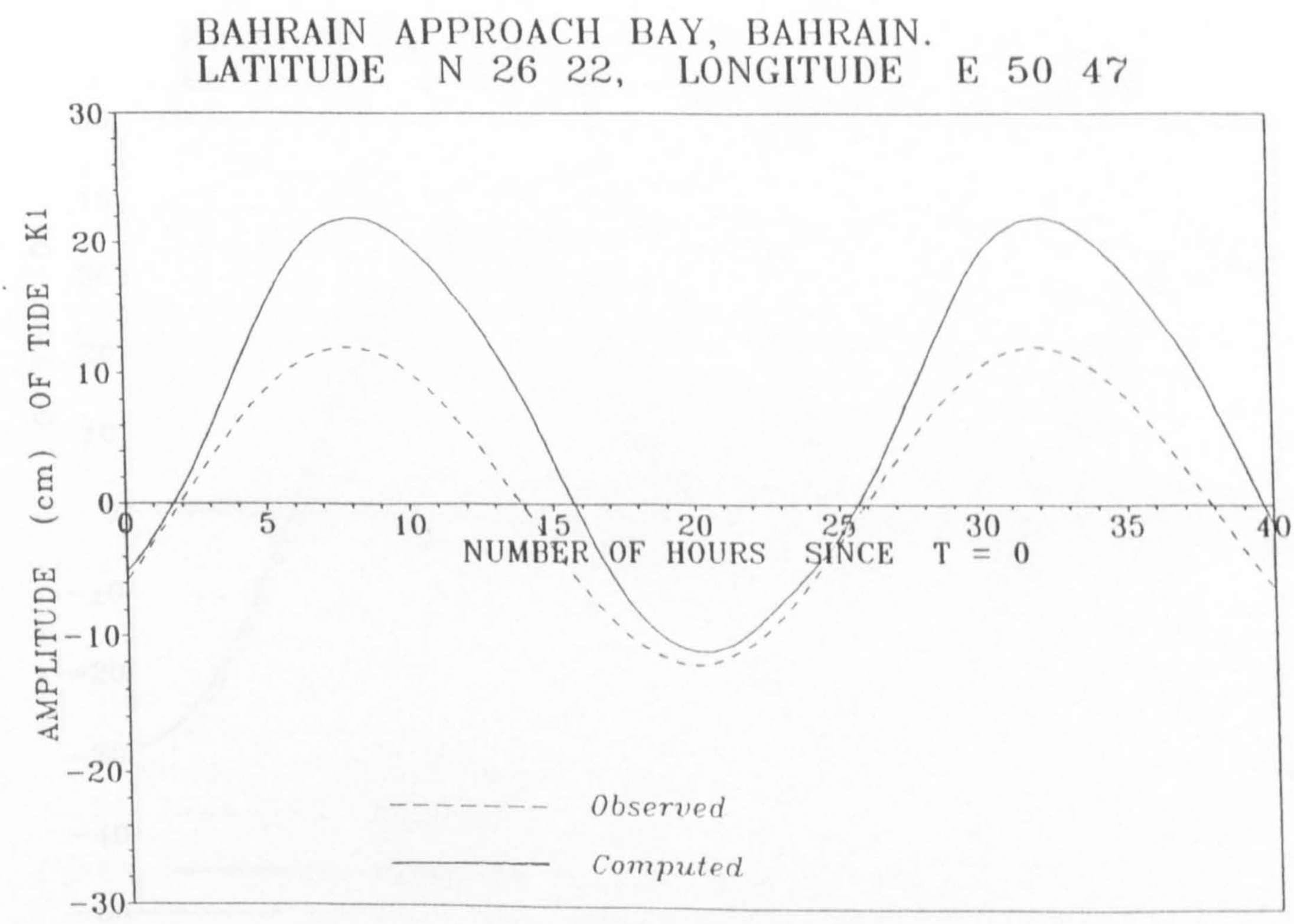

Figure 6.17p Comparison of observed and computed amplitude of tide K_1 at Bahrain Approach Bay, Bahrain

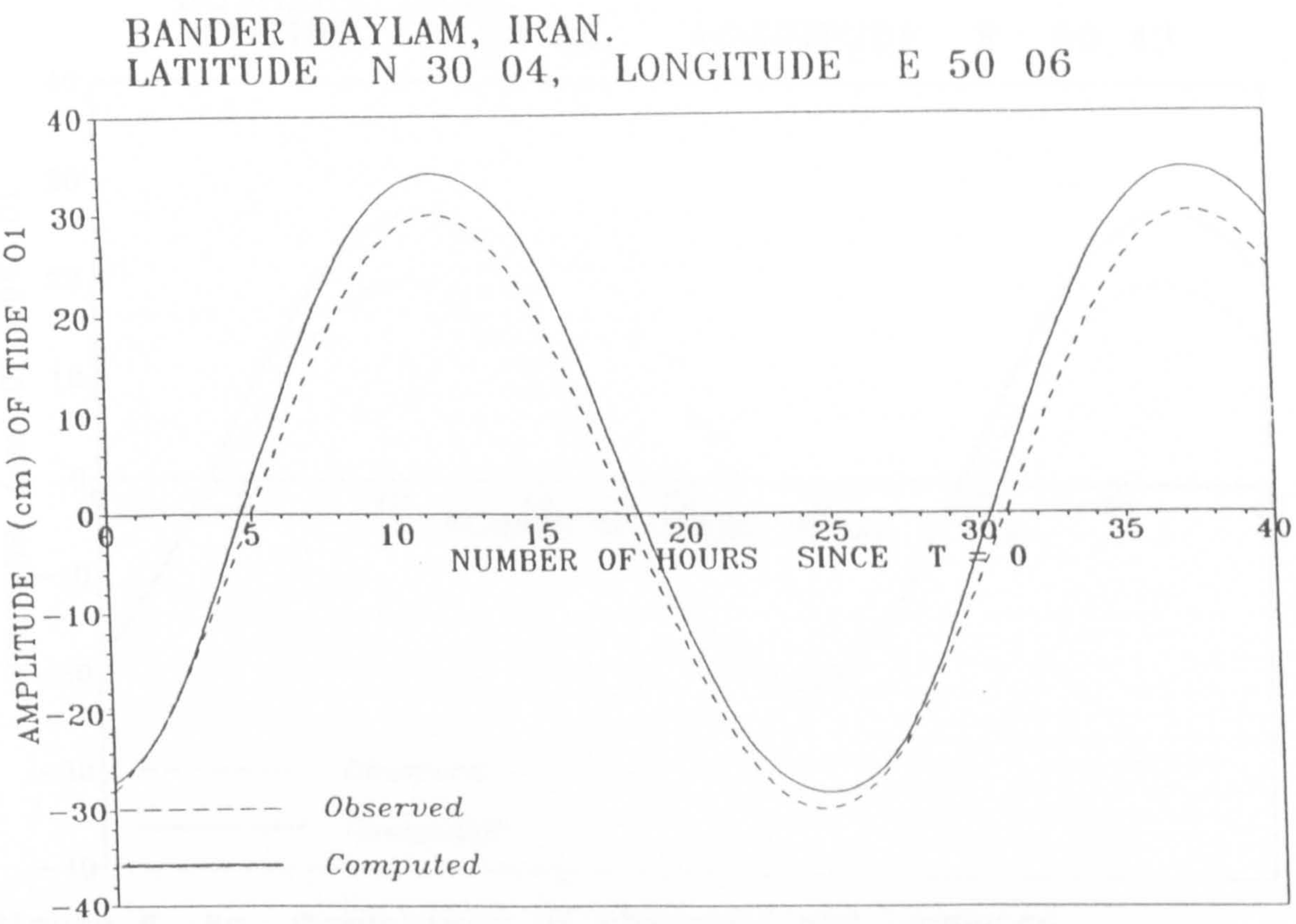

Figure 6.18a Comparison of observed and computed amplitude of tide O_1 at Bander Daylam, Iran

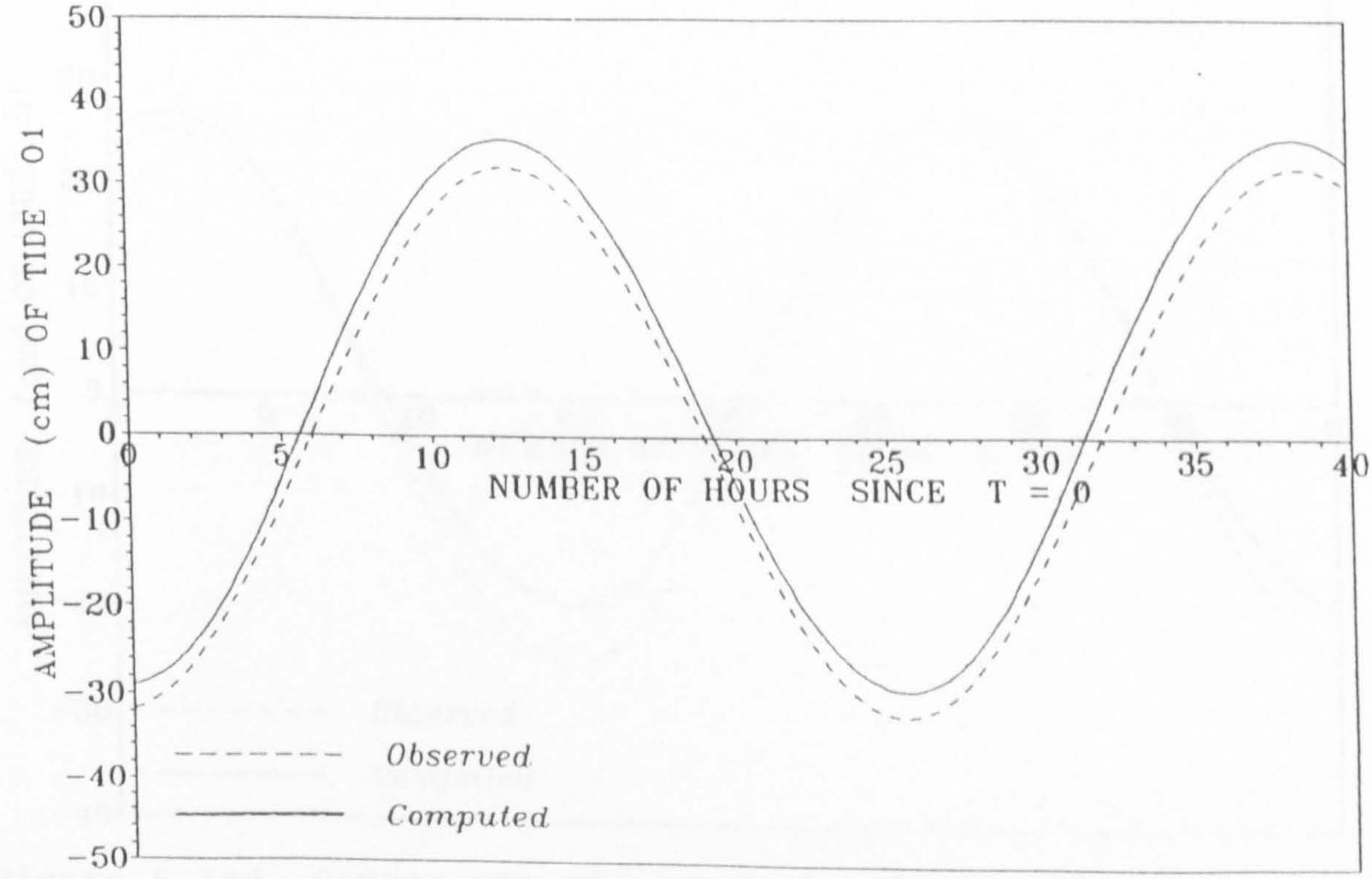

Figure 6.18b Comparison of observed and computed amplitude of tide O_1 at Khor Musa, Iran

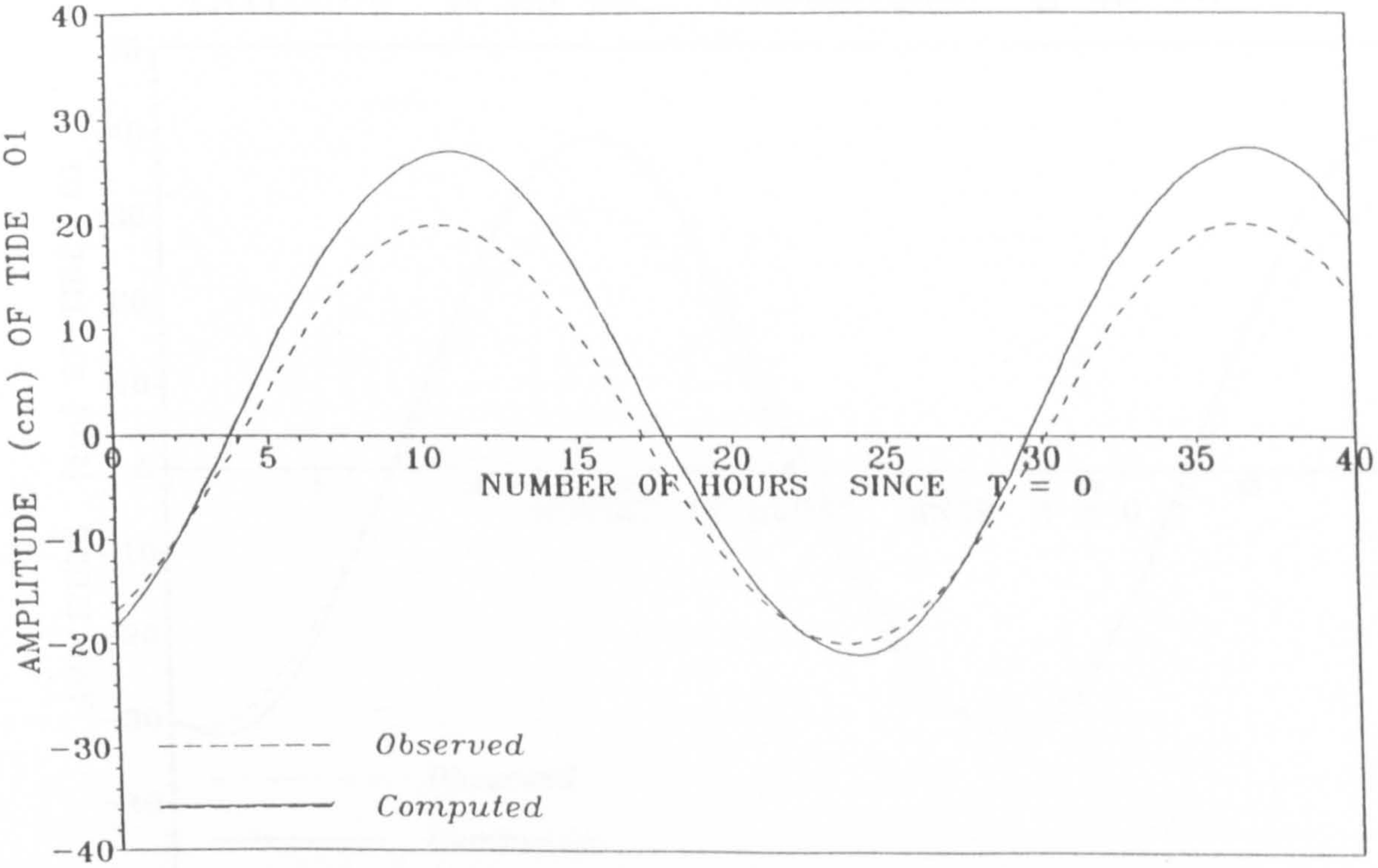

Figure 6.18c Comparison of observed and computed amplitude of tide O_1 at Bushehr, Iran

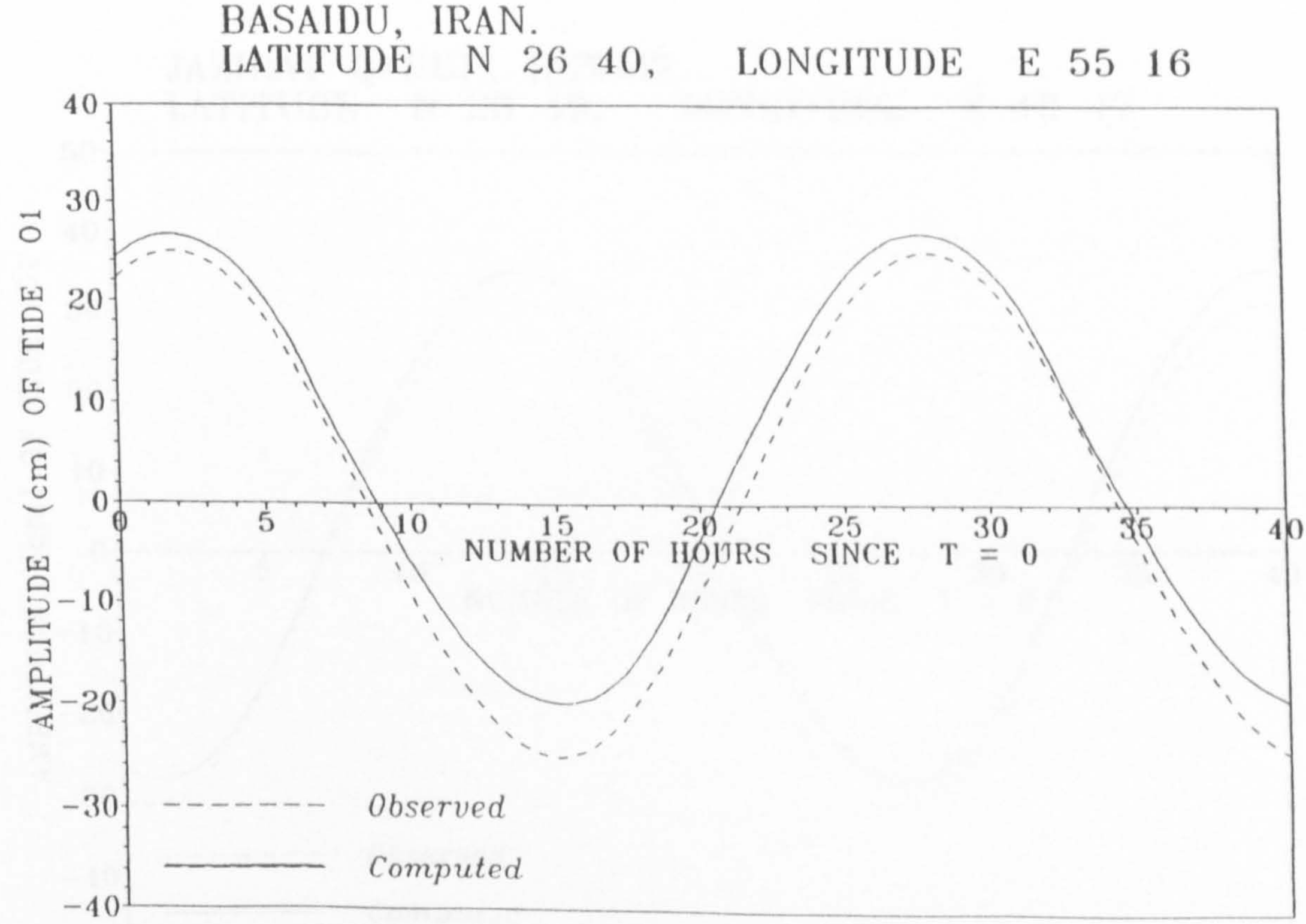

Figure 6.18d Comparison of observed and computed amplitude of tide O_1 at Basaidu, Iran

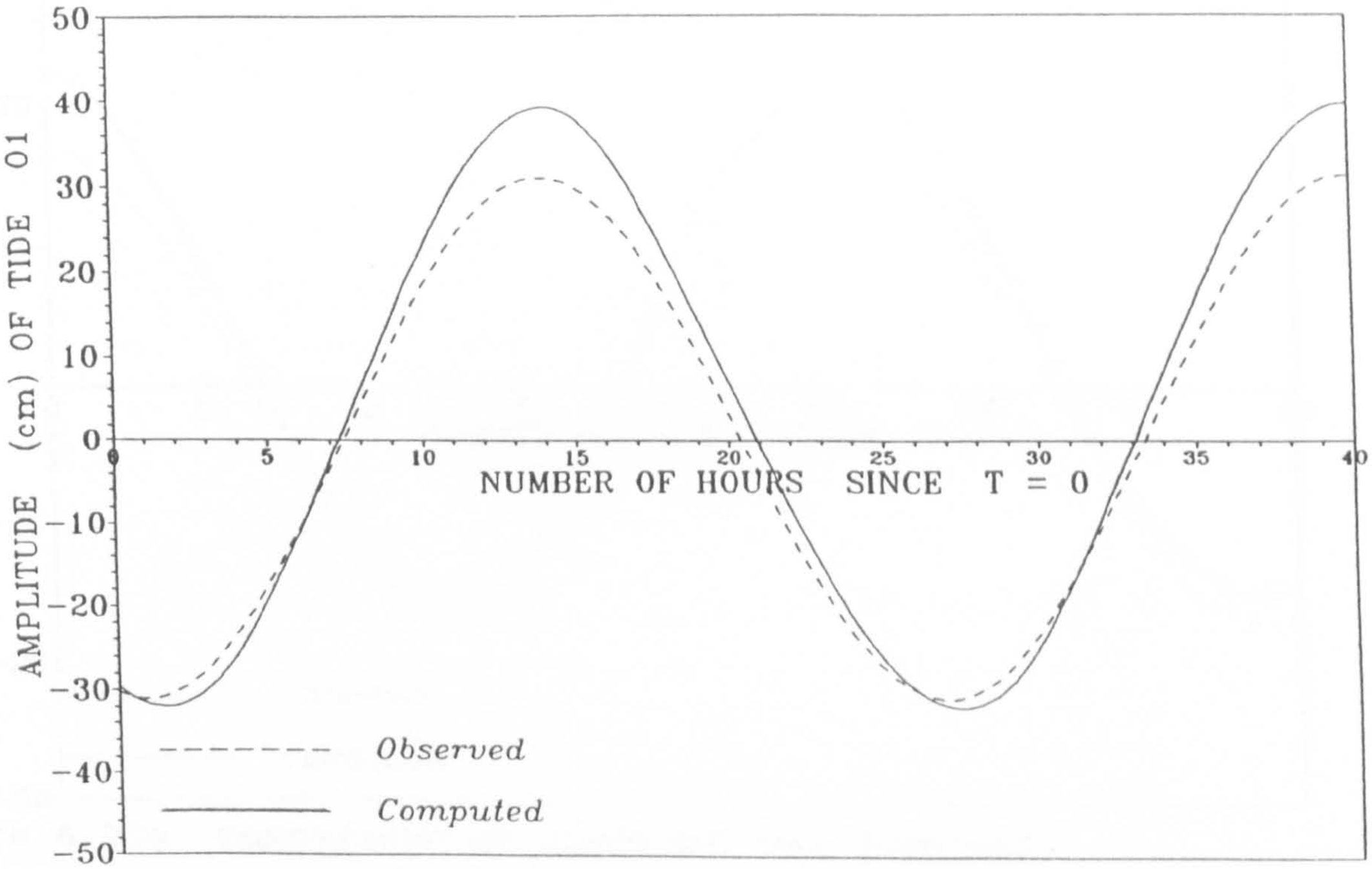

Figure 6.18e Comparison of observed and computed amplitude of tide O_1 at Mina Al Ahmadi, Kuwait

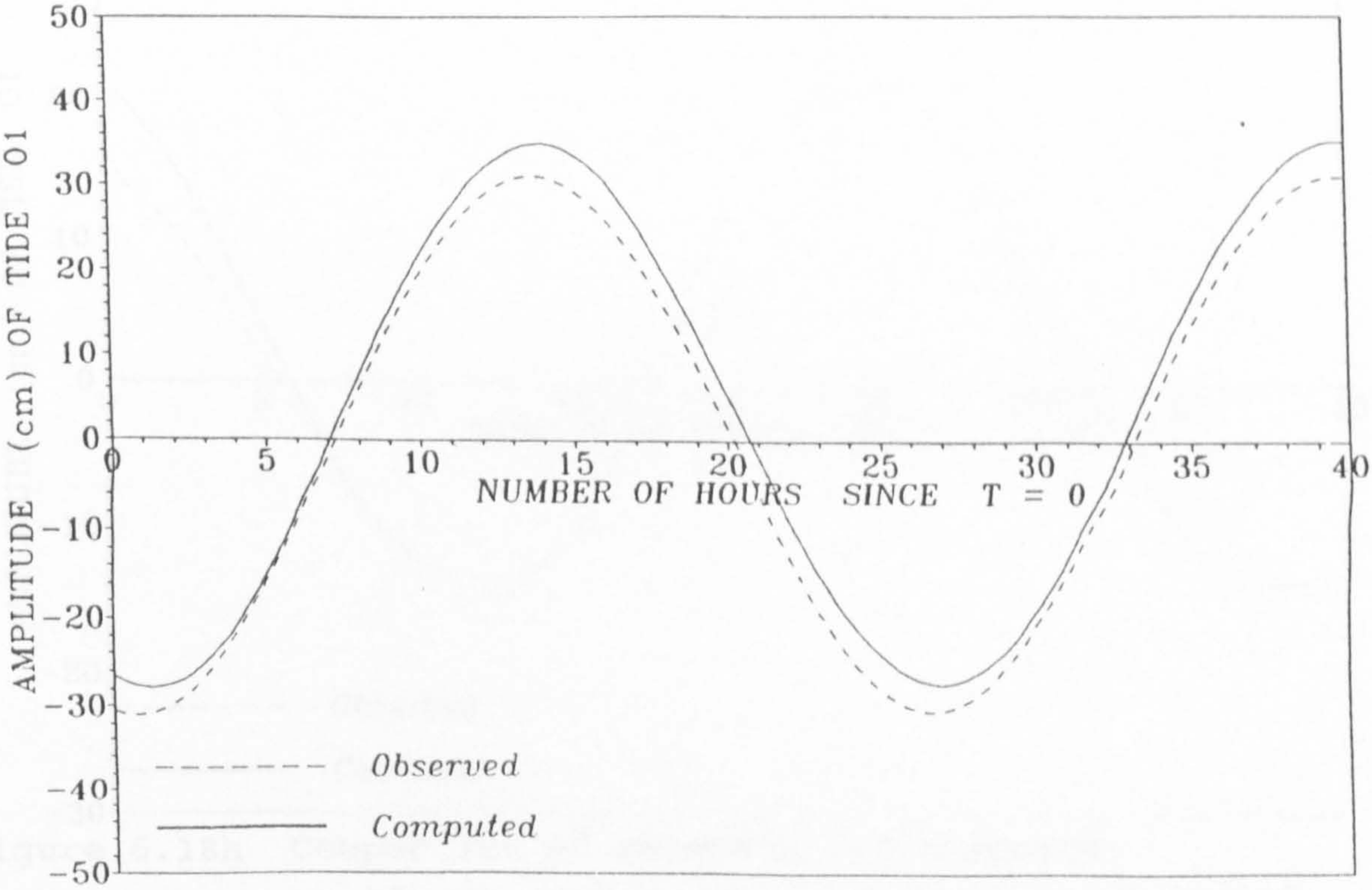

Figure 6.18f Comparison of observed and computed amplitude of tide O_1 at Jazirat Qaruh, Kuwait

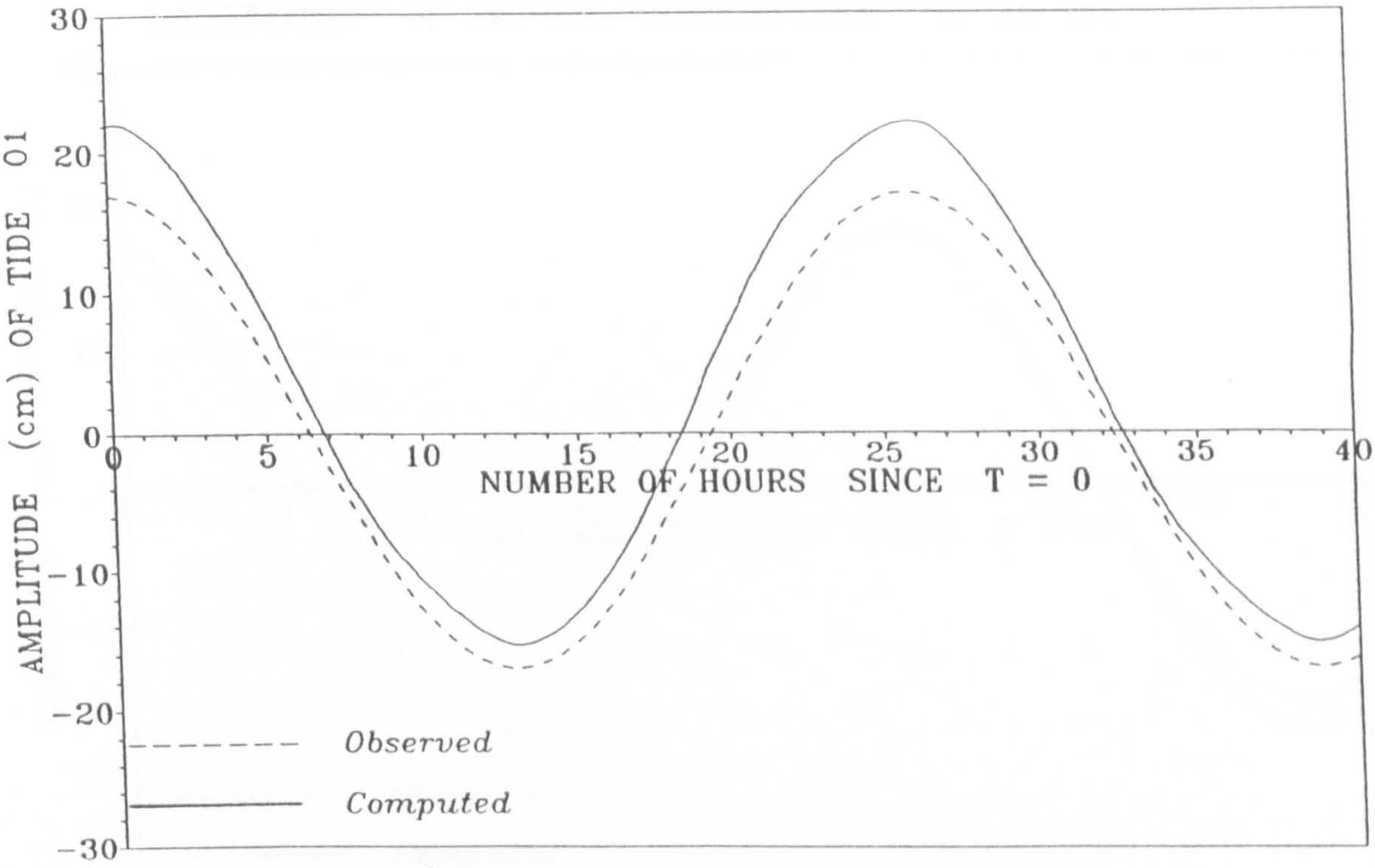

Figure 6.18g Comparison of observed and computed amplitude of tide O_1 at Ad Dawhah, Qatar

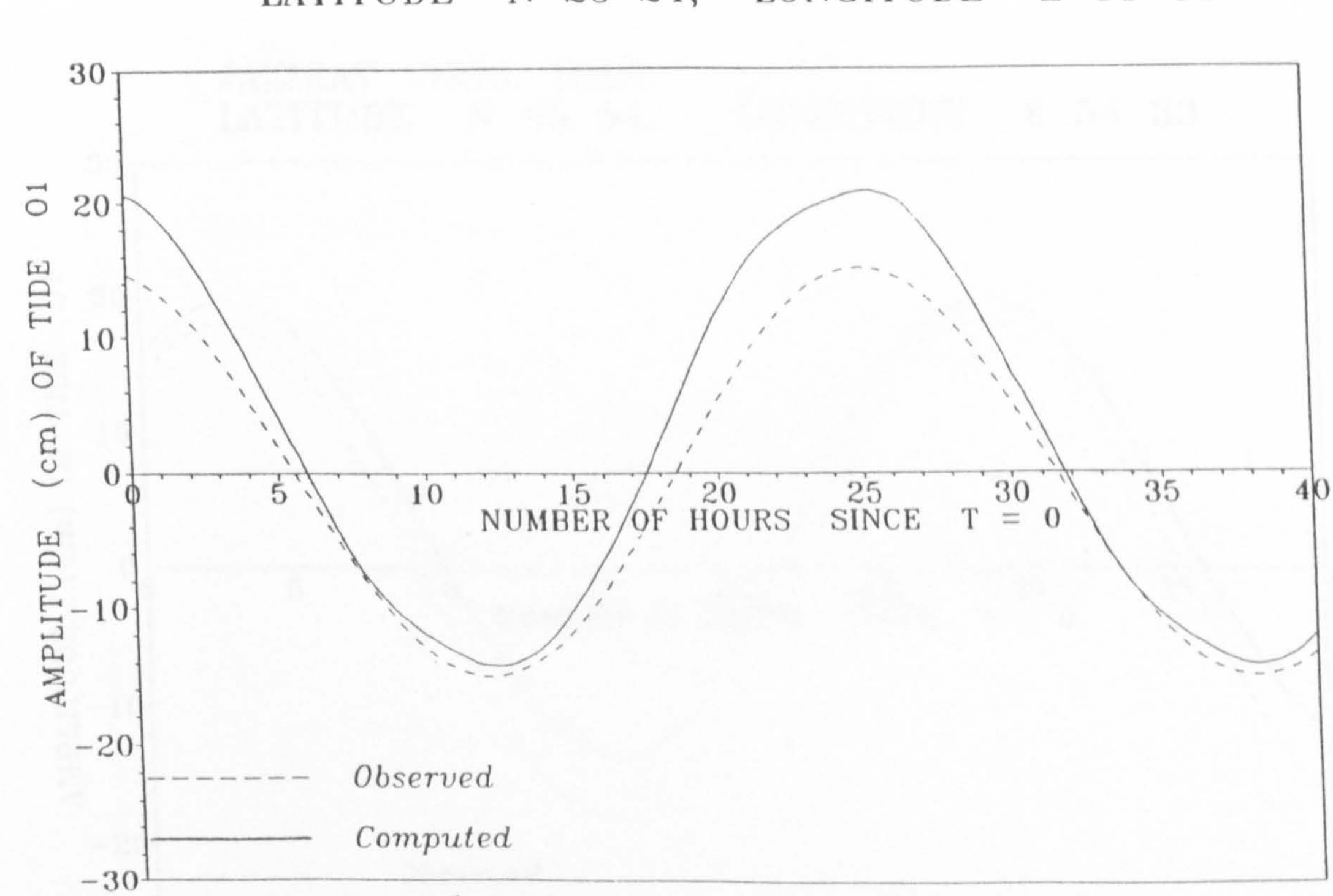

Figure 6.18h Comparison of observed and computed amplitude of tide O_1 at Al Jazirat Al Aliyah, Qatar

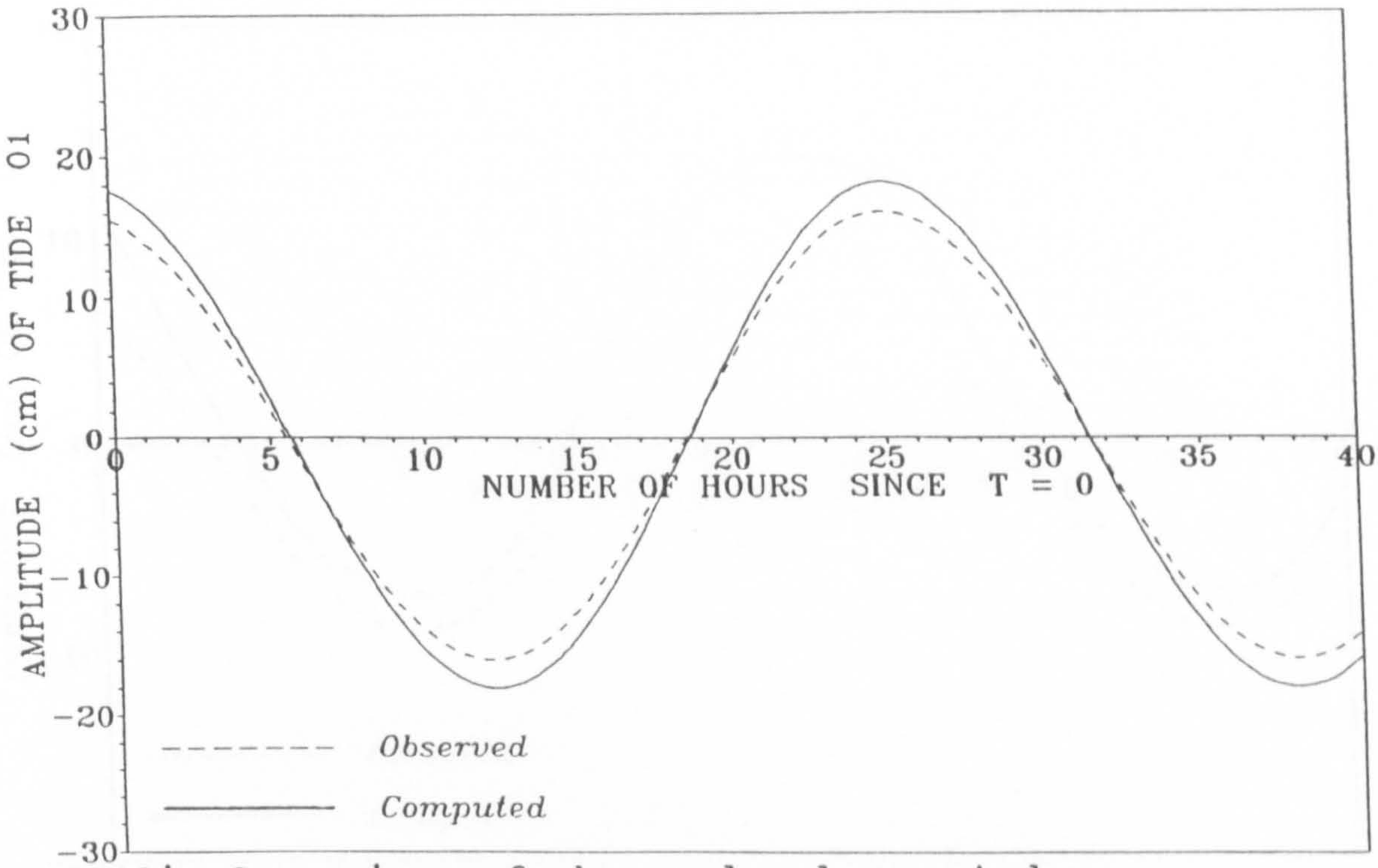

Figure 6.18i Comparison of observed and computed amplitude of tide O_1 at Khawr Al Quway, Strait of Harmouz, Oman

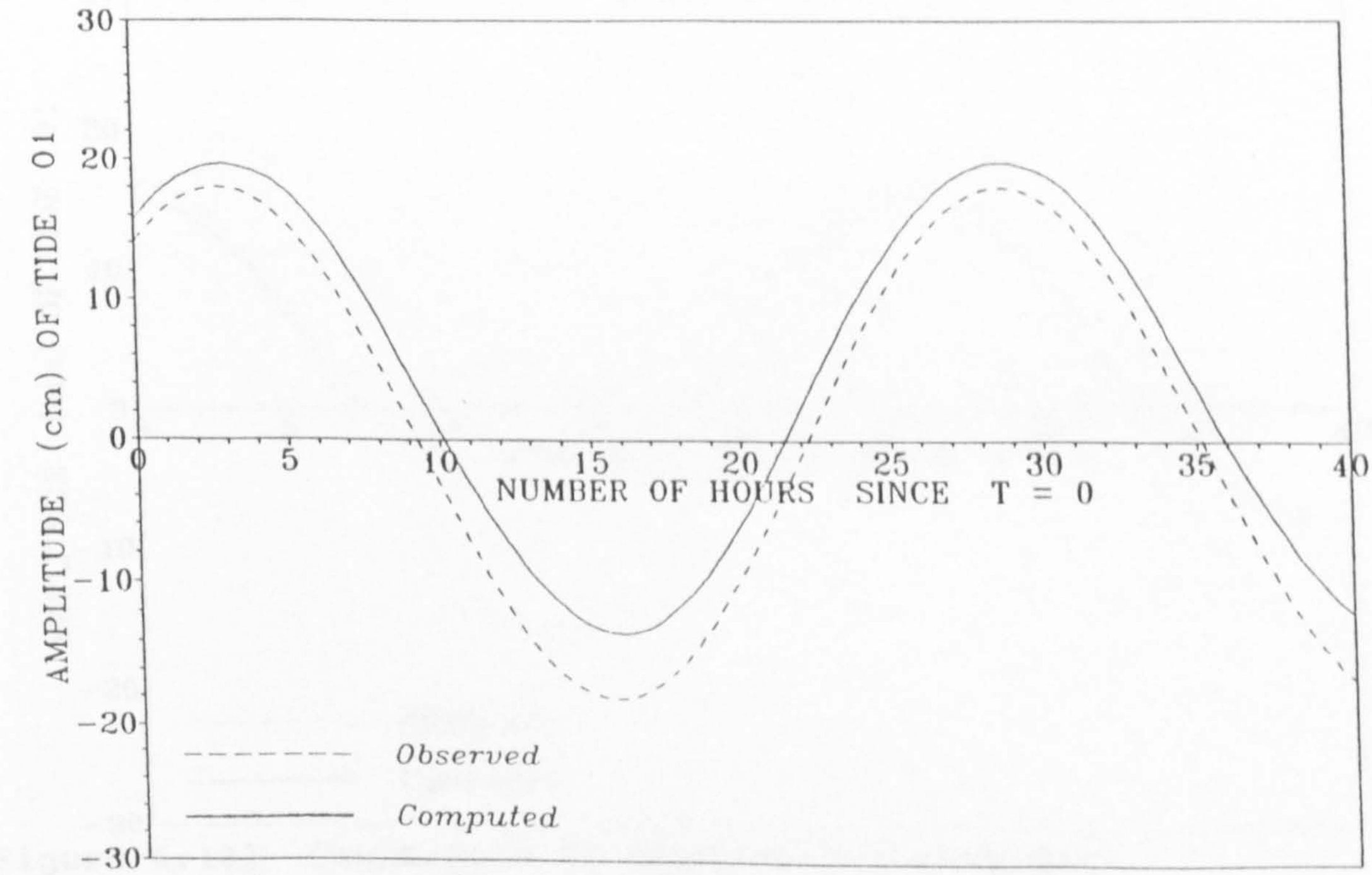

Figure 6.18j Comparison of observed and computed amplitude of tide O_1 at Jazirat Sirri, Iran

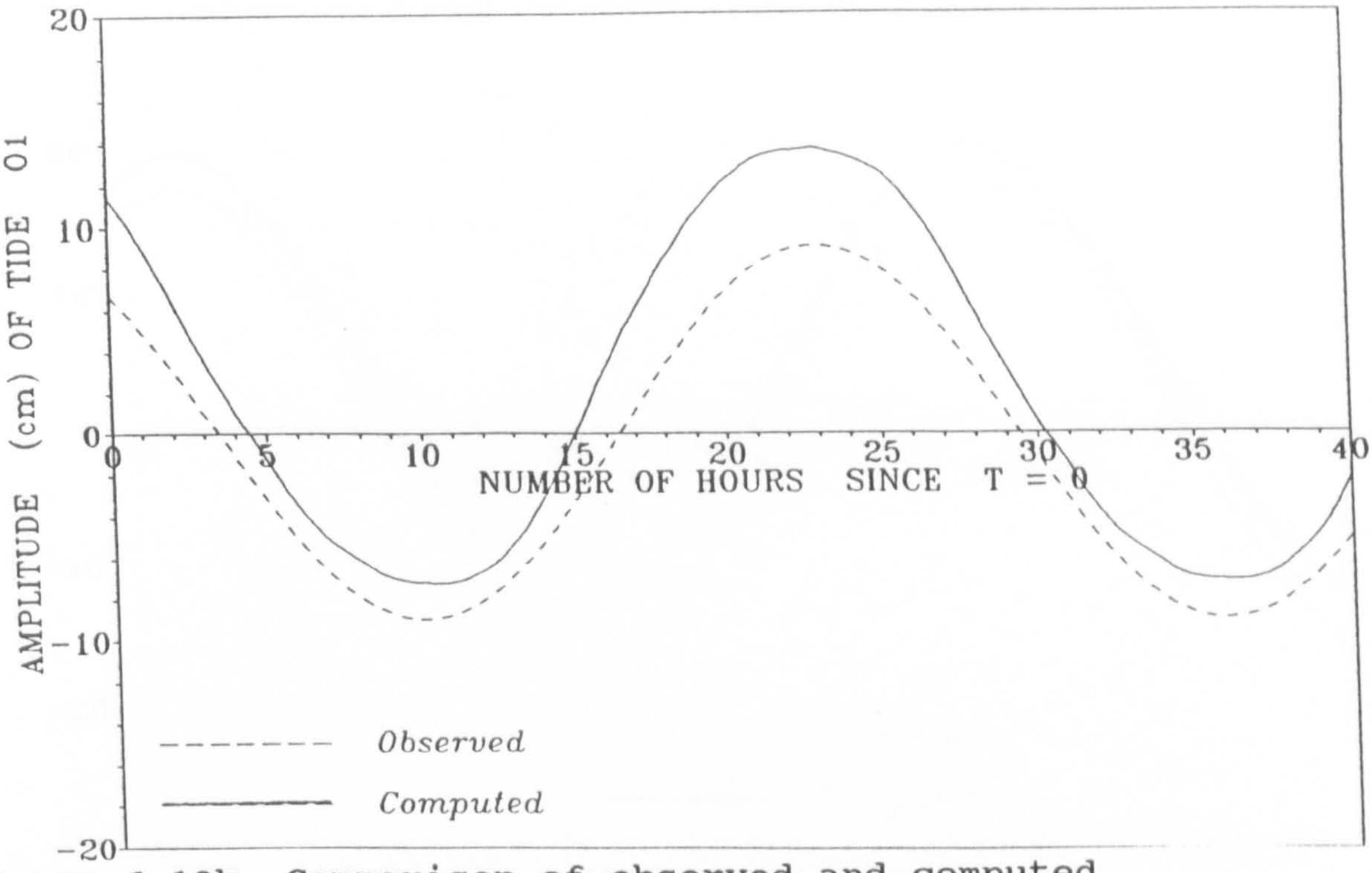

Figure 6.18k Comparison of observed and computed amplitude of tide O_1 at Jabal Al Fuwayrif, Qatar

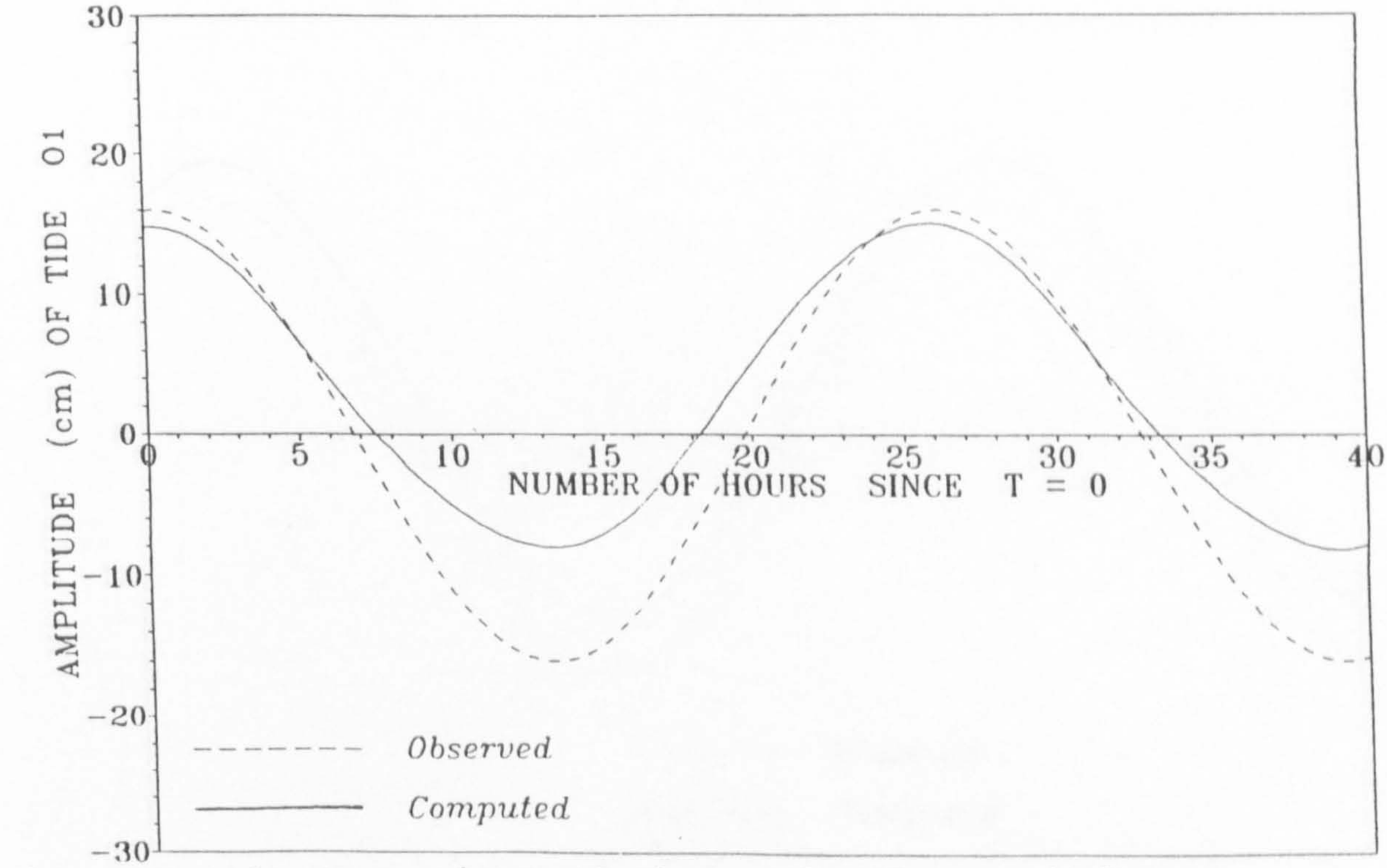

Figure 6.18l Comparison of observed and computed amplitude of tide O_1 at Khawr Khesab, Strait of Harmouz, Oman

JAZIRAT DAS, QATAR.
LATITUDE N 25 10, LONGITUDE E 52 53

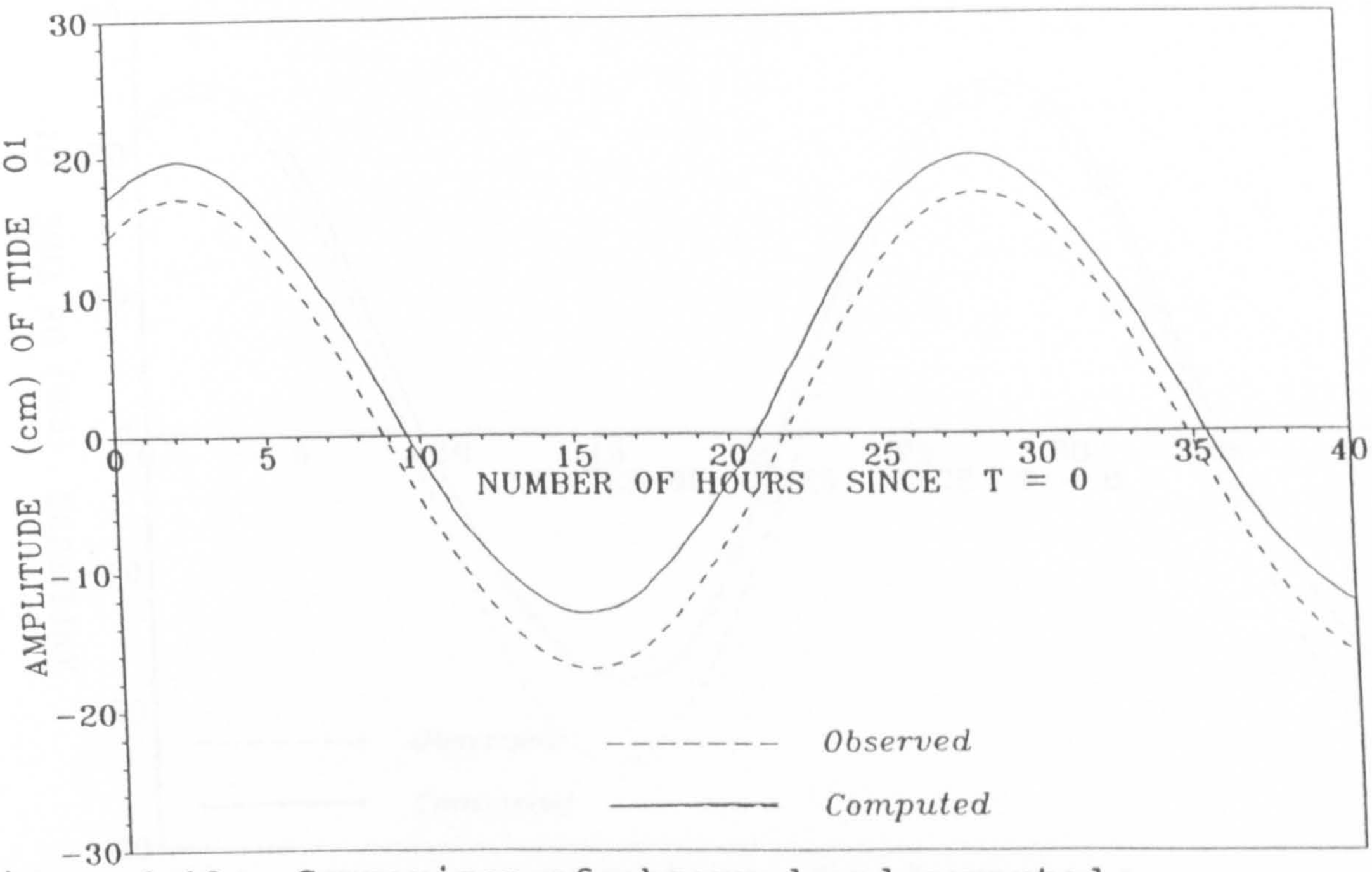

Figure 6.18m Comparison of observed and computed amplitude of tide O_1 at Jazirat Das, Qatar

ZIRKU TERMINAL, UAE.
LATITUDE N 25 02, LONGITUDE E 53 01

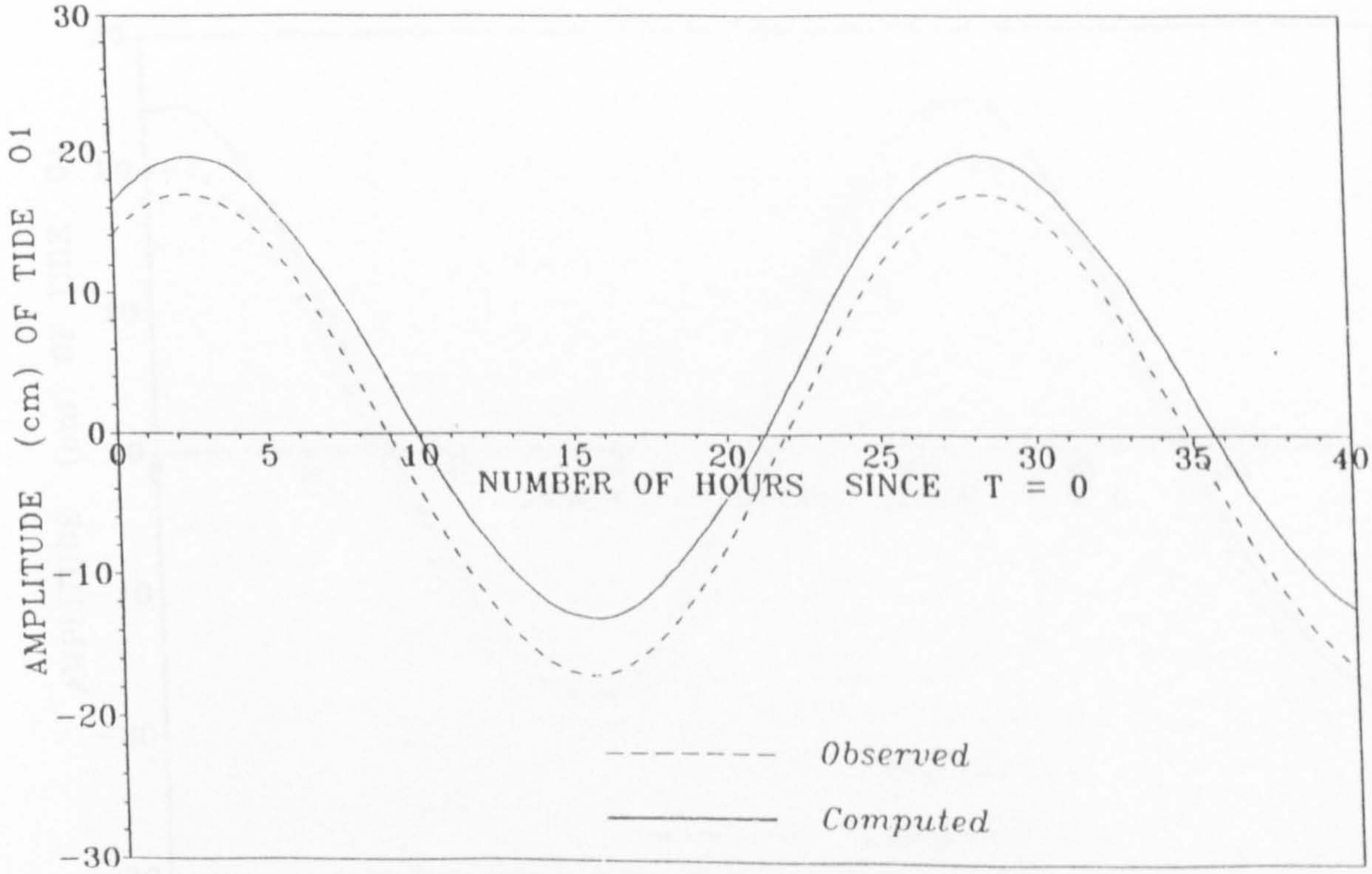

Figure 6.18n Comparison of observed and computed amplitude of tide O_1 at Zirku Terminal, UAE

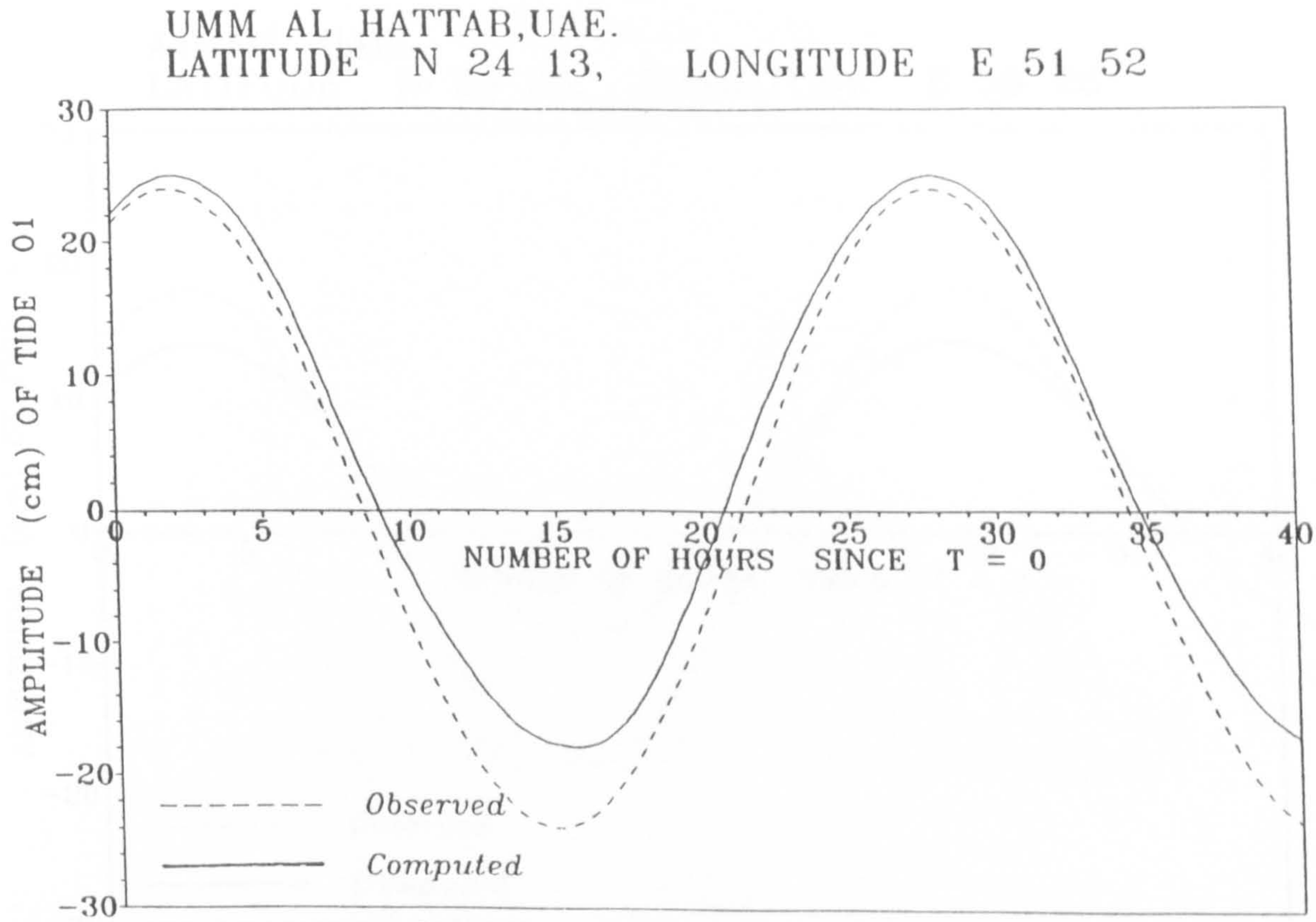

Figure 6.18o Comparison of observed and computed amplitude of tide O_1 at Umm Al Hatab, UAE

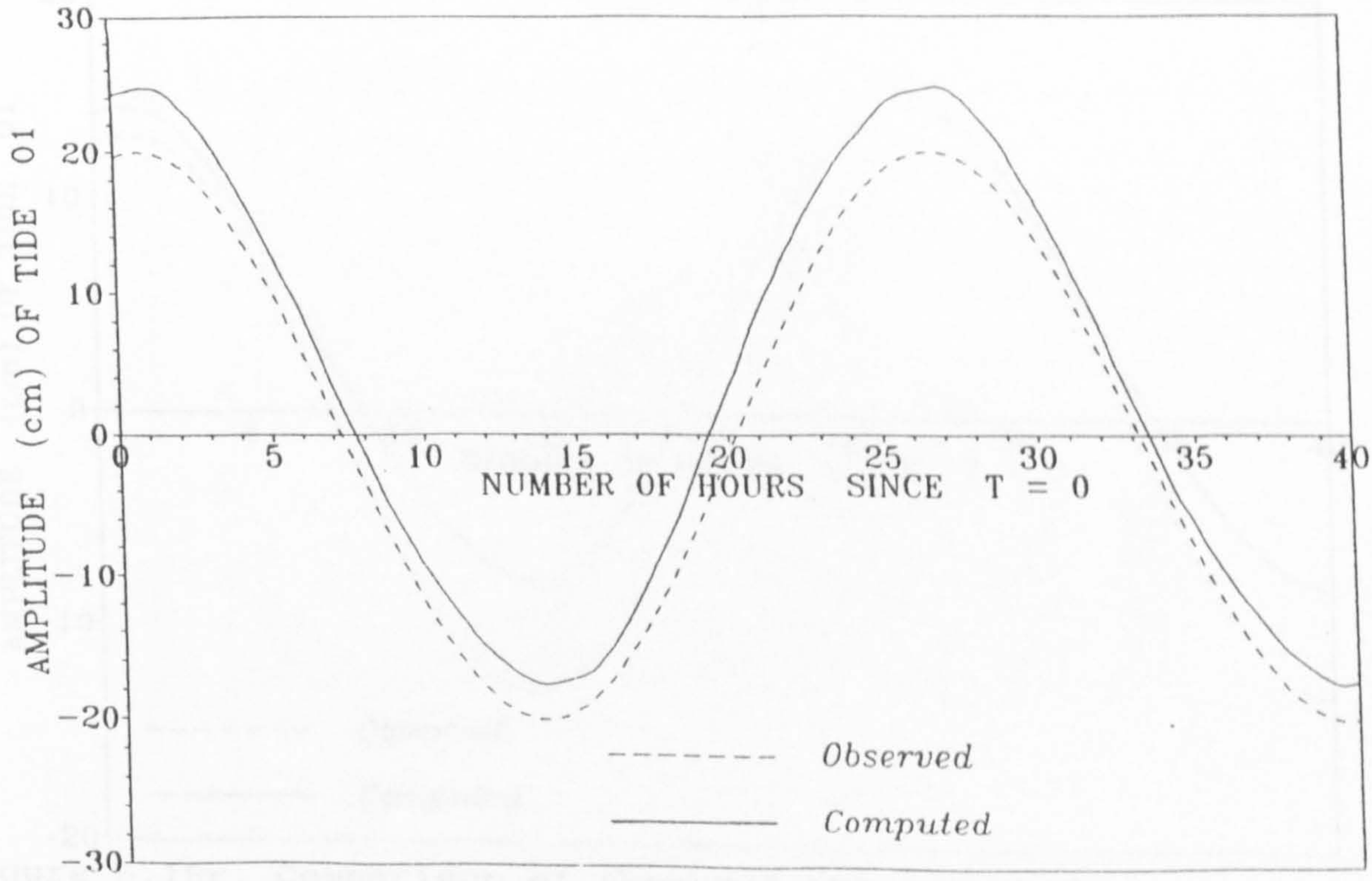

Figure 6.18p Comparison of observed and computed amplitude of tide O_1 at Musay'Id Harbour, Qatar

AJMAN, UAE.
LATITUDE N 25 25, LONGITUDE E 55 26

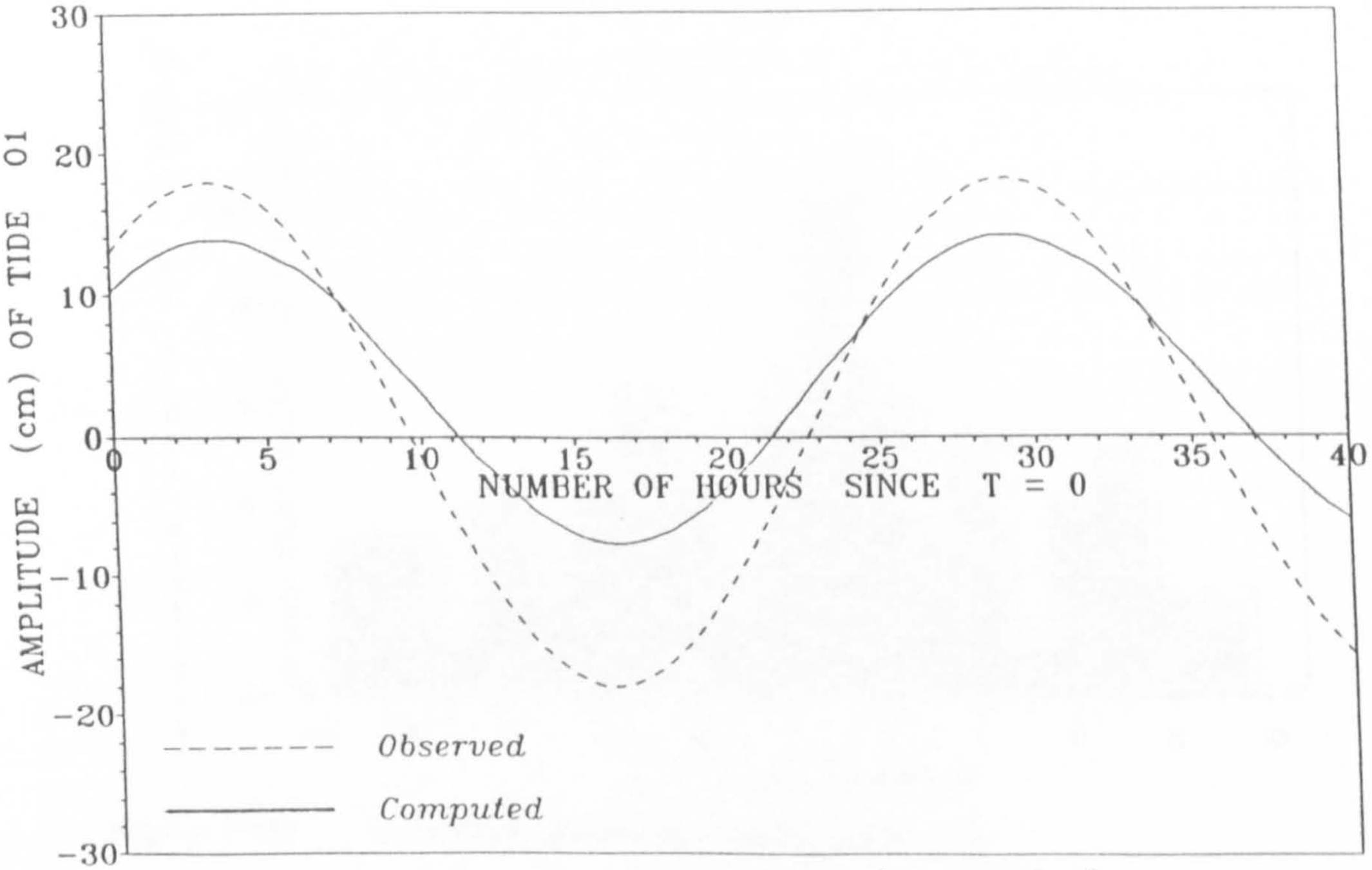

Figure 6.18q Comparison of observed and computed amplitude of tide O_1 at Ajman, UAE

BUKHA, STRAIT OF HARMOUZ OMAN.
LATITUDE N 26 03, LONGITUDE E 56 08

Figure 6.18r Comparison of observed and computed amplitude of tide O_1 at Bukha, Strait of Harmouz, Oman

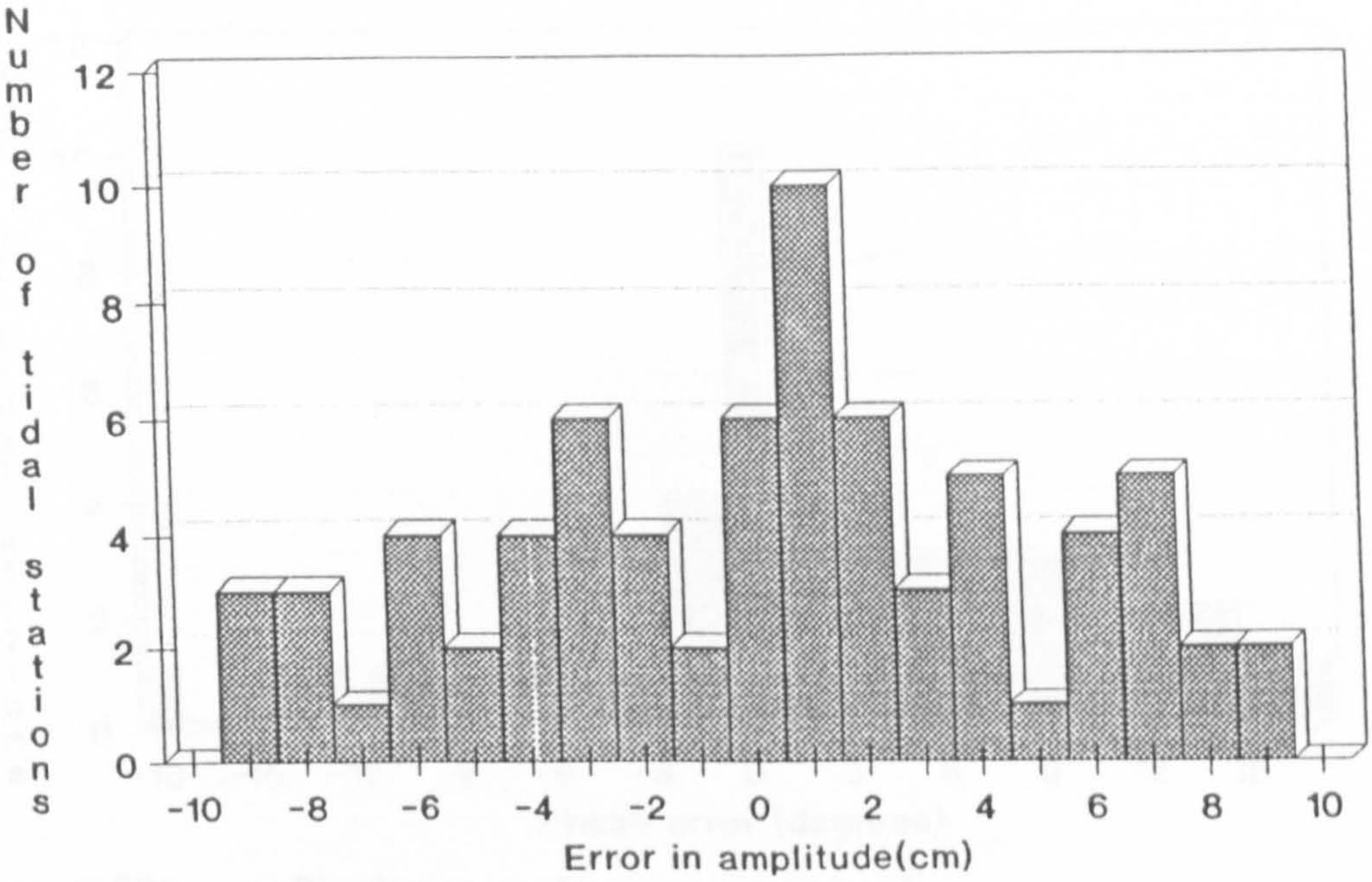

Figure 6.19a Distribution of errors in Amplitude of tide M_2

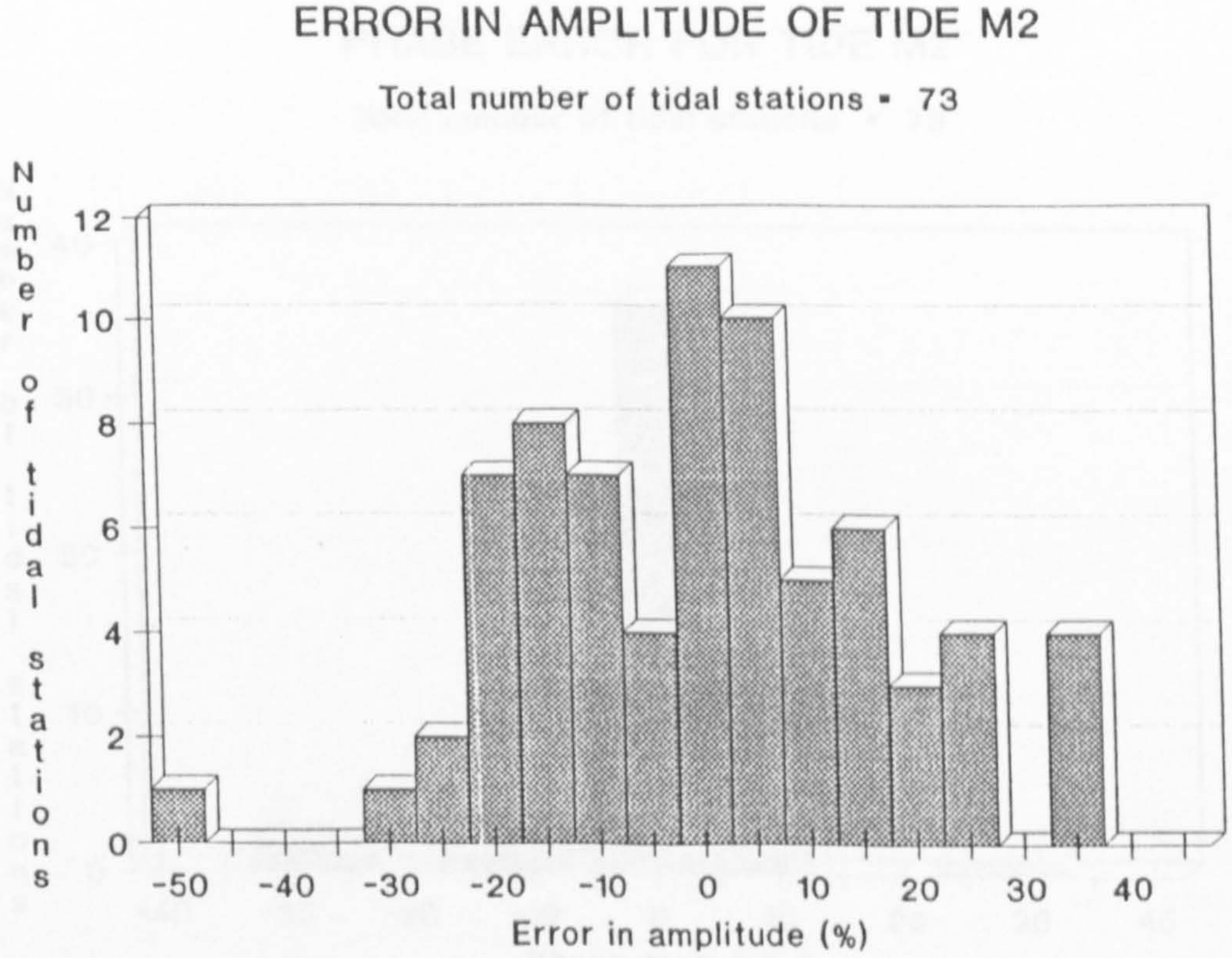

Figure 6.19b Distribution of % errors in Amplitude of tide M_2

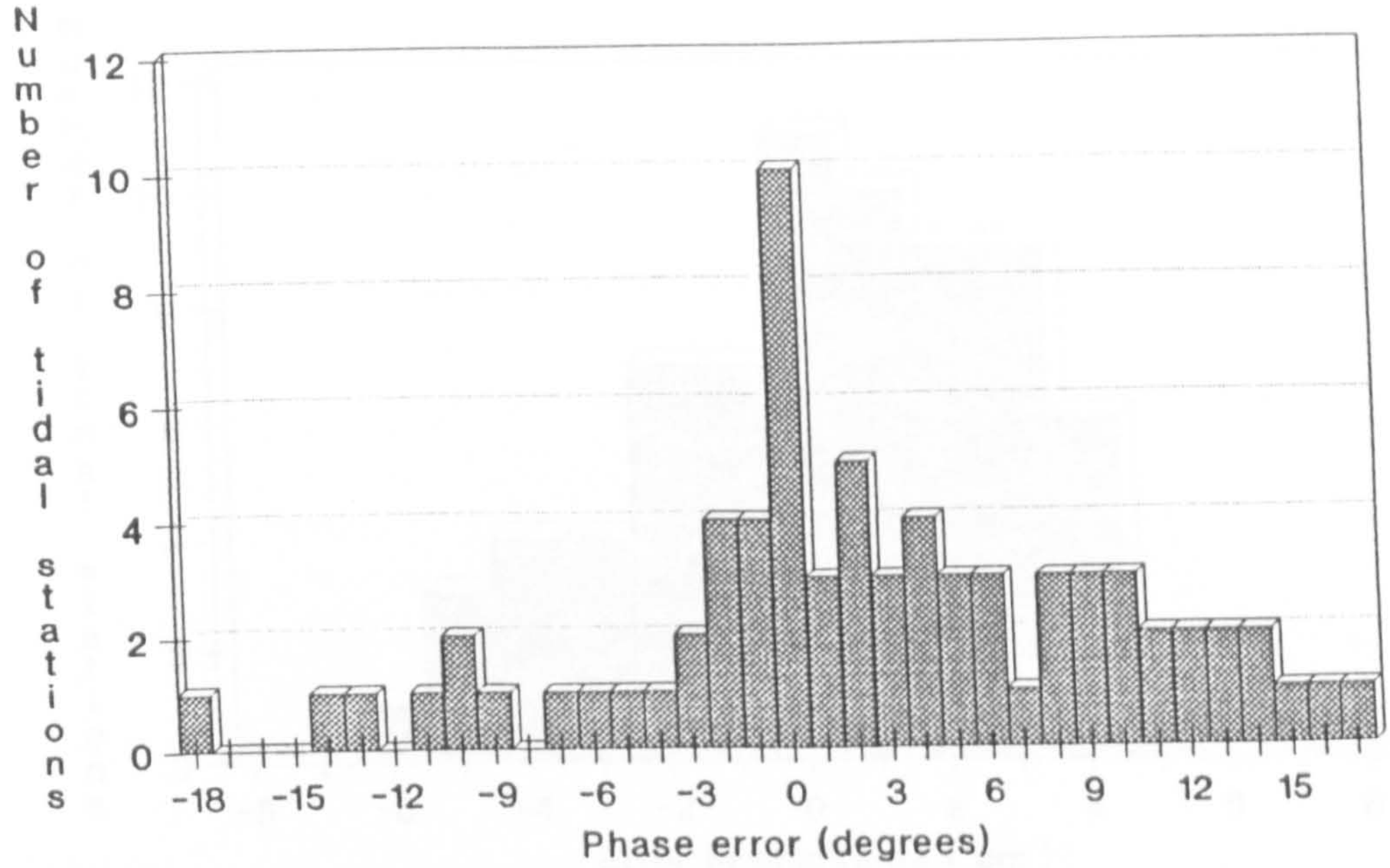

Figure 6.20a Distribution of phase errors for tide M_2

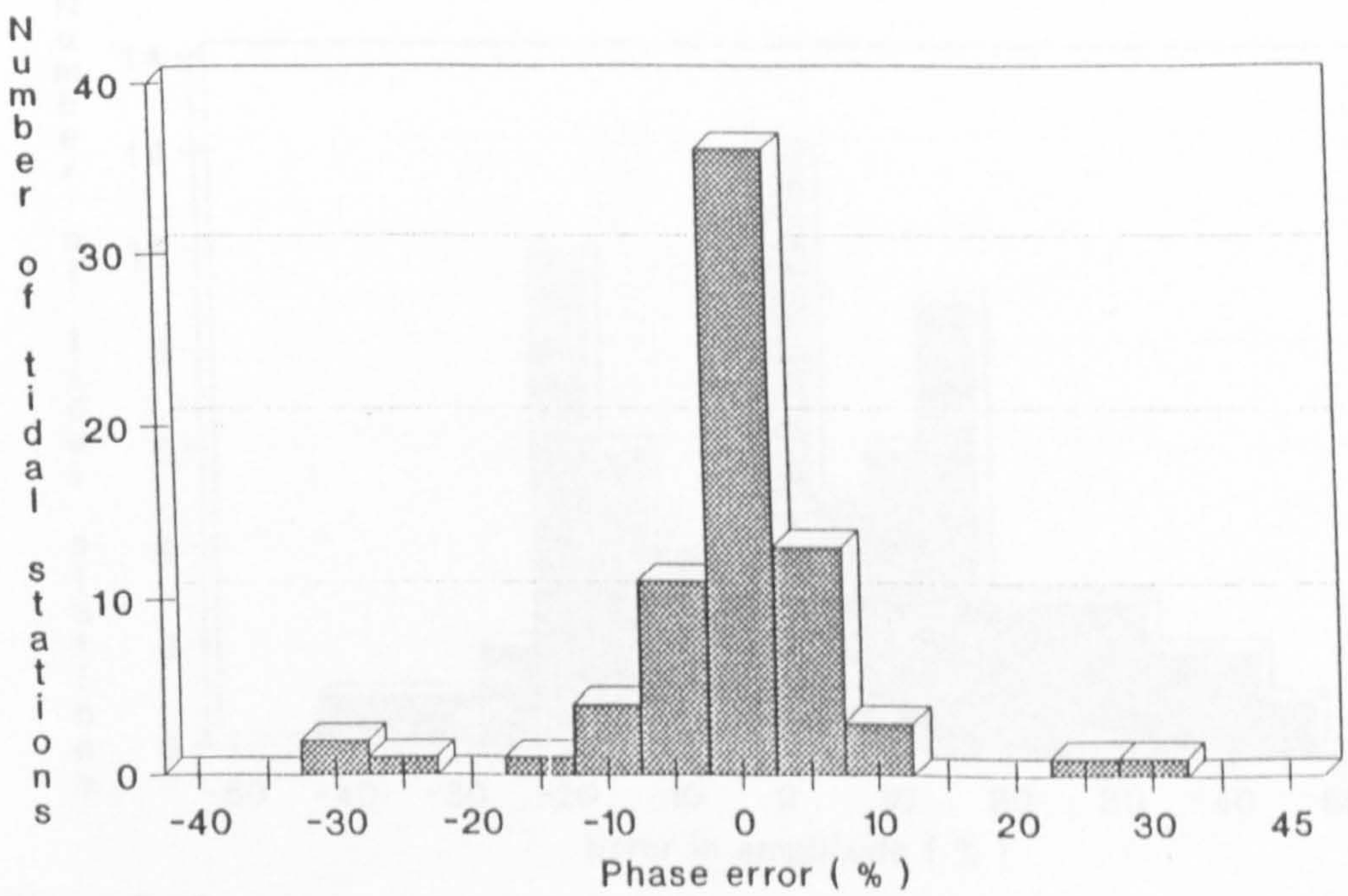

Figure 6.20b Distribution of % phase errors for tide M_2

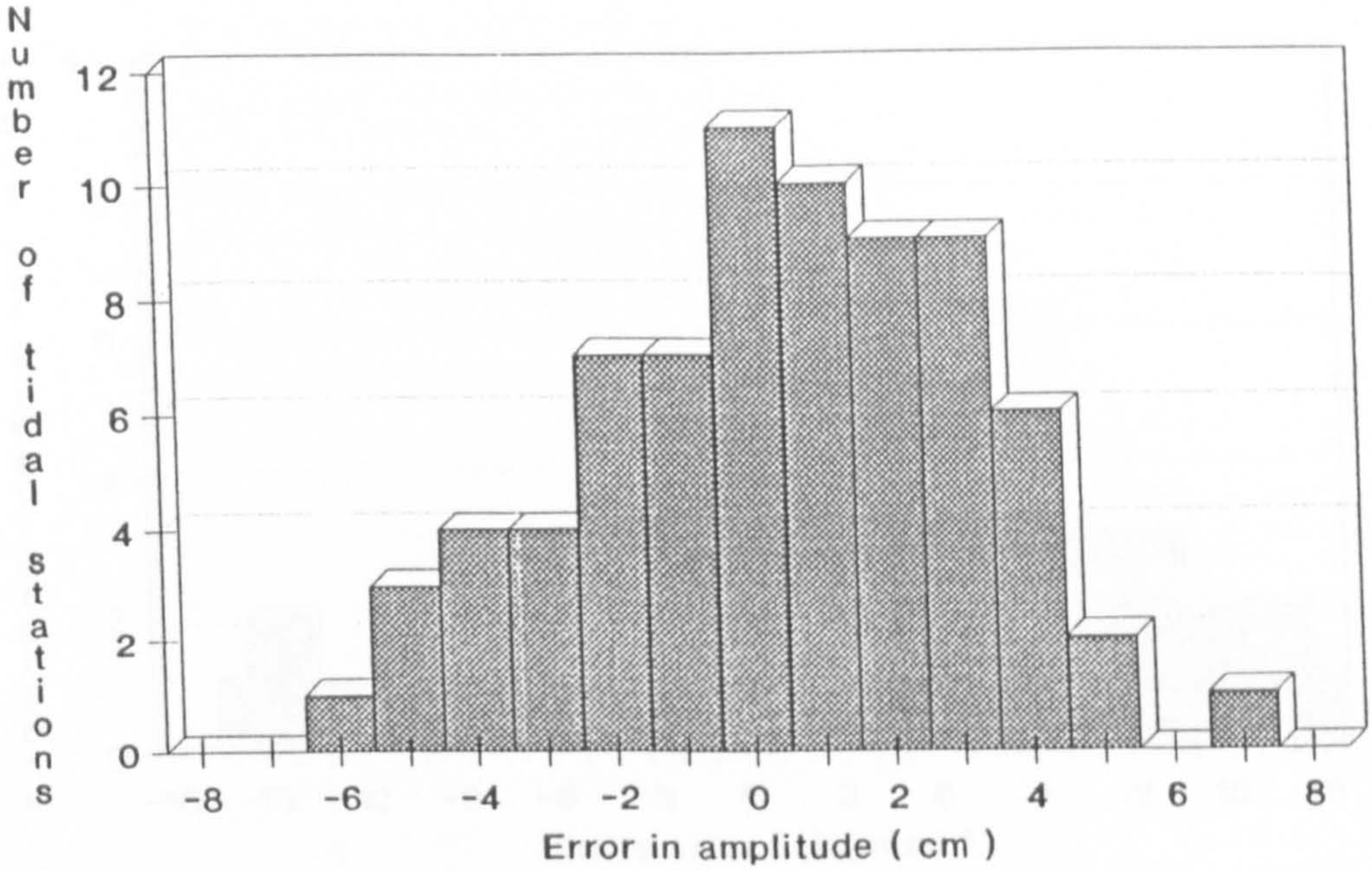

Figure 6.21a Distribution of errors in Amplitude of tide S_2

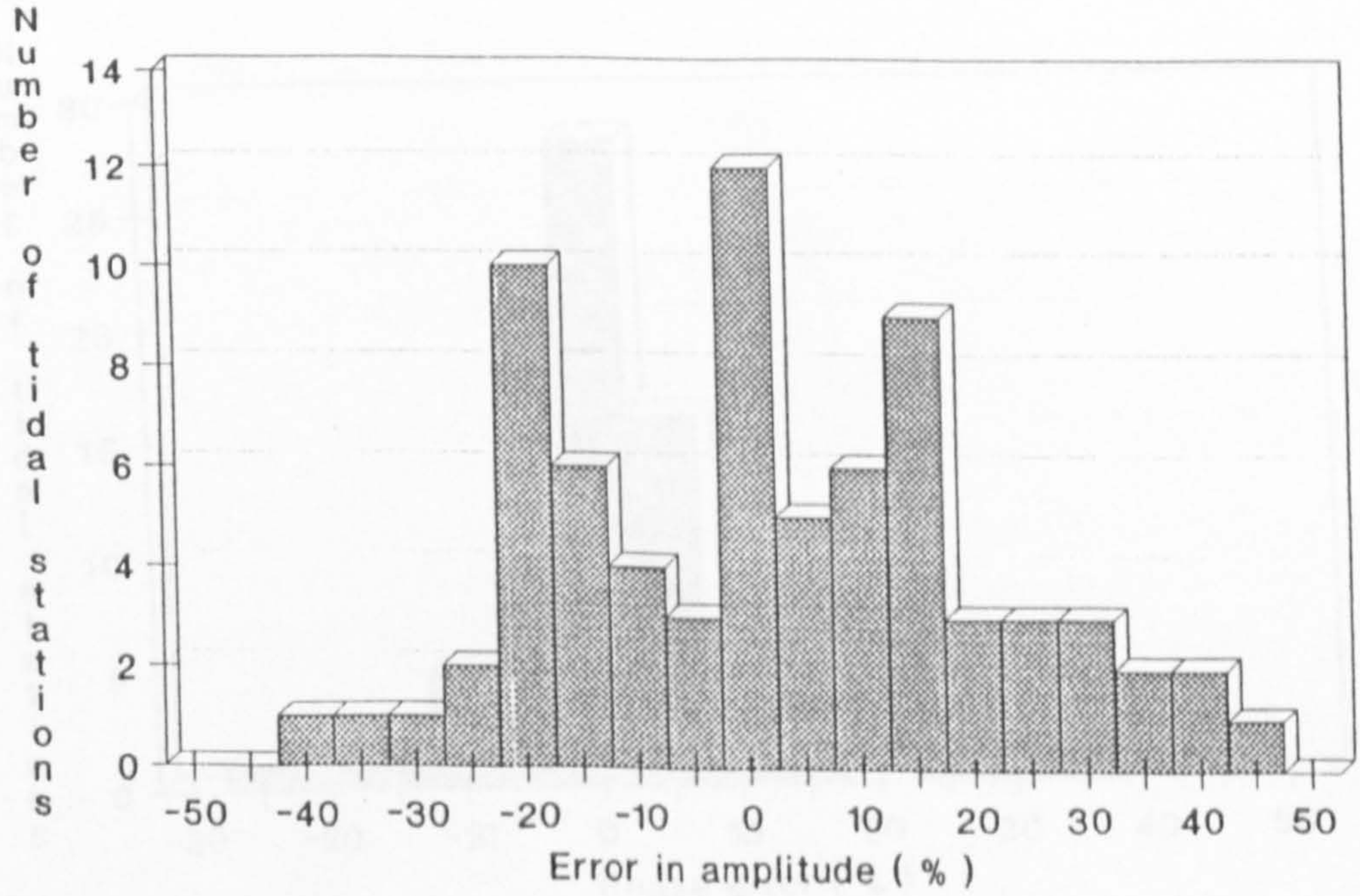

Figure 6.21b Distribution of % errors in Amplitude of tide S_2

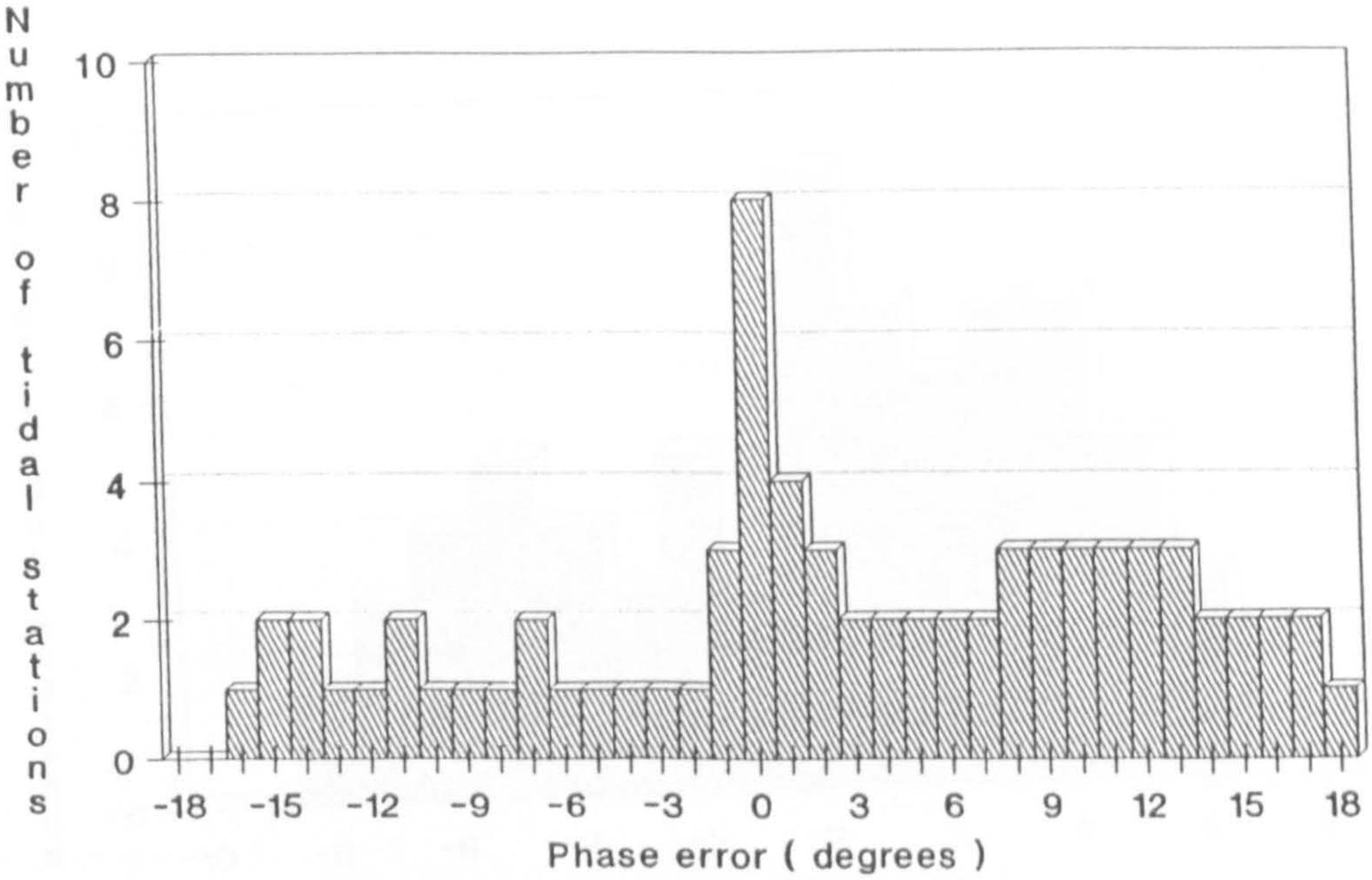

Figure 6.22a Distribution of phase errors for tide S_2

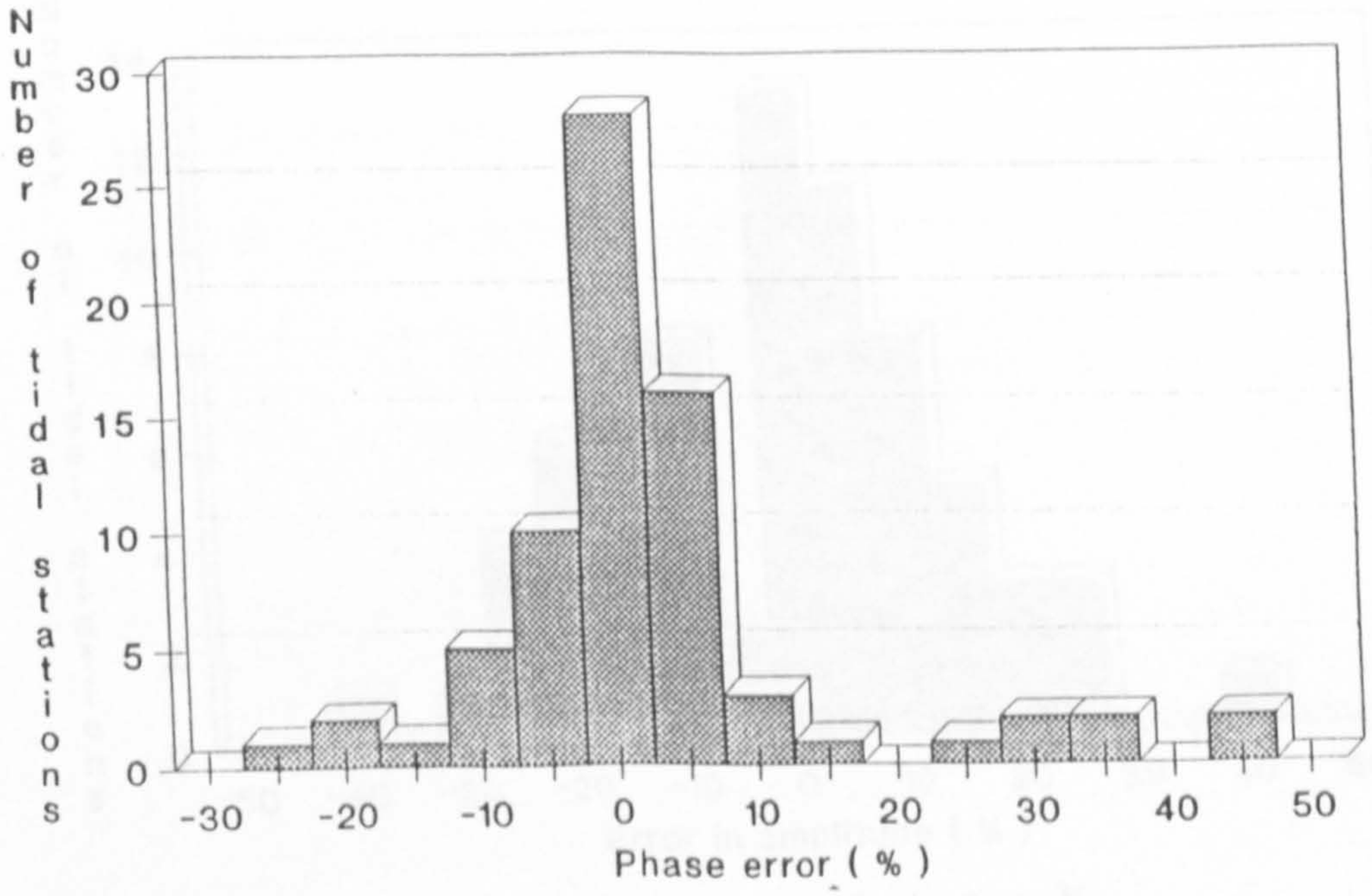

Figure 6.22b Distribution of % phase errors for tide S_2

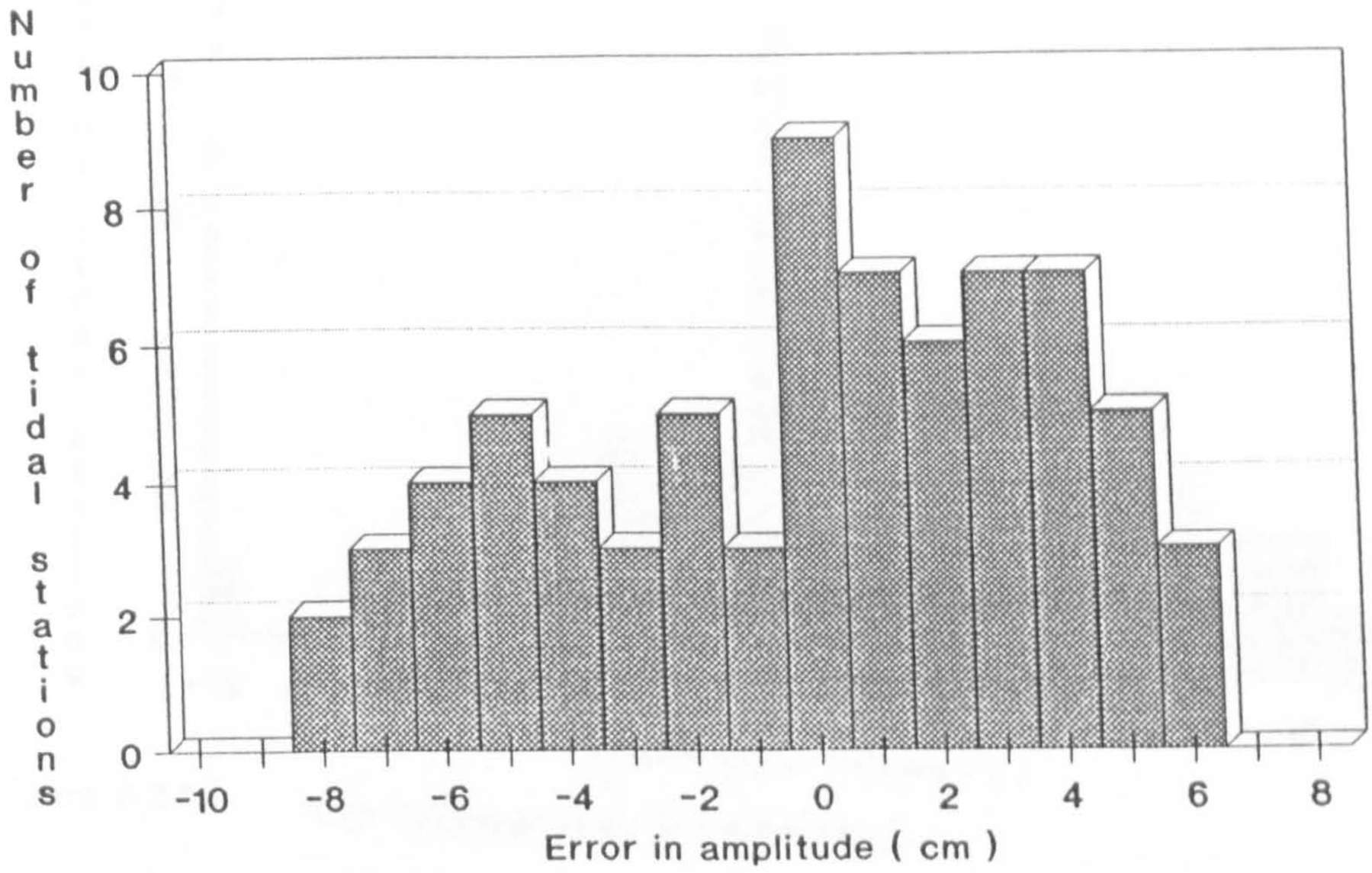

Figure 6.23a Distribution of errors in Amplitude of tide K_1

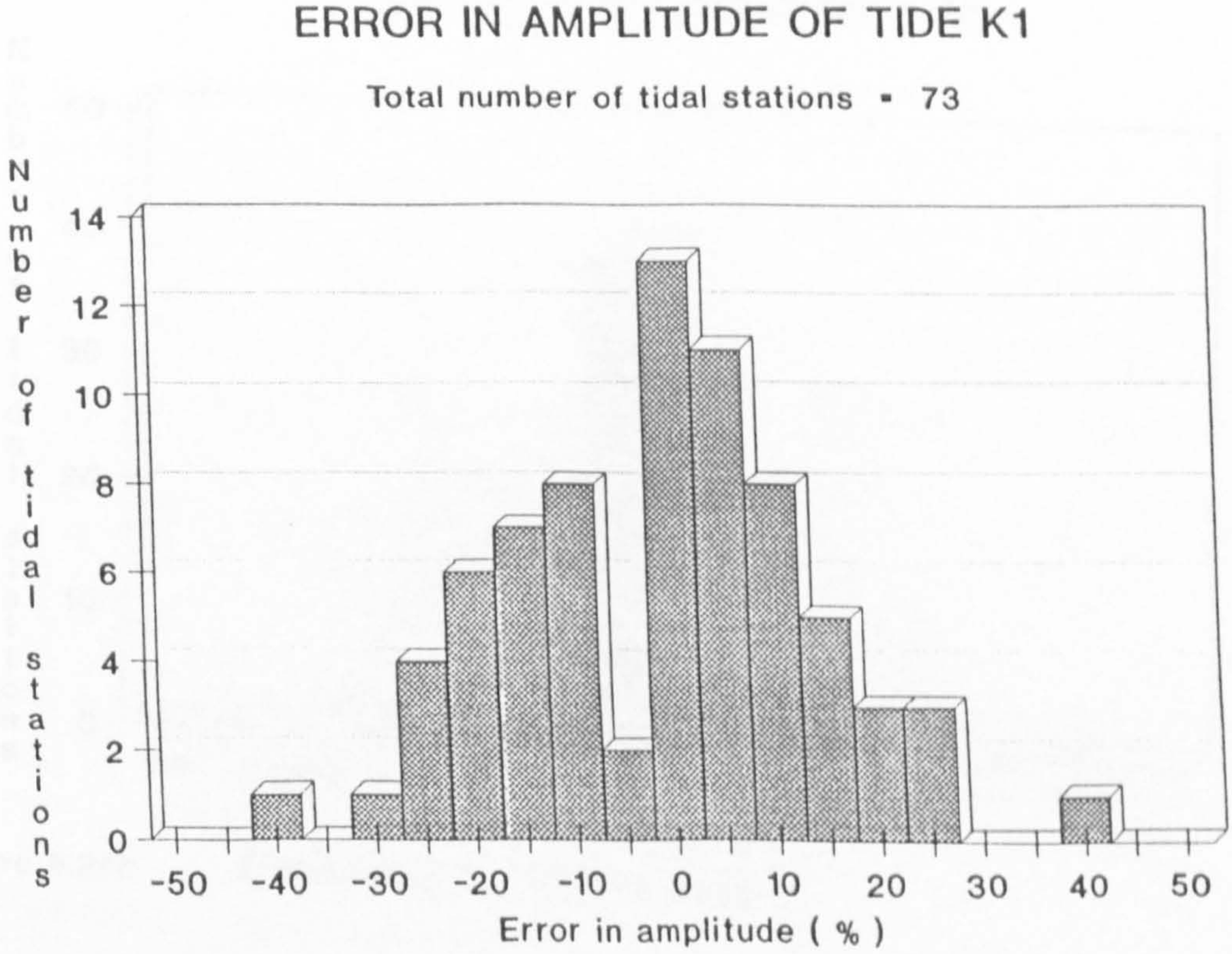

Figure 6.23b Distribution of % errors in Amplitude of tide K_1

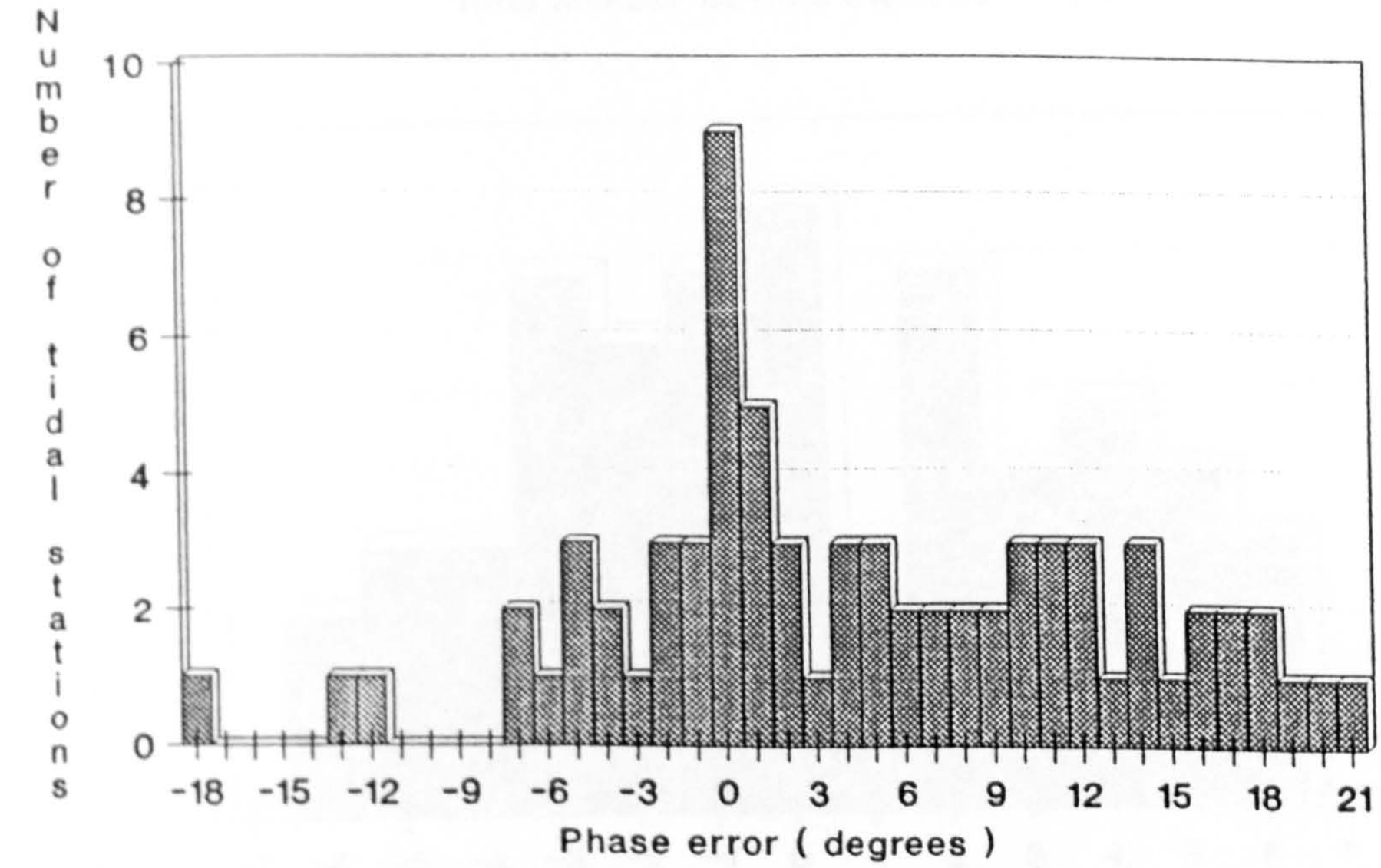

Figure 6.24a Distribution of phase errors for tide K_1

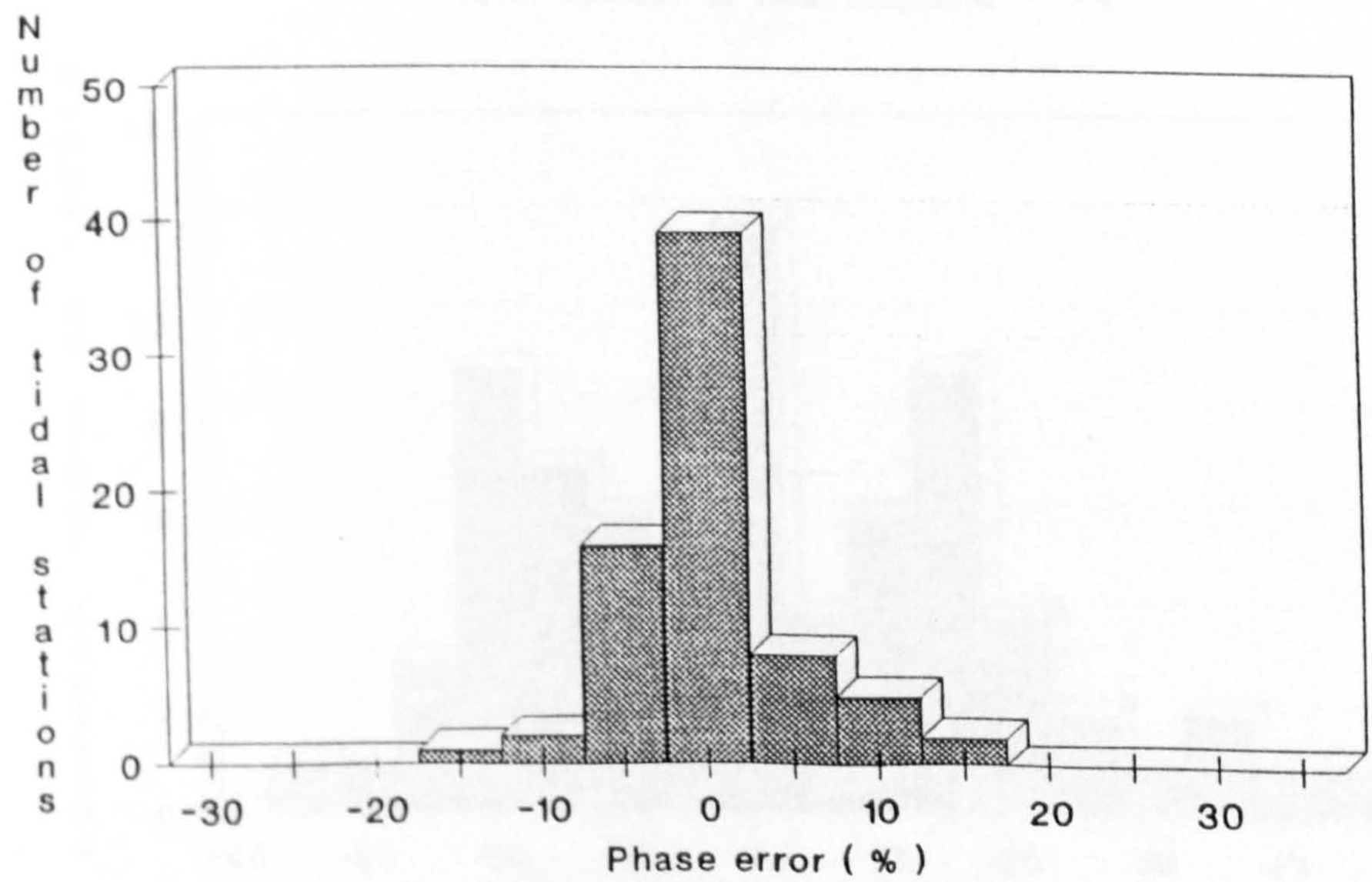

Figure 6.24b Distribution of % phase errors for tide K_1

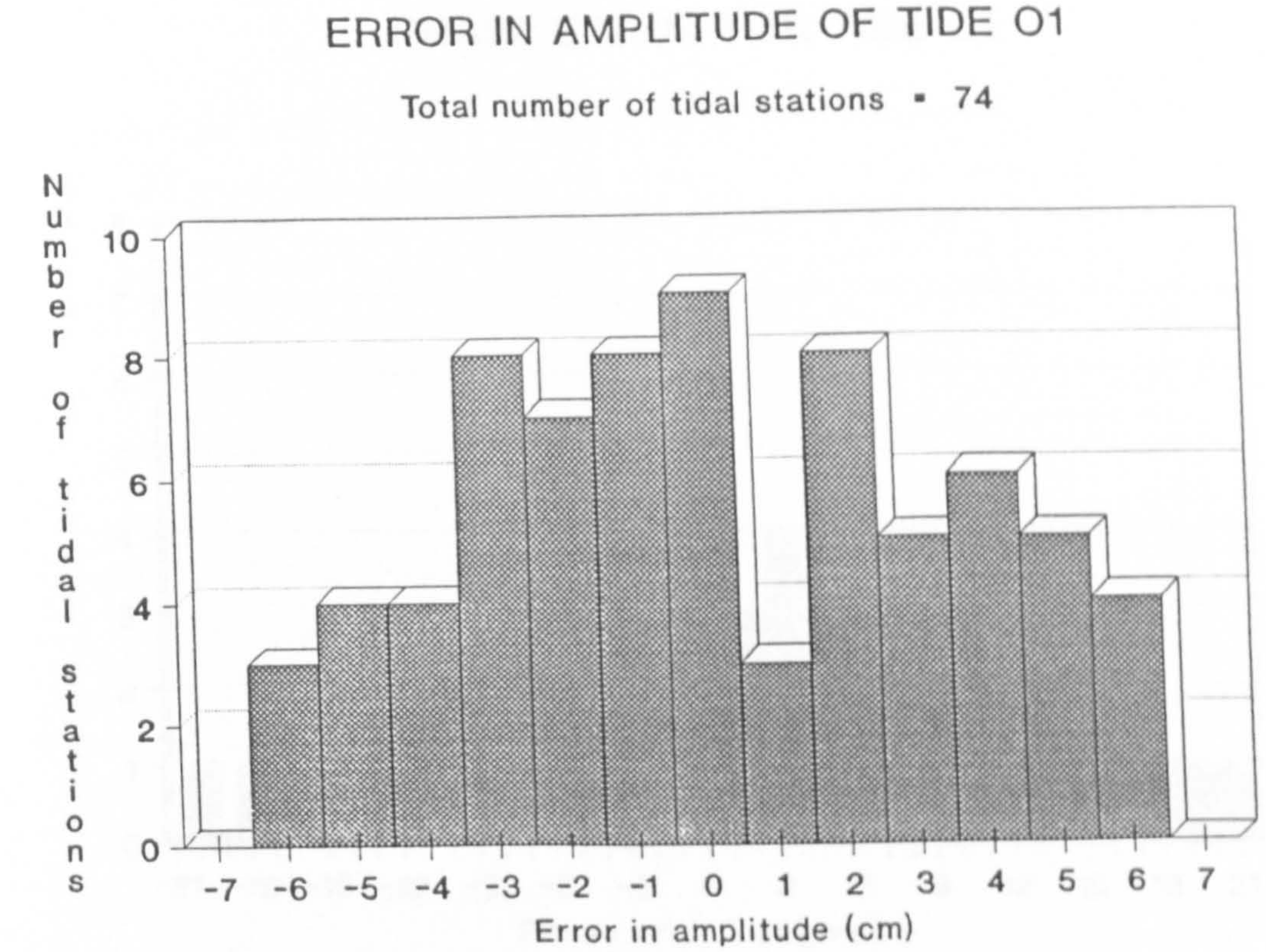

Figure 6.25a Distribution of errors in Amplitude of tide O_1

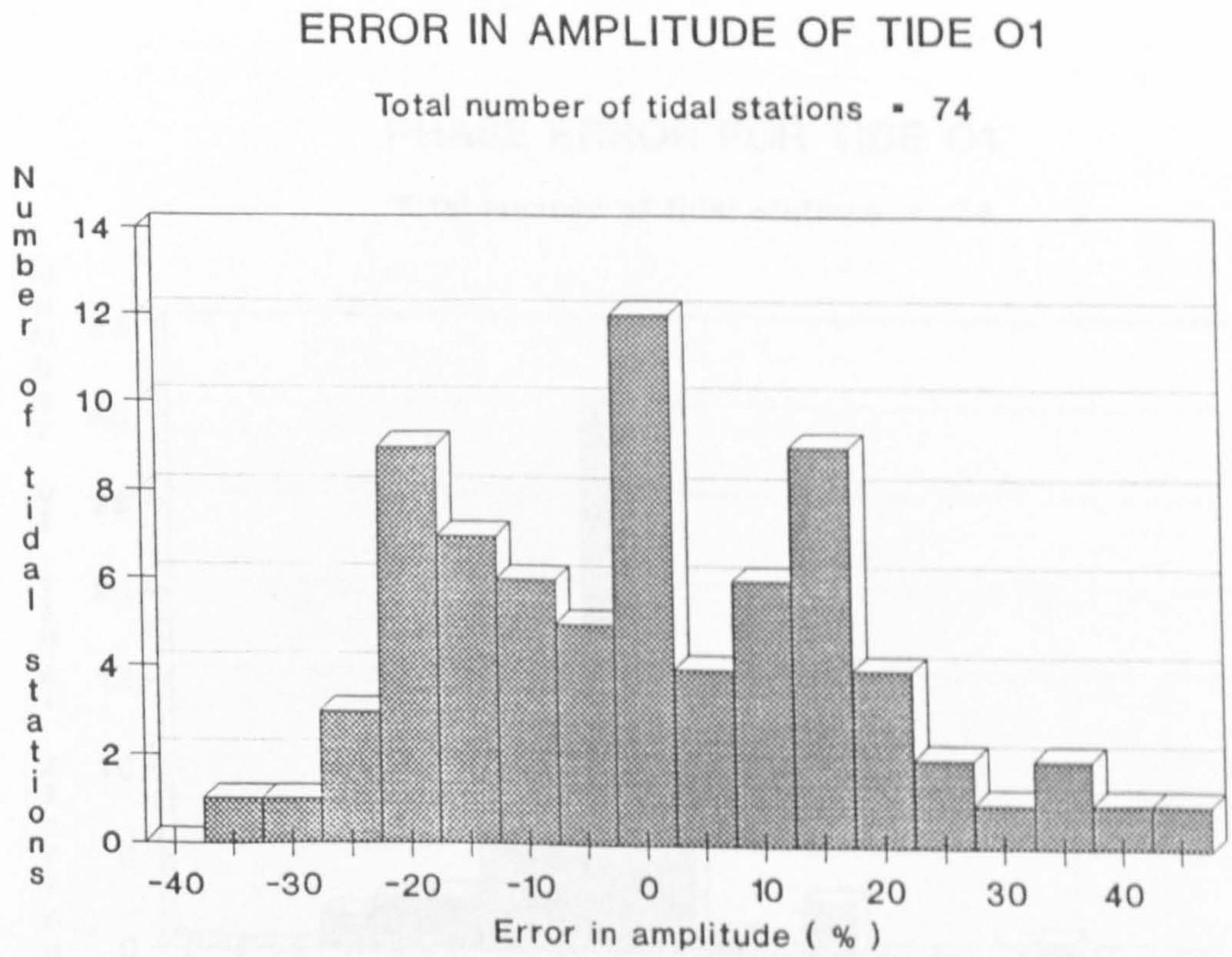

Figure 6.25b Distribution of % errors in Amplitude of tide O_1

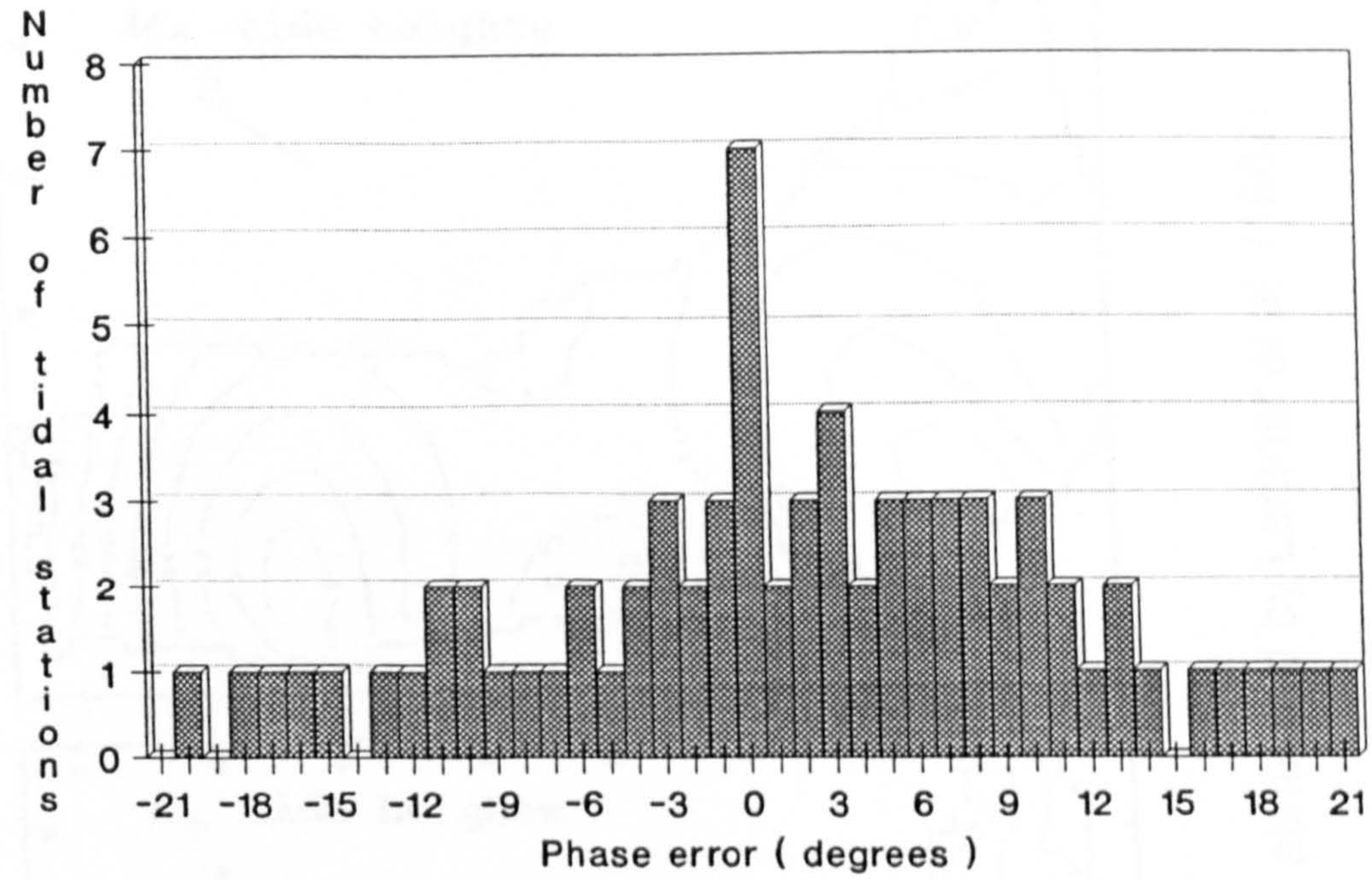

Figure 6.26a Distribution of phase errors for tide O_1

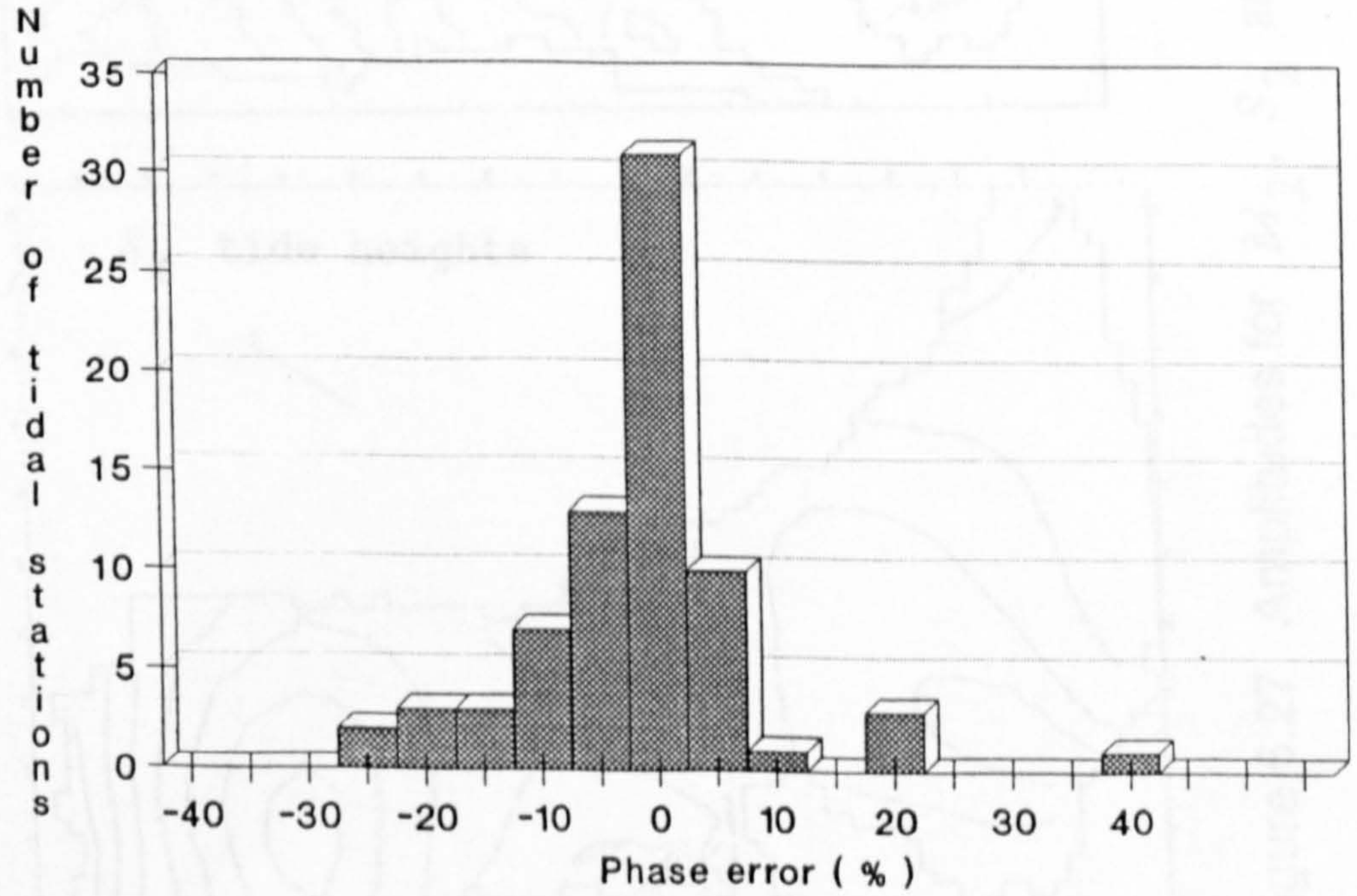

Figure 6.26b Distribution of % phase errors for tide O_1

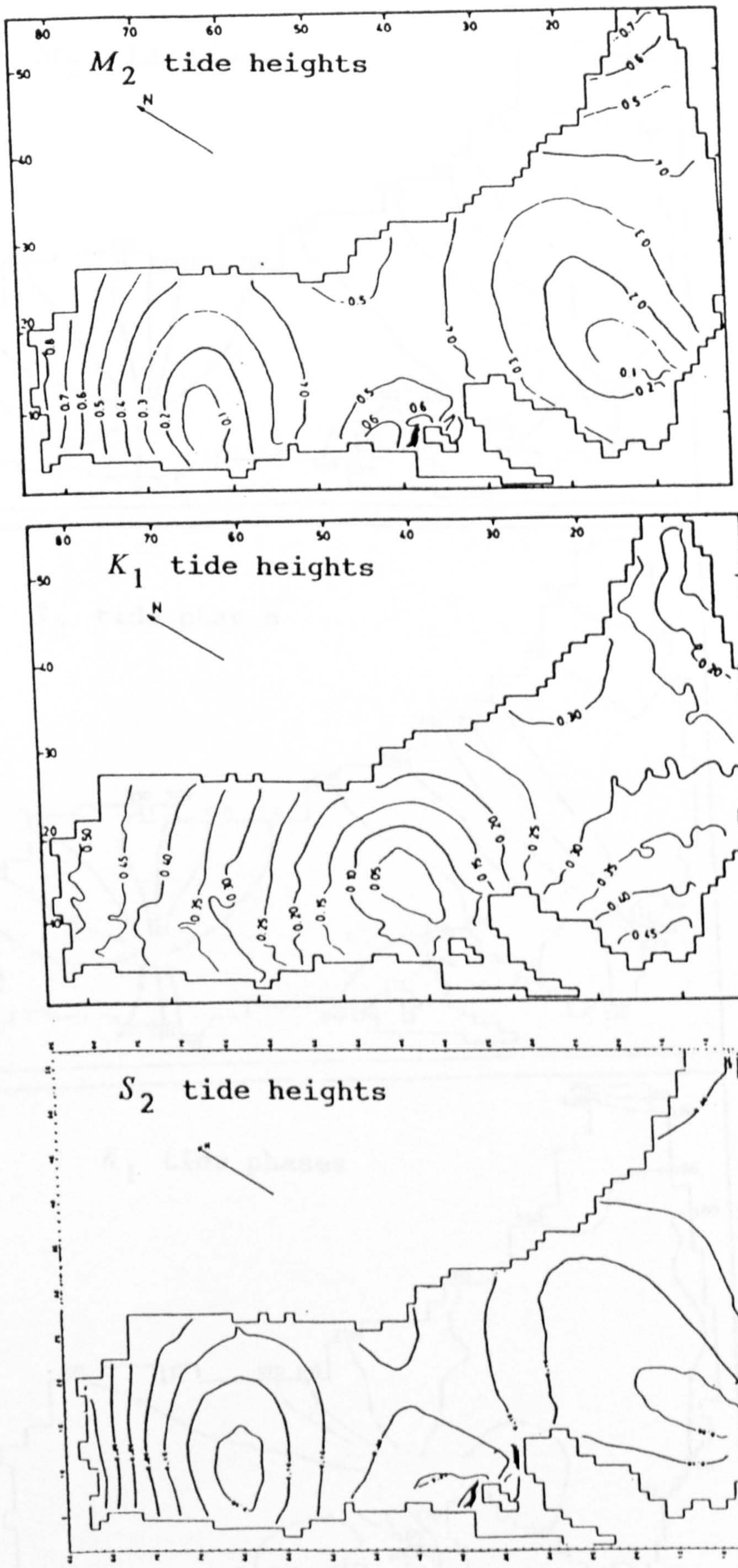

Figure 6.27 Amplitudes for M_2, S_2 and K_1 in metres simulated by Lardner et al (1982).

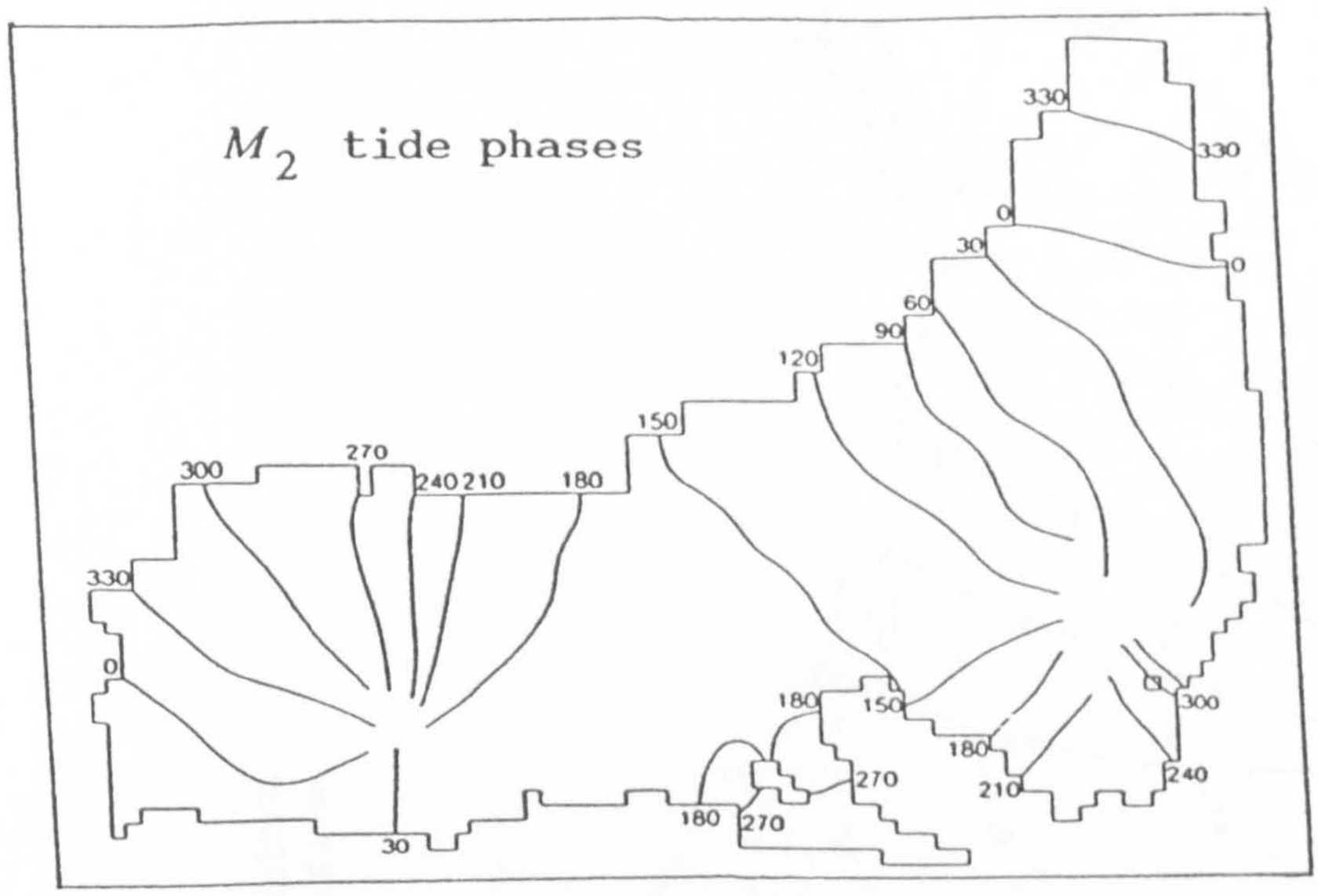

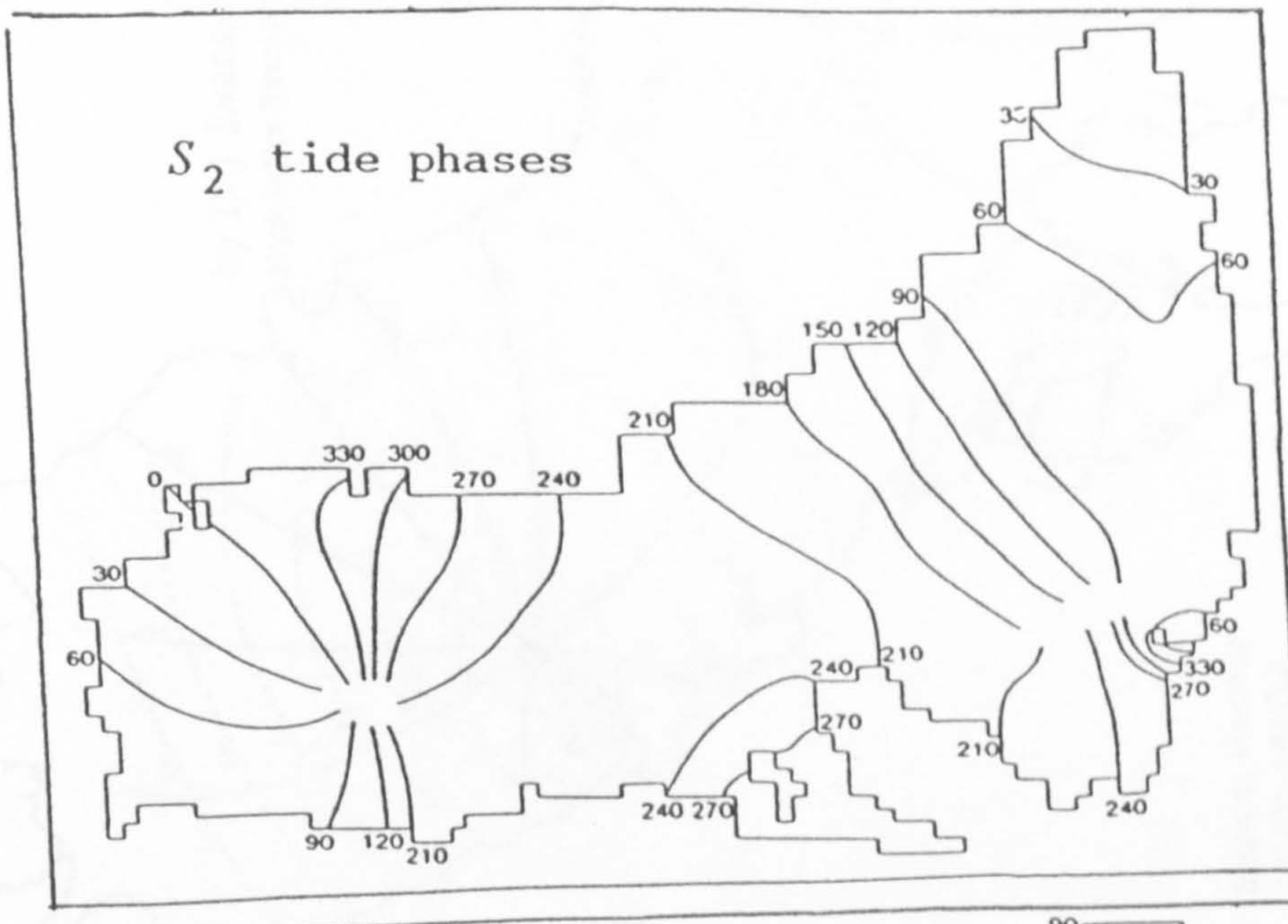

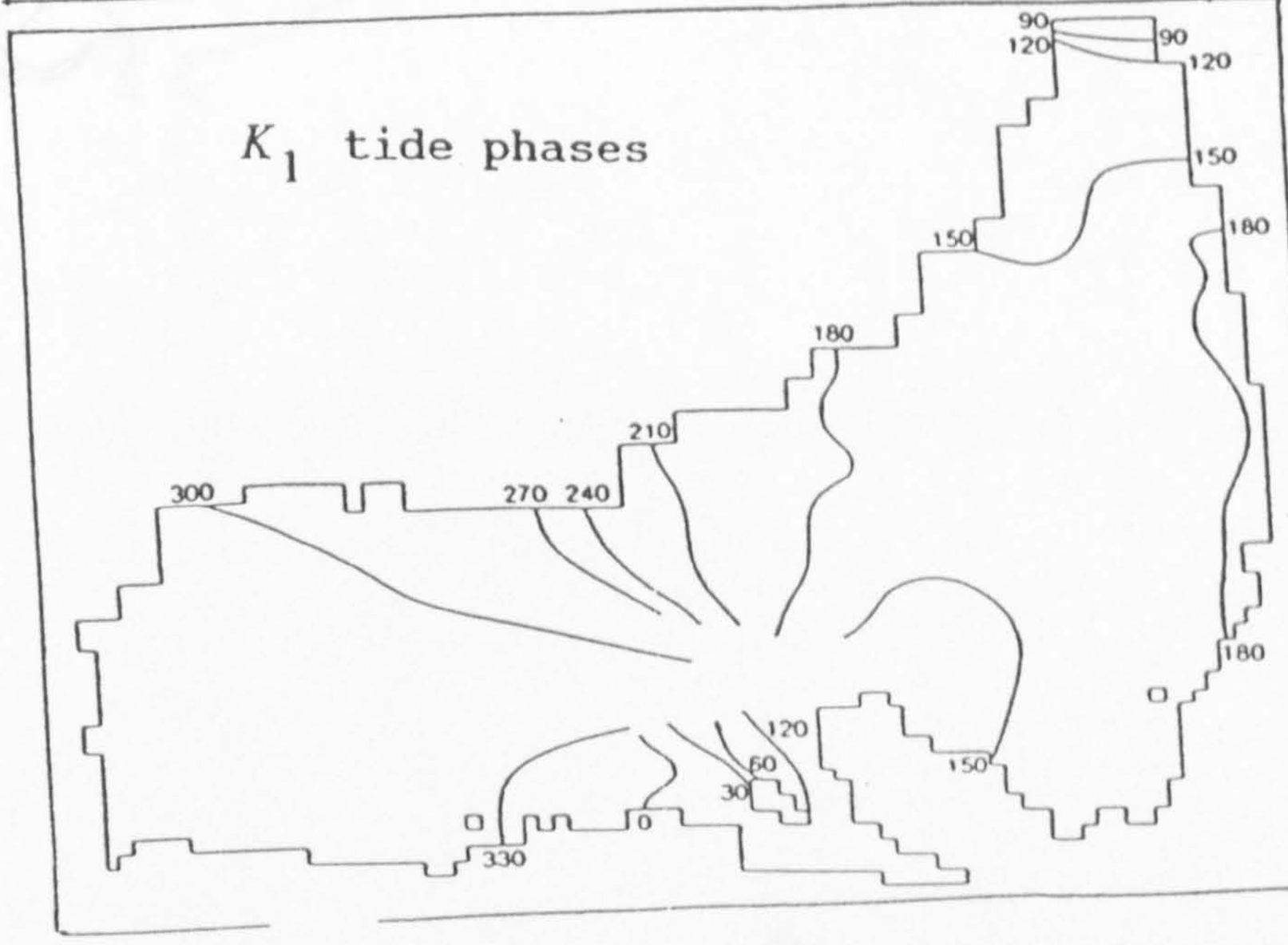

Figure 6.28 Phases for M_2, S_2 and K_1 in degrees simulated by Lardner et al (1982).

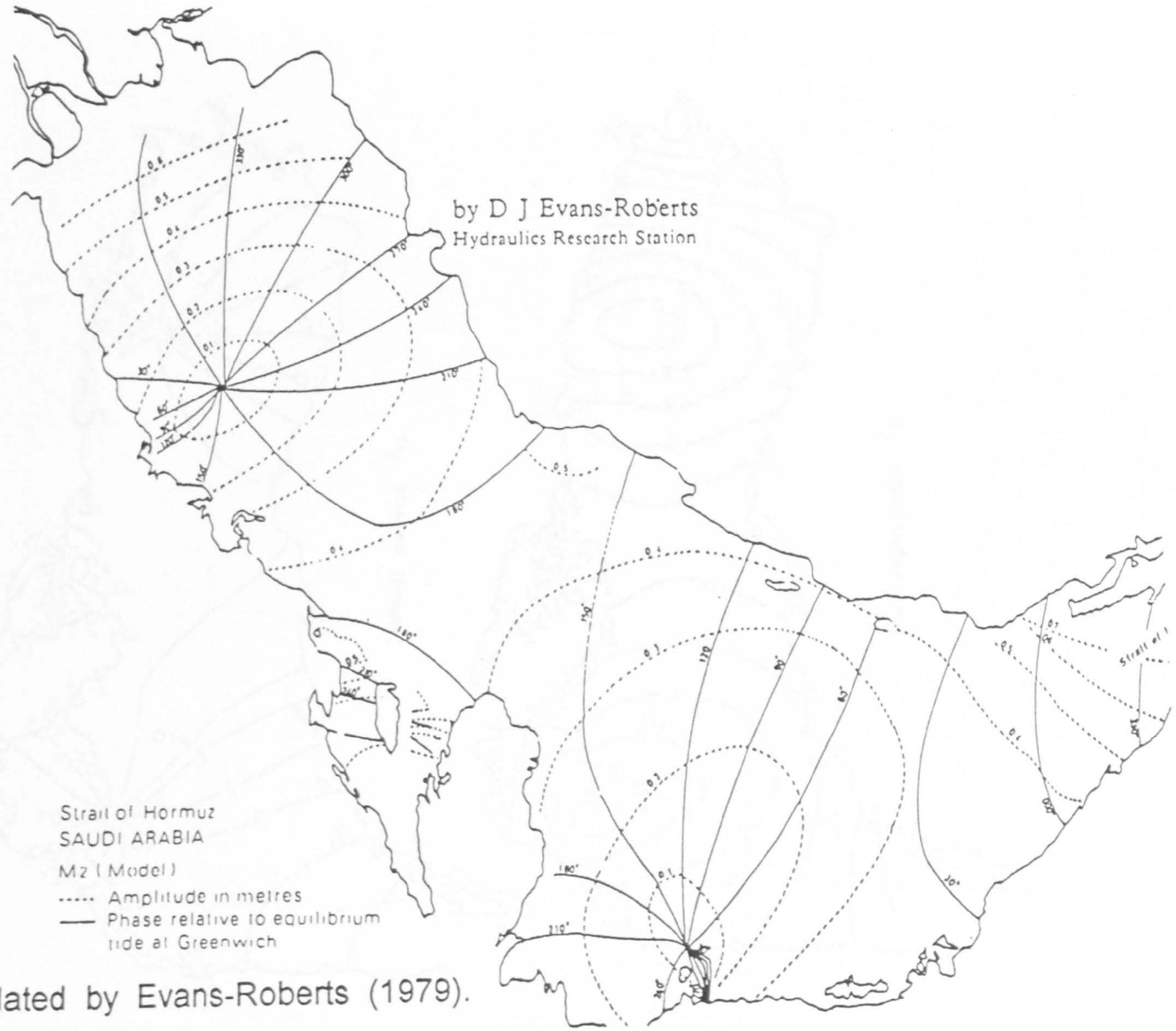

Figure 6.29 The M_2 simulated by Evans-Roberts (1979).

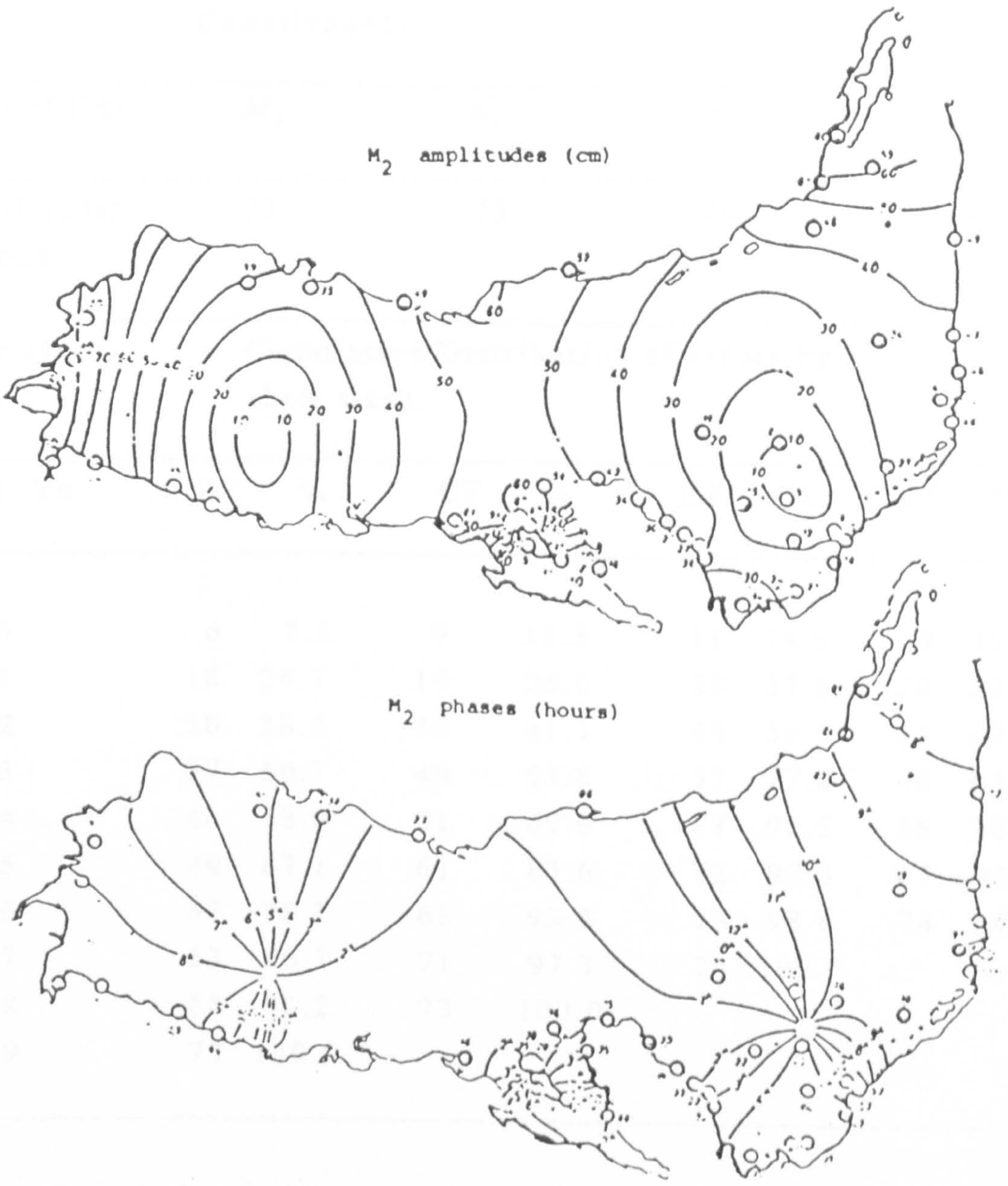

Figure 6.30 Amplitudes and phases for M_2 simulated by Von Trepka (1968).

Table 6.5 Analysis of Error in Amplitude of Tidal Constituents.

Name of tide	M_2		K_1		S_2		O_1	
No. of Tidal stations	73		73		74		74	
Error class (cm)	Cumulative Distribution of errors by their sizes.							
From To	CF	%	CF	%	CF	%	CF	%
0 0	6	8.2	9	12.3	11	14.9	9	12.2
-1 1	18	24.7	19	26.0	28	37.8	20	27.0
-2 2	28	38.4	30	41.1	44	59.5	35	47.3
-3 3	37	50.7	40	54.8	57	77.0	48	64.9
-4 4	46	63.0	51	69.9	67	90.5	58	78.4
-5 5	49	67.1	61	83.6	72	97.3	67	90.5
-6 6	57	78.1	68	93.2	73	98.6	74	100
-7 7	63	86.3	71	97.3	74	100.0		
-8 8	68	93.2	73	100.0				
-9 9	73	100.0						

CF = Cumulative Frequency

Table 6.6 Analysis of Percentage Error in Amplitude of Tidal Constituents.

Name of tide	M_2		K_1		S_2		O_1	
No. of Tidal stations	73		73		74		74	
% Error class (cm)	Cumulative Disribution of errors by their sizes.							
From To	CF	%	CF	%	CF	%	CF	%
0 0	11	15.1	13	17.8	11	14.9	12	16.2
-5 5	25	34.3	26	35.6	20	27.0	21	28.4
-10 10	37	50.7	42	57.5	30	40.5	33	44.6
-15 15	51	69.9	54	74.0	45	61.6	49	66.2
-20 20	61	83.6	63	86.3	58	78.4	62	83.8
-25 25	67	91.8	70	95.9	63	85.1	67	90.5
-30 30	68	93.2	71	97.3	67	90.5	69	93.2
-35 35	72	98.6	71	97.3	70	94.6	72	97,3
-40 40	72	98.6	73	100.0	73	98.6	73	98.6
-45 45	72	98.6			74	100.0	74	100.0
-50 50	73	100.0						

CF = Cumulative Frequency

Table 6.7 Analysis of Phase Error of Tidal Constituents.

Name of tide	M_2		K_1		S_2		O_1	
No. of Tidal stations	73		73		74		74	
Error class (cm)	Cumulative Distribution of errors by their sizes.							
From To	CF	%	CF	%	CF	%	CF	%
0 0	10	13.7	9	12.3	8	10.8	7	9.5
-1 1	17	23.3	17	23.3	15	20.3	12	16.2
-2 2	26	35.6	23	31.5	19	25.7	17	23.0
-3 3	31	42.5	25	34.3	22	29.7	24	32.4
-4 4	36	49.3	30	41.1	25	33.8	28	37.8
-5 5	40	54.8	36	49.3	28	37.8	32	43.2
-6 6	44	60.3	39	53.4	31	41.9	37	50.0
-7 7	46	63.0	43	58.9	35	47.3	41	55.4
-8 8	49	67.1	45	61.6	39	52.7	45	60.8
-9 9	53	72.6	47	64.4	43	58.1	48	64.9
-10 10	58	79.5	50	68.5	47	63.5	53	71.6
-11 11	61	83.6	53	72.6	52	70.3	57	77.0
-12 12	63	86.3	57	78.1	56	75.7	59	79.7
-13 13	66	90.4	59	80.8	60	81.1	62	83.8
-14 14	69	94.5	62	84.9	64	86.5	63	85.1
-15 15	70	95.9	63	86.3	68	91.9	64	86.5
-16 16	71	97.3	65	89.0	71	96.0	66	89.2
-17 17	72	98.6	67	91.8	73	98.6	68	91.9
-18 18	73	100.0	70	95.9	74	100.0	70	94.6
-19 19			71	97.3			71	96.0
-20 20			72	98.6			73	98.6
-21 21			73	100.0			74	100.0

CF = Cumulative Frequency

Table 6.8 Analysis of Percentage Phase Error of Tidal Constituents.

Name of tide	M_2		K_1		S_2		O_1	
No. of Tidal stations	73		73		74		74	
% Error class (cm)	Cumulative Distribution of errors by their sizes.							
From To	CF	%	CF	%	CF	%	CF	%
0 0	36	49.3	39	53.4	28	37.8	31	41.9
-5 5	60	82.2	63	86.3	54	73.0	54	73.0
-10 10	67	91.8	70	95.9	62	83.7	62	83.7
-15 15	68	93.2	73	100.0	64	86.5	65	87.8
-20 20	68	93.2			66	89.2	71	96.0
-25 25	70	95.9			68	91.9	73	98.7
-30 30	73	100.0			70	94.6	73	98.7
-35 35					72	97.3	73	98.7
-40 40					72	97.3	74	100.0
-45 45					74	100.0		

CF = Cumulative Frequency

REFERENCES

Adamec, D., Elsberry, R.L. and Garwood, R.W. 1981 "An embedded mixed-layer-ocean circulation model". *Dynamics of Atmospheres and Oceans, vol. 6, pp. 69-96.*

Admiralty Co-tidal chart Persian Gulf No 5081, *Hydrographer of the Navy*, U.K. 1976.

Admiralty Tide Tables, vol. 2, pp. 343-436, *Hydrographer of the Navy*, U.K. 1988.

Admiralty Chart no. 2858, *Hydrographer of the Navy*, U.K. 1988.

Airy, G.B. 1842. Tides and Waves. *Encyclopaedia Metropolitana 5.*

Al-Deghaiter, 1984. "MEPA marine weather service operational models". El-Sabh, I. (editor) Oceanographic modelling of the Kuwait Action Plan region, UNESCO Report in *Marine Sciences* no. 28, p. 70.

Apelt, C.J. and Richter, N.J. 1985. "Modelling barrier reef tides in the Mackay region". *Civil Engrg Trans, vol. CE27*, pp 166-173.

Arnold, R. and Noye, J. 1982.in *Numerical Solutions of Partial Differential Equations.* ed by J.Noye, pp. 437-453, North-Holland, Amsterdam.

Backhaus, J. 1980. "On currents in the German Bight: a three-dimensional non-linear tidal model". *Lecture notes on Coastal and Estuarine Studies* no. 1, Springer Verlag, Amsterdam.

Bahrain Coastguard Directorate (depth) Chart, (prepared by S. Ahmed S. Khalifa A Gafoor Al-Sadha, in Arabic), Muharraq, Bahrain 1963.

Banks, J.E. 1974. "A mathematical model of a river shallow sea system used to investigate tide,surge and their interaction in the Thames-Southern North Sea region", *Phil. Trans. R. Soc.* Lond., *vol. A 275*, pp. 567-609.

Barlow, E.W. 1932a. "Currents in the Persian Gulf, northern portion of the Arabian Sea, Bay of Bengal, etc, I. summary of previous knowledge". *The Marine Observer*, *vol. IX*, no. 99, pp. 58-60.

Barlow, E.W. 1932b. "Currents in the Persian Gulf, northern portion of the Arabian Sea, Bay of Bengal etc., II-the S.W. monsoon period". *The Marine Observer*, *vol. ix*, no. 105, pp. 169-171.

Barlow, E.W. 1932c. "Currents in the Persian Gulf, northern portion of the Arabian Sea, Bay of Bengal etc., III- the N.E. monsoon period and general summary". *The Marine Observer*, *vol. IX*, no.108, pp. 223-227.

Bashir, M., Al-Hawaj, A.Y., Twizell, E.H. and Khaliq, A.Q.M. 1990. "An explicit finite difference model for tidal flows in the Arabian Gulf", in W.L. Hogarth and B.J. Noye (editors) *Computational Techniques and Applications* CTAC-89, New York, pp. 295-302.

Basson, P., Burchard, J., Hardy, J. and Price, A. 1977. *Biotopes of the western Gulf.* Arabian American Oil Co., Dhahran. p. 27.

Bauer, S. 1979. "Three-dimensional irregular-grid finite difference model of wind-induced water level fluctuations and currents in a homogeneous lake with application to Lake Geneva". *Communication du Laboratorie d'Hydraulique*, report no. 41. Ecole Polytechnique Federale de Lausanne, Switzerland.

Beam, R.M., Warming, R.F. and Yee, H.C. 1982. "Stability analysis of numerical boundary conditions and implicit difference approximations". *J. of Computational Physics*, 48, pp. 200-222.

Beckers, P.M. and Neves, R.J. 1985. "A semi-implicit tidal model of the North European Continental Shelf", *Appl. Math. Modelling*, *vol. 9*, pp. 395-402.

Blegvad, H., 1944. "Fishes of the Iranian Gulf". *Danish Scientific Expeditions in Iran* (1935-1938), pt 3, Copenhagen, pp. 1-247.

Blumberg, A.F. and Kantha, L.H. 1985. "Open boundary condition for circulation methods". *J Hydraul Engrg*, III, pp. 237-250.

Brewer, P.A., Fleer, S., Kadar, D., Shafer, D. and Smith, C. 1978. "Chemical oceanographic data from the Persian Gulf and Gulf of Oman". *Woods Hole Oceanographic Institution Technical Report*, WHOI-78-37, pp. 105.

British Admiralty 1941. "Water movements and related information, Persian Gulf (sheet II)". *Oceanographical Chart* no. 13 C.6120.

Chen, H.S. 1978. "A storm surge model study, a finite element storm surge analysis and its application to a bay-ocean system". *vol II Special Report no. 189 Appl Marine Sci and Ocean Engrg.*

Chiang, W.L. and Lee, J. 1982. "Simulation of large-scale circulation in harbours". J of the Waterway, Port, Coastal and Ocean division. *Proceedings of the Amer Soc of Civil Engineers vol. 108*, no. WW1, pp. 17-31.

Courant, R., Friedrichs and Lewy, H. 1928. " Uber die partiellen Differenzen-Gleichungen der mathematischen Physik", *Mathematische Annalen*, 100, pp. 32-74.

Crean, P.B., Backhaus, J. and Lee, D.K. 1983. "Three-dimensional numerical model studies of tidal residual and density-driven circulation in a deep bathymetrically complex coastal sea between Vancouver Island and the mainland". *18th. General Assembly of IUGG, Coastal and Near Shore Processes; abstract IUGG-21-9,* p 907.

Dantzig, D.van and Lauwerier, H.A. 1960 "The North Sea problem". *Proc. Kon. Ned. Akad.* v Wet., Ser A63 and 64, Amsterdam.

Darwin, G.H. 1907 "Reports of a committee for the harmonic analysis". (*British Assoc Advancement of Sciences*,1883-1886) see also Scientific Papers, Univ. Press, Cambridge.

Davies, A.M. and Heaps, N. 1980. "Hydrodynamic modelling of stratified flows using a spectral formulation". *Int symp on stratified flows, Norw Inst of Tech*, Trondheim, pp. 579-581.

Davies, A.M. 1985. "On determining the profile of steady wind-induced currents". *Appl. Math. Modelling*, 9, pp. 409-418.

Davydov, L.M. and Maksimov, A.V. 1984. "One-dimensional mathematical model of water dynamics and transport of dissolved substances in estuaries". *Soviet Meteorology and Hydrology,* no. 10, pp. 85-90.

Defant, A. 1961.Physical Oceanography, vols 1 and 2, Pergamon Press, Oxford.

Defense Mapping Agency, USA 1975. Sailing Directions for the Persian Gulf. *Hydrographic Center, Washington D.C.*

Dippner, J.W. 1984. " OIPASIPA- a powerful tool for contingency planning". El-Sabh, I.(ed) Oceanographic Modelling of the Kuwait Action Plan Region, *UNESCO Report in Marine Sciences, no. 28.*

Doodson, A.T. 1921. "The harmonic development of the tide-generating potential". *Proc. Roy. Soc.* Lond: A 100, pp. 305-328.

Dronkers, J.J. 1964. Tidal computations in rivers and coastal waters. North-Holland Pub. Co., Amsterdam.

Dubach, H.W. 1964. "A Summary of temperature-salinity characteristics of the Persian Gulf". *Publication NODC-G-4, National Oceanograpgic Data Center*, Washington D.C., U.S.A.

Duff, G.F.D. 1983. "A Special ADI model for the Laplace tidal equations". *Comp. & Math. with Applic.* no. 9, pp. 507-516.

Elahi, Kh.Z. and Sundermann, K. 1979. "Tidal currents in the Northern Arabian Sea". *Int. Indian Ocean Expedition no. 14*, Florida (Research Report).

Elahi, Kh.Z. and Rashid, K. 1981. "Mathematical model of the northern Arabian Sea". *Ocean Management, vol. 6*, no.2-3, pp. 149-158.

Elahi, Kh. 1984. "Simulation of large scale circulation in the Indian Ocean". *Computer Methods in Applied Mechanics and Engineering.*

El-Sabh, M.I. (editor) "Oceanographic modelling of the Kuwait Action Plan region. *UNESCO Reports in Marine Sciences*, no. 28.

Emery, K. 1956. "Sediments and water of the Persian Gulf". *Bull. of the Am. Assoc. of Pet. Geologist*, 40, pp. 2354-2383.

Evans-Roberts, D. 1979. "Tides in the Persian Gulf". *Consulting Engineer*, vol. 1, pp. 46-48.

Falconer, R. 1984. "Temperature distributions in tidal flow field". *J of Environmental Eng, vol. 110*, no. 6, pp. 1099-1116.

Falconer, R. 1985. "Residual currents in Port Talbot harbour: a mathematical model study". *Proc of the Institution of Civil Engineers* (London), *vol. 79* part 2, pp. 33-53.

Flather, R.A. 1976. "Results from a storm surge prediction model of the North-West European Continental Shelf for April, November and December, 1973", *IOS Rep.* no. 24, Bidston Observatory, England, 33p.

Flather, R.A. and Heaps, N.S. 1975. "Tidal computations for Morecombe Bay". *Geophys. J. R. Astr. Soc.*, 42, pp. 489-517.

Galt, J.A. 1984. "Trajectory analysis and simulation of oil spill movement". El-Sabh, M.I. (ed) Oceanographic Modelling of the Kuwait Action Plan Region, *UNESCO Report in Marine Sciences, no. 28.*

Galt, J.A.,Payton, G.M. and Waterbayasmi, G. 1984. "Application of trajectory analysis for the Nowruz oil spill". El-Sabh, M.I. (ed) Oceanographic Modelling of the Kuwait Action Plan Region, *UNESCO Report in Marine Sciences, no. 28.*

Gopalkrishnan, T.C. 1983. "Numerical analysis of a moving boundary problem in coastal hydronamics". *Int. Jour. Num. Methods in Fluids, vol. 3*, pp. 179-200

Gottlieb, D.,Gunzburger, M. and Turkel, E. 1982. "On numerical bounding treatment of hyperbolic systems for finite difference and finite element methods". *SIAM J. of Num. Anal.*, 4, pp. 671-682.

Goursat, E. 1923. Cours d'analyse mathematique. Tome III, Gautier-Villars, Paris.

Goussebaile, J., Hecht, F., Labadie, G. and Reinhart, L. 1984. "Finite element solution of the shallow water equations by a quasi-direct decomposition procedure". *International J for Numerical Methods in Fluids vol. 4*, no. 12, pp. 1117-1136.

Grasshoff, K. 1976. "Review of hydrographical and productivity conditions in the Gulf region, marine sciences in the Gulf area". *UNESCO Technical Papers in Marine Science*, 26.

Griffiths, D.K., Pingree, R.D. and Sinclair, M. 1981 "Summer tidal fronts in the near-arctic regions of Foxe Basin and Hudson Bay". *Deep-Sea Research, part A : Oceanographic Research Papers, vol. 28*, no. 8A, pp. 865-873.

Guohong, F. 1984. "Two-dimensional numerical model for tidal motion in the Taiwan Strait". *Marine Geophysical Researches*, vol. 7, no. 1-2, pp. 267-276.

Gustafsson, B. 1975. "The convergence rate for difference approximations to mixed initial boundary value problems". *Math. of Computation*, vol. 26, pp. 391-406.

Hadamard, J. 1923. Lectures on Cauchy's problem in linear partial differential equations, Dover Publs., New York.

Hamilton, G.D., Soileau, C.W. and Stroud, A.D. 1982. "Numerical modelling study of Lake Pontchartrain". *J of the Waterway, Port, Coastal and Ocean Division, Proc. of the American Soc. of Civil Engineers*, vol. 108, no. WW1, pp. 49-64.

Hansen, W. 1962. "Hydrodynamical methods applied to oceanographic problems", *Proc. symp. math. hydrodyn. phys. ocean*, Institut fur Meereskunde, Universitat Hamburg, pp. 24-34.

Hartman, M., Lange, H., Seibold, E. and Walger, E. 1971. "Surface sediments in the Persian Gulf and Gulf of Oman, I. Geologic-hydrologic setting and first sedimentological results", *"Meteor" Forschungsergebnisse, series C. no 4*, pp. 1-76.

Heaps, N.S. 1980. "Spectoral method for the numerical solution of the three-dimensional hydrodynamics equations for tides and surges". *Lecture Notes on Coastal and Estuarine Studies*, no. 1, Spriger Verlag.

Hendershott, M.C. 1977. "Numerical models of ocean tides". *The Sea, vol. 6*, p 47.

Henry, F., Ahlert, R.C., Peskin, R.L. and Vichnevetsky, R. 1984. "Numerical model of pollution transport in estuaries". *Water Resources Bull, vol. 20*, no. 6, pp. 833-839.

Henry, F., Ahlert, R.C., Peskin, R.L. and Vichnevetsky, R. 1984. "Numerical esterine flow model". *Water Resources Bulletin*, vol. 20, no.6, pp. 823-831.

Hill, M.N. 1962. The Sea, vol 1, Physical Oceanography. Intersci Publ., New York.

Hires, R.I., Oey, L. and Mellor, G.L. 1983. "Prediction of oil spill trajectories in New York harbour". Civil Engrg for Practicing and Design Engineers, vol. 2, no. 6, pp. 585-602.

Holly, F.M. and Usseglio-Polatera, J. 1984. "Dispersion simulation in two-dimensional tidal flow". *J of Hydraulic Engineering, vol. 110*, no. 7, pp. 905-926.

Holz, K.P. 1981. "Numerical modelling of tidal dynamics in estuaries". *Proc. Eighth Canadian Congress of Applied Mechanics*, June 7-12, 1981, pp. 155-160.

Howarth, M.J. and Jones, J.E. 1981. "Comparison of numerical model and observed currents during a storm surge period". *Estuarine, Coastal and Shelf Science, vol. 12, no. 6*, pp. 655-663.

Hughes, P. and Hunter, J. 1979. "A Proposal for a physical oceanography program and numerical modelling of the KAP region". *Project for KAP 2\2*, UNESCO, Paris.

Hunter, J.R. 1980. "An interpretive computer model of oil slick motion". *Paper presented at Oceanology International 80*, Brighton, U.K. 1980.

Hunter, J.R. 1982. "The physical oceanography of the Arabian Gulf: a review and theoretical interpretation of previous observations". *First Gulf Conference on Environment and Pollution, Kuwait 1982.*

Hunter, J.R. 1983. "Aspects of the dynamics of the residual circulation of the Arabian Gulf". in *Coastal Oceanography*. edited by Gade, M.G., Edwards, A. and Svenson, H., Plenum Press, pp. 31-42.

Hunter, J. 1984. "A Review of the residual circulation and mixing processes in the KAP region". In : El-Sabh, M.I. [editor] *"Oceanographic modelling of the Kuwait Action Plan region". UNESCO Reports in Marine Sciences, no. 28.*

Johns, B., Sinha, P.C., Dube, S.K., Mohanty, U.C. and Rao, A.D. 1983. "Simulation of storm surges using a three-dimensional numerical model: an application to the 1977 Andhra cyclone". *Quart. J. R. Met. Soc.* no. 109, pp. 211-224.

Kassler, P. 1973. "The Structural and geomorphic evolution of the Persian Gulf". In: Purser, B. (editor) *The Persian Gulf*. Springer-Verlag, New York, Heidelberg, Berlin, pp. 11-32.

Kawahara, M., Kobayashi, M. and Nakata, K. 1983. "Multiple level finite element analysis and its applications to tidal current flow in Tokyo Bay". *Appl Mathematical Modelling, vol. 7*, no. 3, pp. 197-211.

Kielmann, J. 1983. "Some results from a numerical multi-layer baroclinic circulation model of the Baltic Sea". *18th. General Assembly of Interational Union of Geodesy and Geophysics, IAPSE-Abstract*, Hamburg 15-17 Aug, 1983.

King, I. 1985. "Strategies for finite element modelling of three dimensional hydrodynamic systems". *Adv Water Resources, vol.8,* no. 2, pp. 69-76.

Kinmark, I.P. and Gray, W.G. 1984. "Two-dimensional analysis of the wave equation model for finite element tidal computations". *International J for Numerical Methods in Engineering, vol 20,* no. 2, pp. 369-383.

Koske, P. 1972. "Hydrographic conditions in the Persian Gulf on the basis of observations aboard R.V. Meteor in spring 1965". *Meteor Forschungsergebnisse,* series A, no. 11, pp. 58-73.

Kreiss, H.O. 1970. "Initial boundary value problems for hyperbolic systems". *Comm. on Pure and Appl. Math.* vol. 23, pp. 272-298.

Kreiss, H.O., Gustafsson, B. and Sundstrom, A. 1972. "Stability theory of difference approximations for mixed initial boundary value problems,II". *Math. of Computations,* vol. 26, pp. 649-686.

Krohn, J. 1984. "Global ocean tide model with high resolution in shelf areas". *Marine Geophysical Researches, vol.7,* no.1-2 Oct 1984, Geod Features of the Ocean Surf and their Implic, Hamburg, Aug 1983, pp. 231-246.

Kullenberg, G. 1983. *Mixing processes in the North Sea and aspects of their modelling, North Sea dynamics.* ed. Sundermann and Lenz, Springer Verlag, pp. 349-369.

Laevastu, T., Clancy, M. and Stroud, A. 1974. "Computation of tides, currents and dispersal of pollutants in Lower Bay and approaches to New York with fine and medium grid size hydrodynamical-numerical models". *Naval Environment Prediction Research Facility Tech* no. 3-74.

Laevastu,T. 1975. "Multi-layer hydrodynamical-numerical models". *Proc. of the Symp. on Modelling Techniques,* ASCE, San Fransisco, California.

Lamb, H. 1932. Hydrodynamics. 6th. ed. Cambridge Univ. Press, also Dover Publs., New York, 1945.

Lardner, R., Belen, M.S. and Cekirge, H.M. 1982. "Finite difference model for tidal flows in the Arabian Gulf". *Comp. and Maths. with Appls. vol.8,* pp. 425-444.

Lardner, R.W., Lehr, W., Fraga, R. and Sarhan, M. 1988. "A model of residual currents and pollution transport in the Arabian Gulf". *Appl. Math. Modelling, no.* 12, pp. 379-389.

Leendertse, J. 1967. *Aspects of computational model for long period water wave propagation,* Rand Corp. Rep. RM-5294-PR.

Leendertse, J., Liu, S.K. and Nelson, A.B. 1975. "Three-dimensional model for estuaries and coastal seas". vol. II, *Aspect of Computation,* R-1764-OWRT, Rand Corp, California.

Lehr, W.J. 1984. "A brief survey of oceanographic modelling and oil spill studies in the KAP region". El-Sabh, M.I. ed. *Oceanographic Modelling of the Kuwait Action Plan Region, UNESCO Reports in Marine Sciences, no.28,* pp. 4-11.

Le Provost, C. 1983."Models for tides in the KAP region", *Symp. on oceanographic modelling of the KAP region,* UPM, Saudi Arabia.

Le Provost, C. 1984. "Model for tides in the KAP region". In: El-Sabh, M.I.(editor) "Oceanographic modelling of the Kuwait Action Plan region". *UNESCO Reports in Marine Sciences, no. 28.*

Lorentz, H.A. 1926. "Verslag staatcommissie Zuiderzee, 1918-1926" (report of the government Zuiderzee Commission) Alg. Landsdrukkerij, The Hague.

McCammon, C. and Wunsch, C. 1977. "Tidal charts of the Indian Ocean north of 15°*S*". *J. of Geo. Research, vol. 82*, no. 37, pp. 5993-5998.

Marchuk, G.I. and Kagan, B.A. 1984. Ocean Tides: mathematical models and numerical experiments. Pergamon Press, Oxford.

Massau, J. 1900. "Memoire sur l'integration graphique des equations aux derivées partielles". *Ann. Ass. Ing. Ecoles de Grand.*

Matsuda, Y. 1979. "A water pollution prediction system by the finite element method". *Advances in Water Resources, vol. 2*, pp. 22-34.

Matthews, C.P., Samuel, M. and Al-Attar, L.H. 1979. "The oceanography of Kuwait waters: some effects of fish population on the environment". *Annual Research Report 1979*, KISR, Kuwait.

Matthews, J.B. and Mungall, J.C. 1972. "A Numerical tidal model and its application to Cook Inlet, Alaska". *J. Mar. Res.* no. 30, pp. 27-38.

Miller, H.P. 1984. "Numerical three-dimensional free surface circulation model for the South Biscayne Bay, Florida". *Appl. Math. Modelling, vol. 8*, pp. 313-318.

Mitchell, A. R. and Griffiths, D. F., 1980, " *The Finite Difference Method in Partial Differential Equations*" Wiley, New York.

Murty, T.S. and Henry, F. 1983. "Tides in the Bay of Bengal". *J of Geophysical Research, vol. 88*, no. 10, pp. 6069-6076.

Murty, T.S. and El-Sabh, M.I. 1983. "Movement of oil slicks in the Arabian Gulf during stormy periods". Paper presented at the *Symposium on Oceanographic Modelling of the Kuwait Action Plan Region, Dhahran, Oct 15-18.* 1983.

Murty, T.S. and El-Sabh, M.I. 1984. in Oceanographic modelling of the Kuwait Action Plan region, *UNESCO Reports in Marine Science, (report of a symposium-workshop, UPM, Dahran, Saudi Arabia).*

Nihoul, J.C. 1978. "Three-dimensional modelling of marine circulation". in C.A.Brebbia (editor), *Applied Numerical Modelling.* Pentech Press, pp. 73-81.

Noye, J., May, R.L. and Teubner, M.D. 1981. "Three-dimensional numerical model of tides in Spencer Gulf". *Ocean Management, vol. 6,* no. 2-3, pp. 137-147.

Oliger, J. and Sundstrom, A. 1978. "Theoretical and practical aspects of some initial boundary value problems in fluid dynamics". SIAM J. of Appl. Math., 35, pp. 419-446.

Owen, A. 1984. "Artificial diffusion in the numerical modelling of the adjective transport of salinity". *Appl Mathematical Modelling, vol. 8,* no. 2, pp. 116-120.

Perrone, T.J. 1979. "Winter shamal in the Persian Gulf". *Naval Environmental Prediction Research Facility, Monteray, California, Technical Report* I.R.-79-06, August 1979. Second printing, January 1981.

Picard, E. 1950. Lecons sur queques types simples des equations aux derivees partielles. Nouveau tirage, Gauthier-Villars, Paris.

Pond, S. and Pickard, G.L. 1983. *Introductory Dynamical Oceanography.* 2nd. ed. Pergamon Press, Oxford.

Post, J. 1984. "Simulation models for pollutant transport in marine environment - capabilities and limitations". El-Sabh, M.I.(ed) Oceanographic Modelling of the Kuwait Action Plan Region, *UNESCO Report in Marine Sciences, no 28.*

Proudman, J. 1953. *Dynamical Oceanography*. Methuen, London.

Privett, D. 1959. "Monthly charts of evaporation from the north Indian Ocean (including the Red Sea and Persian Gulf)". *Quart. J. Roy. Meterol. Soc.*, 85, pp. 424-428.

Purser, B.H. and Seibold, E. 1973. "The principal environmental factors influencing Holocene sedimentation and diagenesis in the Persian Gulf". In *The Persian Gulf, Holocene Carbonate Sedimentation and Diagenesis in a Shallow Epicontinental Sea*, edited by Purser, B.H. pp. 1-9, Springer-Verlag, Berlin.

Rath, R.J. and Francis, B.H. 1977. "Modelling methods for predicting oil spill movement". *Technical Report no. PB 277-669, Oceanographic Commission of Washington*. Sea Ale, WA, U.S.A.

Roovers, P., Ozer, J., Mommaerts, J.P. and Adam, Y. 1984. "Simulation of ecological impacts of the new outer-harbour development in Zeebrugge". *Water, Science and Technolgy, vol. 16*, no.3-4, Integr of Ecol Aspects in Coastal Eng Project, Proc of a symp, Rotterdam, June 6-10 1983, pp. 441-446.

Saint Venant, B de. 1871. "Theorie de mouvement non-permanent des eaux, avec application aux crues des rivieres et a l'introduction des mareées dans leur lits". *Compt. Rend. de l'Acad. des Sci.*

Schonfeld, J.C. 1955. "Tides in funnel shaped channels". *Report Rijkswaterstaat*. The Hague.

Schott, G. 1918. "Oceanographie und klimatologie des Persischen Golfes und des Golfes von Oman". *Annalen der Hydrographie und Maritimen Meteorologie*, pp. 1-46.

Sheng, Y.P. 1983. "Mathematical modelling of three-dimensional *coastal currents and sediment* dispersion: model development and application". *Aeronautical Research Associates of Princeton Inc*, Princeton NJ, USA.

Sonu, C.J. 1979. "Oceanographic study in the Strait of Hormouz and over the Iranian shelf in the Persian Gulf". *US Office of Naval Research, final report, contract no. N00014-76-c-0720, TC 3675.*

Spaulding, M.L. and Beauchamp, C. 1983. "Modelling tidal circulation in coastal seas". *J of Hydraulic Engineering, vol. 109,* no, pp. 116-132.

Stelling, G.S. 1984. "On the construction of computational methods for shallow water flow problems". *Rijkswaterstaat Communications, no. 35*, p 226.

Sugden, W. 1963. "The hydrology of the Persian Gulf and its significance in respect to evaporite deposition". *Amer. J. of Sci.*, vol. 261, pp. 741-755.

Sundermann, J. 1966. "Ein Verleich Zwischen der Analytischen und den Numerischen Berechnung Winderzeugter Stromungen und den Wasserstande in Einem Modellmeer mit Anwendungen aug did Nordsee". Mitteilungen des Instituts fur Meerskunde der Universitat Hamburg, no. 4. Universitat Hamburg, Germany.

Sundermann, J. 1971. "Die Hydrodynamisch-numerische Berechnung der Vertikalstruktur von Bewegungsvorgangen in Kanalen und Becken". *Mitt des Int. fur Meerskunde der Universitat Hamburg Nr. 19.*

Sundermann, J. 1974. "Numerical modelling of circulation in lakes". *Proc. of Symp. on Hydrodynamics of Lakes* ED. Graf, W.H., Elsevier Publ., Amsterdam, pp. 1-30.

Szekielda, K.H. 1976. "Spacecraft oceanography". *Oceanogr. Mar. Biol. Ann. Review., vol. 14*, pp. 99-166.

Szekielda, K.H., Salomonson, V. and Allison, L.J. 1972. "Rapid variations of sea surface temperature in the Persian Gulf as recorded by Nimbus 2 HRIR". *Limnology and Oceanography, vol. 17*, no. 2, pp. 307-309.

Taylor, C. 1975. "Tidal propagation and dispersion in estuaries". In Gallagher, R.M. *Finite Element in Fluids, vol. 1*, Wiley, New York, pp. 95-118.

Taylor, G.I. 1920. "Tidal oscillations in gulfs and rectangular basins". *Proc. London Math. Soc*, 2, XX, pp. 148-181.

Trepka, L. von, 1968. "Investigations of the tides in the Persian Gulf by means of a hydrodynamic-numerical model". *Proceedings of symposium on mathematical-hydrodynamical investigations of the physical processes in the sea*. Institut fur Meereskunde der Universitat Hamburg, pp. 59-63.

Twizell, E. H., 1984, " *Computational Methods for Partial Differential Equations"* Ellis Horwood Limited, England.

Uncles, R.J. 1982. "Computed and observed residual currents in the Bristol Channel". *Oceanologica Acta, vol. 5*, no.1, pp. 11-20.

Verboom, G.K., Stelling, G.S., and Officier, M.J. 1982. "Boundary conditions for the shallow water equations" in *Engineering Applications for Computational Hydraulics*, vol. 1, (Abbott, M. and Cunge, J.A. editors), Pitman, London.

Villain, C. 1944. Cours de marees. 1943-44. *Service Central Hydrographique*, Paris.

Wang, D. 1983. "Two-dimensional branching salt intrusion model". *J of Waterway, Port, Coastal and Ocean Engineering, vol. 109,* no. 1, pp. 103-112.

Warren, B.A. 1966. "Medieval Arab references to the seasonal reversing currents of the north Indian Ocean". *Deep-Sea Research, vol. 13*, pp. 167-171.

Wennick, C. and Nelson-Smith, A. 1977. *Coastal oil pollution evaluation study for the Kingdom of Saudi Arabia, vol. 2.* IMCO, London, p. 28.

Wiegel, R.L. 1964. Oceanographic Engineering, Prentice Hall, Englewood Cliffs, New Jersey.

Wilders, P., Stijn, Th van, Stelling, G.S. and Fokkema, G.A. 1988. "A fully implicit splitting method for accurate tidal computations", *Int. J. Numer. Methods Eng, vol. 26,* pp. 2707-2721.

Williams, R. 1979. *Meteorologic and Oceanographic Data handbook.* Arabian American Oil Co., Dhahran.

Zeidler, R. 1976. "Coastal dispersion of pollutants", *J. of Waterways, Harbours and Coastal Eng.*, Div ASCE, vol. 102, pp. 235-250.

Bibliography

Argintaru, V. and Willis, D.H. 1984. "Simulation of the tidal propagation in the Bay of Fundy using a hybrid model", *Math. and Cumputers in Simulation*, vol.26 no.1, pp. 39-42.

Bermejo, R. 1990. "A finite element model of two-layer ocean circulation", *Int. J. for Numerical Methods in Engineering*, vol. 29, pp. 665-678.

Caldwell, H.G.and Pincock, D.G. 1980. "Modelling a model of the tides on the St. Lawrence seaway", *Simulation*, vol.34 no.5, pp. 147-154.

Casulli, V. 1990. "Semi-implicit finite difference methods for the two-dimensional shallow water equations", *J. of Comp. Physics*, 86, pp. 56-74.

Casulli, V. and Cheng, R.T. 1990. "Stability analysis of Eulerian-Lagrangian methods for the one-dimensional shallow-water equations", *Appl. Math. Modelling*, vol.14, pp. 122-131.

Cathers, B. and O'Connor, B.A. 1993. "Picard iteration convergence analysis in a Galerkin finite element approximation of the one-dimensional shallow water equations", *Numerical Methods for Partial Differential Equations*, 9, pp. 77-92.

Coffou, E. and Limic, N. 1985. "Minimization problem in residual current modelling", *Appl. Math. Modelling*, vol.9 no.5, pp. 325-330.

Copeland, A.H., Segall, R.S., Ringo, C.D. and Moore, B. 1991. "Mathematical modelling of inverse problems for oceans", *Appl. Math. Modelling*, vol 15, Nov/Dec, pp. 586-595.

Csanady, G.T. "Circulation in the Coastal Ocean". *D.Reidel Publishing Co.*, Dordrecht, Netherlands, 1982.

Davies, A.M. and Owen, A. 1979. "Three dimensional numerical sea model using the Galerkin method with a polynomial basis set", *Appl. Math. Modelling*, vol. 3, Dec, pp. 421-428.

Davies, A.M. 1983. "Numerical modelling of stratified flow: a spectral approach", *Continental Shelf Res.*, vol.2, no.4, pp. 275-300.

De Goede, E.D. 1992. "Numerical methods for the 3D shallow water equations on vector and parallel computers", *Appl. Numerical Math.*, 10, pp. 3-18.

Flather, R.A. 1976. "A tidal model of the North-West european continental shelf", *Mémoires Société Royale des Sciences de Liège*,6e Série, tome X, pp. 141-164.

Gade, H.G., Edwards, A. and Svendsen, H. "Coastal oceanography". *Plenum Press*, New York, 1982.

Glaister, P. 1987. "Difference schemes for the shallow water equations", University of Reading, Dept. of Mathematics, *Numerical Analysis Report 9/87*.

Guohong, F. 1984. "Two-dimensional numerical model for tidal motion in the Taiwan Strait", *Marine Geophysical Res.*, vol.7 no.1-2, pp. 267-276.

Heaps, N.S. and Jones, J.E. 1985. "A three-layered spectral model with application to wind-induced motion in the prescence of stratification and a bottom slope", *Continental Shelf Res.*, vol.4, no.3, pp. 279-319.

Heemink, A.W. 1988. "Two-dimensional shallow water flow identification", *Appl. Math. Modelling*, vol.12, April, pp. 109-118.

Huthnance, J.M. 1983. "Simple models for Atlantic diurnal tides", *Deep-Sea Res.*, part A: Oceanographic Research Papers, vol.30 no. 1A, pp. 15-29.

IMCOS, 1974. "Handbook of the weather in the Gulf", *IMCOS Marine Ltd.*, London, IM 102.

James, A. 1982. "Mathematical modelling of estuaries and coastal waters", *Water, Science and Tech.*, vol.14 no.9-11, pp. 1109-1123.

King, I.P. 1985. "Finite element modelling of stratified flow in estuaries and reservoirs", *Int. J. for Numerical Methods in Fluids*, vol.5 no.11, pp. 943-955.

Kawahara, M. and Hasegawa, K. 1978. "Periodic Galerkin finite element method of tidal flow", *Int. J. for Numerical Methods in Engineering*, vol. 12, pp. 115-127.

Lardner, R.W. and Smoczynski, P. 1990. "A vertical/ horizontal splitting algorithm for three-dimensional tidal and storm surge computations", *Proc. R. Soc.* Lond., April, pp. 1-20.

MacAyeal, D.R. 1984. "Numerical simulations of the Ross Sea tides", *J. of Geophysical Res.*, vol.89 no. C1, pp. 607-615.

Meissner, U. 1978. "An explicit-implicit water-level model for tidal computations of rivers", *Computer Methods in Appl. Mech. and Engineering*, 13, pp. 221-232.

Mitsoulis, E. 1987. "Use of double nodes in the numerical simulation of multilayered flows of immiscible fluids", *Communications in Appl. Num. Methods*, vol.3, pp. 71-76.

Monin, A.S. and Ozmidov, R.V. "Turbulence in the Ocean". *D.Reidel Publishing Co.*, Dordrecht, Netherlands, 1985.

Navon, I.M. 1979. "Finite-element simulation of the shallow-water equations model on a limited-area domain", *Appl. Math. Modelling*, vol.3, pp. 337-348.

Navon, I.M. 1979. "ADIF, a Fortran IV program for solving the shallow-water equations", *Computers and Geosciences*, vol.5, pp. 19-39.

Nikanorov, A.M. and Swain, W.R. 1981. "Application of mathematical models to large aquatic ecosystems", *J. of Great Lakes Res.*, vol.10 no.3, pp. 235-239.

Speer, P.E. and Aubrey, D.G. 1985. "Study of non-linear tidal propagation in shallow inlet/estuarine systems part II: theory", *Estuarine Coastal Shelf Sci.*, vol.21 no.2, pp. 207-224.

Owen, A. 1980. "A three-dimensional model of the Bristol Channel", *J. of Physical Oceanography*,vol.10, pp. 1290-1302.

Peraire, J., Zienkiewicz, O.C. and Morgan, K. 1986. "Shallow water problems: a general explicit formulation", *Int. J. for Num. Methods in Engineering*, vol.22, pp. 547-574.

Priestley, A. 1987. "Roe type schemes for the 2-D shallow water equations", University of Reading, Dept. of Mathematics, *Numerical Analysis Report 8/87*.

Reddy, A.S. 1982. "Higher order accuracy finite-difference schemes for hyperbolic conservation laws", *Int. J. for Num. Methods in Engineering*, vol.18, pp. 1019-1029.

Schwiderski, E.W. 1984. "Combined hydrodynamical and empirical modeling of ocean tides", *Marine Geophysical Res.*, vol.7 no.1-2, pp. 215-229.

Sharif, M.A.R. and Busnaina, A.A. 1988. "An investigation into the numerical dispersion problem of the skew upwind finite difference scheme", *Appl. Math. Modelling*, vol.12, pp. 98-108.

Tabuenca, P. and Cardona, J. 1992. "Numerical model for the study of hydrodynamics on bays and estuaries", *Appl. Math. Modelling*, vol.16, pp. 78-85.

Townson, J.M., Davies, M.E. and Matsoukis, P. 1980. "Numerical simulations of the Bristol Channel tide", *Proc. of Inst. of Civil Engrs.*, vol.69 pt.2, pp. 671-685.

Walters, R.A. 1988. "A finite-element model for tides and currents with field applications", *Communications in Appl. Num. Methods*, vol.4, pp. 401-411.

Walters, R.A. and Cheng, R.T. 1979. "A two-dimensional hydrodynamic model of a tidal estuary", *Advances in Water Resources*, vol.2, Dec., pp. 177-183.

Williams, R.T. and Zienkiewicz, O.C. 1981. "Improved finite element forms for the shallow-water wave equations", *Int. J. for Num. Methods of Fluids*, vol.1, pp. 81-97.

Withum, D., Holz, K.-P. and Meissner, U. 1979. "Finite element formulations for tidal wave analysis", *Computer Methods in Appl. Mech. and Engineering*, 17/18, pp. 699-716.

Zienkiewicz, O.C., Szmelter, J. and Peraire, J. 1990. *Computer Methods in Appl. Mech. and Engineering*, 78, pp. 105-121.